Epitaxy on substrates with hexagonal lattice symmetry.

by

Max Willi Hermann Braun

Submitted in partial fulfilment of the
requirements for the degree

Doctor of Science

in the Faculty of
Mathematical and Physical Sciences
University of Pretoria
PRETORIA

16th November, 1987

ACKNOWLEDGEMENTS

To my promoter Prof Jan H. van der Merwe, who gave me so much independence to pursue the paths I wished to travel down, and yet gave me both target and guidance towards some sensible work.

To all the staff and colleagues in the Physics department, who bore the brunt of my efforts to transmit enthusiasm over some minor victory or other, and the department head, Prof E.K.H. Friedland for his consideration and patience.

To the staff and director of the Buro for Computer Services, BUREK, for providing me with powerful computing facilities, and hours and hours of computer time, and the special attention I received from everyone.

To the Deans of Faculty for their encouragement and personal interest in the progress of my research,
Prof H.P. van der Schijff, Prof P.J. Zietsman and Prof N. Sauer, the present Dean.

To Alan Carr for freely sharing his enthusiasm for and knowledge of microcomputers.

To my family, for extreme forbearance and support while embroiled in my work and ignoring their very existence!

To my father, who started me on this long road to academic achievement.

DEDICATION

To the memory of my mother who always encouraged me, but didn't see the completion of my work.

ABSTRACT

Epitaxy on substrates with hexagonal lattice symmetry.

by

Max Willi Hermann Braun

PROMOTER: Prof Jan H. van der Merwe

DEPARTMENT: Physics

DEGREE: D.Sc.

A general description of epitaxy between thin films and substrates of any crystal symmetry was developed from a model in which both overgrowth and substrate are initially kept rigid (Chapter 3). The overgrowth-substrate interaction is described by Fourier series, usually truncated, defined on the surface reciprocal lattice vectors of the crystal faces in the interface (Chapter 2). Energy considerations lead directly to a criterion for the existence of epitaxial configurations which occur when a pair of surface reciprocal lattice vectors of the substrate and overgrowth coincide. This criterion is analogous to the von Laue criterion and Bragg equation in diffraction theory, and has a geometrical realization related to the Ewald construction. Generalized, the formulation allows the calculation of misfit strain, (Chapter 4) and the description of interfacial structures in terms of misfit dislocation arrays or verniers (Chapter 5) - the spacing, line sense and Burgers vectors are obtained from the reciprocal lattice for an interface between crystals of the most general and diverse symmetry. The most general structures can be treated with convenient unit cells by using structure factors.

Parallel to the predictions from reciprocal space, the homogeneous misfit strain (Chapter 4), the interfacial atom positions after relaxation (Chapter 5) and misfit and strain energies (both chapters) were obtained by direct numerical minimization of the total interfacial energy of a large (1105 atoms) but finite system.

SAMEVATTING

Epitaxy on substrates with hexagonal lattice symmetry.

deur

Max Willi Hermann Braun

PROMOTER: Prof Jan H. van der Merwe

DEPARTEMENT: Fisika

GRAAD: D.Sc.

'n Algemene beskrywing van epitaksie tussen dun films en substrate met enige kristalsimmetrie is ontwikkel vanaf 'n model waar beide die opgroeisel en die substraat eers star beskou is (Hoofstuk 3). Die opgroeisel-substraat interaksie is beskryf deur Fourier reekse, gewoonlik verkort, wat in terme van die resiproke roostervektore van die strukture van die raakvlakke gedefiniëer is. Energie oorwegings lyf direk na 'n voorwaarde vir die bestaan van epitaksiale konfigurasies wat bestaan as 'n oppervlak resiproke roostervektor van die opgroeisel saamval met 'n verplasingsvektor van die substraat resiproke rooster, wat onder meer atoomry-passing tot gevolg het. Hierdie voorwaarde is analoog aan die von Laue voorwaarde en Bragg vergelykings van diffraksieteorie, en lei na 'n geometriese daarstelling verwant aan die Ewald konstruksie. Na veralgemening, kan die homogene wanpas vervorming (Hoofstuk 4) en die tussenvlak struktuur in terme van die wanpasontwrigtings of wanpas nonius begrippe (Hoofstuk 5) uit die resiproke ruimte formulering bereken word. Die spasiëering, lynrigting en Burgersvektore kan van die resiproke rooster verkry word vir kristalle van die mees algemene en verskillende strukture. Die mees ingewikkelde strukture kan beskryf word in gerieflike eenheidselle deur struktuurfaktore te gebruik.

Afsonderlik van die voorspellings van die resiproke ruimte, is die homogene wanpasvervorming (Hoofstuk 4), die atoomposisies in die tussenvlak tydens lokale vervorming (Hoofstuk 5), sowel as wanpas

To calculate the interfacial atom positions and energies a numerical Finite Element formulation was used.

Systems with fcc{111} or bcc{110} overgrowths on fcc{111} or hcp{0001} substrates were considered. The effect of the substrate symmetry, overgrowth size and anisotropy of the overgrowth elastic constants were studied. Configurations such as Kurdjumov-Sachs (KS), Nishiyama-Wassermann (NW) and a pseudomorphic phase (2DC) were explained, while several other higher order configurations were predicted. The inherent difference in nature between the KS and NW and their relationship to the 2DC were emphasized. Deviations from the ideal orientation of KS linked to anisotropy for systems undergoing misfit strain were discovered. Deviations were also linked to crystal growth.

There was excellent agreement between the reciprocal space and direct energy minimization results, and the combined reciprocal lattice and energy minimization approach proved to be very useful both for prediction and interpretation.

en vervormingsenergië (albei hoofstukke) deur direkte numeriese minimering van die totale tussenvlakenergie van 'n groot maar eindige sisteem (1105 atome) verkry. Die atoomposisies en die energië tydens lokale vervorming is bereken deur 'n Eindige Element formulering toe te pas.

Stelsels met fcc{111} of bcc{110} opgroeisels op fcc{111} of hcp{0001} substrate is beskou. Die effek van substraat simmetrie, opgroeisel grootte en die anisotropie van die opgroeisel se elastiese konstantes is ondersoek. Die bestaan van konfigurasies soos die Kurdjumov-Sachs (KS), Nishiyama-Wassermann (NW) en 'n pseudomorfe fase (2DC) is verklaar, terwyl verskeie ander hoër-orde konfigurasies voorspel is. Die inherente verskil in eienskappe tussen die KS en die NW konfigurasies en hul verband met die 2DC is uitgewys. Afwykings van die ideale oriëntasie van KS, gekoppel aan die anisotropie vir sisteme wat vervorming ondergaan is ontdek. Afwykings is ook aan die kristalgroeimodus gekoppel.

Daar was uitstaande ooreenstemming tussen die resiproke ruimte en direkte energie minimering resultate. Die kombinasie van resiproke rooster en direkte energie minimering is uiters nuttig bewys by voorspelling en interpretasie van epitaksiale sisteme.

CONTENTS

NOTATION

Below is a list of symbols and a short description of their meanings in alphabetical order, in the priority order Lower case, Upper case, Italic, Script, Greek. Symbols without sub- or superscripts are listed with higher priority than those with added labels.

The symbols used in Chapter 1 - the introductory chapter, are not listed here where their usage differs from the rest of the text. The reason is that Chapter 1 discusses the work of several authors, and a notation close to that of the original author's was kept. As the expressions in this chapter are self contained, in that definitions of the symbols are given with each discussion, these definitions are not repeated here.

Bold-face characters represent vector, tensor or matrix quantities, for example, $\mathbf{a}_1$, $\mathbf{b}_2$, $\mathbf{e}_x$, $\mathbf{N}$, $\boldsymbol{\varepsilon}$.

a	dimensional parameter, substrate
a_o	conventional lattice parameter, substrate (cubic lattice parameter for cubic crystals Hexagonal basal parameter for hcp crystals)
a_1, a_2	lengths of the substrate direct basis vectors
$\mathbf{a}_1$,$\mathbf{a}_2$	direct lattice basis vectors, substrate
$\mathbf{a}_1^*$, $\mathbf{a}_2^*$	reciprocal lattice basis vectors, substrate
a_{nn}	bulk nearest neighbour distance, substrate
A, $\mathcal{A}$	refer to elastic constants
$\mathbf{A}$	$=\begin{bmatrix} a_{11} & a_{12} \\ a_{21} & a_{22} \end{bmatrix}$, General linear transformation matrix
$\mathbf{A}$	$=\begin{bmatrix} \alpha_x & \frac{1}{2}\gamma_{xy} \\ \frac{1}{2}\gamma_{xy} & \alpha_y \end{bmatrix}$, Linear transformation matrix due to 2- dimensional strains, $\varepsilon_x = \alpha_x - 1$, $\varepsilon_y = \alpha_y - 1$ and γ_{xy}
$\mathbf{A}^* = \mathbf{A}^{-1}$	as $\mathbf{A}$, but in reciprocal space
$\mathbf{A}_1$, $\mathbf{A}_2$	coincidence lattice basis vectors, substrate
A_{hk}	Fourier Coefficients, cosine series
α	angle between $\mathbf{a}_1$ and $\mathbf{a}_2$
α_x, α_y	refer to $\mathbf{A}$
α_x^*, α_y^*	refer to $\mathbf{A}^*$, with $\alpha_x^* = 1+\varepsilon_x^*$, $\alpha_y^* = 1-\varepsilon_y^*$
α_0 to α_8	coefficients of the biquadratic interpolating polynomial used in the Lagrangian element
b	dimensional parameter, overgrowth
b_o	conventional lattice parameter, overgrowth

b_1, b_2	lengths of the overgrowth basis vectors
$\mathbf{b}_1$, $\mathbf{b}_2$	direct lattice basis vectors, overgrowth
$\mathbf{b}_1^*$, $\mathbf{b}_2^*$	reciprocal lattice basis vectors, overgrowth
$\mathbf{b}_1'$, $\mathbf{b}_2'$	strained lattice basis vectors, overgrowth
b_{nn}	bulk nearest neighbour distance, overgrowth
$\mathbf{B}_M$	Burgers vector of the misfit dislocations
B_{hk}	Fourier coefficients, sine series
$\mathbf{B}_s$	matrix of derivatives of the shape functions, for a given node "s"
$[\mathbf{B}_s]$, $[\mathbf{B}_s]^e$	shape function derivative matrix for elements
$[\mathbf{B}_S]$	shape function derivative matrix for the system
β	angle between $\mathbf{b}_1$ and $\mathbf{b}_2$
β'	angle between $\mathbf{b}_1'$ and $\mathbf{b}_2'$, strained overgrowth
conj(ζ)	complex conjugate of the comples number ζ
c_θ, $c_{\theta\beta}$	refer to transformation parameters
c_{11}, c_{12}, c_{44}	refer to elastic constants
C_{ij}	refer to elastic constants
c_{11}, c_{12}, c_{44}	refer to elastic constants
$d\varepsilon_v$	virtual strain field
$d\mathbf{v}$	virtual displacement field
$[d\mathbf{v}^s]$	matrix of virtual displacements of element nodes
$d\mathfrak{V}_e$	infinitesimal volume of integration of element "e"
$d\mathfrak{D}_e$	infinitesimal area of integration of element "e" $= d\mathfrak{V}_e/t_e$
$\text{Discr}_{x_0y_0}$	discriminant calculated at x_0y_0 , needed for stationary point conditions
D_{ij}	refer to elastic constants
D_θ, $D_{\theta\alpha}$	refer to transformation parameters
$\mathfrak{V}_e$	integration domain, volume of the element "e"
$\mathfrak{D}_e$	integration domain, area of the element "e", $= \mathfrak{V}_e/t_e$
δ_{ij}	Kronecker delta
$\delta\mathbf{q}$	$= \mathbf{q}_b - \mathbf{q}_a$ absolute misfit, dislocation line propagation vector
∂	partial derivative
Δ, Δ_j	stacking fault parameter, strength of a basis feature or of j'th feature
Δ, ∇	"up-triangle", "down-triangle", resp. Refers to stacking order

elastic constants

c_{11}, c_{12}, c_{44}	cubic, unmodified elastic constants
c_{11}, c_{12}, c_{44}	cubic, modified elastic constants
C_{ij}	modified elastic constants in cartesian coordinates local to the plane
D_{ij}	2-dimensional modified elastic constants, in local coordinates, with plane stress boundary conditions enforced. These are the final constants which actually get used
λ, μ, ν	isotropic or Voigt averaged Lamé constant, shear modulus and Poisson ratio
$\mathcal{H}, \mathcal{A}$	unmodified anisotropy factor and ratio
H, A	actual (required) anisotropy factor and ratio

$e_{\text{superscripted}}$	refers to single element or element no "e"
$\mathbf{e}_x, \mathbf{e}_y$	unit vectors of a cartesian coordinate system
E_T	Total energy
$\mathbf{E}_x, \mathbf{E}_y, \mathbf{E}_z$	as $\mathbf{e}_x$ and $\mathbf{e}_y$ but after strain
$\mathcal{E}$	energy per interfacial atom
$\mathcal{E}_{el}$	strain energy per interfacial atom for a bounded island
$\mathcal{E}^{\infty}_{el}$	strain energy per interfacial atom for an infinite island
$\mathcal{E}_G$	total misfit energy for G atoms = $G\mathcal{E}_{mis}$
$\mathcal{E}_{mis}$	misfit energy per interfacial atom
$\mathcal{E}^{0}_{hk}$	contribution to rigid misfit energy of the h,k substrate Fourier term
$\mathcal{E}^{+}_{hk}$	as $\mathcal{E}^{0}_{hk}$ but due to the basis atom specifically
ε	2-dimensional strain matrix
ε_{ij}	general strain tensor components
$\varepsilon_x, \varepsilon_y, \gamma_{xy}$	2-dimensional normal and shear strains
$\varepsilon^*_x, \varepsilon^*_y, \gamma^*_{xy}$	strains in the reciprocal lattice
f, f_{ab}	misfit, one-dimensional system, parameters a, b
f_i, f'_i	misfit, in i'th direction, residual misfit after strain

f_{hk}^{pq}	misfit, between $[p\ q]^*$ and $[h\ k]^*$ reciprocal lattice directions of overgrowth and substrate resp.
	misfit between lattice row spacing in the directions perpendicular to the atomic rows lying along the $[q\ \bar{p}]$ and $[k\ \bar{h}]$ direct lattice directions
F^0	structure factor due to the relative displacement of the overgrowth and substrate
F^{pq}	overgrowth reciprocal lattice structure factor $= F^0(1+F^+)$
F^+	overgrowth structure factor due to basis feature at $x_b^+,\ y_b^+$
F_{hk}	substrate structure factor, of h,k Fourier harmonic $= 1+F_{hk}^+$ or $1 + \sum_j \Delta_j F_{hk}^{(j)}$
$F_{hk}^+,\ F_{hk}^{(j)}$	contribution of the single or j'th substrate basis feature to F_{hk}
$\mathbf{F}^B,\ [\mathbf{F}_S]^B$	dimensionless column matrix of system nodal loads, with boundary conditions applied
$\mathcal{F}$, $[\mathcal{F}_S]$	column matrix of system nodal loads
$\mathcal{F}^e,\ [\mathcal{F}_s]^e$	column matrix of nodal loads on finite element "e"
ϕ	angle through which a strained overgrowth has also rotated to achieve an epitaxial orientation
$\varphi_e,\ \theta_e,\ \psi_e$	Eulerian angles used in $\mathcal{L}_{ij}$
G	no of interfacial atoms in the overgrowth
$\mathcal{G},\ \mathcal{G}'$	appears in the misfit energy expression for the rigid and homogeneously strained overgrowths resp, corrects for symmetry
γ_0	$= hx_0 + ky_0 = \mathbf{q}\cdot\mathbf{r}_0/2\pi$, the translational contribution to the overgrowth structure factors F^0
γ_{xy}	$= 2\varepsilon_{xy}$ shear strain. also refer to ε_x etc.
h, k	integers, components of a reciprocal lattice displacement vector
	integers, characterize Fourier harmonics components of a wave vector $\mathbf{q}(h,k)$ in the substrate reciprocal lattice
$\bar{h},\ \bar{k}$	negative indices
h+k	order of the Fourier harmonic h,k

H	multiplicative factor, normalizes a substrate potential to maximum value 1
H, $\mathcal{H}$	refer to the symbol used differently as elastic constant
$\mathcal{Im}(\eta)$, $\mathcal{Re}(\eta)$	imaginary and real parts of complex number η
$\mathbf{k}$, $[\mathbf{k}_{S'S}]$	system stiffness matrix
$\mathbf{k}^e$, $[\mathbf{k}_{s's}]^e$	element stiffness matrix
$\mathbf{K}$, $[\mathbf{K}_{S'S}]$	dimensionless system stiffness matrix
$[\mathbf{K}_{s's}]^e$	dimensionless element stiffness matrix
$\mathbf{K}^B$	dimensionless system stiffness matrix, boundary conditions included
KS, KS^1	Kurdjumov-Sachs epitaxial orientations $\langle\bar{1}\ 2\ \bar{1}\rangle$fcc$\{1\ 1\ 1\}$ ∥ $\langle 0\ 1\ \bar{1}\rangle$bcc$\{1\ 1\ 0\}$
KS^j	higher order matching with geometric properties related to KS epitaxial orientation
κ	relative strength of overgrowth basis feature
L	no of finite elements
L_{hk}	geometric scaling factor, inverse of Λ_{hk}
ℓ	Van der Merwe configurational parameter
λ	Lamé constant, refer to elastic constants
λ_D	$=2\pi/\lvert\delta\mathbf{q}\rvert$ misfit dislocation spacing
λ_{hk}	wave-length associated with wave vector $\mathbf{q}(h,k)$
Λ_{hk}	scaling factor, appropriate to Fourier sublattice h,k
M, N	overgrowth island size parameters
$\mathcal{M}$, $\mathcal{N}$	no of finite element nodes in the $\mathbf{b}_1$-direction and $\mathbf{b}_2$- direction resp
μ	shear modulus, refer to elastic constants
$\mathbf{n}$	unit normal vector
N_s, N_1 to N_9	shape functions of the bi-quadratic Lagrangian element
$N_{s,x}$, $N_{s,y}$	$=\partial N_s/\partial x$ etc, partial derivatives of shape functions
$\mathbf{N}_s$	matrix of shape functions for element node no "s"
$\mathbf{N}_S$	as $\mathbf{N}_s$, but for the system node no "S"
$[\mathbf{N}_s]$	partitioned matrix of element shape functions
$[\mathbf{N}_S]$	partitioned matrix of system shape functions
NW, NW^1	Nishiyama-Wassermann epitaxial orientations $\langle 0\ 1\ \bar{1}\rangle$fcc$\{1\ 1\ 1\}$ ∥ $\langle 0\ 1\ \bar{1}\rangle$bcc$\{1\ 1\ 0\}$
NW^j	higher order matching with geometric properties related to NW epitaxial orientation
ν	Poisson ratio, refer to elastic constants

∇, Δ	"down-triangle", "up-triangle", resp. Refers to stacking order
ω^F_{hk}	rotation angle of Fourier sublattice h,k wrt the fundamental lattice
Ω, Ω^B	overgrowth volume per interfacial atom for infinite an bounded islands, before strain
p, q	as for h, k , but refer to the overgrowth reciprocal lattice
$\bar{p}$, $\bar{q}$	negative indices, overgrowth reciprocal lattice
$\mathbf{p}(x,y)$	(continuous) distribution of external forces
P	$= \nu/Wr^2$ an (isotropic) strain energy parameter
$\mathbf{q}$	wave vector, either general or substrate
$\mathbf{q}_a$, $\mathbf{q}_b$	wave vector, substrate, overgrowth resp.
$\delta\mathbf{q}$	absolute misfit, dislocation line propagation vector
$\mathbf{q}_0$	lowest order wave vector
$\mathbf{q}_b$	wave vector or reciprocal lattice vector, overgrowth
$\mathbf{q}_{hk}$	reciprocal lattice vector, substrate
$\mathbf{q}(h,k)$	wave vector expressed in substrate coordinates
$\mathbf{q}^{pq}$	reciprocal lattice vector, overgrowth
$\mathbf{q}(p,q)$	wave vector expressed in overgrowth coordinates
$\mathbf{q}_r$	reference wave vector (misfit dislocations)
q_x, q_y	cartesian components of an overgrowth reciprocal lattice vector, normally before strain
Q_x, Q_y	cartesian components of a substrate reciprocal lattice vector
$\mathcal{Q}_{hkl}$	surface migration activation energy, {hkl} surface
$r = b_{nn}/a_{nn}$	ratio of nearest neighbour distances, an important geometric parameter
$\mathbf{r}$	general position
$\mathbf{r}_b$	overgrowth position
$\mathbf{r}_0$	displacement of overgrowth origin wrt substrate
R	$= (1-\nu)/Wr^2$, (isotropic) strain energy parameter
R_θ	Operator, rotates function arguments through θ specifically, R_{120}, R_{180}, R_{240}
$\mathcal{Re}(\zeta)$, $\mathcal{Im}(\zeta)$	Real and Imaginary parts of the complex number ζ
sgn( )	sign of a number, -1 if negative, +1 otherwise
s_θ, $s_{\theta\beta}$	refer to transformation parameters
$_s$subscript or ^{s}superscript :	element node number index, indicates that the quantity labelled with "s" is an element quantity

S	$= h^2 + hk + k^2$, special quantity used for coincidence calculations
S subscript	system node number index, indicates that the quantity subscripted with S is a system quantity
σ	2-dimensional stress matrix
σ_{ij}	general stress tensor components
σ_x, σ_y, σ_{xy}	2-dimensional normal and shear stresses
transformation parameters:	
r_{11}, r_{21}, r_{12}, r_{22}	geometric ratios
c_θ, s_θ, $c_{\theta\beta}$, $s_{\theta\beta}$	angular parameters (overgrowth /substrate)
D_θ, T_θ, $T_{\theta\alpha}$, $T_{\theta\alpha}$	angular parameters (inverse)
r'_{11}, c'_θ, D'_θ etc	refer to strained overgrowth
t_e	thickness of the finite element "e", = thickness of the overgrowth
^{T} (superscripted)	transposed matrix
T_θ, $T_{\theta\alpha}$	refer to transformation parameters
$\mathcal{A}_{ij}$	elements of the transformation matrix from cubic to local surface coordinates used to transform the elastic constant tensor
θ, θ'	angle between $\mathbf{b}_1$ (or $\mathbf{b}'_1$) and $\mathbf{a}_1$, orientation of the unstrained and strained overgrowth wrt the substrate
$\mathbf{u} = (u_x, u_y)$	displacement field
$\mathbf{u}$	column matrix of system nodal displacement components
$\mathbf{u}^e$, $[\mathbf{u}^s]$	column matrix of element nodal displacements
$\mathbf{U}$, $[\mathbf{U}_s]$	as $\mathbf{u}$, system displacements, but boundary conditions included
u_i, u_x, u_y	displacement components in cartesian coordinates
$V(\mathbf{r})$, $V(x,y)$	adatom-substrate interaction potential
V_{cos}, V_{sin}	symmetric and antisymmetric truncated series respectively
V_{hk}	coefficients of the Fourier series, h,k non-negative
$V_{\mathbf{q}}$	coefficients of the general Fourier series
W	overall calibration factor, has units of energy, used in potential expressions
w	strain energy per unit volume
w_σ	virtual work density due to the stress field
W_σ	virtual work due to the stress field

$W_{\mathbf{p}}$	virtual work due to the applied force distribution $\mathbf{p}(x,y)$
x, y	position in the fixed coordinates relevant to each model, specifically: expressions involving the substrate alone or with a rigid overgrowth only, abrreviated form of x_a, y_a; otherwise position in fixed cartesian coordinates
x_1, x_2, x_3	position components in fixed cartesian coordinates
x_0, y_0	special position, substrate coordinates
x^+, y^+	position of the basis atom or feature, substrate
x_a, y_a	position components, substrate symmetry coordinates $\mathbf{r} = x_a\mathbf{a}_1 + y_a\mathbf{a}_2$
x_b, y_b	position components, overgrowth coordinates $\mathbf{r} = x_b\mathbf{b}_1 + y_b\mathbf{b}_2$
x_b^+, y_b^+	position of basis atom or feature, overgrowth
$\mathbf{X}$, X_1, X_2	general position, usually in matrix form, components
ξ, η	normalized coordinates, local to a finite element, range from -1 to +1
$\mathbb{Z}$	set of all integers (standard mathematical symbol)
{ }	general crystallographic indexed plane, or reciprocal lattice direction
[ ]	crystallographic indexed direct lattice direction
[ ]*	reciprocal lattice direction or wave vector
$[A_j]$	matrix with single entries A_j
$[\mathbf{A}_j]$	partitioned matrix, the entries are themselves matrices, $\mathbf{A}_j$
< >	general indexed crystallographic direction

CHAPTER 1

INTRODUCTION

An overview of the study reported here is presented.

Additionally the approaches to the related problems taken by other authors and the relationship of their models to those used here are described in summary fashion.

The procedure which was followed, the progression from a rigid model, through a model allowing homogeneous misfit strain and finally a misfit dislocation model is outlined.

CHAPTER 1

INTRODUCTION

The epitaxial growth of crystals of different species remains a subject of technological as well as fundamental interest. Several theoretical treatments exist, which achieve some success, and yet appear to fail to explain the occurrence, or non-occurrence of epitaxy in one or other system. This is mainly because several factors influence epitaxy in ways not always easily included in those models amenable to analytical treatments, or even when numerically based, to easy and hence useful interpretation. The symmetries, or lack of them, in the interfaces frequently make analytical treatment impossible.

The intention of this study was to find unifying factors of the more successful models, modify and apply them to systems which have symmetries more difficult to treat than the usual four fold symmetry. Specifically, the primary system modelled consisted of a bcc{110} overgrowth on an fcc{111} (or hcp{000.1}) substrate. Dealing with the symmetries lead to the development of a generalized approach - a formulation of the epitaxial problem in reciprocal space.

The reciprocal space formulation is first derived from a model in which both the substrate and the overgrowth are rigid. The definition of *Ideal Epitaxial Configurations* leads naturally to this.

The formulation is extended to the prediction of energy minimizing *misfit strain* accommodation, and the predictions are compared to the results obtained by direct (numerical) interfacial energy minimization, with excellent agreement.

In the most complex case, which includes interfacial features such as dislocations, the geometry of the dislocations, their spacing, orientation, line sense and Burgers vectors are obtained

analytically from the reciprocal space formulation, even for the most general interfaces. The detailed relaxation and strain fields in this third case are treated numerically, and the interfacial structures obtained are correlated with the features predicted from the reciprocal lattice.

A geometric realization of the reciprocal lattice epitaxial criterion is introduced. This is a simple construction in the reciprocal space of the surfaces, analogous to that introduced by Ewald in diffraction theory.

The effects of anisotropy are considered explicitly and do not complicate any of the calculations to any extent, but do introduce several interesting effects.

1.1 AN OVERVIEW OF THE MODELS USED

Three approaches were used, and listed in order of increasing sophistication are

a) the *rigid* model, in which the overgrowth island and the substrate are both held rigid, and the overgrowth is allowed both rigid body degrees of freedom, translation and rotation.
b) the *homogeneous strain* model, where the rigidity requirement on the overgrowth is partially relaxed, and the island is allowed to strain homogeneously, in order to calculate the *misfit strain* if present, and
c) the *dislocation model* and its associated *finite element* description, where the homogeneous strain requirement is relaxed, and the overgrowth is allowed to strain differentially with position. This is the most complex.

The achievement of equilibrium by epitaxial systems is dependent on temperature and the availability of energy to overcome various energy barriers (Peierls barriers to dislocation motion, barriers

to the rigid rotation of islands and so forth) and therefore stable equilibrium is defined by minimum free energy. The attainment of equilibrium is driven by free energy gradients, facilitated by thermal fluctuations. Because of the regularity of both crystals and misfit dislocations, if any, the dominant contribution to the free energy is the absolute energy itself so that the equilibrium configuration may be adequately characterized by the condition that total energy is minimized. (Van der Merwe 1964, 1966, Van der Merwe and Ball 1975).

The three models share the basic description of the epitaxial system.

Based on the work of Van der Merwe (*full references below with the short discussion*), the overgrowth is considered a thin homogeneous layer, primarily a monolayer, which has the structure of the crystal it would form were it part of a bulk material - that is a slice from the bulk. This assumption is probably more valid here where close packed planes are modelled than in general low-coordination planes.

The atoms of the overgrowth interact with the rigid substrate through a single particle potential expressed as a Fourier series, which mirrors the symmetry of the substrate crystal surface. The atoms within the overgrowth interact by stress fields, within the harmonic approximation, observable as strains of the overgrowth island when energetically allowed. The description allows factors such as the binding strength of the substrate to the overgrowth to be included, as well as the geometric features of both the overgrowth and substrate symmetries. The models therefore all go beyond simple purely geometric models.

Rigid model

The simplest treatment assumes that both the substrate and the overgrowth are rigid, and correlates minima in the interaction energy (or misfit energy) between the entire overgrowth and the

substrate with ideal realizable epitaxial configurations. This energy is calculated as a function of the ratio between the nearest neighbour distances in the two crystal types in the bulk, and the relative azimuthal orientation.

This rigid model shows that these *energy minima in fact occur when wave vectors characterizing the terms in the Fourier expansion*, (which in their turn correspond to particular atomic rows), *coincide with reciprocal lattice translation vectors of the overgrowth*. This result which is inevitable from the energy treatment is clearly direct row-matching, or when higher order terms are involved, coincidence matching.

The natural result that row matching as seen in the reciprocal lattice characterizes the *ideal* epitaxial configurations suggests a construction of the Ewald type, in terms of which insight into the geometric and energetic aspects of epitaxy is particularly easily obtained.

Among the successes of this description are the prediction of Nishiyama-Wassermann and Kurdjumov-Sachs (Bruce *e.a.* 1977, 1978 a,b and Van der Merwe 1982 a,b,c) orientations for the bcc{110} / fcc{111} epitaxial system, and some higher order configurations occurring at the same or other orientational angles, all achieved with very little effort.

While this rigid model clearly defines the orientations which may be assumed by systems with nearest neighbour ratios close to the ideal, predictions of epitaxy for other systems is at best speculative. For this reason the requirement that the overgrowth is kept rigid is relaxed in the second model.

The inclusion of homogeneous strain

The overgrowth island is considered an elastic sheet, which strains in response to the interaction with the substrate. However, in this

second case, the strain allowed is restricted to homogeneous strain. The energy of misfit and deformation are minimized together, again as a function of orientation and nearest neighbour ratio. As strain and rotation are separable quantities, the orientation is uniquely definable. The nearest neighbour ratio is once again the ratio of bulk nearest neighbour distances. The relative values of strain constants are determined by the *configurational parameter* (ℓ, see below) first introduced by Frank and Van der Merwe for one-dimensional cases and later extended to more general cases.

Anisotropy in the elastic constants is treated explicitly, and this treatment yields the result that the degree of anisotropy in fact changes the ideal azimuthal angle defining the orientation from the angles expected for rigid systems. This may be used to explain deviations from exact ideal orientations when they occur. Predicted from the model for instance are deviations from the angle for the Kurdjumov-Sachs configuration derived from the geometry alone, caused purely by the anisotropy of the elastic constants.

This homogeneous strain model also predicts and allows the study of perfect two-dimensional coherent or pseudomorphic matching between the substrate and overgrowth lattices in some cases.

The reciprocal lattice construction is also used to predict the strain necessary for achieving row-matching, subject to minimum strain energy, again separate from re-orienation by rotation. Again the energy considerations, and the geometric considerations (with strain energy taken into account) correlate. An important result is that some orientations cannot be achieved from the coherent matching configuration by strain alone, but in fact *must* rotate. This has implications if the island has grown coherently, but later, due to thickening for example, a one-dimensional matching orientation becomes energetically more favourable. If the island cannot rotate to the required orientation, exact row matching in that orientation will not be possible. Intermediate configurations will result, either secondary or higher order row-matching

(coincidence matching), with orientations away from the ideal, or local matching, with edge or screw dislocation networks may be observed.

Local strain and matching situations need a relaxation of the homogeneous strain restriction, and require a more complex formulation allowing more degrees of freedom. This is the purpose of the third model.

Inclusion of local strain

The homogeneous strain limitation is relaxed in this most complex treatment, and the overgrowth is again considered an elastic sheet, but is allowed to strain locally. This allows the inclusion of misfit dislocations, and a rich but ordered interfacial structure is observed. The many degrees of freedom in a large island preclude analytical treatment at this level, and a finite element formulation is used. The effect of local relaxation on the energy behaviour is studied, and some structural information is obtained for systems which are orientated both at and away from the ideal orientations for several nearest neighbour ratios.

The misfit dislocations, or vernier where relaxation is insignificant, are all described in terms of the reciprocal lattice, and in fact their spacing, orientation and Burgers vectors etc. as predicted from the reciprocal lattice, are all correlated with the actual interfacial structure which results from the Finite Element model.

The models are applied progressively, first the ***rigid model***, then the ***homogeneous strain model***, and finally the ***misfit dislocation*** or ***finite element***, local strain, ***model***. The system studied by all three methods has the overgrowth as bcc{110} material, growing on an fcc{111} substrate (or, in fact, because of the finite Fourier series which models the substrate, an hcp{00.1} substrate).

As a model study the case of fcc{111} overgrowth on the fcc{111} substrate is also considered by the rigid, reciprocal space treatment.

1.2 EXISTING APPROACHES

Several models and studies exist which could be applied to the sytems under study, and which certainly influenced the approach taken here. These are described in the order in which the number of degrees of freedom allowed for in the system increases, from purely geometric (no energy considerations at all), through to semiclassical quantum mechanical approaches.

1.3 GEOMETRIC MODELS

Bollman's O-Lattice Theory

Bollmann (1967 a,b ,1970), has developed a direct space lattice geometric theory for describing the matching of differing crystal systems, or like systems in different orientations.

Obtainable from the theory is the space lattice (which may consist of lines, planes or points periodically placed) which defines regions of the two crystals where *equivalent* points of the crystals, related by an affine transformation, coincide in space. If the structures coincide only at lattice points, (or are infinitesimally away from coincidence at lattice points), the lattice is the Coincidence lattice of Friedel (1926) or Ranganathan (1966). The generalization, the O-lattice, includes random positions in the crystal unit cells which are related by the transformation and coincide.

The O-lattice is defined as follows:
(The overgrowth quantities are indicated with superscripted b, the substrate with a.)

1. Two crystal lattices are related by a linear transformation (matrix $\mathbf{A}$), such that *every* lattice point of the second (overgrowth) lattice is the image of a lattice point of the first (substrate) lattice. They are then elements of related equivalence classes, and

$$\mathbf{R}^b = \mathbf{A}\mathbf{R}^a, \text{ and } \mathbf{R}^a = \mathbf{A}^{-1}\mathbf{R}^b.$$

2. If the point $\mathbf{R}^b$ is exactly at a substrate lattice translation vector from $\mathbf{R}^a$, i.e. at $\mathbf{R}^a+\mathbf{t}^a$, where $\mathbf{t}^a$ is any substrate lattice translation vector, then $\mathbf{R}^b$ is in coincidence with the point $\mathbf{R}^a+\mathbf{t}^a$, and $\mathbf{R}^b$ is denoted by $\mathbf{R}^o$, and called an O-lattice point.

Hence the coincidence points are solutions of the equation

$$\mathbf{R}^o = \mathbf{A}^{-1}\mathbf{R}^o+\mathbf{t}^a ,$$

from which

$$(\mathbf{I}-\mathbf{A}^{-1})\mathbf{R}^o = \mathbf{t}^a .$$

For the general case, $\mathbf{R}^a$ is not necessarily a lattice point of the substrate lattice, and the solutions of the above equation define the O-lattice. Where $\mathbf{R}^a$ is in fact a lattice site, the special case of the Coincidence lattice is defined.

3. Depending on the rank of the matrix $(\mathbf{I}-\mathbf{A}^{-1})$, the solutions of $\mathbf{R}^o$ may be points, (rank = 3), lines, (rank = 2) or planes, (rank = 1). For the highest rank, the transformation $\mathbf{A}$ images all the points of the substrate lattice, useful for a stepped surface, while rank = 2 images all points in a plane, and rank = 1, points on a line.

4. The dislocation lines, (or in general cell walls, or moiré lines) lie on intersection of the interface with the Wigner-Seitz cell boundaries of the O-lattice in an isotropic material. For

anisotropic materials, the dislocation lines still bisect the lines joining nearest neighbour O-lattice points, but do not necessarily form straight lines along the Wigner-Seitz cell walls (Chapter 12 of Bollmann 1970).

These O-lattice points have two significant features (Fletcher *e.a.* 1975): (*i*) Because of the symmetry of both crystals about the O-lattice, no matter what local elastic relaxation may take place when the physical interface is formed, the O-lattice points will remain stationary, and (*ii*) the O-lattice gives directly the positions of the intensity maxima in the moiré pattern obtained by superposing the interface atoms of the two undistorted, rigid crystals.

Stated another way, the O-lattice structures in interfaces coincide with the possible location of misfit dislocation lines for a pair of crystals, (strictly in the case of small misfit and large dislocation spacing), for a given orientation and scale. Therein lies its importance. As pointed out by Jesser (1973), the Moiré lines do not necessarily coincide with the *only* possible dislocations line arrays which can accommodate the misfit, as dislocation interactions frequently cause new arrays to be constructed from the old.

The theory is generally applied in the determination of matching planes and orientations which give the largest density of coincidence, as the interfacial interaction energy is assumed to be inversely dependent on this coincidence density.

In applying this energy criterion, any monotonically decreasing function of coincidence density is useful. Other than this principle there is no energetic basis for the theory - it is purely geometric, and highly successful within this context.

The analysis proceeds in direct space, which tends to obscure the periodicities inherent in the lattices as well as the dependence of

low energy configurations on these periodicities. Later models, which include interfacial energy directly, in fact show this dependence.

Bruce and Jaeger's moiré model

This model (Bruce *e.a.* 1977, 1978 a, b) is an essentially geometric model, and directly linked to the moiré patterns used for interpretation of the O-lattices of Bollmann's model.

Nets of disks corresponding to interfacial atoms of the substrate and overgrowth crystals, appropriately scaled and arranged as in the bulk material, are superimposed parallel to the interface. Those areas of the patterns produced in this way, where disks overlap extensively are regarded as high-energy areas, unfavourable for the simulated epitaxy.

This is a procedure for simulation rather than a model, and as such is completely taken up in the more generalized description of Bollman's model. Its noteworthy success in predicting the Kurdjumov-Sachs and Nishiyama-Wassermann epitaxial orientations for the bcc{110}/fcc{111} system confirms the importance of the geometry of the crystal interface which modulates the chemical-electronic interactions between the crystals.

As in Bollmann's model, although the model is very successful, there is not an energetic basis included explicitly in the model, more a phenomenological assumption. Again, the decision for matching is based on the matching of direct space moire constructions, involving many elements, making analytical manipulation more difficult than an appropriate reciprocal space formulation.

Lattice fitting considerations of Takayanagi e.a.

Takayanagi *e.a.* (1978) in a review on experimental work done on several systems, analyzed the results geometrically, by direct comparison of the lattice-row spacings in the observed bulk crystal types for the orientations observed to occur frequently. Their key conclusion is that the epitaxy is frequently related to near or exact row-matching. However, reservations about the purely geometric approach were expressed by them, and they concluded that strain and the interaction energy must be included in any more complete geometric theory.

1.4 GEOMETRIC MODELS WHICH INCLUDE INTERFACIAL ENERGY

Van der Merwe's Rigid Overgrowth/Fourier Substrate Model and the Model of Reiss

As in the previous models, the overgrowth is modelled as a rigid island, in which the atoms are at fixed positions relative to one another, and the only degrees of freedom are the rigid body motions, translation and rotation as a whole. Van der Merwe (1982,a,b,c) in the most extensive discussion of the model, has included the effect of the overgrowth-substrate interaction by using a truncated Fourier series which expresses the adatom-substrate interaction potential. The Fourier series contains the symmetry of the substrate explicitly. A similar approach was taken by Kotzé *e.a.* (1974), who have employed the model in a discussion of the merits of different epitaxial combinations with NaCl substrates, as well as overgrowth size effects. Reiss (1968) calculated the dependence of overlayer-substrate interaction energy between square interfacial meshes on misfit and small axial misorientations.

The basic assumption in the analysis is that the tendency to epitaxy between the two crystals is favourable for configurations (orientation and relationship between the lattice parameters) which minimize the interfacial energy. Sharply defined deep minima would imply a strong epitaxial tendency to the particular orientation, while the absence of such a minimum favours incoherence, or may simply mean the fact that too few degrees of freedom are included.

The use of the truncated Fourier series to represent the adatom-substrate interaction potential has been used in the interface studies from the Frenkel-Kontorowa model (1938), through the pioneering work of Frank and Van der Merwe (1949,a,b, 1950, a,b), and more generalized work later. The coefficients of the series have been estimated from Lennard-Jones 6-12 or similar potentials, (Mackenzie 1950, Steele 1973, Stoop 1986, Stoop *e.a.* 1987), which all confirm that the magnitude of Fourier terms decrease rapidly with increasing order, although the actual rate of decrease may differ for different surfaces. The overall amplitude of the interaction has been linked to binding and surface diffusion energy results, by Van der Merwe (1964) and the energy of adhesion in thicker layers (Van der Merwe 1979), which gives the interaction energy quantitative respectability.

The interfacial energy in this model consists only of the total adatom-substrate interaction potential, expressed as a sum of the interaction energies of all the overgrowth atoms. For G island atoms in the interface, this energy becomes (Van der Merwe and Braun, 1985)

$$V_G = W\left\{G+\sum_{i=1}^{4} V_i C_i(x_0,y_0)K(M;p_i,q_i)\right\} ,$$

in the case of an fcc{111} overgrowth on a bcc{110} substrate - the relevant system studied by Van der Merwe with this model.

The symbols have the meanings:

$$G = (2M+1)^2 + 4M^2 ,$$

the number of atoms of a rectangular overgrowth island which lie in

the interface, where 2M+1 is the number of atoms along the outer edges of the island, and 2M is the number of atoms in the rows just before the outer edges (in both horizontal and vertical directions).

The functions

$$K(M;p,q) = \frac{\{\sin[\pi(2M+1)p]\,\sin[\pi(2M+1)q] + \sin \pi 2Mp \sin \pi 2Mq\}}{\sin \pi p \sin \pi q} ,$$

behave like delta functions as M approaches ∞ , with arguments

$$p_{2,1} = [r \sin \beta \cos(\alpha \pm \theta)]/(\sin \alpha \cos \alpha) ,$$
$$q_{2,1} = [r \cos \beta \sin(\alpha \pm \theta)]/(\sin \alpha \cos \alpha) ,$$
$$p_3 = 2r \sin \beta \cos \theta / \sin \alpha \quad , \quad q_3 = 2r \cos \beta \sin \theta / \sin \alpha ,$$
$$p_4 = 2r \sin \beta \sin \theta / \cos \alpha \quad , \quad q_4 = 2r \cos \beta \cos \theta / \cos \alpha ,$$

and the coefficients $C_i(x_0,y_0)$ are structure factors arising from the translation of the central adatom from a potential minimum expressed in the substrate coordinate system.

Factors V_i and W arise from the Fourier expression for the interaction energy between the overgrowth atoms and the bcc{110} substrate.

$$V/W = 1 + V_1 \cos 2\pi x + V_2 \cos 2\pi y + V_3 \cos 2\pi(x-y) + V_4 \cos 2\pi(x+y) ,$$

where W is an energy calibration term, and V_i are the Fourier coefficients. The position is expressed in terms of a rhombic substrate coordinate system, as $x\mathbf{a}_1 + y\mathbf{a}_2$, written as (x,y) with

$$\mathbf{a}_1 = \tfrac{1}{2}a_o[\bar{1}\ 1\ 1] \quad , \quad \mathbf{a}_2 = \tfrac{1}{2}a_o[1\ \bar{1}\ 1] ,$$

where a_o is the cubic lattice parameter. The ratio, r, of nearest neighbour distances, b_{nn} and a_{nn} ($= \sqrt{3}\, a_o/2$), respectively, (or atomic size in close packed planes), where $r \equiv b_{nn}/a_{nn}$, is seen to be a key parameter.

The angles are α (54.74°), the half-angle between $\mathbf{a}_1$ and $\mathbf{a}_2$, and β (60°), is the half-angle between

$$\mathbf{b}_1 = \tfrac{1}{2}b_o[\bar{1}\ 0\ 1] \text{ and } \mathbf{b}_2 = \tfrac{1}{2}b_o[1\ \bar{1}\ 0] ,$$

where $b_o = 2\sqrt{b_{nn}}$ is the cubic lattice parameter. The orientation angle θ is measured anticlockwise from the parallel alignment of $[0\ \bar{1}\ 1]$ fcc with $[0\ 0\ 1]$ bcc, the Nishiyama-Wassermann orientation.

The significance of V_G is clear, when it is seen that this total interfacial (misfit) energy has a sharp minimum, due to the delta-function-like behaviour of the functions $K(M;p,q)$, when p and q become integers, (with p+q even because of the effect of the structure factors C_i). The abrupt minima in misfit energy define the Ideal Epitaxial Configurations. The normalized depths of these minima provide a measure of the tendency to epitaxy (called epitaxial strength by Van der Merwe) of the particular system.

The prediction of the occurrence of these epitaxial configurations on the basis of energy arguments is the major success of this model.

The further development of this model undertaken here (in Chapter 3) enhances the interpretability considerably:

It is to be noted that the coefficients, V_i, correspond to the two-dimensional substrate (surface) reciprocal lattice directions $[1\ 0]^*$ for V_1, $[0\ 1]^*$ for V_2, $[1\ 1]^*$ for V_3 and $[1\ 1]^*$ for V_4 (Van der Merwe *e.a.* 1985). The quantities p_i, q_i will be shown to be components of these reciprocal vectors in the overgrowth surface reciprocal lattice. That p_i,q_i are integers (such that p_i+q_i is even in this case) at the ideal epitaxial orientations means that the vector $[p_i\ q_i]^*$ is a reciprocal lattice translation vector of the overgrowth lattice.

It is the simultaneous matching of a single substrate and overgrowth reciprocal lattice translation vector which defines an ideal epitaxial orientation. This in turn implies the matching of

lattice rows, whether successive rows, or in coincidence fashion, as noted by Matthews (1972, 1975) in orientation and spacing.

This geometric relationship, obtained from energy arguments, leads to a geometric construction, introduced here in Chapter 3, in terms of which the properties of the reciprocal spaces of the overgrowth and substrate crystals are used to determine epitaxial orientations, the misfit strains, and dislocation densities in simple analytical fashion.

The muffin-tin model of Gotoh and Arai

Gotoh and Arai (1986, see also Gotoh *e.a.* 1987) have described a geometric model which also provides good agreement with experiment, and, like Van der Merwe's model, includes the adatom-substrate interaction as an atomic potential. The key difference is that the adatom-substrate potential is defined as a muffin-tin potential (Ashcroft *e.a.* 1975 ch 11) as follows.

Within the primitive unit cell, circular equipotentials are defined up to a cut-off radius from the force centres at the corners of the cell. The cut-off radius trisects the diagonal. A positive potential is defined about the origin, while negative, inverted equipotentials are defined about the 1/3 and 2/3 positions along the diagonal. These inverted force centres correspond to the intended adatom positions. For the fcc{111} surface modelled in this fashion, the potentials are defined sinusoidally as

$$\phi(r) = \cos \frac{\sqrt{3}\pi r}{a_{nn}} , \quad \text{for } 0 < r < \frac{\sqrt{3}}{6} a_{nn} ,$$

where a_{nn} is the atomic nearest neighbour distance. In areas not covered by this definition, the potential is zero.

Because of the nature of the potential, defined piecewise, the model can only be used numerically, and unfortunately forces interpretation to be linked purely to direct space. Geometric properties of the model, such as row-matching are inferred rather than a natural result of analysis, and because of their rather

specific nature, are difficult to generalize. The predictions which have been made from the model are for the bcc{110}/fcc{111} system, and confirm the occurrence of the Kurdjumov-Sachs and Nishiyama-Wassermann orientations for this system, as predicted from the Van der Merwe model (Van der Merwe 1982, a,b,c, Van der Merwe *e.a.* 1985) and in the present work.

The model does also predict the relative strengths of epitaxial tendencies as it is linked to energy considerations.

For calculations in which Fourier expressions for the energy are not optimal, the essentially one-dimensional nature of the muffin-tin potential may prove to be an advantage, although there is a serious shortcoming in the discontinuity in the derivative for force calculations. The computer time saved with such a potential may be considerable, when compared with a Fourier expression involving several terms, particularly when many mobile atoms, as opposed to a rigid model, are involved. This may yet prove to be the most significant contribution of the model.

The Rigid overgrowth/particle pair potential model of Ramirez e.a.

Ramirez, Rahman and Schuller (1984) have performed a rigid-lattice, atomistic model calculation for bcc{110}/fcc{111} epitaxy, using both a Lennard-Jones 6-12 potential as well as an exponential central potential

$$\phi(r) = 4 \exp[-\tfrac{8}{3}(r^2-1)]\{\exp[-\tfrac{8}{3}(r^2-1)] - 1\} .$$

A Lennard-Jones potential was fitted to the exponential potential to obtain the same potential depth and hard core radius, with

$$\phi(r)^{LJ} = 4\left[\frac{1}{r^{12}} - \frac{1}{r^6}\right] .$$

The degrees of freedom included in the calculation were vertical distance from the substrate, relative position, orientation and the ratio of fcc/bcc lattice parameters, a quantity easily reducible to the ratio of nearest neighbour distances used here.

The calculation confirms the assumption inherent in all the previously described rigid overgrowth models, namely that the distance between the fcc and bcc planes does not affect the qualitative discussions, because the symmetry of the problem, translational as well as rotational does not get affected by the vertical displacement of a rigid overgrowth.

Although the agreement with their experimental work is excellent, it is reported by Ramirez *e.a.* that this agreement is by no means perfect, particularly when the predictions of the model are extended to superlattice growth. This is ascribed to the fact that elastic relaxation and strain as well as the specific chemistry, (such as directional effects of the interatomic bonds perhaps), are not taken into account, by either the rigid overgrowth itself, or the central potentials used.

This model is also successful in predicting the occurrence of the Kurdjumov-Sachs and Nishiyama-Wassermann orientations in the bcc{110}/fcc{111} eptaxial system. This once again confirms the prime importance of geometric considerations in this at least.

Again this is an essentially numerical model, although the form of the model lends itself to Fourier analysis analytically, as suggested by Seeger (1987, Private Communication). Without the calculation of the Fourier expansion however, the difficulty of generalization associated with this model is common to the model of Gotoh *e.a.* described above.

The Pseudopotential Epitaxial model of Batra

Batra (1984) has proposed a first-principles model for the calculation of the energy of an epitaxial system. Its application involved the application of a self-consistent pseudopotential calculation of the energetics of a small aluminium island, 4 to 5 atoms per layer consisting of from 1 to 5 layers, on a small germanium substrate, again about 4 lattice sites in about 2 layers (actually 5 layers of atoms). The orientation modelled is the relationship (001)[100]Al ∥ (001)[110]Ge.

The overgrowth is kept to pseudomorphic geometry, i.e. the interatomic distances and structure of the overgrowth in the interface match the substrate. The aluminium atoms are rigidly kept in their bulk structure, except that the interplanar distance is slightly reduced, while the germanium atoms are fixed in their bulk positions. The distance between the substrate and overgrowth is allowed to optimize.

Essentially therefore the application described by Batra is a rigid island/rigid substrate model, in which the overgrowth-substrate interaction is calculated using pseudo-potential methods.

Useful information obtained from the model is an estimate of the energy amplitude W as used in the truncated Fourier series interfacial potentials such as Van der Merwe's model described above.

The question of orientation and accommodation with misfit dislocation has not been addressed by Batra, probably linked to the rather small islands considered. Clearly this model is still in its early stages of usefulness.

1.5 STRAINED OVERGROWTH, MISFIT DISLOCATION AND ATOMISTIC APPROACHES

The preceding models have all assumed a rigid overgrowth, and therefore their results are specific to systems with geometric relationships which are close to the ideal configurations predicted by these models. In other words, systems for which strain is not an important considertaion.

Models of thin films, particularly if lattice parameters are not close to the ideal most certainly must, at least a priori, take account of strain.

Models of epitaxial growth of thin films which have achieved particular success are the one-dimensional model of Frank and van der Merwe (1949 a,b) and its further development to 2 dimensions. In these models the overgrowth is modelled in "Ball-and-Spring" form as in the Frenkel-Kontorowa (Frenkel *e.a.* 1938) model. The overgrowth atoms are represented as balls, connected by springs, which experience a positional force due to a sinusoidal overgrowth-substrate interaction potential. Epitaxy of dissimilar systems is modelled by choosing the natural length of the springs different from the period of the substrate potential. These formulations lead to finite difference equations, which may be solved numerically. By approximating the chain of springs by a continuum, approximate differential equations are constructed which are analytically solvable in one-dimensional form, or in separable two-dimensional cases. Below, the one-dimensional case will be described, as well as the weakly coupled limit of a non-separable two-dimensional case, which is the model applicable to the systems studied here.

Thicker overgrowths have been treated as elastic continua in the Peierls-Nabarro (Nabarro 1947, 1967, Van der Merwe 1950, 1963a,b, 1964, Jesser *e.a.* 1967, Ball *e.a.* 1970, Ball 1970) model, again with a truncated Fourier series as the overgrowth substrate interaction, realized as a shear stress, or as periodically repeating parabaloids. The substrate has also been allowed to relax elastically.

Half-infinite systems are formulated also as continua, as a limiting case of the thickening overgrowth,(Van der Merwe 1964) or in the formulation due to Fletcher, (see Fletcher *e.a.* 1975 for a review), as collections of atoms experiencing a particle pair interaction potential between overgrowth and substrate atoms. Volterra dislocation models have also been formulated, for example by Brooks (1952), and Nabarro (1970), as well as Matthews (1966,1975, Jesser *e.a.* 1967, 1968 a,b,c) who introduced the threading dislocation mechanism for the introduction of dislocations into the interface.

These thick-overgrowth models (other than that due to Fletcher) are not discussed here, as strictly, the models and the systems studied here are monolayer or near monolayer systems.

The essential departure from the previous approaches, is the complementary approach in which the geometric models, formulated in reciprocal space, are generalized to include strained systems, and are used with numerical solutions of finite systems. The strained systems both in the case of homogeneously strained overgrowths and systems with local strain and misfit dislocations are formulated as elastic continua. The elastic continuum is discretised for numerical solution in the local strain case (discussed in chapter 5) in terms of a Finite Element formulation which preserves the continuum nature of the interaction between the overgrowth atoms as understood in the harmonic approximation. This continuum formulation of the thin-film systems provides the link between the Frenkel-Kontorowa models of thin films and the Peierls-Nabarro models of thicker overgrowths.

The One-Dimensional and weakly coupled Two-Dimensional thin film models.

The first application of the Frenkel-Kontorowa models to thin films was that of Frank and Van der Merwe (1949 a,b). The development of this model is briefly described here.

The assumptions on which the description is based are that the interface is an abrupt and atomically flat interface, that the substances are immiscible, and the substrate may be treated as rigid. The structure of the overlayer after elastic relaxation results from the equilibrium minimum energy criterion that the total energy consisting of elastic strain energy and the overgrowth-substrate interaction energy is minimized.

The substrate is the source of a periodic potential, with period a and overall amplitude or energy calibration factor, W,

$$V = \tfrac{1}{2}W[1-\cos(2\pi x/a)].$$

The position relative to the origin is measured from a minimum (trough) position in the potential V, as the displacement x. The amplitude W will be large for strong bonding and small for weak bonding (Van der Merwe, 1964).

The overgrowth is simulated by a linear chain of atoms connected by springs of natural length b and constant k.

Each potential trough and corresponding overgrowth atom may be designated by the integer n, indicating the n^{th} position from the origin along the axis. This defines a reference configuration, in which the n^{th} atom and the n^{th} potential minimum coincide, the pseudomorphic or exact fit configuration. The positions of the atoms may therefore be written as

$$x_n = a(n + \xi_n) ,$$

where ξ_n is the displacement of the n^{th} atom from the corresponding exact fit position of the n^{th} trough, in units of a. (If the overgrowth is rigid, $x_n = nb$.)

The tangential force on the overgrowth atom at x due to the substrate will be

$$F = -\partial V/\partial x = -(\pi/a)W \sin(2\pi x/a).$$

The forces experienced by the n^{th} atom arise from this interaction, and the tension on the springs connecting the atoms. The extension of the springs about atom n are given as

$$e_{n\,n+1} = (x_{n+1} - x_n - b) = a[(n+1) + \xi_{n+1} - n - \xi_n - b/a] ,$$
$$= (\xi_{n+1} - \xi_n + 1-b/a)a = (\xi_{n+1} - \xi_n - f)a ,$$

and

$$e_{n-1\,n} = (x_n - x_{n-1} - b) = (\xi_n - \xi_{n-1} - f)a .$$

Here $b/a-1$ has been replaced by the natural misfit f between the overgrowth and substrate systems. This is related to the natural

beat wavelength as $b/f = ab/(b-a) = \left[\frac{1}{a} - \frac{1}{b}\right]^{-1}$, the difference between the inverse wave lengths of the two periodic systems. From these expressions the resultant force on the n^{th} atom is

$$F_n = k(e_{n\ n+1} - e_{n-1\ n}) - (\pi/a)W \sin(2\pi x/a).$$

Equilibrium occurs when $F_n = 0$,

$$\xi_{n+1} - 2\xi_n + \xi_{n-1} = \pi\frac{W}{ka^2} \sin(2\pi\xi_n) = (\frac{\pi}{2\ell^2})\sin(2\pi\xi_n) .$$

The quantity $\xi_{n+1} - 2\xi_n + \xi_{n-1} = \Delta_n^2\xi$ is the central difference of the relative displacement ξ calculated at the position of the n^{th} atom.

The configurational parameter

$$\ell \equiv (ka^2/2W)^{\frac{1}{2}} ,$$

was introduced for this model for the first time by Frank and Van der Merwe, and can be expressed in terms of the constants of an isotropic material as $[\mu\Omega/(1-\nu)r^2W]^{\frac{1}{2}}$ (van der Merwe *e.a.* 1975). When $r \equiv b/a$ is the ratio of the spatial periods, $\Omega \equiv tb^2$ is the volume associated with an interfacial atom, and the spring constant k is expressed as $2\mu t(1-\nu)$. The thickness of the overgrowth is t, while μ and ν are the shear modulus and the Poisson ratio respectively. The importance of this dimensionless parameter lies therein that the rigidity, $\mu/(1-\nu)$, or resistance to strain, is balanced against the need to deform, measured as the ratio r, and the maximum energy per unit volume W/Ω available to drive the deformation. Various forms of this parameter apply to various systems, dependent on the symmetries included in r and Ω, but these quantities are always balanced. Conditions on the type of matching which can be achieved, pure strain, strain with periodic strain fields associated with dislocations, and dislocations alone can be economically expressed in terms of this parameter.

The difference equation may be expressed as a differential equation when the displacements ξ vary slowly with n, in the case that the

misfit f is small, the beat wavelength b/f is large. Expanding ξ_{n+1} and ξ_{n-1} as Taylor series about n, in terms of the now continuous variable n,

$$\Delta_n^2\xi = \xi_{n+1}-2\xi_n+\xi_{n-1} = \frac{d^2\xi}{dn^2} + \frac{2}{4!}\frac{d^4\xi}{dn^4} + \frac{2}{6!}\frac{d^6\xi}{dn^6} + \cdots .$$

Hence, when the derivatives of higher order can be neglected, the governing equation reduces to the famous Sine-Gordon equation, now permeating fashionable physics,

$$\frac{d^2\xi}{dn^2} = \left(\frac{\pi}{2\ell^2}\right)\sin(2\pi\xi_n) .$$

This equation can be integrated, as

$$\frac{d\xi}{dn} = (1-T^2\cos^2\pi\xi)^{\frac{1}{2}}/T\ell$$

and

$$\frac{\pi n}{T\ell} = F[T,\pi(\xi-\tfrac{1}{2})] ,$$

after integrating once more,

where

$$T^2 = 1/[1+\ell^2\left(\frac{d\xi}{dn}\Big|_{n=0}\right)^2],$$

and $F[T,\phi]$ is the incomplete elliptic integral of the first kind, (Abramowitz *e.a.* 1965) and the origin has now been chosen where $\xi = \frac{1}{2}$. The angular argument of the incomplete elliptic integral has a known form, $\pi(\xi-\frac{1}{2}) \equiv \mathrm{am}(\pi n/\ell T)$, from which the relative displacement is given as

$$\xi(n) = \tfrac{1}{2} + \frac{1}{\pi}\,\mathrm{am}(\pi n/\ell T) .$$

This dependence of ξ on n is interpreted as a sequence of misfit dislocations which have soliton-like behaviour, located at half-integer values of ξ, when an atom is located exactly on a peak. These dislocations are separated by intervals of

$$2\ell TK(T)/\pi = a/(b-a) = 1/f$$

overgrowth lattice spacings, where $K(T)$ is the complete elliptic integral of the first kind.

As already defined, when dislocations are absent, the configuration is said to be in the coherent or pseudomorphic state. In this state, a = b, and T = 1, with an infinite dislocation spacing.

If the overgrowth has already strained homogeneously to a lattice spacing b', this strained value is contained in the expressions for the beat wavelength, or dislocation spacing, the *residual misfit*,

$$f' = (b'-a)/a,$$

is accommodated by misfit dislocations spaced at *strained overgrowth* intervals $a/(b'-a)$. Once again, $b' = a$ indicates that dislocations will be infinitely far apart.

Extension to Two-Dimensional systems with rhombic symmetry

Van der Merwe (1980), has extended the original one-dimensional model, to two-dimensional systems with square (Frank and van der Merwe 1949b), rectangular, (Van der Merwe and Ball 1970, Van der Merwe e.a. 1975, Van der Merwe 1979) and finally rhombic symmetry. This latter model is suitable for fcc{111}/bcc{110} interfaces, and is approximately solvable analytically when the two sets of governing equations can be decoupled, and the coupling treated as a perturbation in the continuum limit. The model and method of solution closely follows the one-dimensional case.

The physical assumptions of immiscibility, abrupt and flat interface, rigid substrate and elastic overgrowth are also assumed here. The physical model is therefore essentially the same as the one-dimensional model, with the modification that the two-dimensional nature is treated explicitly.

The governing equations are also set up as a discretized elastic continuum, rather than a ball-and-spring model. But as finite difference equations are arrived at as the mathematical realization of the model, the mathematical picture is in fact similar to the one-dimensional model.

Skew axes are chosen to coincide with the sides of the rhombic primitive cells, and these sides correspond to nearest neighbour distances in both the substrate and the overgrowth. As the diagonals of a rhombus are perpendicular to one another, these

diagonals provide a natural choice of direction of cartesian axes. The elastic strains and constants must therefore be expressed in cartesian coordinates which coincide with the diagonals of the rhombi.

The reference configuration is once again defined to be the configuration in which the overgrowth is deformed to match the substrate exactly. This allows a one-to-one correspondence to be set up between overlayer atoms and substrate lattice points by assigning to the former the same numbers, (m,n).

Although the model has been extended to anisotropic elastic constants by Stoop *e.a.* (1982), the original isotropic model will be discussed here.

The substrate rhombus sides are chosen to have length a and obtuse angle 2α. The overgrowth sides are b and the corresponding angle 2β. The elastic constants are shear modulus μ and Poison ratio ν. The thickness of the overgrowth is t.

The components of tension $\mathcal{T}$ per unit length and the elastic energy density are

$$\mathcal{T}_x = 2\mu(\varepsilon_x+\nu\varepsilon_y)/(1-\nu) \qquad \mathcal{T}_{xy} = \mu t\gamma_{xy}$$

and

$$\mathcal{E}_{el} = \tfrac{1}{2}\mu\left\{\frac{2(\varepsilon_x^2+\varepsilon_y^2+2\nu\varepsilon_x\varepsilon_y)}{1-\nu}+\gamma_{xy}^2\right\},$$

where ε_x and ε_y are the normal strains, and γ_{xy} is the shear strain.

The natural misfits are defined for a general direction i as

$$f_i = (b_i-a_i)/a_i .$$

If the overlayer is strained homogeneously by ε_i', so that the average spacing is b_i', the residual misfit and strain are given by

$$f_i' = (b_i'-a_i)/a_i \qquad \varepsilon_i' = (b_i'-b_i)/b_i ,$$

and clearly

$$f_i' = f_i+\varepsilon_i'b_i'/a_i \simeq f_i+\varepsilon_i' ,$$

from which, $f_i \simeq f_i' + |\varepsilon_i'|$,
emphasizing the accommodation of the misfit f_i by misfit dislocations and misfit strain.

The misfit dislocations are spaced at the beat interval as

$$b_i'/f_i' = (\frac{1}{f_i'}+1)a_i \ .$$

So far the correspondence to the one-dimensional model is evident.

The governing equations are also derived in a similar fashion, but first the relationship between the cartesian and rhombic parameters are needed:

The long diagonal is chosen parallel to the e_x axis, and the short diagonal parallel to the e_y axis. With the obtuse angle 2β, it therefore follows that the length of the diagonals are given as

$$b_x = 2b \sin\beta \quad , \ b_y = 2b \cos\beta \ .$$

The coordinates of the atom (m,n) in rhombic substrate units are given by

$$x^1_{m\ n} = ma + \xi_{m\ n}a \qquad x^2_{m\ n} = na + \eta_{m\ n}a \ .$$

If one indicates the transformation from substrate-rhombic coordinates to cartesian coordinates as

$$x = x(x^1,x^2) = (x^1 - x^2)\sin\alpha \ ,$$

and

$$y = y(x^1,x^2) = (x^1 + x^2)\cos\alpha \ .$$

then the strains are calculated according to the assumption that the strain varies linearly, (as $\varepsilon = \alpha_0 + \alpha_1 x + \alpha_2 y + \alpha_3 xy$), over a single unit cell, as the differences:

$$\varepsilon_x = [x(x^1_{m+1\ n},x^2_{m+1\ n}) - x(x^1_{m\ n+1},x^2_{m\ n+1}) - b_x]/b_x$$

$$\varepsilon_y = [y(x^1_{m+1\ n+1},x^2_{m+1\ n+1}) - y(x^1_{m\ n},x^2_{m\ n}) - b_y]/b_y$$

$$\gamma_{xy} = [x(x^1_{m+1\ n+1}, x^2_{m\ n}) - x(x^1_{m\ n}, x^2_{m\ n})]/b_y + [y(x^1_{m+1\ n}, x^2_{m+1\ n}) - y(x^1_{m\ n+1}, x^2_{m\ n+1})]/b_x \ .$$

Expressed in terms of the substrate displacements these strains are then

$$\varepsilon_x = a\ s_\alpha(\xi_{m+1\ n} - \xi_{m\ n+1} - \eta_{m+1\ n} + \eta_{m\ n+1} - 2f_x)/2bs_\beta \ ,$$

$$\varepsilon_y = a\ c_\alpha(\xi_{m+1\ n+1} - \xi_{m\ n} - \eta_{m+1\ n+1} + \eta_{m\ n} - 2f_y)/2bc_\beta \ ,$$

$$\gamma_{xy} = a\ s_\alpha(\xi_{m+1\ n+1} - \xi_{m\ n} - \eta_{m+1\ n+1} + \eta_{m\ n})/2bc_\beta + a\ c_\alpha(\xi_{m+1\ n} - \xi_{m\ n+1} - \eta_{m+1\ n} + \eta_{m\ n+1})/2bs_\beta \ .$$

where

$$f_x = (b_x - a_x)/a_x = f + b(s_\beta - s_\alpha)/as_\alpha$$
$$f_y = (b_y - a_y)/a_y = f + b(c_\beta - c_\alpha)/ac_\alpha$$
$$s_\alpha = \sin\alpha \ , \ s_\beta = \sin\beta, \ c_\alpha = \cos\alpha \ \text{ and } \ c_\beta = \cos\beta \ ,$$

with f the misfit along the rhombic directions, referred to as the dimensional misfit, while $(s_\beta - s_\alpha)/s_\alpha$ and $(c_\beta - c_\alpha)/c_\alpha$ are measures of the angular misfit.

The equations governing the equilibrium of an interior atom (m,n) say, are obtained from the condition that the total of the strain and overgrowth-substrate interaction energy must be minimized with respect to the displacements $\xi_{m\ n}$ and $\eta_{m\ n}$.
Hence

$$E_T = \sum_{m,n} (V_{m\ n} + \mathcal{E}_{m\ n})$$

so that the equilibrium conditions are given by

$$0 = \frac{\partial E_T}{\partial \xi_{m\ n}} = \frac{\partial E_T}{\partial \eta_{m\ n}} \ .$$

The resulting difference equations can be approximated by partial differential equations with the assumption that $\xi_{m\ n}$ and $\eta_{m\ n}$ vary slowly from lattice point to lattice point, m and n may be treated

as continuous variables. Introducing the Taylor expansions about (m,n),

$$\xi_{m+\delta m\ n+\delta n} = \xi\Big|_{m\ n} + \left[\delta m\frac{\partial}{\partial m} + \delta n\frac{\partial}{\partial n}\right]\xi\Big|_{m\ n} + \tfrac{1}{2}\left[\delta m\frac{\partial}{\partial m} + \delta n\frac{\partial}{\partial n}\right]^2\xi\Big|_{m\ n} + \cdots,$$

where δm, δn are $\pm$ 1 across a cell, leads to the differential equation,

$$\left[\frac{s_\alpha}{s_\beta}\right]^2\partial^2_{m-n}(\xi-\eta)+\left[\frac{c_\alpha}{c_\beta}\right]^2\partial^2_{m+n}(\xi+\eta)+2\nu\frac{c_\alpha s_\alpha}{c_\beta s_\beta}\partial_{mm-nn}\xi +$$

$$+\tfrac{1}{2}(1-\nu)\left\{\left[\frac{s_\alpha}{s_\beta}\right]^2\partial^2_{m+n}(\xi-\eta)+2\frac{c_\alpha s_\alpha}{c_\beta s_\beta}\partial^2_{mm-nn}\xi+\left[\frac{c_\alpha}{s_\beta}\right]^2\partial^2_{m-n}(\xi+\eta)\right\} =$$

$$= \frac{2\pi}{\ell^2}\sin 2\pi\xi$$

with a similar equation, with the rôles of η and ξ and n and m reversed.

The configurational parameter again has the form

$$\ell^2 = \frac{\mu\Omega}{(1-\nu)Wr^2}, \qquad \text{and} \qquad \Omega = \tfrac{1}{2}tb_xb_y = 2tb^2s_\beta c_\beta .$$

The differential symbols are

$$\delta_{m\pm n} \equiv \frac{\partial}{\partial m} \pm \frac{\partial}{\partial n}, \qquad \text{and} \qquad \delta_{mm\pm nn} = \frac{\partial^2}{\partial m^2} \pm \frac{\partial^2}{\partial n^2} .$$

In the approximate solution several types of dislocation networks, and their respective creation energies and stability limits were examined. These were pseudo-edge, pseudo-screw, pure edge and screw as well as mixed configurations. They have respectively, dislocation lines parallel to one of the rhombic sides with Burgers vector, for pseudo-edge, perpendicular to these lines or parallel for the case of pseudo-screw types. The pure dislocations are considered for dislocation lines parallel to the diagonal directions with appropriately perpendicular or parallel Burgers vectors, while the mixed type have the dislocation lines parallel to the rhombic sides, but Burgers vectors parallel or perpendicular to the diagonals. The choices are dictated by the symmetry of the systems.

It was found that for the particular substrate representation chosen, namely the two-term Fourier expression, the types most

likely to accommodate dimensional misfit in general cases are the pseudo-edge types, which however require dislocations arrays parallel to both rhombic directions, because of the coupling of the two governing equations when $\alpha \neq \beta \neq 45^{\circ}$, and particularly when $\alpha \geq 51^{\circ}$. This is the case for bcc{110} growth on fcc{111} substrates, close to the Nishiyama-Wassermann orientation.

In addition for the fcc{111} substrate it appears possible for mixed dislocations aligned parallel to the long (b_y) diagonal to exist, as they are consistent only when α is between 58° and 62°.

The pseudo-screw dislocations parallel to the a_2-axis can accommodate the angular misfit, which the pure screw dislocations cannot, but are accompanied by secondary pseudo-screws parallel to the a_1-axis.

The estimate of stability of coherent matching (which again is relevant in the Nishiyama-Wassermann orientation) is that above 10% the introduction of pseudo-edge dislocation arrays in one direction is energetically favourable. The considerations indicate that the introduction of the pseudo-screw type dislocations may occur only at a still higher critical angular misfit, (defined by $(\beta-\alpha)/\alpha$)).

A reservation concerning the quantitative information, is expressed by Van der Merwe, in that the continuum approximation is at its limits of applicability in the misfits near 10%, the elastic properties considered are isotropic in nature, and that anisotropy may have an important influence on the critical misfits, while the limitation of the substrate potential expression to only two terms is particularly serious.

Stoop and Van der Merwe (1982 a,b,c) have modified the approach taken in this earlier work, by studying an anisotropic system, including more terms in the substrate potential representing a bcc{110} substrate. Their studies were then applied to the

Nishiyama-Wassermann and Kurdjumov-Sachs (with isotropic constants in the latter) orientations of the fcc{111} overgrowth on bcc{110} rigid substrate system.

Stoop and Van der Merwe (1982c) have analyzed this system analytically in terms of this improved formulation, and have arrived at the conclusion that transition from the two-dimensionally coherent or pseudomorphic phase, in which substrate and overgrowth match exactly, in fact proceeds through the formation of pseudo-screw dislocations.

Highlighted in their studies of the Kurdjumov-Sachs orientation is the shortcoming that rotational orientation is not a natural variable in the formulation. The importance of this parameter has been shown in the geometric models of Bruce and Jaeger (1977, 1978) and Van der Merwe (1982) and by the present work. Anisotropy itself certainly introduces difficulties in the analytical manipulations of these finite difference models. In order to allow analytical solution, not unlike the one-dimensional Frank and Van der Merwe model already described, the coordinates in which the strains and displacements are expressed have to be chosen with care, normally a different choice is optimal for different orientations.

Numerical models based on the finite element technique, rather than the finite difference formulations used previously promise to overcome these problems, and the extent to which this has proved possible is described in Chapter 5 of the present work. The cost is of course, that the analysis is numerical rather than analytical, and the information obtainable is of a different, complementary kind.

The Numerically based Finite Difference models of Snyman and Van der Merwe and of Snyman and Snyman

Snyman and Van der Merwe (1974 a,b) presented numerical solutions of the difference equations of the one-dimensional model, extended

to include size effects and free boundaries, and also epitaxy in the case of interfaces with rectangular symmetry. These models are governed by the same assumptions as these described above, but are not solved in the analytic continuum limit. The discrete finite difference equations are solved directly.

Among other results is the qualitative agreement with the analytical treatments by Van der Merwe described above. Another result is that the strongly cusped minima in the interfacial energy per atom with size are smoothed out by the inclusion of the free boundary. This result is in fact also confirmed by the homogeneous strain studies of Chapter 4 in this study.

Snyman and Snyman (1981) extended the finite difference models to the case of an fcc{111} overgrowth on an fcc{111} substrate. This model they applied subject to the condition of zero average strain, misfit accommodation is only allowed by misfit dislocations. This is a severe restriction for finite monolayer islands. The effect of free boundaries was not considered in this model, the inherent complications of this type of condition in a finite difference formulation were therefore avoided. The model was used to study the accommodation of misfit between the two fcc{111} structures, while they were in a fixed, parallel orientation. No orientational variations were studied.

Most important to the present work is the formulation of the adatom-substrate potential energy, which has been generalized in terms of the reciprocal lattice in Chapter 2.

Snyman e.a. included special terms, not deducible directly from the earlier expression of Steele (1973), to account for an energy associated with stacking faults in the fcc lattice, in that the two three-fold symmetry positions in the plane are not equal. Their potential expression is of the form

$$V + W\{[\frac{3}{2} + \cos 2\pi(\frac{x}{a}+\frac{2}{3}) + \cos 2\pi(\frac{y}{a}+\frac{1}{3}) + \cos 2\pi(\frac{x}{a}-\frac{y}{a}+\frac{1}{3})] +$$
$$+ \Delta[\frac{3}{2}+\cos 2\pi(\frac{x}{a}+\frac{1}{3}) + \cos 2\pi(\frac{y}{a}+\frac{2}{3}) + \cos 2\pi(\frac{x}{a}-\frac{y}{a}-\frac{1}{3})]\} ,$$

where Δ had values between 0 and 0.7. They have shown, by the dislocation structures to be expected as the symmetry is increased from three-fold to nearer to six fold symmetry, that this differentiation between minima in the interfacial potential is in fact essential.

The lowest energy position at x = 0, y = 0, while initially surrounded by three maxima, and three equally deep minima, with Δ = 0, is surrounded by three global maxima, and three local maxima, half the height of the others with a stacking fault contribution with Δ = 0.5. These global and local maxima lie on the vertices of a hexagon, to partly restore hexagonal symmetry to the interface, an effect which is carried across to the patterns of dislocation arrays.

A generalized form of this potential is discussed in the present work in Chapter 2, with the generalized inclusion of substrate features such as different types of atoms or stacking fault terms, included in the form of a simple structure factor. Higher order terms are also included in the generalization.

1.6 OTHER MODELS

Other approaches to the description of epitaxy of differing structures which use an atomistic approach have been applied successfully. Fletcher's model in particular has been developed and formulated in the reciprocal lattice. As this is also done with the developments reported here, it is appropriate to discuss some of the features of this model.

The Variational model of Fletcher e.a.

The energy principle on which Fletcher's variational method (Fletcher 1964, Fletcher e.a. 1966, Lodge 1970, Fletcher *e.a.* 1975) is based is the minimization of the energy of the system consisting

of the crystals and the interface. The energy is minimized through variation of the atomic positions in the interface, subject to given constraints on the orientation or form of the bicrystals, as in the models of Van der Merwe, so effectively calculating the structure at 0 K. A necessary simplifying assumption is that the two crystals are immiscible. The interaction between atoms in the overgrowth, the substrate and across the interface are given as pair potentials, such as Morse or Mie potentials. This allows large strains to be considered in principle, without violation of the restrictions based on the harmonic or small strain approximations. This approach is applicable even when the interfacial misfit dislocation density is too high to allow the confident application of dislocation theories.

The substrate is considered to be semi-infinite with an interface boundary of known orientation. The overgrowth on the other hand may be of finite thickness. In the minimization process the structure and the energy of the interface are determined for arbitrary relative orientation, and the assumption is that the actual orientations which will occur, are those which minimize the interfacial energy.

This variational model becomes particularly powerful when formulated in the reciprocal space of the two structures concerned. This was achieved by using the Fourier transform of the interaction potential and the interfacial displacement function. For simplicity it is useful to define coordinates in which a coordinate plane coincides with the interface plane, and the coordinate vectors lying in the plane form the basis of a surface lattice, a set in general for each of the overgrowth types. A general lattice position in the substrate crystal may therefore be written as $\mathbf{R} = \mathbf{R}_s + \mathbf{R}_3$, where $\mathbf{R}_s$ is a surface lattice vector, and $\mathbf{R}_3$ is the remaining vector, also a lattice vector.

The potential experienced by an atom at $\mathbf{r}_b \equiv \mathbf{r}$ of the overgrowth crystal in the field of the substrate atoms at $\mathbf{R}_a$ is given by

$$V(\mathbf{r}) = \sum_{\mathbf{R}_a}^{-} v(\mathbf{r}-\mathbf{R}_a)$$

where the - is used to indicate the summation is over the substrate atoms only. This potential can be written in terms of the Fourier components $V_{\mathbf{q}}$

$$V(\mathbf{r}) = \frac{N}{8\pi^3} \int V(\mathbf{q})\ e^{i\mathbf{q}\cdot\mathbf{r}}\ d\mathbf{q}$$

where N is the (essentially infinite) number of atoms in the crystal, and

$$V(\mathbf{q}) = \frac{1}{N} \sum_{\mathbf{R}_a}^{-} v_{\mathbf{q}}\ e^{-i\mathbf{q}\cdot\mathbf{R}_a}\ ,$$

with

$$v_{\mathbf{q}} = \int v(\mathbf{r})\ e^{-i\mathbf{q}\cdot\mathbf{r}}\ d\mathbf{r}$$

the Fourier transform of the <u>atomic</u> potential.

Rigid Overgrowth and Substrate

It is now possible to write the total interaction energy of the system between the two <u>rigid</u> crystals by summing V(r) over all the atomic positions of the overgrowth crystal,

$$E_T = \sum_{\mathbf{R}_b}^{+} V(\mathbf{R}_b) = \frac{1}{8\pi^3} \sum_{\mathbf{R}_b}^{+} \sum_{\mathbf{R}_a}^{-} \int v(\mathbf{q})\ e^{i[\mathbf{q}\cdot(\mathbf{R}_b-\mathbf{R}_a)]}\ d\mathbf{q}\ .$$

If the vectors $\mathbf{R}_b$ and $\mathbf{R}_a$ are now written in terms of surface and 3rd components, the sum taken over an infinite lateral overgrowth and substrate (even if the largest $\mathbf{R}_3$ vectors are finite) contain kronecker deltas,

$$\sum_{\mathbf{R}_s} e^{i\mathbf{q}\cdot\mathbf{R}_s} = N\,\delta_{\mathbf{q}\,\mathbf{Q}}\ ,$$

where $\mathbf{Q}$ is a reciprocal lattice vector of the surface reciprocal lattice corresponding to the surface basis of the relevant crystal.

Dividing the total energy by the product of the number of atoms in the overgrowth, the average bicrystal interaction energy per atom becomes

$$\varepsilon_I = \frac{1}{2\pi} \left\{ \sum_{R_3\{a,b\}} \int v(q)\, e^{i[q_3(R_b - R_a + r_0)|_3]}\, dq_3 \right\} \delta_{q_s Q_a}\, \delta_{q_s Q_b} ,$$

where r_0 is a translation vector between the overgrowth and substrate direct lattice origins added for generality and $|_3$ indicates the third component of the vector. The key feature of this result is that in the case of this infinite (in the lateral extent at least) interface, the only non-zero terms are due to the coincidence of the reciprocal lattice vectors,

$$q_s = Q_a = Q_b \quad .$$

Comment

This result is similar to that obtained from the van der Merwe rigid model in chapter 3 here, and due to the same reason. Not immediately evident, but clear from the deliberations of chapter 3, is the effect of the finite nature of the overgrowth, namely the delta functions are replaced by deeply cusped functions, the equivalent of the K(M,p,q) functions described above, representing approximate coincidence lattice matching of higher order, as a size effect. The existence of the secondary minima existing in the energy function is therefore an effect of the finite size only. As calculations of Chapter 4 show, also shown by the numerical work of Snyman and van der Merwe, these are smoothed to a large extent if either of the crystals is allowed to strain to equilibrium. The reader is referred to the relevant chapter later in this work for a full discussion.

Misfit Dislocations

A thick overgrowth was treated in terms of the above formulation by Lodge (1970), for which the accommodation of misfit is achieved by

periodic distortions, which themselves may be written in Fourier form as $F\, e^{i\delta Q \cdot r}$. The vectors δQ are selected as the difference of nearly coincident reciprocal lattice vectors. The distortion associated with such a misfit dislocation is then given by the superposition of terms $F_n e^{in\delta Q \cdot r}$, n integer. F_n are determined from energy minimization and are the variational parameters of the problem.

The same results follow from the analysis given in this work, in terms of the construction in reciprocal space based on the extension of Van der Merwe's model as developed here. In addition the case of homogeneous strain, important for thin films, is also discussed here in chapter 4, which is a new example of the power of the reciprocal formulation.

The Lattice Dynamical Formulation due to Novaco and McTague

Novaco and McTague (1977) have formulated the interface problem in the general language of quantum mechanical lattice dynamics, and have been able to draw some general conclusions from the long wavelength (small misfit) static (0 K) and thus classical limit of their equation of motion. For weak adatom substrate interactions, where the Van der Merwe configurational parameter ℓ is much greater than 1, they have described the case of misfit accommodation by Static Distortion Waves in the overgrowth, which are identifiable with the strain fields of misfit dislocations.

Their model is also restricted to rigid, smooth and flat crystalline substrates. The adsorbate monolayer is assumed to be at 0 K, while the adatom-adatom interaction used is formulated as an atomic pair-potential. The lattice dynamics are treated in the harmonic approximation, which is equivalent to accepting continuum linear elasticity theory, but with the pair-potential requirement, with elastic constants which satisfy the Cauchy relations. That the

system is at 0 K, of course allows the assumption that the ground state, or lowest energy state configuration will obtain.

In the harmonic approximation the adatom-adatom Hamiltonian for the monolayer is

$$\hat{\mathcal{H}}_0 = E_L + \sum_j \frac{1}{2M} \hat{\mathcal{P}}_j^{\alpha} \hat{\mathcal{P}}_j^{\alpha} + \sum_{i,j} \tfrac{1}{2}\phi_{ij}^{\alpha\beta} \hat{w}_i^{\alpha} \hat{w}_j^{\beta} \quad ,$$

where summation over the component indices $\alpha, \beta = 1,2,3$, is implicit in the Einstein summation convention, while the explicit summations are over the G atoms all of mass M in the overgrowth island. $\hat{\mathcal{P}}_j^{\alpha}$ and $\hat{w}_j^{\alpha}$, are the α-components of the momentum and displacement (from the equilibrium position) operators of the j^{th} overgrowth atom. The $\phi_{ij}^{\alpha\beta}$ are matrix elements or coupling constants, calculated from the potential applicable at the equilibrium positions, and are in fact the second derivatives of the atomic pair-potentials (see for example Ashcroft *e.a.* 1975, ch 22) assumed to govern the interaction,

$$\phi_{ij}^{\alpha\beta} = \frac{\partial^2 \phi(\mathbf{R}_i - \mathbf{R}_j)}{\partial u^{\alpha}(\mathbf{R}_i) \partial u^{\beta}(\mathbf{R}_j)} \quad .$$

The E_L term defines the zero of the energy scale, and represents the ideal lattice potential energy, or free overgrowth potential energy, with all atoms at equilibrium.

The dynamical matrix is calculated as

$$\mathbf{D}(\mathbf{q}) = \sum_j \left[\phi_{jo}^{\alpha\beta}(\mathbf{R}_j) e^{i\mathbf{q}\cdot\mathbf{R}_j} \right] ,$$

diagonalized and the eigenvalue problem

$$M\omega^2(\mathbf{q})\varepsilon(\mathbf{q}) = \mathbf{D}(\mathbf{q})\varepsilon(\mathbf{q}) \quad ,$$

is solved to yield the polarization vectors $\varepsilon(\mathbf{q})$ and the eigenfrequencies of the normal modes $\omega(\mathbf{q})$. The wave vector $\mathbf{q}$ is a vector lying in the first Brillouin Zone of the overgrowth surface reciprocal lattice.

From these the phonon creation and annihilation operators, $\hat{\alpha}$ and $\hat{\alpha}^{+}$, can be calculated and the displacement operators expressed as

$$\hat{w}_j^{\alpha} = \frac{1}{\sqrt{G}} \sum_{q,l} \varepsilon_l^{\alpha}(q)\, e^{iq\cdot R_j} \left[\frac{\hbar}{2M\omega_l(q)}\right]^{1/2} [\hat{\alpha}_{q\ l} + \hat{\alpha}^{+}_{-q\ l}] \quad .$$

The substrate potential energy is expressed as a (truncated) Fourier Series,

$$V(r) = \sum_{Q_a} V_{Q_a} e^{iQ_a\cdot r} \quad ,$$

where $\{Q_a\}$ is the substrate reciprocal lattice.

The adatom-substrate interaction potential is expressed as a power series of this interaction, truncated after the linear term, which contributes the Hamiltonian

$$\hat{\mathcal{H}}_1 = \sum_j V(R_j) + \sum_j V^{\alpha}(R_j)\hat{w}_j^{\alpha} \quad .$$

The combined Hamiltonian may then be written in terms of the respective operators and dynamic energies as

$$\hat{\mathcal{H}} = E_L + \tfrac{1}{2}\sum_{q,l} \hbar\omega_l(q) + \sum_{q,l} \hbar\omega_l(q)\hat{\alpha}^{+}_{q\ l} + G\sum_{Q_b}\sum_{Q_a} V_{Q_a}\, \delta_{Q_a,Q_b} + i\sqrt{G}\sum_{q,l} (g_{q\ l}\,\hat{\alpha}_{q\ l} - g^{*}_{-q\ l}\,\hat{\alpha}^{+}_{-q\ l}) \quad ,$$

where

$$g_{q\ l} = \sum_{Q_a}\sum_{Q_b} V_{Q_a}\, Q_a^{\beta}\, \varepsilon_l^{\beta}(q)\, \delta_{Q_a+q,Q_b} \left[\frac{\hbar}{2M\omega_l(q)}\right]^{1/2} = -g^{*}_{-q\ l} \quad .$$

The ground state of this Hamiltonian is characterized by nonzero values for the expectation values (averages) $\langle\hat{\alpha}^{+}_{q\ l}\rangle$ and $\langle\hat{\alpha}_{q\ l}\rangle$ of the phonon creation and annihilation operators. These averages are calculated by minimizing the ground-state energy as a function of these values. An immediate consequence of the non-zero nature of

these averages is a static displacement of the atoms in the monolayer from the ideal-lattice sites, which Novaco *e.a.* refer to as a Static Distortion Wave, or is usually referred to in this context as a misfit dislocation, and the displacement as the relaxation associated with a misfit dislocation.

The average displacements for each atom can be calculated from the creation and annihilation operator expectation values as

$$\langle \hat{u}_j^{\alpha} \rangle = \sum_{Q_a, l} \varepsilon_l^{\alpha}(q)\ \eta_l(Q_a)\ \sin[Q_a \cdot R_j] \quad ,$$

with $$\eta_l(Q) = \left[\frac{V_Q\ Q^{\beta} \varepsilon_l^{\beta}(q)}{M\omega^2(q)} \right] \quad .$$

The static displacement of the atom at the j^{th} site varies in the sinusoidal fashion as given by the Fourier expansion. This is the linear response of the monolayer lattice to the external periodic field imposed by the substrate surface.

The terms in the Hamiltonian represent the ideal lattice potential energy, the kinetic energy of the phonon, which in the classical limit is zero at 0 K, the strain energy of the dislocation (or Static distortion wave), the rigid overgrowth-substrate interaction energy, and the misfit dislocation substrate interaction energy respectively.

The rigid misfit energy term is zero unless an overgrowth reciprocal lattice vector Q_b matches a substrate reciprocal lattice vector Q_a in both magnitude and direction. This is the same result as obtained from the Van der Merwe - Reiss rigid model, and by Fletcher *e.a.* This matching for incommensurate lattices is possible for some monolayers, given sufficient binding between overgrowth and substrate by homogeneous strain of course, although Novaco *e.a.* did not consider this accommodation mode.

The dislocation misfit energy term is maximally negative if the $Q_a \cdot \varepsilon_1(q)$ term is maximal, when the polarization vector is parallel to the substrate reciprocal vector, therefore perpendicular to the substrate atomic rows. Since the displacements and therefore the Burgers vector is parallel to the polarization vector, related to the amplitude terms, this alignment gives rise to an edge misfit dislocation type. Further, the dynamic term appearing in the expression for η, contains $\omega(q)$ as a divisor, so that the energy takes its greatest negative value when the propagation vector $q = Q_b - Q_a$ is a minimum, therefore Q_b will tend to align with Q_a, and long wavelength or largely spaced periodic dislocations are favoured. As the Frank and Van der Merwe model shows, this minimizes the incoherency, and maximizes the pseudomorphic regions between dislocation lines.

From the competing dynamic effect, that the frequency of long-wavelength transverse modes is less than that of the longtitudinal (edge) modes, Novaco *e.a.* predict that a small degree of misalignment may well be optimal in some systems, due to the relative weakening of the orienting effect at small angles. This is misalignment in the sense that lattice rows of overgrowth and substrate are not exactly parallel. They do not however consider the effect of size on the strength of the orienting force as it initiates a rigid body motion. Also the effect of temperature, supplying vibrational energy, has in this 0 K limit not been discussed.

The effect of anisotropic elastic constants and the effect on the relationship between the polarization vector and the propagation vector has not been treated by Novaco *e.a.*

Both the question of homogeneous strain and the equilibrium configuration when misfit dislocations are introduced into the interface are discussed in terms of the Van der Merwe type of model in this work. As these calculations are done in the classical

limit, in which the frequencies play no rôle, dynamic effects cannot be treated. However the effect of anisotropy and the misalignments caused by this, does receive explicit attention.

1.7 CONCLUDING DISCUSSION

In this chapter several models of epitaxy have been discussed briefly. The implications of these descriptions on the work done here have been pointed out. In some cases various terms which serve a similar function to those in expressions derived here have been identified, although this identification was not done by the original author. For example in the model of Novaco-McTague the strain and misfit energy terms have been identified, and static distortion waves as the strain fields associated with misfit dislocations.

The development to be followed below begins, in Chapter 2, with the derivation of a suitable expression for an adatom-substrate interaction potential capable of reproducing the full symmetry of the substrate. Coping with the asymmetries introduced by stacking fault effects, or the effect of different atom species in the substrate lead to a *generally applicable* formulation in terms of simple structure factors, or additional potentials.

The first modelling of epitaxy begins in Chapter 3, where the *Ideal Epitaxial Configurations* are defined to be those lattice relationships, scale and orientation, which minimize *misfit energy* without the strain. Necessarily these calculations are performed in terms of a Van der Merwe - Reiss rigid model. As a result the generalized reciprocal lattice formulation, which includes row-matching and used throughout this study, is introduced, as well as a geometric realization of the analytical conditions as a construction in reciprocal space of the Ewald type.

The two-dimensionally coherent phase, and the one-dimensionally coherent row-matching configurations are examined in Chapter 4 subject to the availability of homogeneous, position independent, strain, which is identified with the *Misfit Strain* component of misfit accommodation in the models of Frank and van der Merwe, as extended, described above. This is applied to systems which are not the ideal configurations derived from the rigid case, and includes the two-dimensionally coherent, or pseudomorphic phase which cannot be achieved by non-identical overgrowth and substrate structures without strain. These homogeneous strains, subject to minimum energy criteria are derived both from the reciprocal lattice epitaxy conditions, and by direct minimization of the total interfacial energy, defined for the purpose as the sum of the misfit and strain energies. With anisotropy included, several interesting results are obtained.

The strain fields associated with misfit dislocations are position dependent and are discussed in Chapter 5. The relaxation of the bcc{110} overgrowth as interacting with an fcc{111} substrate, the model system studied here, is obtained numerically from the Finite Element model described here. A novel formulation of the misfit dislocation geometry for general interfaces in terms of the reciprocal lattice is introduced. This yields the *spacing*, *orientation* and *line sense* of the misfit dislocations, as well as their *Burgers vectors* for the most general interface in a formalism fully compatible with the preceding reciprocal lattice conditions. The interfacial atomic positions and the resulting interface structures derived numerically are interpreted in terms of the reciprocal space expressions. One concludes that the combined formulation of the misfit problem in direct and reciprocal space offers a very general and powerful description of misfitting interfaces.

Chapter 6 is the concluding chapter.

CHAPTER 2

SUBSTRATE POTENTIALS

The adatom-substrate interaction potential is developed, initially from a generalized Fourier expression in terms of the reciprocal lattice of the substrate surface. Various features, symmetries and fine structure and their inclusion in a truncated series are discussed. The effect of various Fourier terms and the relative magnitudes of their coefficients are derived, and interpreted both geometrically and physically.

The physical basis for a suitable range of values for the overall energy amplitude and strength of the stacking fault correction are discussed, before a useful simple potential for use in later chapters is proposed.

CHAPTER 2

SUBSTRATE POTENTIALS

The interaction of adatoms with a *rigid* substrate is represented by a potential V, which has the 2-dimensional symmetry properties of the atomic lattice forming the substrate surface. This surface is assumed to be of the same symmetry as the bulk surface in most applications. This potential is periodic and is naturally represented as a (truncated) *Fourier series*. (Frank and van der Merwe 1949, Van der Merwe 1964, Van der Merwe and Ball, 1975, Snyman and Snyman 1981, Stoop 1986).

A general Fourier representation may be given once basis vectors $\mathbf{a}_1$ and $\mathbf{a}_2$, which define a unit cell in the 2-dimensional lattice, have been chosen. Usual choices of basis vectors for the crystal systems which will be discussed are given in Table 2.1.

Table 2.1 *Choice of basis vectors for some crystal systems.*

Face centred cubic : fcc{111} :

$\mathbf{a}_1 = \frac{1}{2}\langle\bar{1}\ 1\ 0\rangle a_o$ $\qquad$ $\mathbf{a}_2 = \frac{1}{2}\langle 0\ \bar{1}\ 1\rangle a_o$

centred at a position of hexagonal symmetry in the two-dimensional close packed {1 1 1} plane, with $\mathbf{a}_2$ rotated through 120° from $\mathbf{a}_1$.

Lattice parameters: $a_{nn} = a = |\mathbf{a}_1| = |\mathbf{a}_2| = a_o/\sqrt{2}$,

where a_o is the conventional cubic lattice parameter.

Hexagonal or Hexagonal close packed basal plane : hcp{0001} :

$\mathbf{a}_1 = a_o\langle 1\ 0\ \bar{1}\ 0\rangle$ $\qquad$ $\mathbf{a}_2 = a_o\langle 0\ 1\ \bar{1}\ 0\rangle$

centred at a point of hexagonal symmetry.

Lattice parameters: $a = |\mathbf{a}_1| = |\mathbf{a}_2| = a_o$, where a_o (with c_o) is the conventional hexagonal lattice parameter.

The basis vectors are illustrated in figure 2.1

The (infinite) Fourier series may be written as

$$V(\mathbf{r}) = \sum_{\{\mathbf{q}\}} V_{\mathbf{q}}\, e^{i\mathbf{q}\cdot\mathbf{r}} \quad , \qquad (1a$$

where $\mathbf{r} = x\mathbf{a}_1 + y\mathbf{a}_2$ is the position of an overgrowth atom with respect to the substrate coordinates, and

$$\{\mathbf{q}\} = \{\mathbf{q} : \mathbf{q} = h\mathbf{a}_1^* + k\mathbf{a}_2^* \; ; \; h,k \in \mathbb{Z}, \; \mathbf{a}_i \cdot \mathbf{a}_j^* = 2\pi\delta_{ij}\} \qquad (1b$$

where $\mathbf{a}_1^*$ and $\mathbf{a}_2^*$ are reciprocal vectors to $\mathbf{a}_1$ and $\mathbf{a}_2$, and h,k are integers. In this representation the perpendicular variation has not been included, as it is implicitly assumed that the overgrowth would have settled at some suitable proximity to the substrate. If necessary, such a variation may be included by allowing a z-dependence in the coefficients $V_{\mathbf{q}}$, as has been done by Steele (1973). Physically $\mathbf{a}_1^*$ and $\mathbf{a}_2^*$ may be interpreted as basis vectors of a *Bravais* lattice (Ashcroft *e.a.* 1975) whose displacement vectors are the wave vectors of wave fronts (phase contours) which are straight lines. This reciprocal lattice has the same rotational symmetry as the direct lattice defined by $\mathbf{a}_1$ and $\mathbf{a}_2$, while

$$e^{i\mathbf{q}\cdot\mathbf{R}} = 1 \quad \text{where} \quad \mathbf{R} = m\mathbf{a}_1 + n\mathbf{a}_2 \;\; \forall \; m,n \in \mathbb{Z} \; . \qquad (2$$

The reciprocal lattice basis vectors may be calculated from $\mathbf{a}_1$ and $\mathbf{a}_2$ by the equations

$$\mathbf{a}_1^* = \frac{2\pi \; \mathbf{a}_2 \times \mathbf{n}}{|\mathbf{a}_1 \times \mathbf{a}_2|} \quad , \quad \mathbf{a}_2^* = \frac{2\pi \; \mathbf{n} \times \mathbf{a}_1}{|\mathbf{a}_1 \times \mathbf{a}_2|} \; , \qquad (3$$

where $\mathbf{n} = \dfrac{\mathbf{a}_1 \times \mathbf{a}_2}{|\mathbf{a}_1 \times \mathbf{a}_2|}$

is a unit vector normal to the plane defined by $\mathbf{a}_1$ and $\mathbf{a}_2$ (Spiegel 1974).

Expanding $\mathbf{q}$ and $\mathbf{r}$ in terms of their basis vectors and applying the condition $\mathbf{a}_i \cdot \mathbf{a}_j^* = 2\pi \; \delta_{ij}$, then $V(\mathbf{r})$ may be written as

$$V(x,y) = \sum_{h,k=-\infty}^{\infty} V_{hk} \; e^{i2\pi(hx + ky)} \; . \qquad (4$$

Through judicious choice of the coefficients, V_{hk} various point symmetries may be imposed on the potential V(x,y), although the fundamental translational symmetry originally implied by the basis vectors $\mathbf{a}_1$ and $\mathbf{a}_2$ will always be retained.

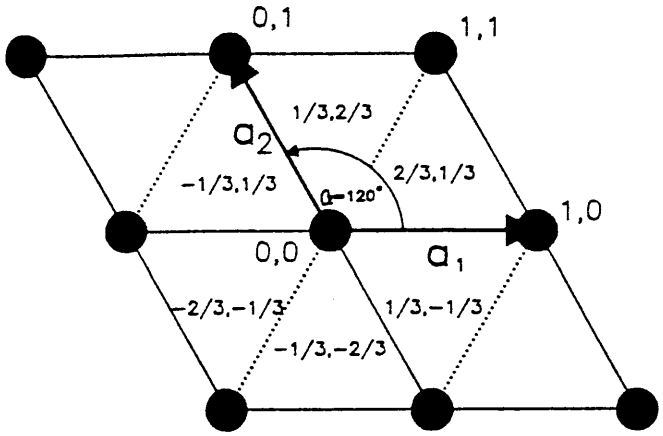

Figure 2.1 Choice of coordinates for hexagonal or three-fold symmetry systems. The unit cell is formed by the positions at 0.0 1.0 0.1 and 1.1. Dotted lines emphasise the equilateral "up" and "down" triangles about 2/3, 1/3 and 1/3, 2/3 and their equivalents.

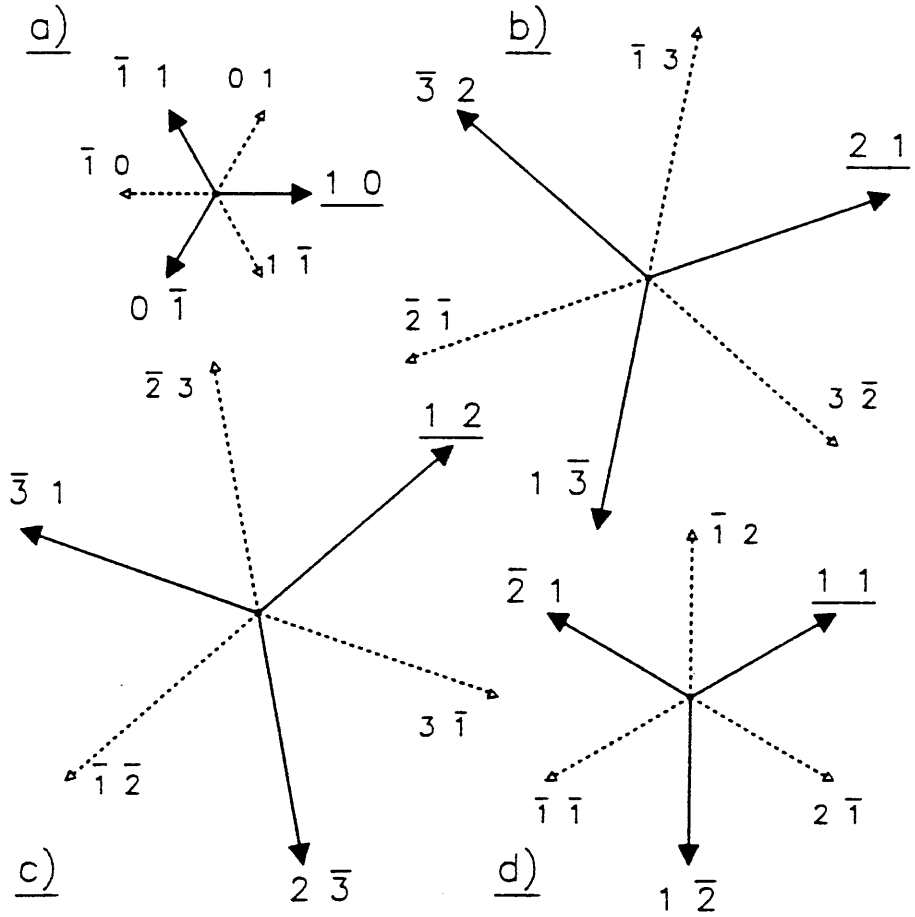

Figure 2.2 Symmetry stars in the three-fold and hexagonal reciprocal spaces (a) fundamental order (b) and (c) third order, (d) second order wave vectors.

Further tailoring of the substrate-adatom interaction potential may be useful, particularly if the basis vectors a_1 and a_2 do not define a primitive unit cell, necessitating the addition of further features to the unit cell. A particularly flexible approach was used by Snyman & Snyman (1981). In generalized form, the method consists of the addition of a further potential $V^+(x,y)$, with the same translational symmetry, but a displaced origin.

Specifically, if $V^o(x,y)$ is the unit-cell potential, and a feature similar to that at the origin in this potential is required at a point

$$r^+ = x^+a_1 + y^+a_2 \ , \qquad (5$$

then $V^+(x,y)$, is simply the unit-cell potential displaced to this position:

$$V(x,y) = V^o(x,y) + V^+(x,y) = V^o(x,y) + V^+(x-x^+,y-y^+) \ . \qquad (6$$

By premultiplying $V^+(x,y)$ with a pre-factor Δ say, this second potential may be an attenuated form of the unit-cell potential, but displaced, and may represent different atomic species in the substrate, or the effect of the atomic layers below the interface. In this way, asymmetry existing in the substrate may be introduced as in the case of local energy differences due to various stacking sequences in fcc and hcp crystal structures. Snyman & Snyman have termed the parameter Δ in this context a stacking-fault parameter.

This representation may be somewhat improved by defining a *structure factor* F_{hk} which includes a term F^+_{hk} for each added potential as follows. Consider as above that the attenuated potential is centred at x^+,y^+ . Then

$$V(x,y) = \sum_{h,k=-\infty}^{\infty} V_{hk} e^{i2\pi(hx+ky)} + \Delta\, e^{i2\pi[h(x-x^+)+k(y-y^+)]}$$

$$= \sum_{h,k=-\infty}^{\infty} V_{hk}[1 + \Delta\, e^{-i2\pi(hx^+ + ky^+)}]e^{i2\pi(hx+ky)}$$

$$= \sum_{h,k=-\infty}^{\infty} V_{hk} F_{hk} e^{i2\pi(hx+ky)} , \qquad (7$$

where

$$F_{hk} \equiv 1 + \Delta e^{-i2\pi(hx^{+}+ky^{+})} \equiv 1 + F^{+}_{hk} \qquad (8a$$

defines the structure factor. This is easily generalized to more features by including further terms as

$$F_{hk} = 1 + F^{+}_{hk} \quad \text{with} \quad F^{+}_{hk} = \sum_{j} F^{(j)}_{hk} = \sum_{j} \Delta_j e^{-i2\pi(hx^{+}_{j} + ky^{+}_{j})} \qquad (8b$$

where the summation and superscript refer to structural terms calculated for each additional feature. Where the Fourier harmonics are related by underlying lattice symmetry, (see below), the structure factors will be the same. In such cases V_{hk} will generally be taken to include the structure factor, and be equivalent to $V_{hk}F_{hk}$, so that expressions are not unnecessarily complicated.

If a second set of basis-vectors are chosen which are lattice displacement vectors of the lattice defined by a_1 and a_2, a potential with coarser translational symmetry, (and possibly a lower order of rotational symmetry), may be constructed. This second potential may represent the effect of surface reconstruction, or coincidence lattices, naturally, with a suitable choice of coefficients. For the case of a superimposed lattice which has the same rotational symmetry as the substrate, a simpler approach based on the physical effect of higher order Fourier levels will be discussed in a separate section below.

Although these possibilities are illustrated, not all of these tailored potentials are useful to the present problem and will be discussed in more detail elsewhere. Specific to our discussion is the creation of an efficient representation of substrate surfaces with hexagonal and related symmetry.

2.1 INTRODUCTION OF SYMMETRY CONDITIONS

3-fold Rotational symmetry

The symmetry inherent in an fcc{111} surface must be 3-fold,i.e. it must be symmetrical under a rotation through 120°.

Letting R_{θ} represent the rotation operator about the origin for the angle θ, then for 3-fold symmetry

$$V = R_{120}\, V = R_{240}\, V \,. \qquad (9a$$

Since this operator (figure 2.1) transforms $\mathbf{a}_1$ into $\mathbf{a}_2$ and $\mathbf{a}_2$ into $-(\mathbf{a}_1 + \mathbf{a}_2)$, it follows that

$$R_{120}\, V(\mathbf{r}) = R_{120}\, V(x\mathbf{a}_1 + y\mathbf{a}_2) = V\{-y\mathbf{a}_1 + (x-y)\mathbf{a}_2\} \,. \qquad (9b$$

Applying the rotation operator R_{120} twice yields the R_{240} operator, and hence:

$$\begin{aligned} R_{240}\, V(\mathbf{r}) &= R_{120}\, R_{120}\, V(\mathbf{r}) = R_{120}\, V\{-y\mathbf{a}_1 + (x-y)\mathbf{a}_2\} \\ &= V\{(y-x)\mathbf{a}_1 - x\mathbf{a}_2\} \,. \end{aligned} \qquad (9c$$

When we apply these transformations to the Fourier expansion one sees that for each term h,k the terms transform as follows:

$$\begin{aligned} R_{120}\, V_{hk}\, e^{i2\pi(hx + ky)} &= V_{hk}\, e^{i2\pi\{-hy + k(x-y)\}} \\ &= V_{hk}\, e^{i2\pi\{kx - (h+k)y\}} \end{aligned} \qquad (10a$$

and :

$$\begin{aligned} R_{240}\, V_{hk}\, e^{i2\pi(hx + ky)} &= V_{hk}\, e^{i2\pi\{h(y-x) - kx\}} \\ &= V_{hk}\, e^{i2\pi\{-(h+k)x + hy\}} \,. \end{aligned} \qquad (10b$$

Already existing in the (unrotated) Fourier expansion are the related terms

$$V_{k;-(h+k)}\, e^{i2\pi\{kx - (h+k)y\}} \text{ and } V_{-(h+k)\ h}\, e^{i2\pi\{-(h+k)x + hy\}} \,. \qquad (10c$$

Clearly on rotation, each of the exponentials transforms into one already existing. For the required rotational symmetry to exist, it is necessary that the coeficients of these exponentials be the same. Then

$$V_{k;-(h+k)} = V_{h\ k} = V_{-(h+k)\ h} \,. \qquad (11$$

(Here, and in eqn 10 c, a semicolon ";" has been introduced into

the subscript notation to avoid confusion between a single subscript "h-k" , and the pair of subscripts "h" and "-k" intended in h;-k. There is no other significance associated with the semicolon.)

Correspondingly, summing only over over non-negative indices, one may write

$$V(x,y) = \sum_{h,k=0}^{\infty} \mathbb{V}_{hk}[e^{i2\pi\{hx+ky\}} + e^{i2\pi\{-(h+k)x + hy\}} + e^{i2\pi\{kx - (h+k)y\}}] + \mathbb{V}_{-h;-k}[e^{-i2\pi\{hx + ky\}} + e^{-i2\pi\{-(h+k)x + hy\}} + e^{-i2\pi\{kx - (h+k)y\}}] \quad (12$$

where $\mathbb{V}_{hk} = V_{hk}$, for $h \neq 0$ and $k \neq 0$, $\mathbb{V}_{hk} = \frac{1}{2}V_{hk}$ for one of h or k = 0 (but not both) and $\mathbb{V}_{00} = \frac{1}{6}V_{00}$, — which makes the required symmetry explicit.

The reciprocal lattice vectors,

$$\mathbf{q}(h,k) = h\mathbf{a}_1^* + k\mathbf{a}_2^*, \ \mathbf{q}\{k,-(h+k)\}, \text{ and } \mathbf{q}\{-(h+k),h\} , \quad (13$$

are related by symmetry and together with $\mathbf{q}(-h,-k)$, $\mathbf{q}\{(h+k),-h\}$ and $\mathbf{q}\{-k,(h+k)\}$ form the six-pointed star shown in figure 2.2 a, where they are plotted in the reciprocal lattice.

2-Fold and Inversion symmetry.

In the case of the fcc{111} surface treated without regard to other atomic layers full hexagonal symmetry exists. This is also true for the hexagonal primitive lattice basal plane, and the same plane in the hcp structure. This hexagonal symmetry may be constructed by adding 2-fold rotational symmetry to the 3-fold symmetry axis through the origin, already considered in the previous paragraph.

Letting R_{180} represent the operator which rotates through 180°, this symmetry requires

$$V(\mathbf{r}) = R_{180}\, V(\mathbf{r}) = V(-x\mathbf{a}_1 - y\mathbf{a}_2)$$

i.e.

$$V(x,y) = V(-x,-y) , \quad (14$$

since this operation tranforms $\mathbf{a}_1$ into $-\mathbf{a}_1$ and $\mathbf{a}_2$ into $-\mathbf{a}_2$.

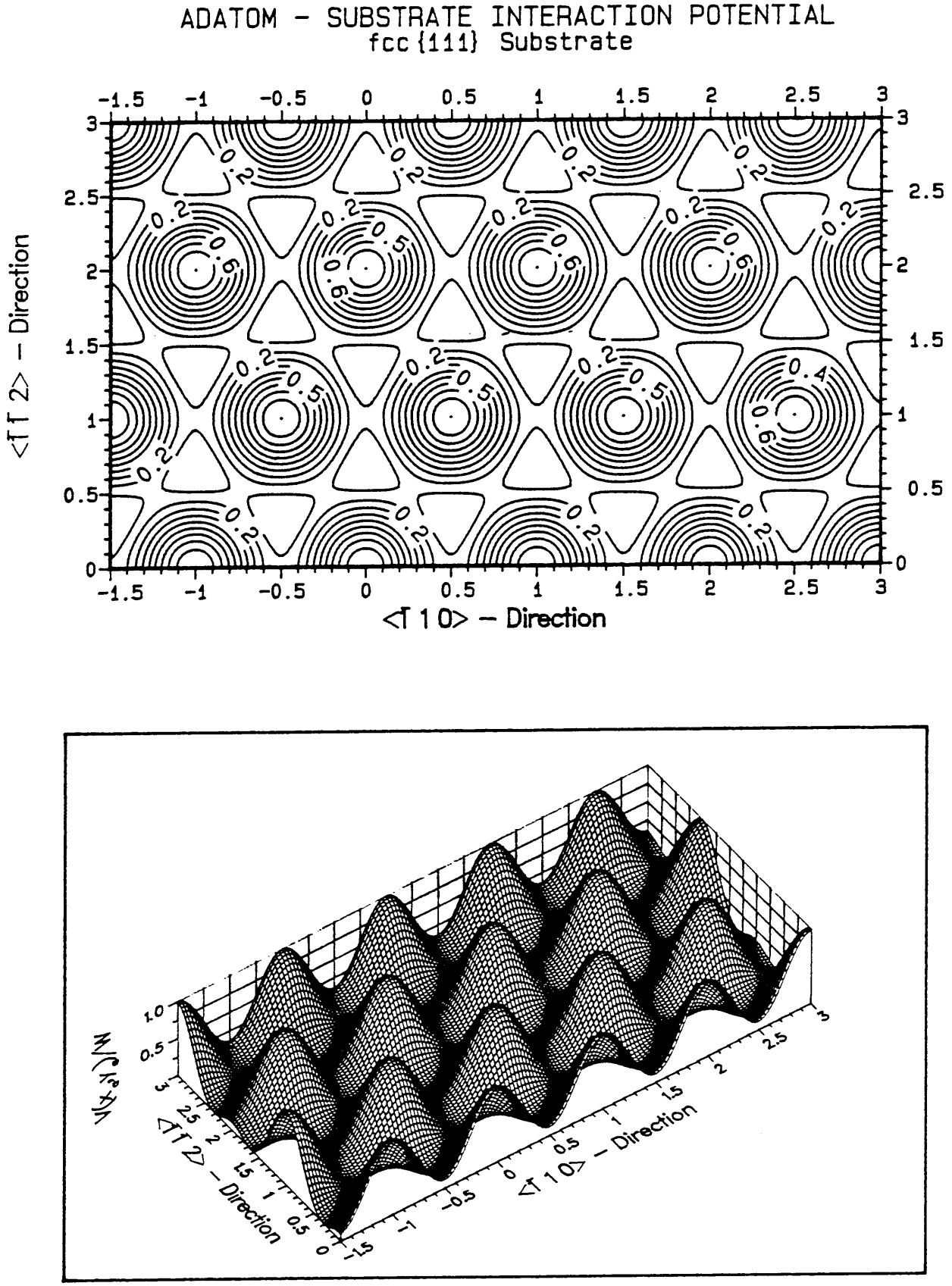

Figure 2.3(a) Simple fundamental potential h = 1, k = 0 cosine terms only, shows full hexagonal symmetry

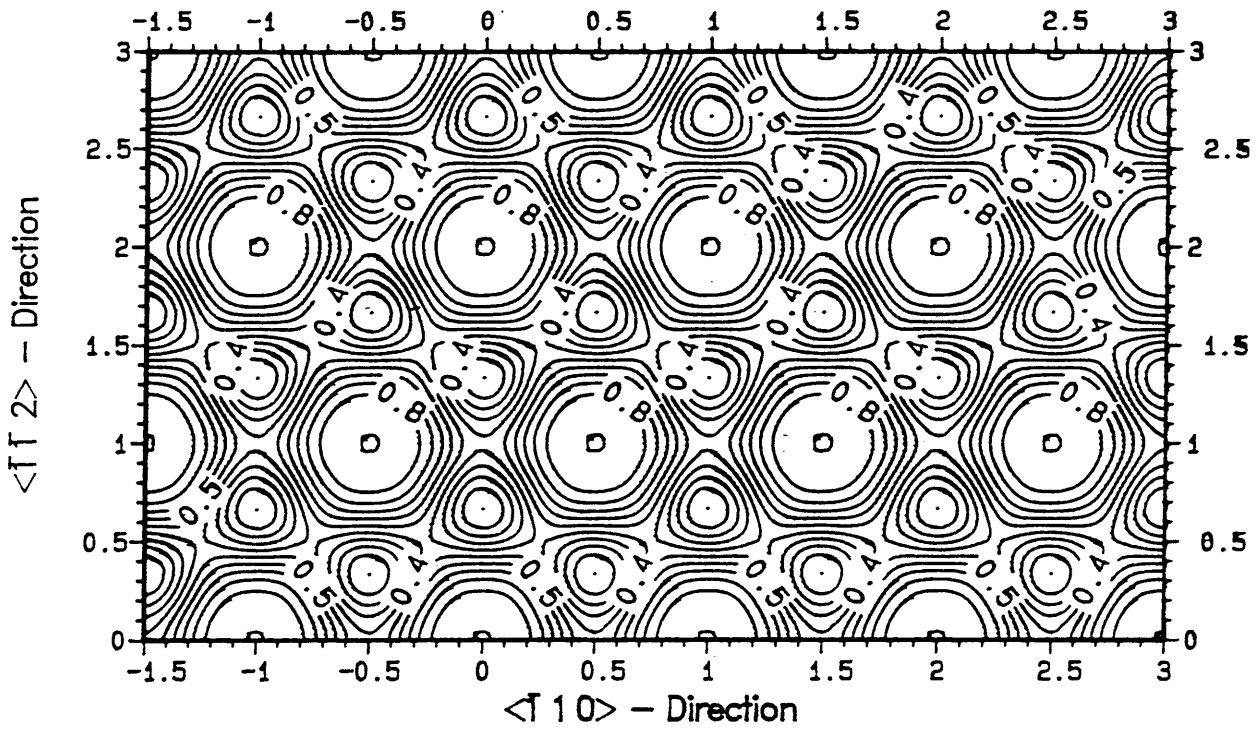

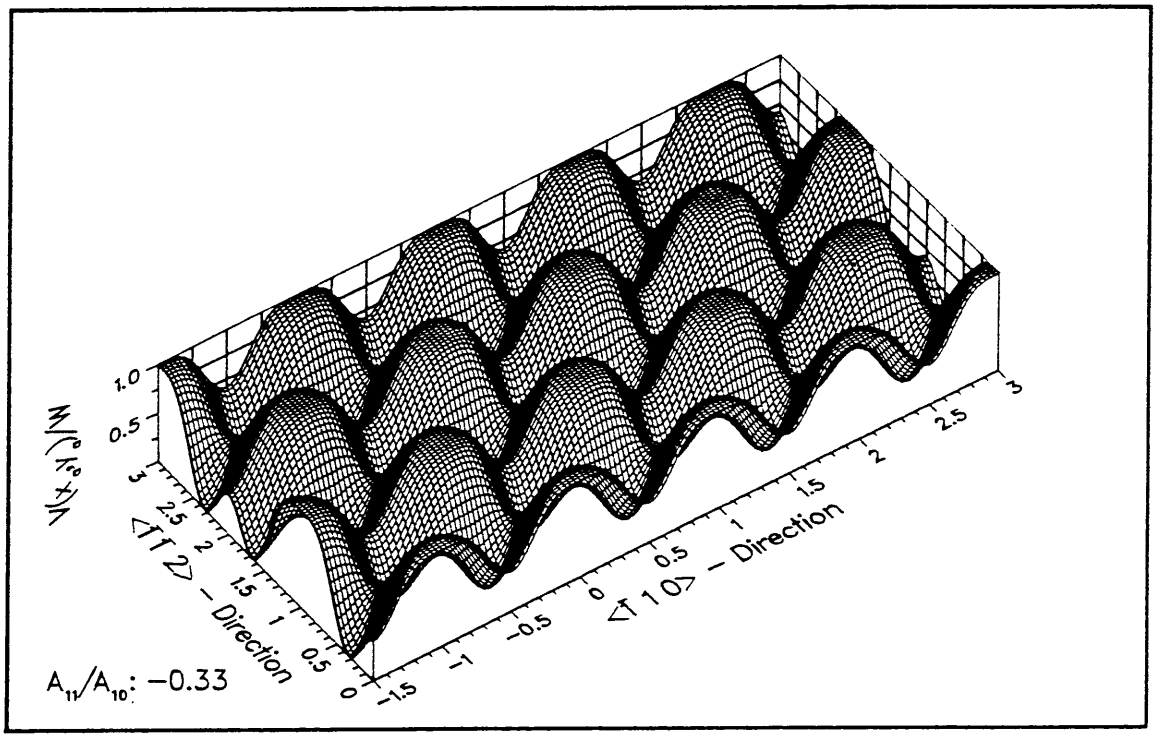

Figure 2.3(b) Potential with fundamental plus h = 1, k = 1 cosine term $A_{11}/A_{10} = -1/3$

Considering, as before, the terms in the expansion related to the term h,k by symmetry namely.

$$V_{hk}\, e^{i2\pi(hx + ky)} \quad \text{and} \quad V_{-h;-k}\, e^{i2\pi(-hx - ky)} \qquad (15$$

it is evident that

$$V_{hk} = V_{-h;-k}\,, \qquad (16$$

since the exponentials transform into one another.

The further requirement that the potentials must be *real*, while the second exponential is clearly the complex conjugate of the first, yields:

$$\text{conj}(V_{hk}) = V_{-h;-k} \quad (\text{with} \quad \text{conj}(V_{-h;-k}) = V_{hk}), \qquad (17$$

from which, for 2-fold symmetry the coefficients V_{hk} (and $\mathcal{V}_{hk}$) are real, and $V_{hk} = V_{-h;-k}$ (as well as $\mathcal{V}_{hk} = \mathcal{V}_{-h;-k}$) .

Since $\cos\theta = (e^{i\theta} + e^{-i\theta})/2$, it follows that under the combined conditions of 3-fold and 2-fold symmetry, i.e. 6-fold -hexagonal- symmetry about the origin, the Fourier expansion further simplifies to:

$$\frac{V(x,y)}{WH} = A_{00} + \sum_{\substack{h,k=0 \\ h\neq 0 \text{ or } k\neq 0}}^{\infty} A_{hk}\,[\cos 2\pi\{hx + ky\} + \cos 2\pi\{-(h+k)x + hy\} + \cos 2\pi\{kx - (h+k)y\}] \qquad (18$$

where we have included the overall factors H and W. The factor H is a normalizing term, normally chosen in such a way that the overall amplitude of V(x,y)/W (from global minimum to global maximum) may be 1, while W has units of energy, and is a calibration factor. The factor W is usually interpreted as a measure of the Binding Strength of the adatom to the substrate, (Van der Merwe 1964, 1980, 1982, Van der Merwe and Ball 1975).

Here, A_{hk} and $\mathcal{V}_{hk}$ are related by

$$WHA_{hk} = 2\mathcal{R}e(\mathcal{V}_{hk}) \qquad (19a$$

when h and k are not both zero, and

$$WHA_{00} = 6\mathcal{R}e(\mathcal{V}_{00})\,. \qquad (19b$$

Inversion Anti-symmetry

Closely related to the inversion symmetry in the two-dimensional lattice under consideration, is anti-symmetry, for which

$$V(x,y) = -V(-x,-y). \qquad (20a$$

Then

$$V_{hk} = -V_{-h;-k} \quad . \qquad (20b$$

This together with the requirement that the potential be real, leads to the conclusion that the coefficients in this case are pure imaginary, i.e.

$$\text{conj}(V_{hk}) = -V_{hk} \quad (\text{and} \quad \text{conj}(V_{-h;-k}) = -V_{-h;-k}). \qquad (21$$

For 3-fold symmetry about the origin (and 6-fold symmetry about the x = 2/3, y = 1/3 positions) the Fourier expansion reduces to sine terms only, and

$$V(x,y) = WHB_{00} + WH \sum_{h,k=0}^{\infty} B_{hk} [\sin 2\pi\{hx + ky\} + \sin 2\pi\{-(h+k)x + hy\} + \sin 2\pi\{kx - (h+k)y\}] \qquad (22$$

where $WHB_{hk} = 2\Im m(V_{hk})$, and B_{00} is chosen so that the minimum of V(x,y) = 0.

Expansion in terms of Trigonometric Functions

Finally, for 3-fold symmetry, which models the fcc{111} surface with stacking fault effects adequately, the expansion may be written with distinct symmetric and antisymmetric parts as a combination of the cosine and sine series as:

$$\frac{V(x,y)}{WH} = (A_{00} + \Delta B_{00}) + \sum_{\substack{h,k=0 \\ h\neq 0 \text{ or } k\neq 0}}^{\infty} A_{hk} [\cos 2\pi\{hx + ky\} + \cos 2\pi\{-(h+k)x + hy\} \cos 2\pi\{kx - (h+k)y\}] + \sum_{\substack{h,k=0 \\ h\neq 0 \text{ or } k\neq 0}}^{\infty} \Delta B_{hk} [\sin 2\pi\{hx + ky\} + \sin 2\pi\{-(h+k)x + hy\} + \sin 2\pi\{kx - (h+k)y\}] \qquad (23$$

Here Δ serves as a parameter giving the strength of the

antisymmetric terms, interpretable as a *stacking-fault parameter* in this context. The B_{hk} are normally chosen to give a structure similar to the cosine series (but symmetrical about a displaced axis). The antisymmetric (sine) series introduces a difference in value between the $x = 2/3, y = 1/3$ and $x = 1/3, y = 2/3$ positions in the surface. These correspond to " up triangle " (Δ) and " down triangle " (∇) " stacking locations respectively in the fcc{111} and hcp{00.1} planes. Often, both energies and forces are needed in a calculation. In this case the sine-series formulation of stacking fault differentiation is computationally more efficient than the displaced potential formulation, as sine and cosine functions transform into one another when differentiated. (Compare figures 2.3 *a* and 2.4 *a*.)

Although a fuller discussion of the selection of numerical values for the various coefficients is still to follow, perspective (wire-mesh) and corresponding contour diagrams for some examples shown in figures 2.3-2.5, are instructive.

2.2 EFFECT OF HIGHER FOURIER ORDERS

Fourier Sublattices

It is evident that each group of three terms (or six for the higher symmetry case) associated with a particular h,k in the symmetry star (refer to figure 2.2 a-d) form a complete duplicate of the fundamental lattice defined by the Fourier level $h = 1, k = 0$, but for a different scale and orientation.

(For convenience the related terms are referred to together as a *Fourier level* or *sublattice* and a single term h,k as an *harmonic*, while $h+k$ is the *order* of the term or level when h and k are both positive.)

The wavelength associated with the wave vector q_{hk} and the orientation of this sublattice, with respect to the basis vectors

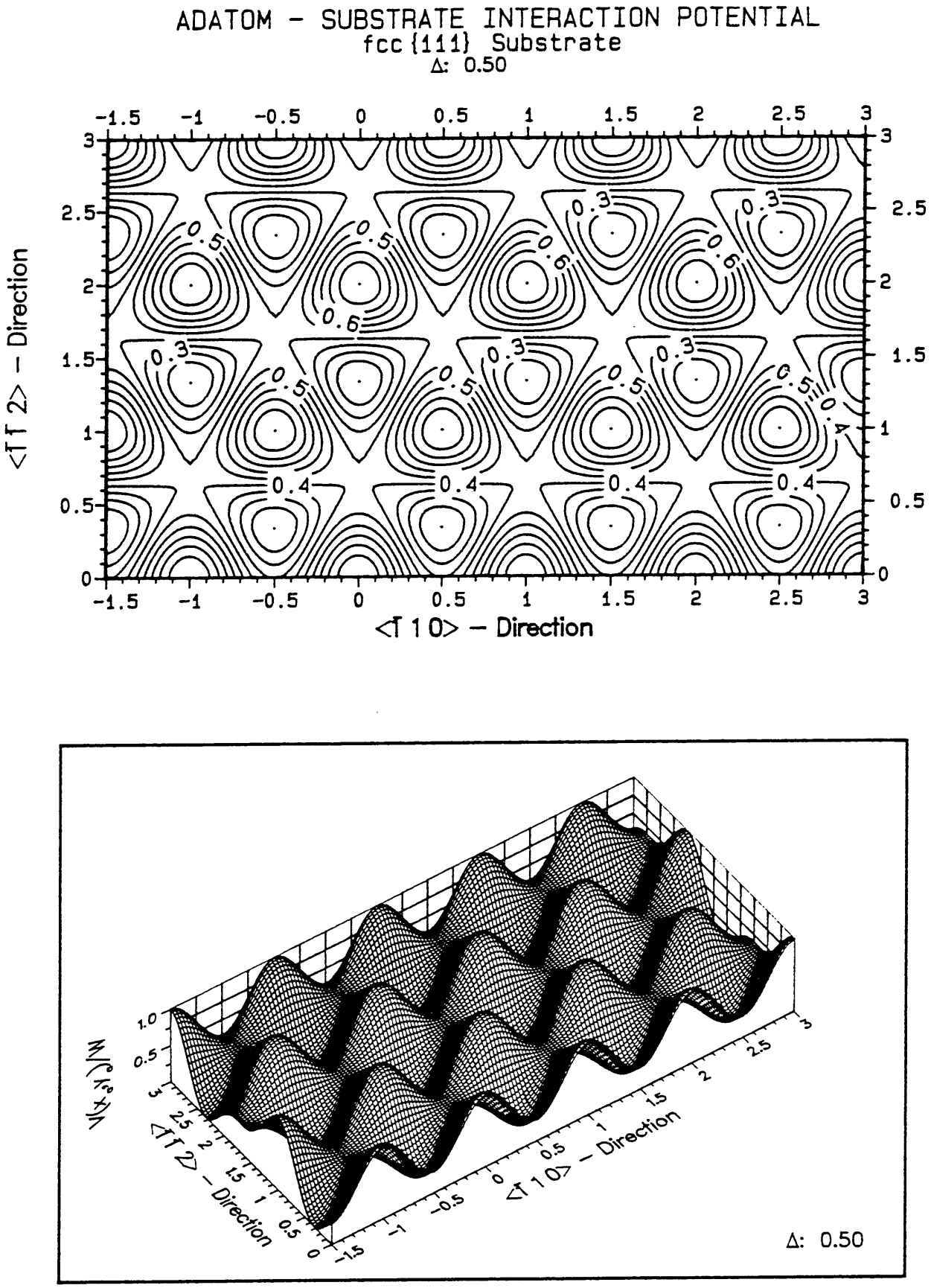

Figure 2.4(a) Potential with stacking fault terms.
Fundamental only $\Delta = \frac{1}{2}$

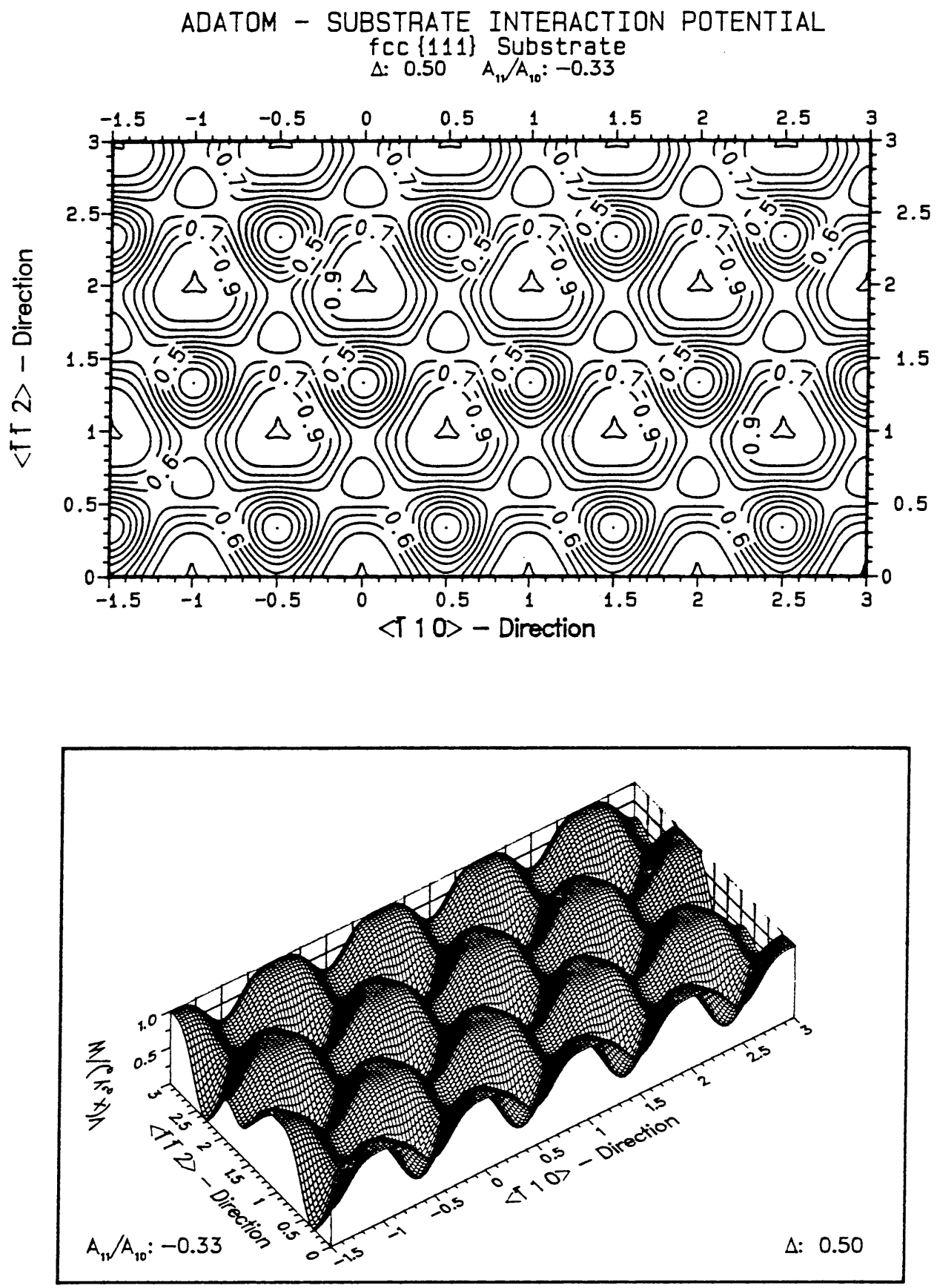

Figure 2.4(b) Potential with stacking fault terms.
Fundamental plus the h = 1, k = 1, cosine terms with A_{11}/A_{10} = - 1/3
$\Delta = \frac{1}{2}$

$\mathbf{a}_1$ and $\mathbf{a}_2$ change. The scale factor and orientation of these Fourier sublattices may be calculated in a number of ways. A useful first stage, is the expression of the basis vectors and their reciprocal set in terms of a suitable Cartesian axis system. We let

$$\mathbf{a}_1 = a\,\mathbf{e}_x \qquad \text{and} \qquad \mathbf{a}_2 = a\left(\frac{\sqrt{3}}{2}\,\mathbf{e}_y - \frac{1}{2}\,\mathbf{e}_x\right), \tag{24}$$

where $\mathbf{e}_x$ and $\mathbf{e}_y$ are the unit vectors of the cartesian system, and

$$\mathbf{a}_1^* = \frac{2\pi}{a}\left(\mathbf{e}_x + \frac{1}{\sqrt{3}}\,\mathbf{e}_y\right) \quad \text{and} \quad \mathbf{a}_2^* = \frac{2\pi}{a}\left(\frac{2}{\sqrt{3}}\,\mathbf{e}_y\right). \tag{25}$$

By choosing the lowest order wave vector of the Fourier terms as the vector

$$\mathbf{q}_o = \mathbf{q}_{1\ 0} = \mathbf{a}_1^*, \tag{26}$$

we can calculate the angle ω_{hk}^F made by a higher order wave vector

$$\mathbf{q}_{hk} = \mathbf{q}(h,k) = h\mathbf{a}_1^* + k\mathbf{a}_2^* = \frac{2\pi}{a}\left\{h\,\mathbf{e}_x + \frac{1}{\sqrt{3}}\,(h+2k)\,\mathbf{e}_y\right\} \tag{27}$$

from

$$\cos w_{hk}^F = \frac{\mathbf{q}_o \cdot \mathbf{q}_{hk}}{|\mathbf{q}_o|\ |\mathbf{q}_{hk}|} = \frac{\frac{1}{2}(2h+k)}{\sqrt{h^2+hk+k^2}}. \tag{28}$$

The scaling factor Λ_{hk} by which the lattice basis vectors are multiplied to give the length of the Fourier sublattice basis vectors, may be calculated from the wavelength λ_{hk} of the wave vector $\mathbf{q}_{hk}$ as:

$$\lambda_{hk} = \frac{2\pi}{|\mathbf{q}_{hk}|} = \frac{a\sqrt{3}}{\sqrt{h^2+hk+k^2}}. \tag{29}$$

Thus

$$\Lambda_{hk} \equiv \frac{\lambda_{hk}}{\lambda_{10}} = \frac{1}{\sqrt{h^2+hk+k^2}}, \tag{30}$$

since $\lambda_{10} = a\,\frac{\sqrt{3}}{2}$.

The Fourier sublattice direct basis vectors, and their reciprocal set can be derived in various ways. One may apply the scaling factors and rotation angles derived above, to obtain $\mathbf{a}_1(h,k)$ and $\mathbf{a}_2(h,k)$ from the direct lattice, and calculate the reciprocal vectors $\mathbf{a}_1^*(h,k)$ and $\mathbf{a}_2^*(h,k)$ by vector formula. Or, noting that

$\mathbf{a}_1^* = \mathbf{q}(1,0)$, one may define the reciprocal vector $\mathbf{a}_1^*(h,k)$ as equal to $\mathbf{q}(h,k)$ and construct the vector $\mathbf{a}_2^*(h,k)$ from this in the same relationship that $\mathbf{a}_2^*$ has to $\mathbf{a}_1^*$, — namely a rotation through 60° — and calculate the direct basis vectors from these. Either method produces identical answers, although the second method is algebraically somewhat simpler.

The results are:

Direct lattice basis vectors for the Fourier sublattice h,k :

$$\mathbf{a}_1(h,k) = \frac{(h+k)\,\mathbf{a}_1 + k\,\mathbf{a}_2}{h^2 + hk + k^2} = \frac{a}{2}\left[\frac{(2h+k)\,\mathbf{e}_x + \sqrt{3}\,k\,\mathbf{e}_y}{h^2 + hk + k^2}\right] \qquad (31a$$

and

$$\mathbf{a}_2(h,k) = \frac{-k\,\mathbf{a}_1 + h\,\mathbf{a}_2}{h^2 + hk + k^2} = \frac{a}{2}\left[\frac{-(h+2k)\,\mathbf{e}_x + \sqrt{3}\,h\,\mathbf{e}_y}{h^2 + hk + k^2}\right], \qquad (31b$$

while the corresponding reciprocal lattice basis vectors are:

$$\mathbf{a}_1^*(h,k) = h\,\mathbf{a}_1^* + k\,\mathbf{a}_2^* = \frac{2\pi}{a}\left[h\,\mathbf{e}_x + \frac{1}{\sqrt{3}}(h+2k)\,\mathbf{e}_y\right] \qquad (32a$$

and

$$\mathbf{a}_2^*(h,k) = -k\,\mathbf{a}_1^* + (h+k)\,\mathbf{a}_2^* = \frac{2\pi}{a}\left[-k\,\mathbf{e}_x + \frac{1}{\sqrt{3}}(2h+k)\,\mathbf{e}_y\right]. \qquad (32b$$

It can be deduced from the preceding discussion, that any property which is dependent on the geometry of the substrate, may be studied by first deriving relevant effects for the fundamental level Fourier terms, h=1,k=0, and by rotating and scaling according to whichever higher order terms are present in the expansion. In the subsequent chapters, this approach will prove useful when predictions of epitaxial orientations are discussed.

The Fourier sublattices of higher orders are related to the fundamental order in Table 2.2.

Table 2.2. Angles of Rotation and Scale Factors of Fourier Sublattices.

Sublattice order	h	k	Λ_{hk}	$\cos \omega^F_{hk}$	ω^F_{hk}
1	1	0	1	1.0	0°
2	1	1	$\frac{1}{\sqrt{3}}$	$\frac{\sqrt{3}}{2}$	30
	2	0	$\frac{1}{2}$	1.0	0
	0	2	$\frac{1}{2}$	$\frac{1}{2}$	60
3	2	1	$\frac{1}{\sqrt{7}}$	$\frac{5}{\sqrt{28}}$	19.1
	1	2	$\frac{1}{\sqrt{7}}$	$\frac{2}{\sqrt{7}}$	40.9
	3	0	$\frac{1}{3}$	1.0	0
	0	3	$\frac{1}{3}$	$\frac{1}{2}$	60
4	2	2	$\frac{1}{\sqrt{12}}$	$\frac{\sqrt{3}}{2}$	30
	3	1	$\frac{1}{\sqrt{13}}$	$\frac{7}{\sqrt{52}}$	13.9
	1	3	$\frac{1}{\sqrt{13}}$	$\frac{5}{\sqrt{52}}$	46.1
	4	0	$\frac{1}{4}$	1.0	0
	0	4	$\frac{1}{4}$	$\frac{1}{2}$	60

Coincidence lattices

An interesting use of these Fourier orders is as an aid to construction of potentials representing reconstructed surfaces, which still retain the fundamental symmetry, but have superimposed on them a coarser periodicity of the same symmetry. Another example is a substrate surface which already has a sub-monolayer overgrowth lattice associated with it, but this second lattice, although sharing point symmetries, has a different lattice parameter and is rotated with respect to the substrate lattice, in such a way that there is coincidence of lattice positions between the coarser overgrowth and finer substrate lattices.

In these cases the relationship between the coarse lattice, and the finer substrate lattice, can be deduced from the table, as the inverse relationships

$$L_{hk} = 1/A_{hk}, \qquad (33$$

and angles of rotation ω^{F}_{hk} .

The relationship between basis vectors of the higher order Fourier sublattices and the basis vectors of the fundamental order is simply given by:

$$\begin{aligned} Sa_1(h,k) &= (h+k)a_1 + ka_2 \quad , \\ Sa_2(h,k) &= -ka_1 + ha_2 \quad , \end{aligned} \qquad (34$$

where $S = h^2 + hk + k^2$.

If one were to chose the coincidence lattice basis vectors as the fundamental basis vectors, the potential expression is simply as before. The dominant coefficients would be chosen by referring to the scale and angular relationships as in the Table 2.2. However, in general it is more suitable to express all positions in terms of the substrate coordinates.

Assuming one has identified suitable basis vectors of the coincidence lattice, $\mathbf{A}_1$ and $\mathbf{A}_2$, and determined which Fourier level h,k will provide basis vectors for the substrate coordinates namely a_1 and a_2, we associate the finer and coarser bases as follows:

$$Sa_1 = (h+k)\mathbf{A}_1 + k\mathbf{A}_2 \quad , \qquad Sa_2 = -k\mathbf{A}_1 + h\mathbf{A}_2 \qquad (35$$

and conversely:

$$\mathbf{A}_1 = ha_1 - ka_2 \quad , \qquad \mathbf{A}_2 = ka_2 + (h+k)a_2 \; . \qquad (36$$

The dominant Fourier terms in the potential when expressed in terms of the coincidence lattice coordinates X and Y are simply

$$A_{10}\,[\cos 2\pi X + \cos 2\pi Y + \cos 2\pi (Y-X)] \qquad (37a$$

and

$$A_{hk}\,[\cos 2\pi\{hX + kY\} + \cos 2\pi\{-(h+k)X + hY\} + \cos 2\pi\{kX - (h+k)Y\}] \qquad (37b$$

as before.

Transforming to substrate coordinates x,y by writing

$$\mathbf{r} = x\mathbf{a}_1 + y\mathbf{a}_2 = X\mathbf{A}_1 + Y\mathbf{A}_2 \qquad (38a$$

then

$$x = hX + kY \quad , \quad y = -kX + (h+k)Y \qquad (38b$$

and conversely

$$SX = (h+k)x - ky \quad , \quad SY = kx - hy \; . \qquad (38c$$

The Fourier sublattice which represents the fundamental order of the substrate lattice is now simply

$$A_{hk}\,[\cos 2\pi\, x + \cos 2\pi\, y + \cos 2\pi(y-x)]. \qquad (39$$

The coarser, coincidence lattice terms become interestingly,

$$A_{10}\,[\cos\tfrac{2\pi}{S}\{(h+k)x - ky\} + \cos\tfrac{2\pi}{S}\{-(kx + hy)\} + \cos\tfrac{2\pi}{S}\{(h+k)y - hx\}] \; . \qquad (40$$

Except for the overall divisor $S = (h^2 + hk + k^2)$, the arguments of the cosine terms are the same as the Fourier level k,h.

The simplest potential representing the substrate potential (as level h,k) together with a superimposed coarser lattice (as level $1,0$), is thus

$$\begin{aligned} V(x,y) = A_{00} &+ A_{hk}\,[\cos 2\pi\, x + \cos 2\pi\, y + \cos 2\pi(y-x)] \\ &+ A_{10}\,[\cos\tfrac{2\pi}{S}\{(h+k)x - ky\} + \cos\tfrac{2\pi}{S}\{-(kx + hy)\} \\ &+ \cos\tfrac{2\pi}{S}\{(h+k)y - hx\}] \end{aligned} \qquad (41$$

where the coefficients A_{00}, A_{hk}, A_{10} already include normalization and calibration factors. Obviously, higher order Fourier terms to provide the fine structure would be added to obtain a faithful representation of a real surface.

As an example one might consider the $(\sqrt{3} \times \sqrt{3})R30^\circ$ coincidence structure (Bauer 1982) observed on fcc{111} surfaces. The $L_{hk} = \sqrt{3}$, requires that $h = k = 1$. The simplest potential representing such a lattice superimposed on the fundamental lattice would be

$$\begin{aligned} V(x,y) = A_{00} &+ A_{11}\,[\cos 2\pi\, x + \cos 2\pi\, y + \cos 2\pi(y-x)] \\ &+ A_{10}\,[\cos\tfrac{2\pi}{3}(2x-y) + \cos\tfrac{2\pi}{3}(x+y) + \cos\tfrac{2\pi}{3}(2y-x)] \; . \end{aligned} \qquad (42$$

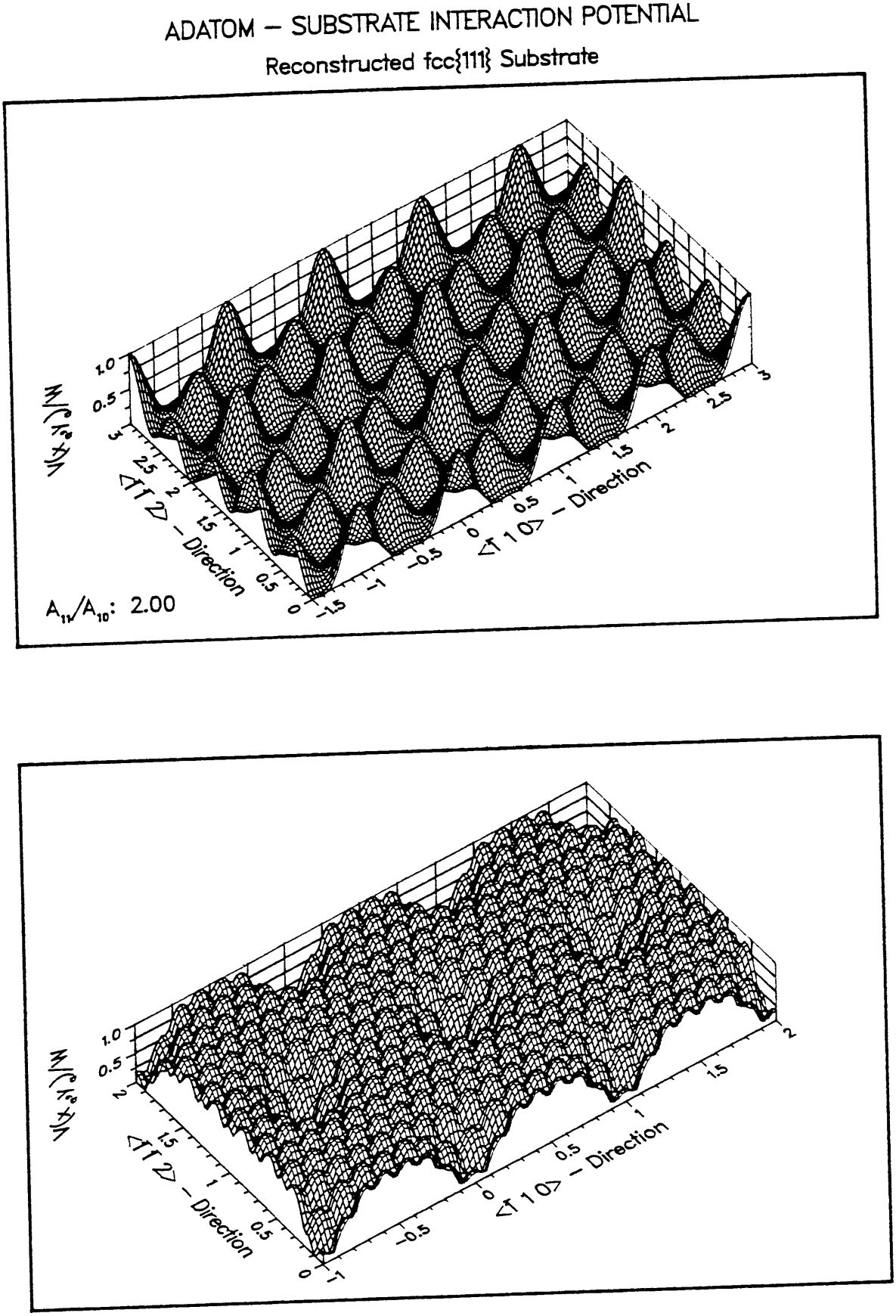

Figure 2.5 Examples of potentials representing reconstructed surfaces

(a) $\sqrt{3} \times \sqrt{3}$ R 30° (eqn 3.42) $A_{11}/A_{10} = 2$ (coincidence surface)

(b) 7 × 7 reconstruction

Such a potential is shown as a surface diagram in figure 2.5 *a* , while an example 7X7 potential is shown in figure 2.5 *b*.

2.3 CHOICE OF NUMERICAL VALUES OF THE FOURIER COEFFICIENTS

Physical considerations

Common to both close-packed structures, fcc and hcp, is the fact that the close-packed planes have six-fold symmetry as their highest symmetry, if the effect of subplanar atoms are ignored. The optimal position of the adatoms in both stuctures is a point of three-fold symmetry, either "up-triangle" Δ, or "down-triangle" ∇. In terms of the coordinates chosen in the expression of the potential, these positions are the $\frac{2}{3},\frac{1}{3}$ or $\frac{1}{3},\frac{2}{3}$ positions respectively. As one of these is the most suitable position for an adatom, these must be positions of minimum energy, usually chosen as zero for convenience. If the stacking order is to be simulated, there must be a difference between these two, and the "up-triangle" position is taken as the global minimum here. The $\frac{1}{3},\frac{2}{3}$ position must then have a non-zero energy, but still be a local mimimum.

The position of six-fold symmetry is a most unfavourable position for the location of an adatom. In the development given here, this position was chosen as the origin of the coordinate system. Correspondingly the global maximum must occur at the origin.

Intermediate values are located at the saddle points between the up and down triangle positions, at $\frac{1}{2},0$ (and positions equivalent by symmetry).

The overall calibration factor, W, is normally estimated from surface diffusion data (Van der Merwe 1982, Venables *e.a.* 1984), or surface binding energy information (Van der Merwe 1964). But, as these data are not very available in general, a range of values is usually considered, and phase diagrams constructed, with either

this W as a parameter, or the van der Merwe Configurational parameter ℓ, which depends on W, as parameter. A fuller discussion is given below.

Mathematical considerations

Consideration of the effect of Fourier sublattices in particular, and higher order Fourier terms in general, indicates that these provide fine structure to the basic potential, and correspondingly, may be chosen to have coefficients that rapidly decrease in magnitude. Previous models have all terminated the Fourier expansion after very few terms, usually one or two orders. Fourier coefficients that have been calculated for adatom potentials in which a central atom pair potential such as the Lennard-Jones interaction $-a/r^6 + b/r^{12}$ or the longer range $-a/r^4 + b/r^7$ were assumed (Mackenzie 1950, Stoop 1986), clearly confirm this tendency. With these remarks in mind, the potential form (for the 6-fold case) rarely exceeds three levels in the subsequent discussions, and may correspondingly be written as:

$$\begin{aligned} V_{cos}(x,y)/WH = A_{00} &+ A_{10}\,[\cos 2\pi(y-x) + \cos 2\pi x + \cos 2\pi(-y)] + \\ &+ A_{11}\,[\cos 2\pi(x+y) + \cos 2\pi(-2x+y) + \cos 2\pi(x-2y)] \\ &+ A_{20}\,[\cos 2\pi(2y-2x) + \cos 2\pi(2x) + \cos 2\pi(-2y)]\,, \end{aligned} \qquad (43$$

where the notation V_{cos} has been introduced for the symmetric truncated series.

The features which the physical nature of the systems that will be studied impose on the potential, are reflected in mathematical conditions limiting the choice of values of the coefficients, A_{00}, A_{10}, etc.

As a global maximum and a global minimum are needed at the origin and $\frac{2}{3},\frac{1}{3}$ positions, respectively, for which the conditions in local terms are necessary, we list the inequalities which must be satisfied, at these points.

An intermediate quantity used in these turning point conditions (Spiegel 1963) is

$$\text{Discr}_{x_0y_0} \equiv \left\{ \left[\frac{\partial^2 V}{\partial x^2}\right] \cdot \left[\frac{\partial^2 V}{\partial y^2}\right] - \left[\frac{\partial^2 V}{\partial x \partial y}\right]^2 \right\}\Big|_{x_0y_0} \qquad (44$$

where, as indicated, all the quantities are calculated at x_0,y_0.

A necessary condition for local maximum, minimum or a saddle point to occur at x_0,y_0 is that both partial first derivatives must be zero. Hence

$$\frac{\partial V}{\partial x}\Big|_{x_0y_0} = \frac{\partial V}{\partial y}\Big|_{x_0y_0} = 0 \qquad (45$$

Once the first-derivative conditions are satisfied, the following are sufficient

(i) Maximum at x_0,y_0 if (46

$$\text{Discr}_{x_0y_0} > 0 \quad \text{and} \quad \frac{\partial^2 V}{\partial x^2}\Big|_{x_0y_0} < 0$$

(ii) Minimum at x_0,y_0 if

$$\text{Discr}_{x_0y_0} > 0 \quad \text{and} \quad \frac{\partial^2 V}{\partial x^2}\Big|_{x_0y_0} > 0$$

(iii) Saddle point at x_0y_0 if

$$\text{Discr}_{x_0y_0} < 0 \ .$$

The fourth case, $\text{Discr}_{x_0y_0} = 0$, provides no information.

Necessary global conditions to be satisfied obviously include the requirements that $V(0,0) > V(\frac{1}{2},0) \geq V(\frac{2}{3},\frac{1}{3})$. These together with the strongly required conditions 46(i) and (ii) above, to be satisfied at $0,0$ and $\frac{2}{3},\frac{1}{3}$ respectively, (while 46(iii) at $\frac{1}{2},0$ should be seen as informative, but may be replaced by a local maximum, or minimum say) lead to the inequalities summarized in Table 2.3, below.

Table 2.3. Allowed ranges of the Fourier coefficients. [Necessary Conditions with minimum at 2/3, 1/3]

(a) A_{20} *not necessarily equal to 0*

Local Conditions:

(*i*) *Maximum at 0,0.*

$A_{10} + 8A_{20} + 3A_{11} > 0$

$A_{11} > -\frac{1}{3}(A_{10} + 8A_{20})$, $A_{20} > -\frac{1}{8}(A_{10} + 3A_{11})$

(*ii*) *Minimum at 2/3,1/3*

$A_{10} + 4A_{20} - 6A_{11} > 0$

$A_{11} < \frac{1}{6}(A_{10} + 4A_{20})$, $A_{20} > -\frac{1}{4}(A_{10} - 6A_{11})$

(*iii*) *Saddle Point at 1/2,0*

$(A_{10} - 4A_{20} - A_{11})^2 > 8(A_{10} - 4A_{20} - A_{11})(A_{11} - 2A_{20})$

$A_{11} >$ *maximum of* $(A_{10} - 4A_{20})$ *and* $\frac{1}{9}(A_{10} + 12A_{20})$

OR

$A_{11} <$ *minimum of* $(A_{10} - 4A_{20})$ *and* $\frac{1}{9}(A_{10} + 12A_{20})$

(*iv*) $A_{10} > 0$, *combining maximum* (*i*) *and minimum* (*ii*) *conditions:*

$-\frac{1}{3}(A_{10} + 8A_{20}) < A_{11} < \frac{1}{6}(A_{10} + 4A_{20})$

$A_{20} >$ *maximum of* $-\frac{1}{8}(A_{10} + 3A_{11})$ *and* $-\frac{1}{4}(A_{10} - 6A_{11})$

Global conditions

(*v*) $V(0,0) > V(2/3,1/3)$

$A_{10} + A_{20} > 0$

(*vi*) $V(0,0) > V(1/2,0)$

$A_{11} > -A_{10}$

(*vii*) $V(2/3,1/3) \leq V(1/2,0)$

$A_{10} + 9A_{20} - 8A_{11} \geq 0$

$A_{11} \leq \frac{1}{8}(A_{10} + 9A_{20})$, $A_{20} \geq \frac{1}{9}(8A_{11} - A_{10})$

(*viii*) *Combined global and local conditions*

$A_{10} + A_{20} > 0$

$A_{11} \geq$ *maximum of* $-\frac{1}{3}(A_{10} + 8A_{20})$ and $-A_{10}$

$A_{11} \leq$ *minimum of* $\frac{1}{6}(A_{10} + 4A_{20})$ and $\frac{1}{8}(A_{10} + 9A_{20})$

$A_{10} > 0 \Rightarrow A_{20} \geq$ maximum of $-\frac{1}{8}(A_{10} + 3A_{11})$, $-\frac{1}{4}(A_{10} - 6A_{11})$ and $\frac{1}{9}(8A_{11} - A_{10})$

Table 2.3 *Allowed ranges of the Fourier Coefficients. (Necessary Conditions with minimum at 2/3, 1/3)*

(*b*) $\underline{A_{20} = 0,\ A_{10} > 0}$

Local conditions
Maximum and minimum

(*ix*) $-\frac{1}{3} A_{10} \leq A_{11} \leq \frac{1}{6} A_{10}$

Saddle point at 1/2,0

(*x*) $A_{11} \leq \frac{1}{9} A_{10}$ *or* $A_{11} \geq A_{10}$

Global conditions

(*xi*) $-A_{10} \leq A_{11} \leq \frac{1}{8} A_{10}$

Combined conditions

(*xii*) $-\frac{1}{3} A_{10} \leq A_{11} \leq \frac{1}{8} A_{10}$

In many cases, a potential with an antisymmetric component such as the stacking fault terms will be required. The displaced potential approach presents no complications, as any expression similar to that used above will need to conform only to the requirements of Table 2.3, before multiplying by the attenuation factor Δ, to be suitable. The truncated sine series however, does need to be examined further, as one needs to know, for example, which minimum position ("up" or "down") is to be made shallower. Furthermore, since the expansion is usually used in attenuated form, one needs only the fundamental Fourier triplet, in most applications. One may therefore introduce the notation V_{sin} for the antisymmetric truncated series:

$$\begin{aligned} V_{sin}(x,y)/WH = B_{00} &+ B_{10}\,[\sin 2\pi(y-x) + \sin 2\pi x + \sin 2\pi(-y)] \\ &+ B_{11}\,[\sin 2\pi(x+y) + \cos 2\pi(-2x+y) + \cos 2\pi(x-2y)] \\ &+ B_{20}\,[\cos 2\pi(2y-2x) + \cos 2\pi(2x) + \cos 2\pi(-2y)] \,. \end{aligned} \qquad (47$$

The major physical features of the potential are due to dominant fundamental terms. The positions of the stationary points and their nature, are correspondingly determined only for those terms.

The necessary condition that the first order partial derivatives must be zero identifies the stationary points in the unit cell ($0 \leq x < 1$, and $0 \leq y < 1$) as 0,0 ; 1/3,2/3 and 2/3,1/3 respectively. The sufficient conditions (i), (ii) and (iii) above, show their nature. Hence,

	0,0	is a saddle point,	(48
	1/3,2/3	is a maximum	
and	2/3,1/3	is a minimum, while $B_{10} > 0$.	

Subject to the requirement that these positions retain these properties when the harmonics 1,1 and 2,0 are included, analogous conditions may be imposed on the coefficients B_{11} and B_{20} as apply to the coefficients of the symmetric expansion V_{cos}. These are summarized in Table 2.4.

Table 2.4. Allowed ranges of the Fourier coefficients in V_{sin} (Necessary conditions)

(a) B_{20} *not necessarily equal to 0*

Local conditions	*Global conditions*
Maximum and minimum	$V(2/3,1/3) <$ *minimum of* $V(2/3,0)$ *and* $V(0,2/3)$
(*xiii*) $B_{10} > 4B_{20}$	(*xiv*) $B_{10} > B_{11} + B_{20}$

Combined conditions

(*xv*) $B_{20} < \frac{1}{4} B_{10}$, $-B_{10} + B_{20} < B_{11} < B_{10} - B_{20}$

(b) $B_{20} = 0$, $B_{10} > 0$ [*by* (*xiii*)]

(*xvii*) $-B_{10} < B_{11} < B_{10}$

Values of the Normalizing Coefficients

The constants A_{00} and B_{00} are chosen in such a way that the minimum value of the potential $V(x,y)$ is zero, so that an overgrowth for which all the atoms are in perfect register with the

substrate, will have zero *misfit* energy. By design, the minimum is at $\frac{2}{3},\frac{1}{3}$, in both subpotentials V_{cos} and V_{sin}, so that this criterion can be applied to A_{00} and B_{00} separately. It easily follows that

$$A_{00} = \frac{3}{2}(1 + \frac{A_{20}}{A_{10}} - 2\frac{A_{11}}{A_{10}})A_{10} \qquad (49a$$

and

$$B_{00} = \frac{3\sqrt{3}}{2}(1 - \frac{B_{20}}{B_{10}})B_{10} \ . \qquad (49b$$

While A_{10} may be chosen to be any (positive) value, usually taken as 1 here, B_{10} will be dependant on A_{10}. As the cosine terms represent the effect of atoms in the surface itself, while the sine terms should represent the effect of a similar surface, below the interface, it is reasonable to require that the overall amplitude of the sine and cosine terms, before attenuation, should be the same. With A_{00} chosen as above, the overall amplitude of the cosine sub-potential is the maximum value, calculated at $0,0$, while the sine value is calculated at $\frac{1}{3},\frac{2}{3}$. Thus, B_{10} is given by

$$B_{10} = \frac{\sqrt{3}}{2}\frac{1 + A_{20}/A_{10}}{1 - B_{20}/B_{10}}A_{10} \ . \qquad (49c$$

The potential at this stage may be written as

$$V(x,y)/WH = V_{cos} + \Delta V_{sin} \qquad (50$$

in which A_{10} is implicitly an overall factor. If the calibration factor W is to be interpretable as the actual energy difference between the minimum and maximum values in the potential, (physically related to, but not always simply, to the magnitude of the maximum binding energy, {Van der Merwe 1982}), H must be a normalizing factor, so that this difference, before calibration is 1. Hence,

$$1/H = (V_{cos} + \Delta V_{sin})\big|_{0,0} = \frac{9}{2}(1 + A_{20}/A_{10})(1 + \frac{\Delta}{2})A_{10} \qquad (49d$$

Clearly, A_{10} is most conveniently chosen as 1.

The energy factor W

The value of W must be known to a sufficient degree if energy judgements need to be made, comparing say, various possibilities

for reducing misfit energy, to pseudomorphic matching in which the misfit energy is reduced to zero - at an energy cost due to elastic deformation of the overgrowth (Van der Merwe 1964, 1975, 1980). However, when all that is required is a purely geometric judgement, with no deformation taken into account, but the misfit energy needs to be minimized, no knowledge of W is needed.

Depending on the materials under study, the value of W will depend heavily on which adsorption mechanism is dominant,- physisorption and chemisorption energies may differ by more than a factor 4 (Forty 1983) in their average values. Metallic bonding approaches the strength of the covalent bonding dominant in chemisorption (Van der Merwe 1966). The values of W for some systems may be estimated from a knowledge of the activation energy, Q, of surface migration (Venables *e.a.* 1984, Van der Merwe 1978, Wetzel *e.a.* 1984). Q is identified with the height of the barrier between atomic locations, usually the saddle point position $\frac{1}{2},0$ for the substrates used here (Bacigalupi and Neustadter 1970).

Clearly the height of this barrier compared to the maximum at $V(0,0) = W$, will depend heavily on the choice of stacking fault parameter and higher order Fourier coefficients such as A_{20}, A_{11} etc. However, the goal is usually the construction of phase diagrams (Van der Merwe 1980, Stoop e.a. 1982, Bauer e.a. 1986), in which the stable epitaxial orientation and misfit accommodation mode are related to nearest neighbour ratio $r = b_{nn}/a_{nn}$, and the Van der Merwe configurational parameter ℓ, where b_{nn} and a_{nn} are the nearest neighbour distances in the overgrowth and substrate crystals, respectively. This implies that an estimate of the range of values of W which are physically reasonable is required more than an exact value for a specific overgrowth - substrate system. Such exact values would require calculation based on quantum mechanical principles or pseudo-potentials, and are still rather scarce. A calculation of this type was performed by Batra (1984) for an Aluminium - Germanium (001) system, and a value of 1.2 eV was found for W.

Bacigalupi & Neustadter (1970) using a Lennard-Jones 6-12 potential have shown that Q is very surface dependent in fcc structures. The extent of this variation is evident from their data in that Q_{hkl}/Q_{111} ranges from an average of 1.99 for the (311)-face to 8.77 for the (210)-face, where Q_{hkl} is the energy appropriate for the particular face (hkl). Ehrlich & Stolt (1980) considered the data reported by Ayrault (1973, Ayrault *e.a.* 1974) for several surfaces of Rhodium, and Bassett and Webber (1978) for Platinum, and compared them to the calculations based on Morse potentials reported by Ayrault. They have suggested that the trends in the dependence of these activation energies on surface type may be general for the fcc metals.

Table 2.5 *Experimental values of surface (self) migration activation energies for several faces*

Rhodium [ES-ae,a]		*Platinum* [ES-b]	*Iridium* [PR-b,bp]
Plane hkl	Q_{hkl} (eV)	Q_{hkl} (eV)	Q_{hkl} (eV)
111	0.15 ± 0.02		0.52
100	0.88 ± 0.07		
110	0.60 ± 0.03	0.84 ± 0.1	
		1.07 [HP]	
		1.02 (Au) [HP]	
311	0.54 ± 0.05	0.69 ± 0.2	1.17
		0.66 [HP]	
331	0.64 ± 0.03	0.84 ± 0.1	

Tungsten [ES-ge] (*bcc*)	*Plane* hkl	Q_{hkl} (eV)
	110	0.92 ± 0.05
	211	0.76 ± 0.07
	321	0.87 ± 0.08

Data from :
ES: Ehrlich & Stolt (1980)- ae: Ayrault & Ehrlich (1974), a: Ayrault (1973), b: Bassett (1973), ge: Graham & Ehrlich (1975)
PR : Prutton (1983) - b : Bassett (1973) bp : Bassett & Parsely (1970)
HP : Halicioglu & Pound(1979)

Prutton (1983) has listed the results reported by Bassett (1973, Bassett *e.a.* 1970) on Iridium, and although there are few, there is agreement with the trends predicted theoretically.

These results and the migration activation energy ratios for various faces are shown in Tables 2.5 and 2.6.

Table 2.6 *Comparison of Normalized Experimental and Theoretical Data.* (*Lennard-Jones* [BN] *and Morse potentials* [ES])

Rhodium : (*L-J* : *averages of* $\sigma/a = 0.6$ and $\sigma/a = 0.7$)

Plane	*L-J*	*Exp* (*111*)	*L-J* (*111*)	*Morse* (*111*)	*Exp* (*110*)	*L-J* (*110*)	*Morse* (*110*)
111	0.083	1	1	1 (0.33)	0.25	0.17	0.09
100	0.404	5.84	4.87	10.0 (3.3)	1.46	0.81	0.91
110	0.500	4.00	6.02	11.0 (3.6)	1.00	1	1
311	0.256	3.59	3.08	13.8 (4.6)	0.90	0.51	1.25
331	0.526	4.27	6.34	16.1 (5.3)	1.07	1.05	1.46

Platinum : (*L-J* : $\sigma/a = 0.7$)

Plane	*L-J*	*L-J* (*111*)	*Exp* (*110*)	*L-J* (*110*)	*Morse* (*110*)
111	0.065	1	-	0.14	-
100	0.37	5.69	-	0.78	-
110	0.475	7.31	1	1	1
311	0.162	2.49	0.63	0.34	0.78
331	0.445	6.85	0.82	0.94	1.20

Iridium : (*L-J* : $\sigma/a = 0.8$)

Plane	*L-J*	*Exp* (*111*)	*L-J* (*111*)
111	0.054	1	1
110	0.361	-	6.64
311	0.070	2.25	1.29

BN : Lennard-Jones data from Bacigalupi & Neustadter (1970)
ES : Morse data from Ehrlich & Stolt (1980)
Experimental data from Table 2.5

By averaging the theoretical and the available experimental data, one may reasonably conclude that the ratio of single adatom migration activation energies Q_{110}/Q_{111}, where Q_{110} refers to the (110) surface, and Q_{111} to the (111), is approximately 6. This leads to a working value of the energy $Q = Q_{111} \approx 0.3$ eV. The Morse

potential tendencies where the ratio is about 10 would lead to a smaller value. The values in parentheses in Table 2.6 for rhodium are best fit values over the entire range, and are probably more reasonable. These were used in the calculation of the average. Interestingly, the average of the tungsten values is close to the fcc (110) values, which leads to an estimate of Q as 0.15 eV. This agrees well with the experimental value for rhodium. Judging from the theoretical tendencies, the energy for iridium may be reasonably considered as indicating the upper reaches of the range. Correspondingly, Q will be in the approximate range from 0.15 eV to 0.5 eV with a reasonable representative value of 0.3 eV.

Van der Merwe (1963) has argued on a basis of bond type that this single atom diffusion energy for the close-packed metal surfaces is about one third of the overall energy amplitude W. Based on this, W ≈ 0.9 eV, and ranges from about 0.45 eV to around 1.5 eV.

Bacigalupi & Neustadter (1970) and van der Merwe (1963) and (1982) in considerations of epitaxy on bcc(110) substrates assume a criterion based on the form of the adatom-substrate interaction potential. This identifies the height at the saddle-point with Q. If one uses only the fundamental Fourier terms in the potential, and no stacking-fault correction, i.e. $\Delta = 0$, then $W = 9\,Q$. If $\Delta = 0.5$, then $W = \frac{45}{13}\,Q \approx 3\,Q$, in agreement with the previous criterion.

Graham & Ehrlich (1974) have reported an energy difference of about 0.5 eV between the lattice and fault positions in a bcc{111}-tungsten surface. If one accepts this value as reasonable, together with a stacking fault parameter $\Delta = 0.5$, it follows from $\delta V = V(\frac{1}{3},\frac{2}{3}) - V(\frac{2}{3},\frac{1}{3}) = W\,\frac{2+\Delta}{2\Delta} = 0.5$ eV, that $W = 1.25$ eV. Interestingly, this agrees with the value of $W = 1.2$ eV calculated by Batra for the aluminium-germanium system. The bcc{111} surface is somewhat rougher than fcc{111}, and this suggests that for the case of fcc{111}, W (or $W(2+\Delta)/2\Delta$) is smaller rather than larger.

Combining the arguments, one may accept with reasonable confidence that W lies in a range from about 0.45 eV to about 1.5 eV, (with an unlikely extreme of $9Q = 9 \times 0.5 = 4.5$ eV). One would expect the smaller range to predominate, with W = 0.9 eV as a useful working value.

As a final comment, after correcting for the difference in meaning of W in the papers by van der Merwe (1982), the values used to model the bcc(110) substrate range from 0.4 eV to 1.2 eV, which is not unlike the range considered here.

The Stacking-Fault Parameter Δ

Inverting the arguments above, which link the stacking-fault parameter to W, the range of Δ which is consistent with W does not go beyond about 0.5. This is further evident when the meaning of Δ is considered, namely as an attenuation factor on the interaction with the potential, in order to represent the effect of atomic layers below the substrate. The adatom interacts with a layer which is largely screened by the substrate atoms, and can be considered at most as a next-nearest-neighbour interaction. These conclusions apply to both methods of including the stacking-fault effects, i.e. the antisymmetric - sine function, and the displaced potential formulation.

The effect of a still deeper layer may be simulated by attenuating the factor once more, with an h=0, k=1 sine level, or structure factor for a basis effect at 2/3, 1/3 (Van der Merwe and Braun 1987). Its parameter may be expected to be no greater that Δ^2, and may be considerably less. The attenuation from lower atomic rows is confirmed by Ramirez *e.a.* (1984) and Stoop (1986), who found in their considerations with pair potentials (as described in the introductory survey) that the greatest interaction is with the first layer, while beyond the third layer the effects are negligible. This result has been confirmed for an Argon (100) oriented model system, with Lennard Jones potentials by Stoop (1986), and Stoop and Snyman (1987).

2.4 CONCLUSION

The form of the adatom-substrate potential used in the subsequent chapters is either an infinite Fourier series in general form, or, for calculations other than purely an examination of second order effects, a fundamental level plus a stacking fault term. The values of W range from 0.1 eV, to about 6eV for various purposes. In the homogeneous, misfit strain model several thousand data systems were examined with two values of W, namely 0.4 eV and 0.9eV. As it was found that these values show the interesting effects, such as transitions between one-dimensional coherence and two-dimensional coherence, (pseudomorphism) these were considered useful and representative. The finite element, misfit dislocation calculations were done on systems with W values of 0.1 eV, 0.4eV, 0.9eV, 1.5eV, 3.0eV and 6eV. However beyond 0.9eV there was very little difference in the qualitative behaviour. The potential itself was of the form

$$\frac{V}{W} = H\Big[A_{00} + A_{10}[\cos 2\pi x + \cos 2\pi y + \cos 2\pi(y-x)] + \Delta\{B_{00}+B_{10}[\sin 2\pi x + \sin 2\pi(-y) + \sin 2\pi(y-x)]\}\Big] \qquad (51a$$

with $A_{10} = 1$, $A_{00} = \frac{3}{2}$, $B_{10} = \frac{\sqrt{3}}{2}$, and $B_{00} = \frac{9}{4}$. (51b

With $\Delta = \frac{1}{2}$, the usual choice, $H^{-1} = \frac{9}{2}(1+\frac{1}{4}) = \frac{45}{8}$. (51c

A generalized force, in the skew axes, which must therefore be transformed to the appropriate coordinates as described in Chapter 5 is obtained by differentiation, so that

$$\left[\frac{F}{W}\right]_x = -\frac{\partial}{\partial x}\frac{V}{W} = 2\pi H\Big[\sin 2\pi x - \sin 2\pi(y-x) - \Delta[\cos 2\pi x - \cos 2\pi(y-x)\Big], \qquad (52a$$

and

$$\left[\frac{F}{W}\right]_y = -\frac{\partial}{\partial y}\frac{V}{W} = 2\pi H\Big[\sin 2\pi y + \sin 2\pi(y-x) + \Delta[\cos 2\pi y - \cos 2\pi(y-x)\Big]. \qquad (52b$$

As formulated here the overall minimum of the potential is at 2/3, 1/3 (up triangle) positions in the cells, while 1/3, 2/3 is a secondary (stacking faulted) minimum (down triangle). The overall maximum is at 0, 0. This substrate potential is illustrated for W = 0.4eV in figure 2.4 a.

In Chapter 3 the misfit energy is calculated, both as a general analytical expression, and for several special cases The misfit energy is defined as the total adatom-substrate potential energy summed over all the overgrowth atoms in the interface, under the condition that the minimum, ideal-fit energy is zero, a condition satisfied by the values given above in eqn 51.

It is the general expression, in terms of the wave vectors q_{hk} which leads to the criterion that epitaxy arises from the matching of reciprocal lattice vectors of the overgrowth to the substrate reciprocal lattice vectors, and vice versa. This development will form a powerful component of the interpretive machinery developed in the following chapters.

CHAPTER 3

IDEAL EPITAXIAL CONFIGURATIONS - RIGID MODEL

The initial model in which the overgrowth island, as well as the substrate are kept rigid is described. The analysis is based on that of Van der Merwe's treatment of the Van der Merwe - Reiss rigid model.

The key assumption, that stable epitaxial configurations minimize the interfacial energy, in this case the misfit energy due to disregistry of the overgrowth and substrate lattices, leads directly to the identification of ideal epitaxial configurations with coincidence of translation vectors of the overgrowth and substrate (surface) reciprocal lattice. The analogy of this criterion to that of von Laue in diffraction theory is used to introduce a geometric construction of the Ewald type, which simplifies later discussions of the epitaxial criteria.

The formulation is applied to the fcc{111} substrate with an fcc{111} overgrowth and a bcc{110} overgrowth. Well-known epitaxial configurations are explained, and higher order variants are discussed.

CHAPTER 3

IDEAL EPITAXIAL CONFIGURATIONS - RIGID MODEL

The first step in the prediction of epitaxial orientations for an epitaxial overgrowth-substrate system involves the determination by essentially analytical methods (by applying the methods of van der Merwe 1982) of *Ideal Epitaxial Configurations*, which may be defined as the scale and orientation relationships giving the best possible degree of fit between the different crystal structures without distortion. The appropriate model, its advantage being simplicity, treats the overgrowth as a rigid island of atoms usually large but finite extent, interacting with a rigid substrate. The overgrowth-substrate interaction is expressed as a Fourier series, defined over the entire set of reciprocal lattice vectors of the substrate reciprocal lattice as described in Chapter 2. Necessarily, for actual numerical calculations one normally uses a truncated form of the series. In this way, quantitative information on the penalty of lattice misfit and misorientation may be obtained, a distinct advantage over purely geometric models (Bollmann 1970, Bruce and Jaeger 1977, 1978).

Analytical predictions from the rigid model concern the two *rigid body* degrees of freedom, namely translation of the island as a whole, and reorientation by rotation about some chosen axis. The influence of the relative magnitudes of the overgrowth and substrate lattice parameters of course is obtained from this model, through the parameter $r=b_{nn}/a_{nn}$, the ratio of the overgrowth and substrate nearest neighbour distances. Particularly useful is the ability of the model to predict *relative* depths of the misfit energy minima, for available orientations, without the necessity of knowing the overgrowth-substrate bonding strength, or the parameter W, the overall energy calibration factor defined in Chapter 2.

A simple generalization of this model, treated in the next chapter, within the harmonic (linear elasticity) approximation (Born and

Huang 1954) allows the inclusion of energy terms due to homogeneous deformation of the island. Further localized relaxation of the overgrowth associated with dislocations is more difficult to treat and is formulated in terms of a *Finite Element Model*, described in Chapter 5. This allows the comparison of the contribution to interfacial energy reduction, by several possible mechanisms such as rotation with misfit vernier, homogeneous deformation or misfit strain, (with misfit vernier), and the introduction of misfit dislocations.

The application of this model to a bcc{110}/fcc{111} epitaxial system is preceded by a generalized development of the model, to assist the interpretation and comparison with other systems, as well as the definition of the various parameters which are to be used. A geometrical construction in the reciprocal space which considerably simplifies the prediction of ideal orientations by essentially row-matching criteria, and their interpretation, is also introduced in this section. This reciprocal space formulation allows predictions of the misfit strains and misfit dislocation densities and Burgers vectors, as will be demonstrated when these further degrees of freedom are introduced in the later chapters.

3.1 MODELLING OF THE EPITAXIAL SYSTEM

Choice of Coordinates

The adatom-substrate interaction potential $V(x,y)$ was developed in terms of substrate coordinates. The positions of atoms in the overgrowth are, however, most easily expressed in another set of coordinates suited to the symmetry of the overgrowth lattice. It is thus appropriate to define the coordinates and transformations between them at this stage. The various parameters are illustrated in figure 3.1. All of the transformations introduced in this chapter are listed in Appendix A.

Substrate:

The substrate coordinate system consists of two basis vectors $\mathbf{a}_1$ and $\mathbf{a}_2$, with an angle α between them and lengths a_1 and a_2 respectively. A general point $\mathbf{r}$ in the substrate coordinates is given by (Chapter 2, Table 2.1 and figure 2.1, eqn 2.3)

$$\mathbf{r} = x\mathbf{a}_1 + y\mathbf{a}_2. \qquad (1$$

If confusion between coordinate systems may occur, the substrate coordinates are also written as x_a and y_a if necessary.

Overgrowth:

The overgrowth coordinate system has basis vectors $\mathbf{b}_1$ and $\mathbf{b}_2$, with an angle β between them and lengths b_1 and b_2 respectively. A general position in the overgrowth is given by

$$\mathbf{r}_b = x_b\mathbf{b}_1 + y_b\mathbf{b}_2 . \qquad (2$$

Origins:

Locate the overgrowth origin at the position

$$\mathbf{r}_0 = x_0\mathbf{a}_1 + y_0\mathbf{a}_2 , \qquad (3$$

in the substrate system.

Orientation:

Let θ be the angle between $\mathbf{b}_1$ and $\mathbf{a}_1$, given by

$$\cos\theta = \mathbf{b}_1\cdot\mathbf{a}_1/(|\mathbf{a}_1||\mathbf{b}_1|) . \qquad (4$$

The sense of the angle may be obtained similarly from the vector cross product of $\mathbf{b}_1$ and $\mathbf{a}_1$. This angle is correspondingly 0 when $\mathbf{b}_1$ is parallel to $\mathbf{a}_1$ and gives the orientation of the overgrowth coordinates relative to the substrate coordinates as an anti-clockwise rotation.

It is sometimes convenient to measure the angle from a different initial orientation, a particular epitaxial orientation for

instance. In that event a subscripting notation will be introduced, for example

$$\theta_{(NW)} = \theta - \theta_{NW} \ , \qquad (5$$

where $\theta_{(NW)}$ is the orientation measured from the 'Nishiyama-Wassermann' (see below) epitaxial orientation, and θ_{NW} is the angle through which the overgrowth is rotated to reach that orientation.

Transformations:

The transformation from overgrowth to substrate coordinates follows from eqns 1-4 and figure 3.1 in a straightforward manner.

Consider the general point r_b, with coordinates x_b, y_b in the overgrowth system and x,y in the substrate system. Then,

$$x = x_b r_{11} c_\theta + y_b r_{21} s_{\theta\beta} + x_0 \qquad (6a$$

and

$$y = x_b r_{12} s_\theta + y_b r_{22} c_{\theta\beta} + y_0$$

where transformation parameters are :

$$r_{11} = b_1/a_1 \ , \quad r_{12} = b_1/a_2 \ , \qquad (6b$$
$$r_{21} = b_2/a_1 \quad\quad r_{22} = b_2/a_2$$

and

$$c_\theta = \sin(\alpha-\theta)/\sin\alpha \ , \quad s_\theta = \sin\theta/\sin\alpha \ , \qquad (6c$$
$$s_{\theta\beta} = \sin(\alpha-\beta-\theta)/\sin\alpha \ , \quad c_{\theta\beta} = \sin(\beta+\theta)/\sin\alpha \ .$$

Clearly, the rotation angle is included in the cosine and sine - like parameters c_θ, s_θ etc, whereas the scale relationships are given by the ratios r_{11}, r_{21} etc, while both sets contain the information regarding lattice types.

Usually it will be convenient to express the ratios r_{ij} in terms of a common ratio

$$r = b_{nn}/a_{nn} \qquad (7$$

where b_{nn} and a_{nn} are the nearest neighbour distances in the overgrowth and substrate crystals respectively. One may then introduce an overall change of scale, without changing the lattice symmetry, simply by changing r.

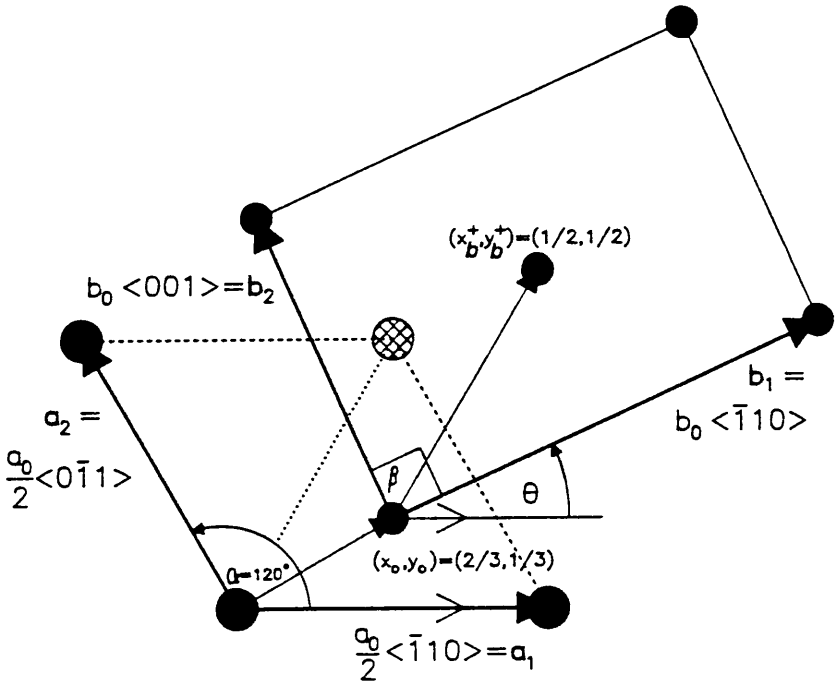

Figure 3.1 Transformation parameters for bcc{110} overgrowth (small circles) on fcc{111} substrate (larger circles).

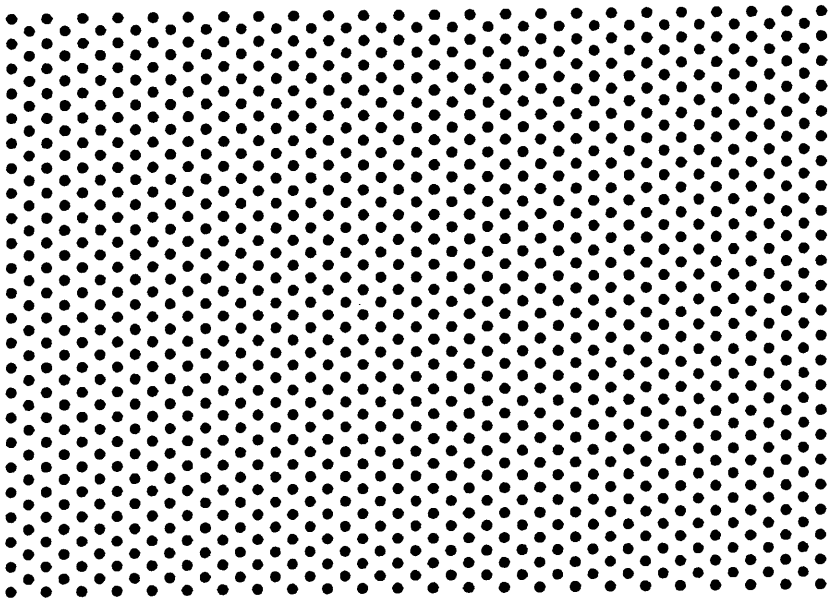

Figure 3.2 The bcc{110} overgrowth island with M = N = 11 and misfit energy given by eqn. 28

In a similar fashion the inverse transformation is

$$x_b = (x-x_0)\frac{D_\theta}{r_{11}} + (y-y_0)\frac{T_{\theta\alpha}}{r_{12}} \quad , \tag{8a}$$

$$y_b = (x-x_0)\frac{T_\theta}{r_{21}} + (y-y_0)\frac{D_{\theta\alpha}}{r_{22}}$$

where

$$D_\theta = \sin(\beta+\theta)/\sin\beta \quad , \qquad T_\theta = -\sin\theta/\sin\beta \quad , \tag{8b}$$

$$T_{\theta\alpha} = \sin(\beta-\alpha+\theta)/\sin\beta \quad , \qquad D_{\theta\alpha} = \sin(\alpha-\theta)/\sin\beta \quad .$$

Adatom-Substrate Potential energy.

The potential energy

$$V(x,y) = \sum_{h,k} V_{hk}\, e^{i2\pi(hx+ky)} \tag{9}$$

was developed for substrate symmetry coordinates in Chapter 2, and the coefficients V_{hk} are assumed to contain the substrate structure factor (Chapter 2 eqns 2.7 and 2.8), F_{hk} where applicable. The arguments of all the Fourier representations are of the form

$$\mathbf{q}_{hk}\cdot\mathbf{r} = 2\pi(hx+ky). \tag{10}$$

As an atom position in the overgrowth island is conveniently expressed in b-coordinates, this argument may be expressed after substituting from the transformation as

$$\begin{aligned} 2\pi(hx+ky) &= 2\pi\,[x_b(hr_{11}c_\theta + kr_{12}s_\theta) + y_b(hr_{21}s_{\theta\beta} + kr_{22}c_{\theta\beta}) \\ &\qquad + hx_0 + ky_0] \\ &= 2\pi\,[x_b p(h,k) + y_b q(h,k) + \varkappa_0] \\ &= 2\pi\,[px_b + qy_b + \varkappa_0]_{hk} \\ &= \mathbf{q}_b\cdot\mathbf{r}_b + \mathbf{q}\cdot\mathbf{r}_0 \quad , \end{aligned} \tag{11a}$$

with

$$\mathbf{q}_b = p\mathbf{b}_1^* + q\,\mathbf{b}_2^* \quad , \tag{11b}$$

where $\mathbf{b}_1^*$ and $\mathbf{b}_2^*$ are reciprocal to $\mathbf{b}_1$ and $\mathbf{b}_2$.

The variables p,q and $\varkappa_0$ have been introduced where

$$p(h,k) = hr_{11}c_\theta + kr_{12}s_\theta$$

and

$$q(h,k) = hr_{21}s_{\theta\beta} + kr_{22}c_{\theta\beta}$$

with

$$2\pi\varkappa_0 = 2\pi(hx_0 + ky_0) = \mathbf{q}\cdot\mathbf{r}_0 \quad . \tag{12}$$

Clearly, p and q are the components of the wave vector **q** expressed in the overgrowth reciprocal lattice. For the sake of clarity,

$$\mathbf{q}(p,q) = \mathbf{q}_b \ , \tag{13}$$

will be used to indicate the wave vector expressed in the overgrowth reciprocal lattice. The variables p and q contain the effect of any change of the overgrowth *orientation* or *unit cell* parameters, relative to the substrate coordinates. τ_0 is affected only by a rigid-body (overall) *translation* of the overgrowth.

The inverse transformation is obtained as

$$h(p,q) = p\,\frac{D_\theta}{r_{11}} + q\,\frac{T_\theta}{r_{12}}$$

and

$$k(p,q) = p\,\frac{T_{\theta\alpha}}{r_{21}} + q\,\frac{D_{\theta\alpha}}{r_{22}} \ . \tag{14}$$

The single adatom at x_b,y_b has a potential energy (of misfit) $V(x_b,y_b)$, given by (from eqns 9, 11 and 12),

$$\begin{aligned} V(x_b,y_b) &= \sum_{h,k=-\infty}^{\infty} V_{hk}\, e^{i2\pi\,[hx(x_b,y_b)+ky(x_b,y_b)]} \\ &= \sum_{h,k=-\infty}^{\infty} V_{hk}\, e^{i2\pi(px_b+qy_b+\tau_0)_{hk}} \\ &= \sum_{h,k=-\infty}^{\infty} V_{hk}\, e^{i\mathbf{q}_b\cdot(x_b\mathbf{b}_1+y_b\mathbf{b}_2)+\mathbf{q}\cdot\mathbf{r}_0} \ . \end{aligned} \tag{15}$$

The number of terms and the choice of coefficients V_{hk} naturally depend on the symmetries required in the substrate.

3.2 MISFIT ENERGY OF A RIGID OVERGROWTH

If one now constructs the island and calculates the misfit energy for each atom and sums over all the overgrowth atoms, one arrives at the misfit energy of the overgrowth island. While the island is rigid,(or the island has homogeneously deformed), the position of each overgrowth atom follows a simple linear formula. This allows the order of summation to be changed around, so that every Fourier term is first summed over all the overgrowth atoms. This form is

easily interpretable and leads to simple row-matching criteria. These will be derived below.

A useful intermediate result, frequently encountered in diffraction theory is the sum of exponential terms of the form,

$$\mathcal{F}_M^{M'}(p) = \sum_{m=-M}^{M'} e^{i2\pi\, mp} = \sum_{m=-M}^{M'} e^{i\mathbf{q}_b \cdot m\mathbf{b}_1}$$

$$= \frac{\sin \pi(M+M'+1)p}{\sin \pi p} \cdot e^{i\pi(M'-M)p} \,. \qquad (16$$

Consider an island constructed in the following way:

Translate a lattice point (the origin) M times by $\mathbf{b}_1$, and M times by $-\mathbf{b}_1$, so that *there are* 2M *unit cells lying along the* $\mathbf{b}_1$ *direction.* Repeat this row of lattice points 2N times along the $\mathbf{b}_2$ direction in the same manner as before *to yield* 2Mx2N *unit cells.* After placing an atom at each lattice point, this island contains

$$G = (2M+1) \times (2N+1) \qquad (17$$

lattice atoms. The m,n'th atom is then located at

$$\mathbf{r}_b^{m,n} = m\,\mathbf{b}_1 + n\,\mathbf{b}_2 \,, \qquad (18$$

where m and n run from -M to M and -N to N respectively. The contribution to the misfit energy of this atom due to the h,k'th Fourier term is

$$V_{hk}\, e^{i2\pi(px_b+qy_b+\gamma_0)hk} = V_{hk}\, e^{i2\pi(pm + qn +\gamma_0)hk} \,. \qquad (19$$

Summing over all the atoms in the island gives the contribution of the h,k'th Fourier term as

$$\varepsilon_{hk}^0 = V_{hk} \sum_{m=-M}^{M} \sum_{n=-N}^{N} e^{i2\pi(pm + qn + \gamma_0)hk}$$

$$= V_{hk}\, e^{i2\pi\gamma_0} \sum_{m=-M}^{M} e^{i2\pi\, pm} \cdot \sum_{n=-N}^{N} e^{i2\pi\, qn}$$

$$= V_{hk}\, e^{i2\pi\gamma_0}\, \mathcal{F}_M^M(p) \cdot \mathcal{F}_N^N(q)$$

$$= V_{hk}\, e^{i2\pi\gamma_0}\, \frac{\sin \pi(2M+1)p}{\sin \pi p} \cdot \frac{\sin \pi(2N+1)q}{\sin \pi q}$$

$$\equiv V_{hk}\, e^{i2\pi\gamma_0}\, \mathcal{FQ}^1(M,p) \cdot \mathcal{FQ}^1(N,q) \,, \qquad (20$$

where the quotient of the sines with argument 2M+1 has been denoted by $\mathcal{F}Q^1$.

Non-primitive structures

Frequently additional (basis) atoms are required in the unit cell, which allow other symmetries to be constructed from the underlying lattice symmetry. Consider the contribution to the misfit energy of the atom at $x_b^\dagger, y_b^\dagger$ (both > 0) referred to the m,n'th unit cell, and located at $m+x_b^\dagger, n+y_b^\dagger$ in the island coordinates. The h,k'th Fourier term contributes, analogous to eqn 19,

$$V_{hk}^\dagger e^{i2\pi(pm + qn + \gamma_0^\dagger)_{hk}} . \qquad (21$$

Here $V_{hk}^\dagger$ refers to the potential experienced by the non-lattice atom, which may be a different type to the lattice atom, while

$$\gamma_0^\dagger(h,k) = \gamma_0 + px_b^\dagger + qy_b^\dagger . \qquad (22$$

Usually $V_{hk}^\dagger = \kappa V_{hk}$ for all Fourier harmonics so that κ is an overall calibration factor.

The complete island may now be constructed from the combination of lattice and basis atoms by the addition of a basis atom to each lattice atom. However with the basis atom displaced from the lattice atom in the same way for each pair, a mirror or two-fold symmetry inherent in a centred lattice, for example, would be destroyed. Two methods for constructing an island which retains the inherent mirror symmetry may be conceived. The first method results in an island with more lattice atoms than basis atoms, while the second results in an island with more basis atoms than lattice atoms. Naturally the misfit energy will differ slightly in each of the three cases for a finite island, asymmetric, excess lattice and excess basis atoms, but for an infinite island these differences disappear.

Island with an excess of lattice atoms

The additional atoms are added to the interior of every unit cell in the island, giving a total of (2M)X(2N) basis atoms at the

positions $m+x_b^+, n+y_b^+$, where m and n run from -M to M-1 and -N to N-1 respectively. The misfit energy due to the basis atoms is then

$$\varepsilon_{hk}^+ = \kappa V_{hk}\, e^{i2\pi[\gamma_0+p(x_b^+-\frac{1}{2})+q(y_b^+-\frac{1}{2})]}\, \frac{\sin\pi(2M)p}{\sin\pi p}\cdot\frac{\sin\pi(2N)q}{\sin\pi q}\ . \qquad (23$$

Therefore, the misfit potential energy of an island with centre at x_0, y_0 in the substrate coordinates and (2M)X(2N) *unit cells*, each containing a lattice and a basis atom, (and further lattice atoms at the upper and right edges) with

$$G = (2M+1)X(2N+1) + (2M)X(2N)$$

atoms, is, using eqns 20 and 23,

$$\begin{aligned}\varepsilon_G &= \sum_{h,k}\varepsilon_{hk} = \sum_{h,k}(\varepsilon_{hk}^0 + \varepsilon_{hk}^+)\\ &= \sum_{h,k} V_{hk}\, F^0 \left\{\frac{\sin\pi(2M+1)p}{\sin\pi p}\cdot\frac{\sin\pi(2N+1)q}{\sin\pi q} + \right.\\ &\qquad \left. + F^+ e^{-i\pi(p+q)}\,\frac{\sin\pi(2M)p}{\sin\pi p}\cdot\frac{\sin\pi(2N)q}{\sin\pi q}\right\}_{hk}\\ &= \sum_{h,k} V_{hk}\, F^0 \left\{(1+F^+)\frac{\sin\pi(2M+1)p}{\sin\pi p}\cdot\frac{\sin\pi(2N+1)q}{\sin\pi q} - F^+\mathcal{F}(M,N)\right\}_{hk}\ . \end{aligned} \qquad (25$$

For the last expression, the same island was constructed from (2M+1)X(2N+1) *unit cells* and the basis atoms from the upper and right-hand edges were subtracted. Introduced here are the structure factors:

$$F^0 = e^{i2\pi\gamma_0} = e^{i\mathbf{q}\cdot\mathbf{r}_0} \qquad (26a$$

for the lattice atom, and

$$[1 + F^+(p,q)]_{hk} = [1 + \kappa\, e^{i2\pi(px_b^+ + qy_b^+)}]_{hk}\ , \qquad (26b$$

due to the basis atom in each unit cell, and the term:

$$\mathcal{F}(M,N)_{hk} = \left\{e^{i2\pi(Mp+Nq)}\left[e^{-i\pi(2M+1)p}\,\frac{\sin\pi(2M)p}{\sin\pi p} + \right.\right.$$
$$\left.\left. + e^{-i\pi(2N+1)q}\,\frac{\sin\pi(2N)q}{\sin\pi q} + 1\right]\right\}_{hk} \qquad (27$$

corrects for the unwanted basis atoms at the edges. This correction term may be neglected for larger islands, in which M and N become large, as these terms are at most $\approx$ 2M or 2N, while the dominant term approaches (2M+1)X(2N+1).

Island with an excess of basis atoms

The second type of symmetrical island (the type shown in figure 3.2 for the bcc{110} island) is the type which is in fact useful for implementation of the boundary conditions of Chapter 5, and will therefore be used in subsequent expressions in Chapter 4, and the finite island misfit energy calculations of this chapter. Primarily the difference of course arises from the choice whether the origin is at a lattice or non-lattice position.

In the second method symmetry is restored by adding basis atoms along the lower and left edges when the island is constructed from 2MX2N *unit cells*. Equivalently, removing lattice atoms from the lower and left edges of an island constructed from (2M+1) X (2N+1) *unit cells* yields the same island.

The misfit energy of a symmetric island constructed from 2M *unit cells* repeated in the $\mathbf{b}_1$-direction and 2N *cells* in the $\mathbf{b}_2$-direction, and symmetrized by the *addition* of nonlattice atoms along the lower and left hand edges is, per interfacial atom,:

$$\varepsilon_G = \sum_{h,k} V_{hk} F^0 \left\{ (1+F^+) \frac{\sin \pi(2M+1)p}{\sin \pi p} \cdot \frac{\sin \pi(2N+1)q}{\sin \pi q} + F^+ \mathcal{G}(M,N) \right\}_{hk} . \quad (28$$

The structure factors have the same form as above and the term:

$$\mathcal{G}(M,N)_{hk} = \left\{ e^{-i2\pi[(M+1)p+(N+1)q]} \left[e^{i2\pi(M+1)p} \frac{\sin \pi(2M+1)p}{\sin \pi p} + e^{i2\pi(N+1)q} \frac{\sin \pi(2N+1)q}{\sin \pi q} + 1 \right] \right\}_{hk} \quad (29$$

corrects for the additional basis atoms at the lower and left edges.

The behaviour of the misfit energy (per interfacial atom) is illustrated in figures 3.3 and 3.4 for the island M=N=11, with basis atoms at $x_b^+ = y_b^+ = \frac{1}{2}$.

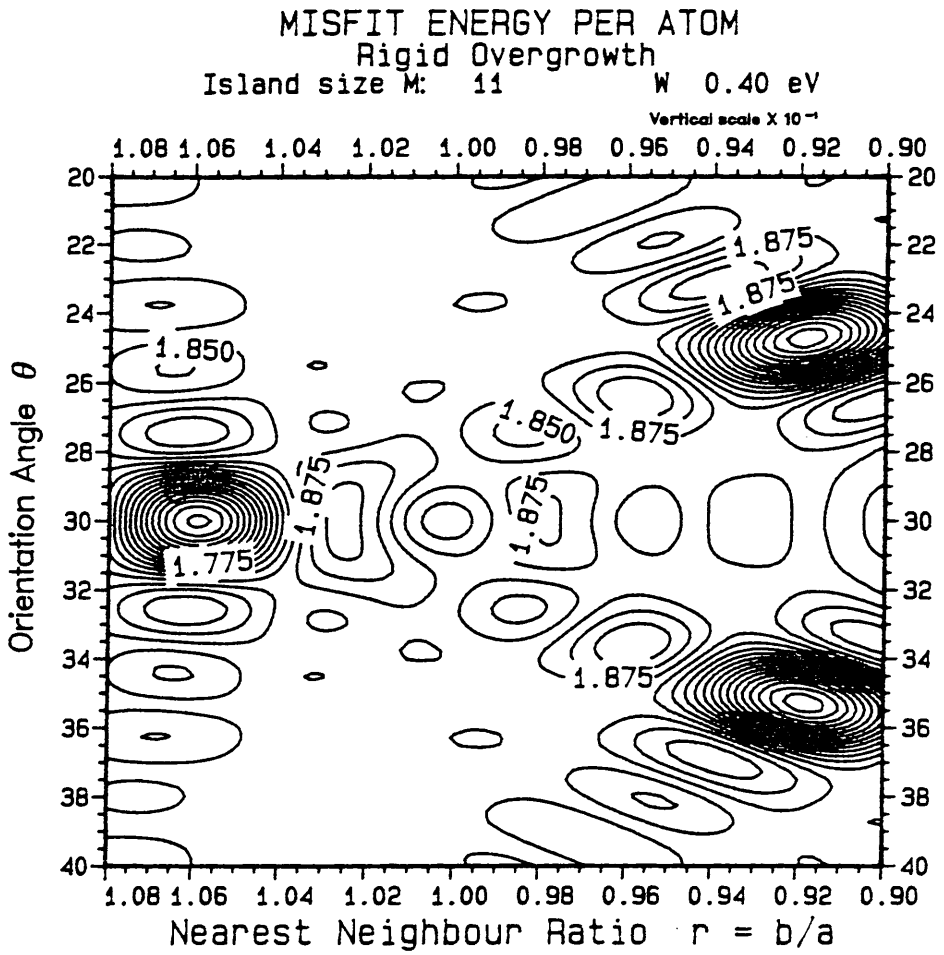

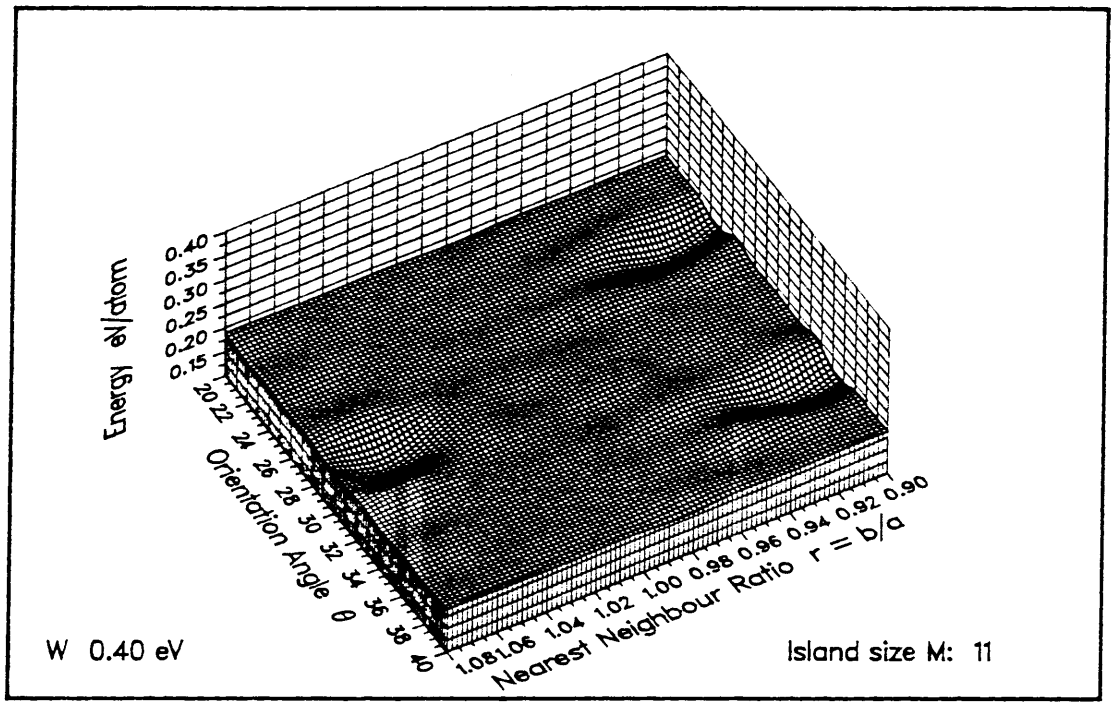

Figure 3.3(a) The misfit energy per atom for the island used in subsequent chapters. $A_{11} = 0$ $\Delta = \frac{1}{2}$ $M = N = 11$

Note the secondary minima radiating from the dominant minima at the ideal epitaxial configurations.
Substrate parameters are those of equation 2.51(b) and (c)

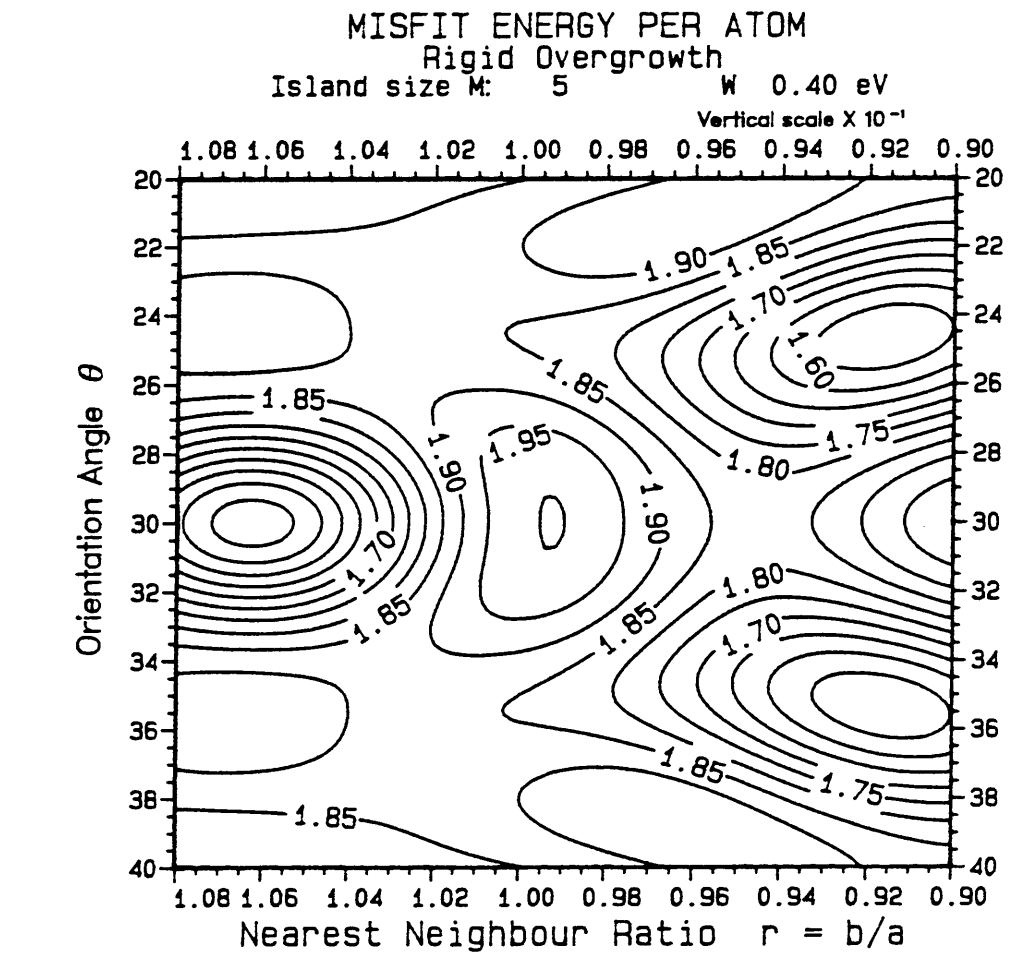

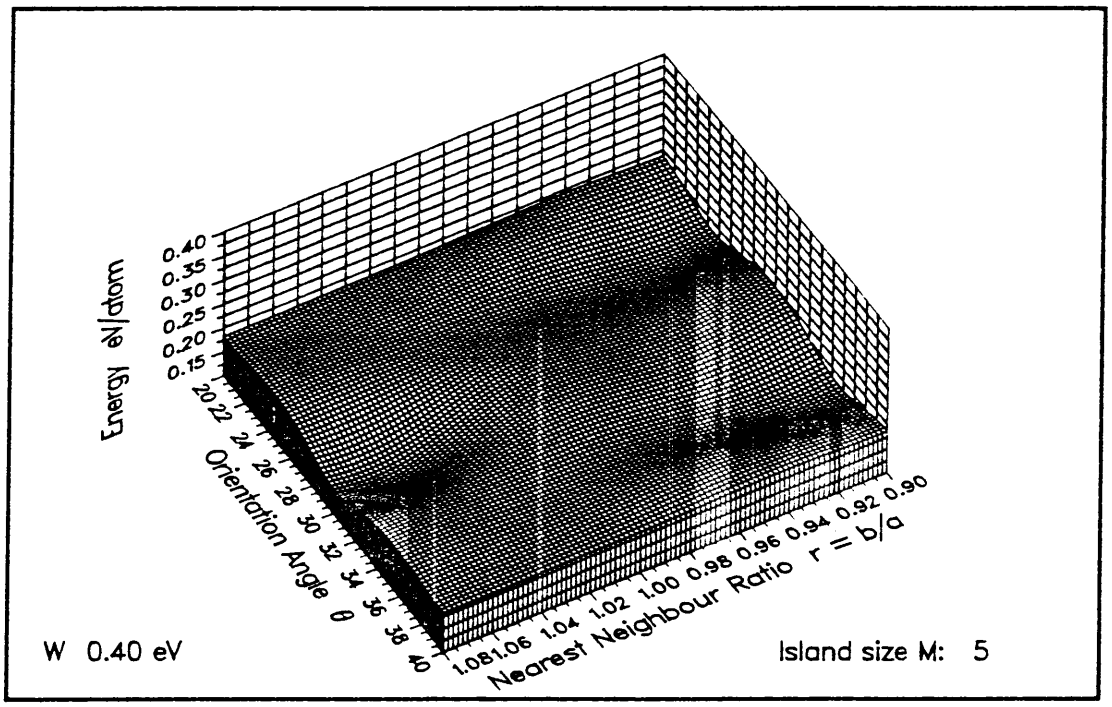

Figure 3.3(b) As in 3.3(a) illustrating the effect of the size of the island. $A_{11} = 0$ $\Delta = \frac{1}{2}$ $M = N = 5$

Note the width of the energy minima around the ideal epitaxial configurations and the widely spaced secondary minima.

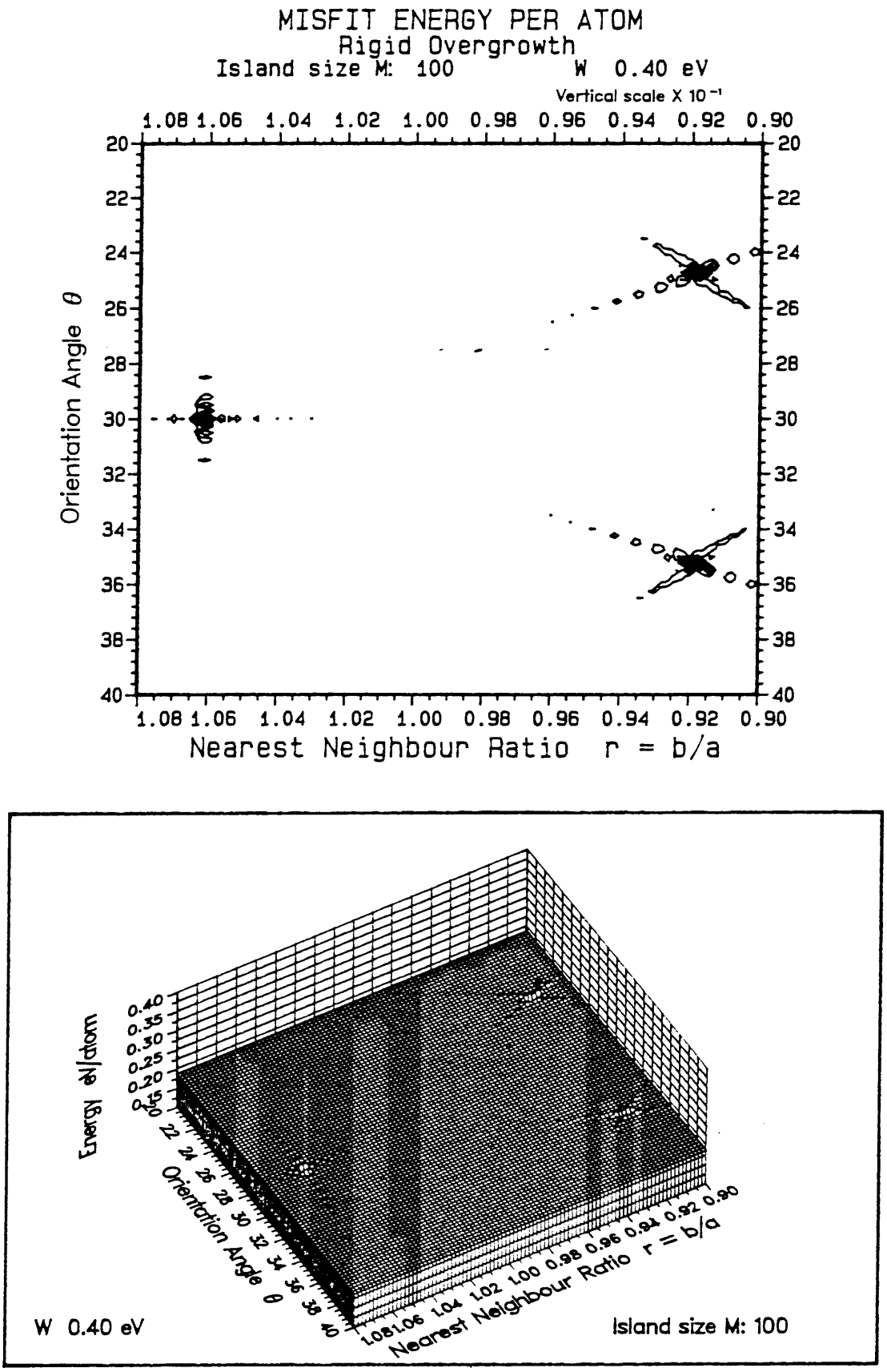

Figure 3.3(c) As in 3.3(a) illustrating the effect of the size of the island. $A_{11} = 0$ $\Delta = \frac{1}{2}$ $M = N = 100$

Note the extreme narrowness of the minima at the ideal epitaxial configurations and the almost featureless plateau away from the ideal configurations. The secondary minima are extremely shallow and close

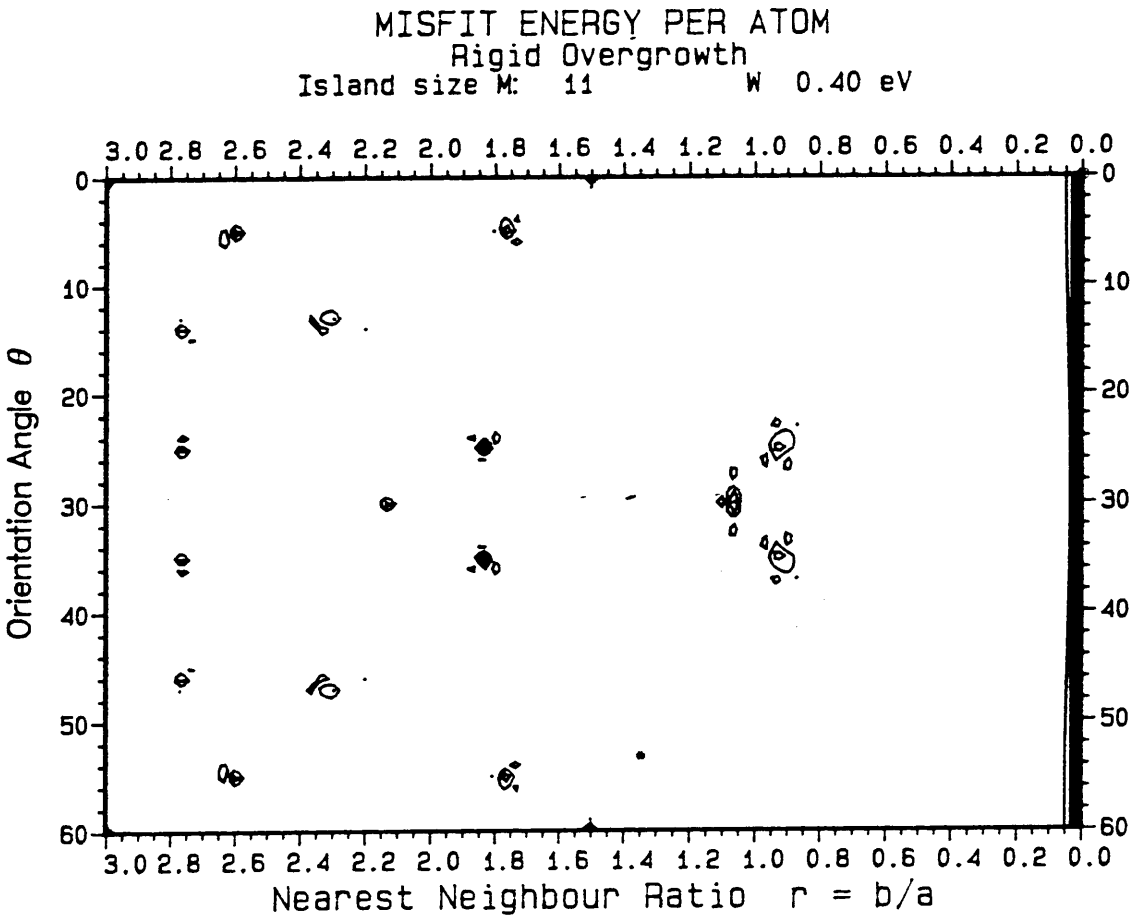

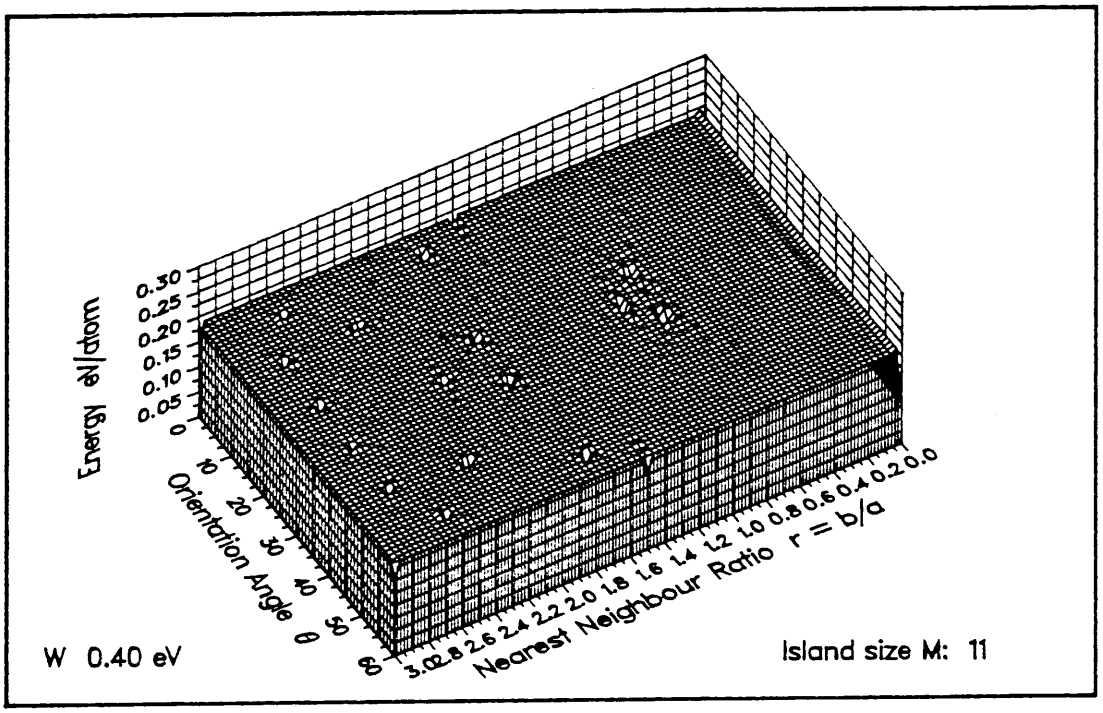

Figure 3.4(a) Same island as in Figure 3.3(a) $A_{11} = 0$ $\Delta = \frac{1}{2}$ showing a wide range of configurational parameters.

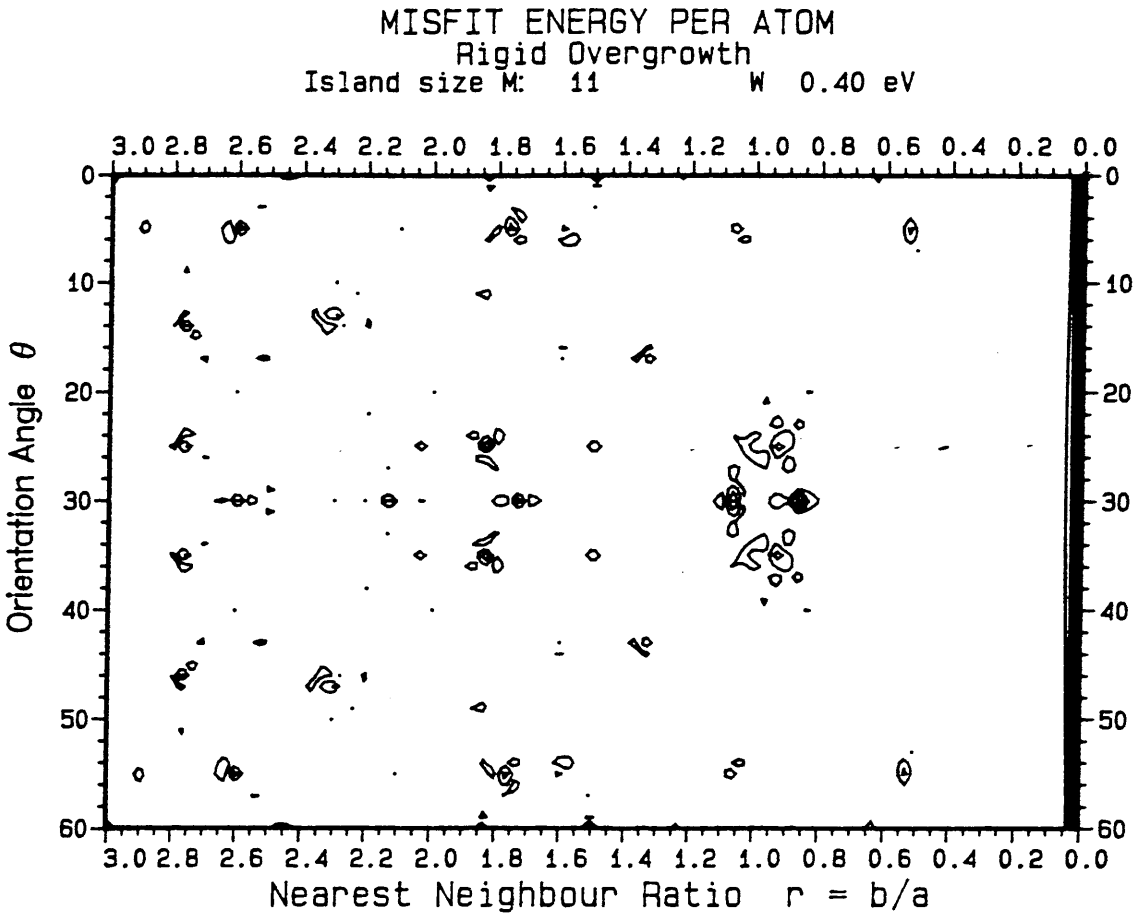

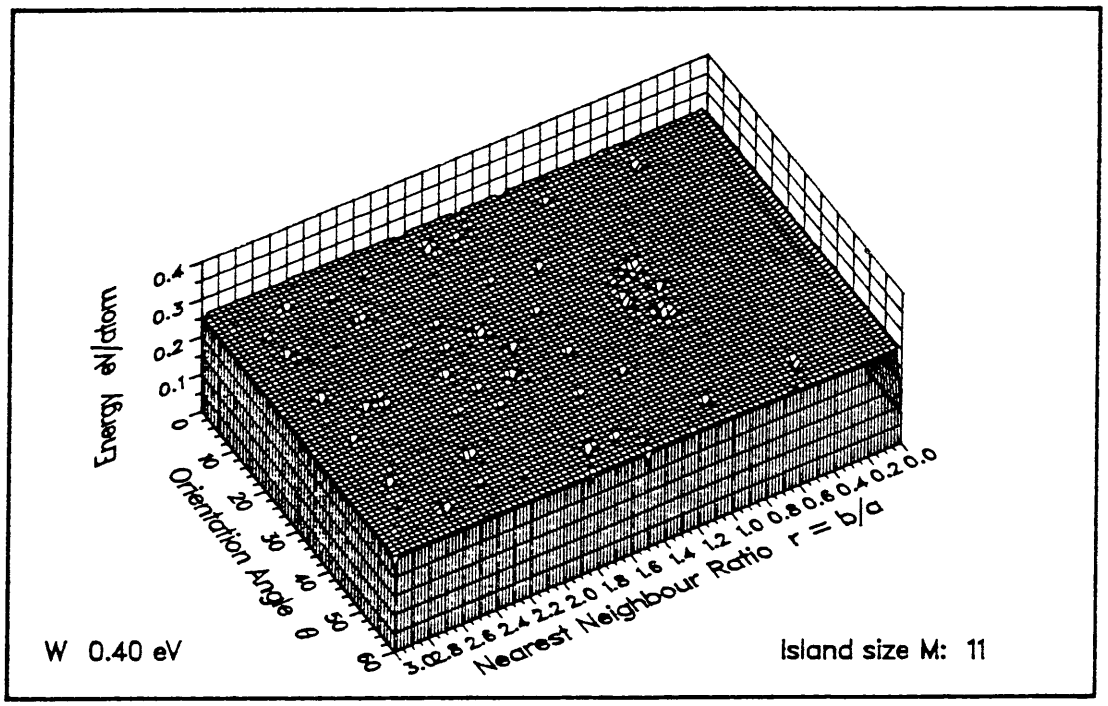

Figure 3.4(b) Same island as in Figure 3.4(a) and 3.3(a) but showing the effect of second order substrate terms $A_{11}/A_{10} = -1/3$ $\Delta = \frac{1}{2}$

Other islands

With $\mathcal{F} = \mathcal{G} = 0$ in the expressions above, eqns 25 and 28, the misfit energy of the asymmetric island with the same number of lattice and basis atoms is arrived at, while $F^+ = 0$ results in the energy of an island without basis atoms.

Clearly additional basis atoms can be accommodated by adding structure factors, so that

$$F^+ = \sum_j F^{(j)} = \sum_j \kappa_j \, e^{i2\pi[px_b^{(j)} + qy_b^{(j)}]}, \qquad (30$$

with the summation being taken over all the basis atoms in a single unit cell, with the j-th basis atom at $x_b^{(j)}, y_b^{(j)}$ in the unit cell.

Trigonometric potential expression

The expressions for the total misfit energy are easily modified for the potential expressed as expansions in the trigonometric functions. Cosine series yield the real parts of the preceding expressions, and sine series the imaginary parts. Clearly the quotients $\mathcal{F}(M,p) \equiv \sin \pi(2M)p/\sin \pi p$, $\mathcal{F}^1$ etc are not affected by the type of expansion, although the structure factors are, becoming cosine terms for a cosine subsrate potential and sine terms for a sine expansion.

3.3 SELECTION OF IDEAL EPITAXIAL CONFIGURATIONS

General Considerations

The structure dependent terms F^+ need to be known for interpretation, although some general conclusions may be drawn purely from the quotients at this stage.

Clearly critical values of the total misfit energy will occur when p and q are simultaneously integers, as then the denominators sin πp and sin πq become zero:

This means that a lattice translation vector in the substrate reciprocal lattice must also be a translation vector of the overgrowth reciprocal lattice for ideal epitaxy to occur, hence,

$$\mathbf{q}^{pq} = \mathbf{q}_{hk} \quad , \text{ with p,q,h,k all integer.} \qquad (31$$

This is a necessary condition for epitaxy in an ideal configuration, minimizing the misfit energy, and defines the concept of an *Ideal Epitaxial Configuration*, within the rigid model.

Here there is a clear analogy with the diffraction conditions due to von Laue (Busch *e.a.* 1976, Kittel 1966) in crystallography. This simple result has some far reaching consequences.

Consequences

(I) Shared wave vector implies parallel lattice rows.

Suppose that the reciprocal lattice vector shared by both reciprocal lattices is the vector $\mathbf{q}$, with (integer) components h,k *and* p,q in the substrate and overgrowth reciprocal lattices respectively. If one further considers that the wave vectors are normal to wave fronts, which in this case coincide with rows of lattice points, then these rows may be identified in several ways. The components of the wave vectors themselves provide indices analogous to Miller-indices of planes in 3-dimensional crystals. Alternatively, the direction along the rows is easily determined by the condition (analogous to the zone-law) that these directions are also perpendicular to the wave vector.

It is always true that the wave vector,

$$\mathbf{q} = [h\ k]^{*} \perp [k\ \bar{h}], \qquad (32$$

where the notation [ ] indicates a direction in the lattice, and [ ]* indicates direction in the reciprocal lattice. In keeping with normal practice the overbar "$\bar{h}$" is used to indicate a negative index $-h$. Hence the lattice row $(h\ k)$ lies along the direction $[k\ \bar{h}]$.

The same is true of the overgrowth lattice rows. In the overgrowth the reciprocal lattice vector with components p,q is perpendicular to the row indexed as $(p\ q)_b$ and lying along the lattice direction $[q\ \bar{p}]_b$, where the subscript has been introduced to indicate an overgrowth lattice direction.

Necessarily, as the vector $\mathbf{q}$ is perpendicular to rows in the substrate and the overgrowth simultaneously, these rows must be *parallel* in the ideal epitaxial orientation.

(II) Parallel rows must have the same spacing.

The spacing between matching rows is also easily determined from the wave vector, as

$$d_{hk} = \lambda_{hk} = \frac{2\pi}{|\mathbf{q}(h,k)|} = 2\pi \div \sqrt{h^2\mathbf{a}_1^*\cdot\mathbf{a}_1^* + 2hk\mathbf{a}_1^*\cdot\mathbf{a}_2^* + k^2\mathbf{a}_2^*\cdot\mathbf{a}_2^*}\ , \qquad (33a$$

for the wave vector expressed in the substrate reciprocal lattice, and as

$$d^{pq} = \lambda^{pq} = \frac{2\pi}{|\mathbf{q}(p,q)|} = 2\pi \div \sqrt{p^2\mathbf{b}_1^*\cdot\mathbf{b}_1^* + 2pq\mathbf{b}_1^*\cdot\mathbf{b}_2^* + q^2\mathbf{b}_2^*\cdot\mathbf{b}_2^*}\ , \qquad (33b$$

in the overgrowth reciprocal lattice. For the ideal lattice epitaxial configuration,

$$d_{hk} = d^{pq}\ . \qquad (33c$$

This means in practice that the spatial period of rows of atoms which are brought into parallel orientation must be equal in substrate and overgrowth crystals. (This requirement is the analog of the Bragg condition of crystallography)

(III) Misfit in directions perpendicular to the matched rows is Zero.

Misfit is frequently related to the direction of accommodation, so if the x-directions are brought into match this is usually expressed as $f_x = (b_x - a_x)/a_x = 0$. Because of the condition of equal spacing of matched rows, the misfit in a direction perpendicular to the rows must be

$$f_{hk}^{pq} = (d^{pq} - d_{hk})/d_{hk} = 0 \qquad (34$$

This zero misfit direction may often be indexed as a lattice displacement vector, but not always. This fails in particular, if the direct axes are skew, as there is not always a low index direction available in the lattice which is parallel to a given reciprocal lattice vector. The direction in the substrate direct lattice parallel to the matching wave vector would satisfy

$$[u\ v] \perp [k\ \bar{h}] \text{ , i.e., } \qquad (35a$$

$$uk - vh(a_2/a_1)^2 + (vk-uh)(a_2/a_1)\cos\alpha = 0 .$$

From this it follows that

$$u[k-h(a_2/a_1)\cos\alpha] = v[h(a_2/a_1)^2-k(a_2/a_1)\cos\alpha] \text{ ,}$$

with a useful solution

$$u = h(a_2/a_1)^2 - k(a_2/a_1)\cos\alpha \quad , \quad v = k - h(a_2/a_1)\cos\alpha . \qquad (35b$$

A simple lattice direction however does exist if $(a_2/a_1)^2$ and $(a_2/a_1)\cos\alpha$ are rational so that u and v can be scaled to integer values. For the common case for which a rectangular unit cell can be constructed, (as then $\cos\alpha = 0$), the equations all simplify somewhat. Rectangular unit cells (not necessarily primitive cells) can always be constructed for a 2-dimensional Bravais lattice if either a mirror line or equivalently a two-fold axis lies *in* the plane (Kittel 1966, Strozier 1975). This symmetry occurs on all except the *Oblique* 2-dimensional lattice type which has at most a two-fold axis perpendicular to but not in the plane.

Similar considerations naturally apply to the overgrowth.

(*IV*) ***Construction.*** (Refer to figure 3.5)

A construction, analogous to the well-known Ewald construction, may be designed which allows the quick determination of whether a substrate row of atoms can be brought into coincidence with a row in the overgrowth. This also simplifies the qualitative discussion pertaining to these considerations in real crystals.

(*i*) *Choose the substrate lattice row which is to be matched with the overgrowth. Express this direction in terms of the substrate direct lattice direction* $[k\ \bar{h}]$.

(*ii*) *Determine the substrate reciprocal lattice vector normal to this row,* $\mathbf{q} = [h\ k]^*$. *Plot this vector to a suitable scale in the substrate reciprocal lattice. The effect (if such a term exists) of the substrate structure factor*

$$F_{hk} \equiv 1 + \Delta\, e^{-i2\pi(hx^+ + ky^+)} = 1 + F^+_{hk}\ , \qquad (36$$

(from Chapter 2, eqn 2.8) *associated with each potential term as* $V_{hk}\, F_{hk}\, e^{i\mathbf{q}\cdot\mathbf{r}}$ *must be included at this stage.*

(*iii*) *Plot the overgrowth reciprocal lattice to the same scale and with the origin at the start of the vector* $\mathbf{q}$. *Incorporate all selection rules required by the structure factor* (from eqns 26 and 30)

$$F^{pq} \equiv F^o(1+F^+). \qquad (37$$

(*iv*) *Draw a circle centred at the origin, and through the end of* $\mathbf{q}$. *This circle forms the locus of the end-point of* $\mathbf{q}$ *when this vector is rotated through* 360°.

Any reciprocal lattice point which lies on this circle will describe an overgrowth reciprocal lattice translation vector, equal in length to $\mathbf{q}$. *When the overgrowth lattice is rotated so that a lattice point lying on the circle will coincide with* $\mathbf{q}$, *the overgrowth and substrate* atomic *rows with the same spacings in both lattices and perpendicular to the vector* $\mathbf{q}$ *will be parallel and*

in an Ideal Epitaxial Configuration. *The reciprocal lattice vector* **q** *with its components in the respective lattices uniquely defines the appropriate atomic rows and their orientations.*

The overgrowth structure factor

$$F^{pq} = F^0[1+F^+(p,q)] \qquad 35'$$

must be included, as this represents extra atomic rows between the lattice rows, which may cancel the misfit energy gain exactly, or largely as $F^0(1\pm\kappa)$, so that in analogy with diffraction theory, where the structure factor causes selection of diffraction conditions, some ideal configurations suitable for the lattice island are not suitable once the basis atoms are added to the island. For the same reason, the effect of the substrate structure factor

$$F_{hk} = 1 + F^+(h,k) = 1 + F^+_{hk} \qquad (36'$$

must be taken into account during the selection of the substrate reciprocal lattice vector **q**. This assures that matching of *atomic* rows, as opposed to lattice rows in fact defines Ideal Epitaxial Configurations.

(V) *Broadening of reciprocal lattice points with a decrease in island size.*

Away from the critical states, the delta-function behaviour of the quotients $\mathfrak{f}\mathfrak{q}^1$ (in eqns 25 and 28) assures a rather featureless plateau of misfit energy, particularly for large islands. This is shown in figure 3.3. For small islands the critical states are broadened, with undulations of decreasing amplitude as p and q deviate from ideality. The wavelength of these undulations is proportional to 2/(2M+1), effectively the width of the principle potential well.

This has the effect of broadening the size of the overgrowth reciprocal lattice points to families of concentric circles (or rectangles for a rectangular island), allowing epitaxial orientations away from the ideal value, and possibly matching conditions dictated by secondary rather than the central minimum.

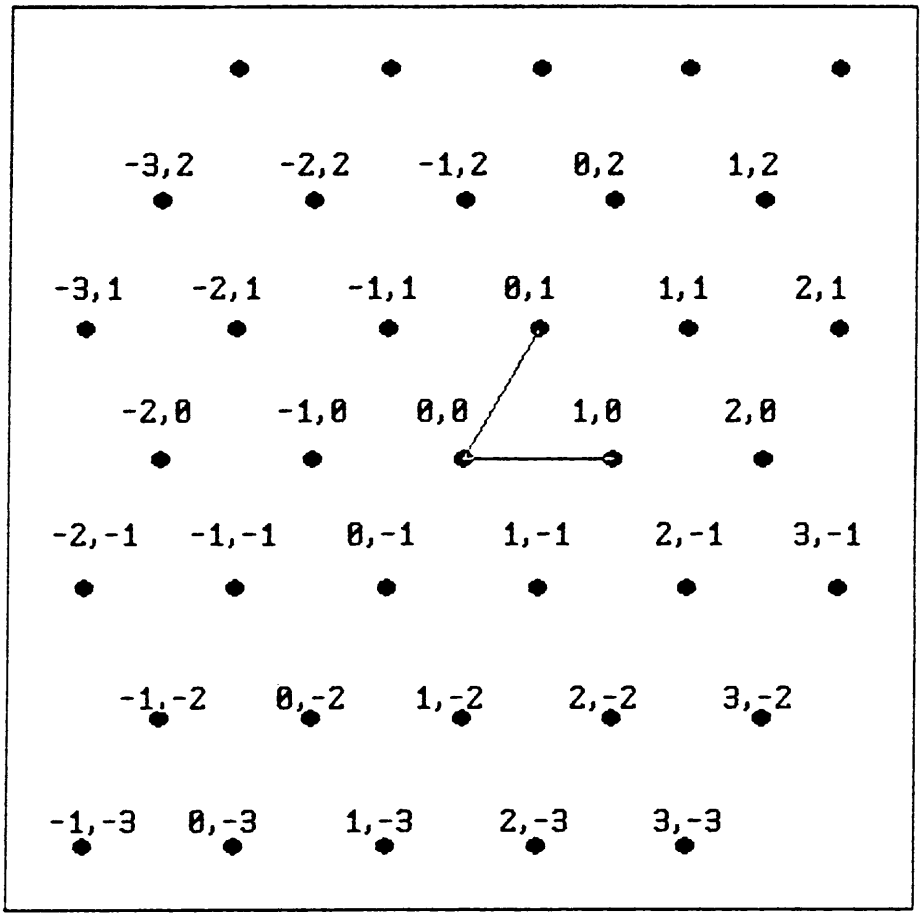

Figure 3.5(a) Reciprocal lattice of the substrate surface

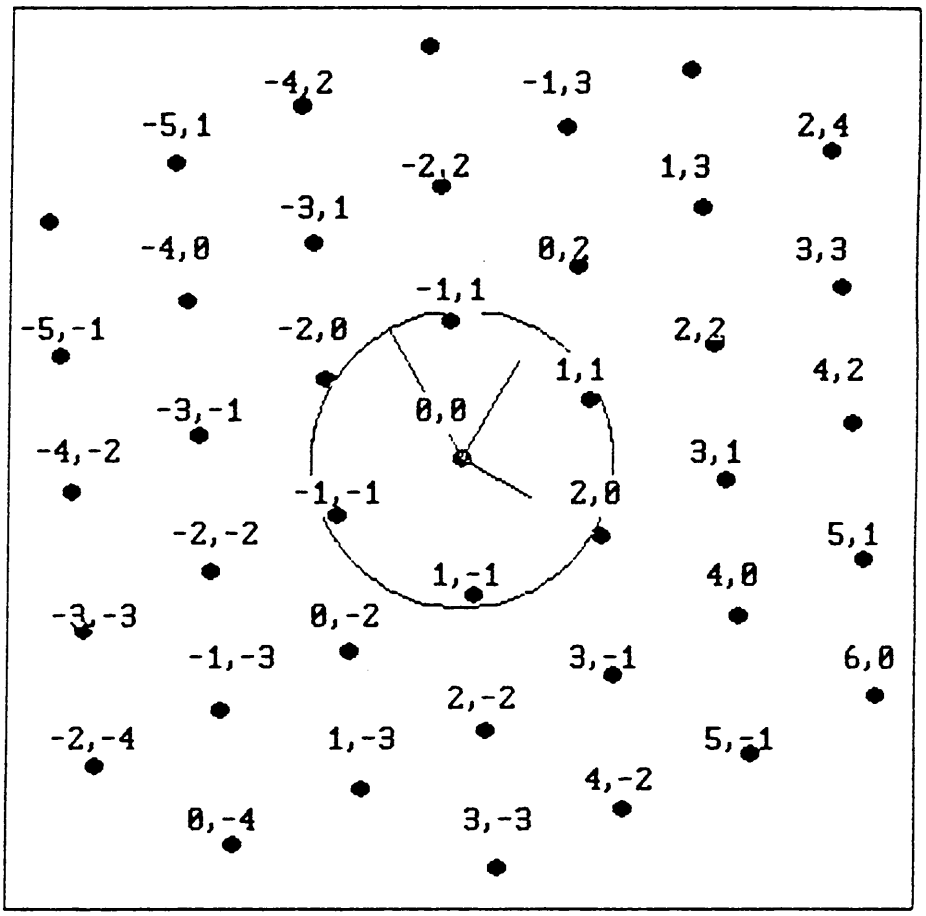

Figure 3.5(b) Reciprocal lattice of the overgrowth surface showing the "Ewald" circle passing through the end of the substrate reciprocal lattice vector $[\bar{1}\ 1]^*_a$, shown.

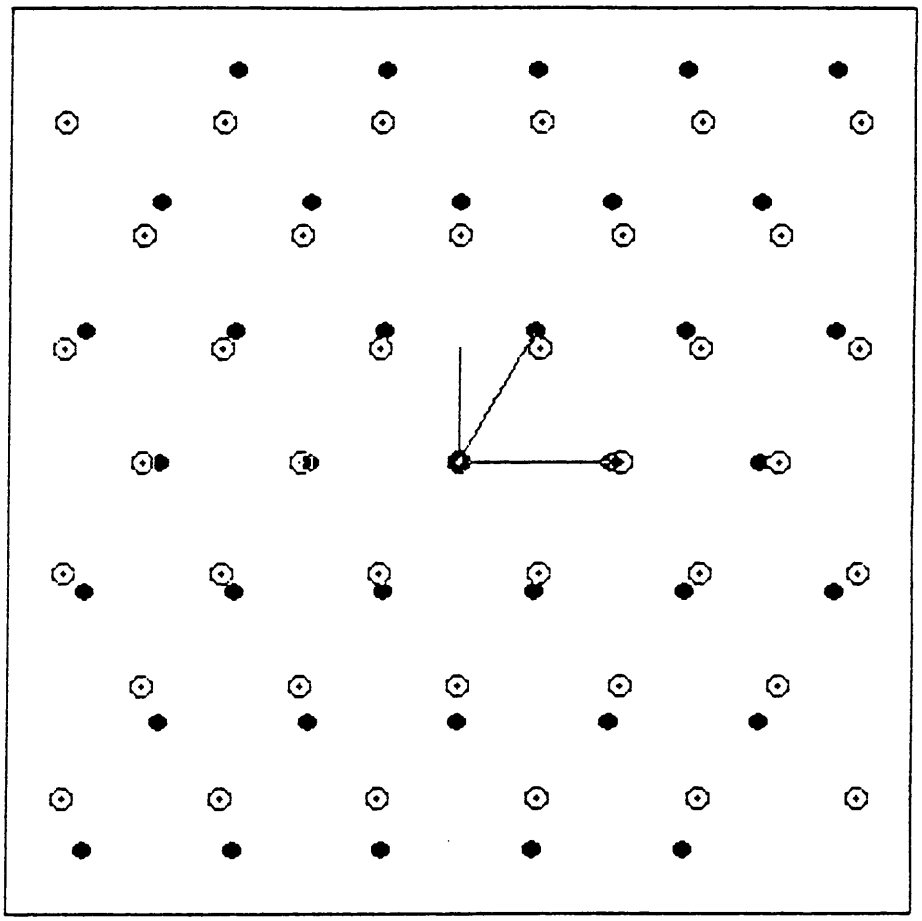

Figure 3.5(c) Superposed substrate and overgrowth reciprocal lattices for nearest neighbour ratio $r = b_{nn}/a_{nn} = 1$, orientation $\theta = 30^{\circ}$. This figure may be obtained by superposition and rotation of figures 3.5(a) and (b).

The size of the spot parallels the effect of the optical diffraction pattern of a small opening in relation to a large one.

This means that for small islands, the matching criteria are somewhat relaxed, so that these crystals may orient towards a scattering of orientations early in their growth, possibly coinciding with the ideal orientation, even if their lattice parameters deviate from the ideal values.

Degree of misfit in non-ideal and real systems

Most generally, real systems will not conform exactly to the nearest neighbour ratios required for ideal epitaxy, and in fact $d_{hk} \neq d^{pq}$, where h,k are components of a substrate reciprocal lattice translation vector $\mathbf{q}_{hk}$, and p,q are the components of an overgrowth reciprocal lattice point $\mathbf{q}^{pq}$ lying close to the circle in the construction. (All components are integer in this case.) In order to achieve epitaxy, the discrepancy needs to be made up by distortion of the overgrowth reciprocal lattice until the point lies on the circle, or the introduction of misfit dislocations. How the lattice will distort will depend on the amount of energy needed in the process, and the degree of anisotropy in the elastic constants. This problem will be addressed in the next two chapters.

Assuming that the overgrowth and substrate are oriented so that $\mathbf{q}^{pq}$ is parallel to $\mathbf{q}_{hk}$, the only misfit is dimensional in that direction. The misfit which needs to be accommodated by the system is given by the ratio of the difference in the row spacing, to the spacing between the rows in the substrate as:

$$f_{hk}^{pq} = \frac{d^{pq} - d_{hk}}{d_{hk}} = \frac{\lambda^{pq} - \lambda_{hk}}{\lambda_{hk}} = \frac{1/|\mathbf{q}^{pq}| - 1/|\mathbf{q}_{hk}|}{1/|\mathbf{q}_{hk}|} = \frac{|\mathbf{q}_{hk}|}{|\mathbf{q}^{pq}|} - 1 \quad . \quad (38$$

It follows that the degree of change of lattice parameters necessary can be expressed as the length ratio, or as the misfit, depending on convenience. In terms of the geometric construction,

these quantities are determined simply from the lengths of the reciprocal lattice vectors.

For the important case where the change in lattice parameter is achieved as an overall (isotropic) change of scale, the ratio $|\mathbf{q}^{pq}|/|\mathbf{q}_{hk}|$ directly gives the factor by which the nearest neighbour ratio $r = b_{nn}/a_{nn}$ must be multiplied.

If the vectors $\mathbf{q}^{pq}$ and $\mathbf{q}_{hk}$ are not parallel, the angle between the vectors provides the angle through which the overgrowth needs to rotate in relation to the substrate to achieve epitaxy. This angle θ_R may be shown from vector algebra to be given by:

$$\cos(\theta_R) = \frac{\mathbf{q}_{hk} \cdot \mathbf{q}^{pq}}{|\mathbf{q}_{hk}| \cdot |\mathbf{q}^{pq}|} \quad , \tag{39}$$

which can be seen directly from the reciprocal space construction. The sense is obtained from the vector cross product.

Finally, the epitaxial orientations are normally expressed as crystallographic directions which are parallel, in terms of the three-dimensional basis vectors of the bulk crystal. The conversion from the local 2-dimensional basis vectors $\mathbf{a}_1$ and $\mathbf{a}_2$ is straight-forward. For example consider the vectors:

$$\mathbf{a}_1 = \langle u\ v\ w \rangle \quad \text{and} \quad \mathbf{a}_2 = \langle U\ V\ W \rangle \ . \tag{40a}$$

The reciprocal lattice vector $[h\ k]^*$, conforms to the lattice row $[k\ \bar{h}]$, (eqn 32) so that the appropriate direction is

$$k\mathbf{a}_1 - h\mathbf{a}_2 = \langle ku-hU\ \ kv-hV\ \ kw-hW \rangle \ . \tag{40b}$$

Similar considerations apply to the overgrowth crystallographic directions.

3.4 APPLICATION TO SOME SPECIAL SYSTEMS

fcc{111}/fcc{111} epitaxial system

The basis vectors, unit cell structure, transformations and other relevant rigid model parameters for this system are given in Table 3.1. From the reciprocal space construction the possible overgrowth/substrate row matching orientations are rapidly determined. Because both overgrowth and substrate have the same structure, the strongest reduction in misfit energy is possible (not surprisingly) when the nearest neighbour distances, and hence the unit cells, are the same. Other possibilities are evident once this criterion is not satisfied, however, but matching then occurs among relatively high-index directions. The possible orientations as predicted from the row-matching criterion, are summarised in Table 3.2.

As discussed in Chapter 2, the Fourier amplitudes of higher orders in the adatom-substrate interaction potential are somewhat less than the fundamental, and lowest orders. The tendency to epitaxy is decided by how much the interfacial energy may be lowered by minimizing the misfit through assuming an epitaxial orientation. This energy gain is heavily dependent on the Fourier coefficients - physically by the actual nature of the overgrowth-substrate interaction. In this epitaxial system, without overgrowth basis atoms, the only relevant structure factors are the substrate stacking fault term, and the F^0 displacement term. While the structure factor is used to induce asymmetry, the parts of the Fourier expansion other than this factor may have the full symmetry of the lattice. Since all Bravais lattices have inversion symmetry, a cosine expansion is suitable and correspondingly only the real parts of the structure factors F_{hk} and F^0 are involved. These have sufficiently simple forms to be easily interpreted.

$$\mathrm{Re}(F^0) = \cos 2\pi\left(h\tfrac{2}{3} + k\tfrac{1}{3}\right) = \begin{cases} 1 & 2h+k = 3m \quad ,m \text{ any integer} \\ -\tfrac{1}{2} & \text{otherwise} \end{cases} . \qquad (41$$

Table 3.1 Parameters for the fcc{111}/fcc{111} epitaxial system.

Substrate Lattice

$\mathbf{a}_1 = \frac{1}{2}\langle\bar{1}\ 1\ 0\rangle a_o$ $\qquad$ $\mathbf{a}_2 = \frac{1}{2}\langle 0\ \bar{1}\ 1\rangle a_o$

$|\mathbf{a}_1| = |\mathbf{a}_2| = \frac{a_0}{\sqrt{2}} = a_{nn}$, *where* a_o *is the cubic lattice parameter and* $\alpha = 120^\circ$

Position of minimum: $x_0 = \frac{2}{3}$, $y_0 = \frac{1}{3}$

Position of the substrate stacking fault peaks: (basis effect)

$x^+ = \frac{1}{3}$, $y^+ = \frac{2}{3}$

Structure Factor:

$$(1+F^+) = 1 + \Delta e^{-i2\pi(hx^+ + ky^+)} = 1 + \Delta e^{-i2\pi(h+2k)/3}$$

$$= \begin{cases} 1+\Delta & (h+2k)=3m \\ 1-\Delta\mathcal{Z}^2 & (h+2k)=2n\neq 3m \\ 1-\Delta\mathcal{Z}^1 & \text{otherwise} \end{cases}$$

where $\mathcal{Re}(\mathcal{Z}^1) = \mathcal{Re}(\frac{1}{2} - i\frac{\sqrt{3}}{2}) = \frac{1}{2}$ *and* $\mathcal{Re}(\mathcal{Z}^2) = \mathcal{Re}(\frac{1}{2} + i\frac{\sqrt{3}}{2}) = \frac{1}{2}$, *with* m,n *integer.*

Island Lattice

$\mathbf{b}_1 = \frac{1}{2}\langle\bar{1}\ 1\ 0\rangle b_o$ $\qquad$ $\mathbf{b}_2 = \frac{1}{2}\langle 0\ \bar{1}\ 1\rangle b_o$

$b_{nn} = \frac{b_0}{\sqrt{2}} = |\mathbf{b}_1| = |\mathbf{b}_2|$, *where* b_o *is the cubic lattice parameter and* $\beta = 120^\circ$

Transformation parameters

Scale relationships:

$r = b_{nn}/a_{nn} = b_0/a_0 = r_{11} = r_{12} = r_{21} = r_{22}$

Angular relationships:

$c_\theta = \sin(\alpha-\theta)/\sin\alpha = 2\cos(30-\theta)/\sqrt{3}$,

$s_\theta = \sin\theta/\sin\alpha = 2\sin\theta/\sqrt{3}$

$s_{\theta\beta} = \sin(\alpha-\beta-\theta)/\sin\alpha = -2\sin\theta/\sqrt{3}$,

$c_{\theta\beta} = \sin(\beta+\theta)/\sin\alpha = 2\cos(\theta+30)/\sqrt{3}$

$D_\theta = \sin(\beta+\theta)/\sin\beta = c_{\theta\beta}$, $T_\theta = -\sin\theta/\sin\beta = s_{\theta\beta}$

$T_{\theta\alpha} = \sin(\beta-\alpha+\theta)/\sin\beta = s_\theta$, $D_{\theta\alpha} = \sin(\alpha-\theta)/\sin\beta = c_\theta$

Table 3.2 *Ideal Epitaxial Orientations*
fcc{111}/fcc{111}

	Matched vectors in reciprocal space		*Parallel Surface lattice*		*Directions Crystallographic*		*Geometric Parameters*	
	a	b	a	b	a	b	r	
	h k	p q	k $\bar{h}$	q $\bar{p}$			(b_{nn}/a_{nn})	θ°
A)	1 0	1 0	0 $\bar{1}$	0 $\bar{1}$	<0 1 $\bar{1}$>	<0 1 $\bar{1}$>	1	0
B)	1 1	2 0	1 $\bar{1}$	0 $\bar{2}$	<$\bar{1}$ 2 $\bar{1}$>	<0 1 $\bar{1}$>	1.1547	30
C)	2 0	1 2	0 $\bar{2}$	2 $\bar{1}$	<0 1 $\bar{1}$>	<$\bar{2}$ 3 $\bar{1}$>	1.3229	30
D)	1 2	0 3	2 $\bar{1}$	3 0	<$\bar{2}$ 3 $\bar{1}$>	<$\bar{1}$ 1 0>	1.1339	19.11
E)	1 3	2 2	3 $\bar{1}$	2 $\bar{2}$	<$\bar{3}$ 4 $\bar{1}$>	<$\bar{1}$ 2 $\bar{1}$>	0.9608	16.10
F)		0 4		4 0	<$\bar{3}$ 4 $\bar{1}$>	<$\bar{1}$ 1 0>	1.1094	13.90

One can show that if (2h+k) is a multiple of 3, then so are the associated quantities, [with i=-(h+k)] : 2i+h, 2k+i, h+2k, i+2h and k+2i. Correspondingly, in a given Fourier level, as defined in Chapter 2, the structure factor has the same value for each harmonic. As seen from Table 3.1, the stacking-fault structure factor has the same property.

Van der Merwe (1982), has associated a measure of the tendency to epitaxy with each of the ideal configurations. This is calculated from the terms in the expression for the total misfit energy which reach peak values at ideality. The total misfit energy, expressed in units of WH, and per atom is given by:

$$\mathcal{E} = A_{00} + \frac{1}{G} \sum_{\substack{h,k=0 \\ h\neq 0 \text{ or } k\neq 0}}^{\infty} A_{hk} F^0 [1+F^+_{hk}(\Delta)] \left\{ [\mathcal{F}\mathcal{Q}^1_p \mathcal{F}\mathcal{Q}^1_q]_{hk} + [\mathcal{F}\mathcal{Q}^1_p \mathcal{F}\mathcal{Q}^1_q]_{ih} + [\mathcal{F}\mathcal{Q}^1_p \mathcal{F}\mathcal{Q}^1_q]_{ki} \right\} \quad (42$$

where i = -(h+k) and G = (2M+1)X(2N+1) is the number of interfacial atoms in the island.

The *Epitaxial Strength* is then defined as the contribution to the misfit energy, per atom, of the terms which peak - those for which p and q are integer. Because of the rather special symmetry of

this epitaxial system - both overgrowth and substrate have 6-fold symmetry in the reciprocal lattices - all three terms of a particular Fourier level peak simultaneously, as coincidence of one pair of reciprocal lattice points implies pairing of the others, by symmetry.

The structure factor $F^{o}[1+F^{+}_{hk}(\Delta)]$ must be negative if A_{hk} is positive to contribute to a reduction in the misfit energy. As F^{o} contains the position of the central atom, this requirement determines the displacement of the island. Depending on p,q therefore, the island will translate to maximize the misfit energy reduction.

Completely Coherent Configuration $r = 1, \theta = 0^{o}$

The first epitaxial configuration listed in Table 3.2 deserves special mention. In this case $r = 1$, and $\theta = 0^{o}$. In other words, the substrate and overgrowth systems match perfectly in the configuration called the *Completely Coherent Configuration* by Van der Merwe (1982). All reciprocal lattice points, and hence all direct lattice rows and atoms match. The misfit energy is correspondingly reduced to *zero*, and this configuration will have the maximum epitaxial strength of all.

Table 3.3 lists the epitaxial strengths and the directions in which misfit is eliminated for the unique configurations. In this and in Table 3.2 the order of the matched reciprocal vectors may be reversed, so that the ratio r will be inverted. These are not treated as separate configurations, although it must be noted that the epitaxial strength *in this model* is dependent on the substrate Fourier level, and not on the overlayer reciprocal lattice vector. Also not explicitly listed are the configurations which are equivalent by symmetry, and specifically rotations through $-\theta$.

Table 3.3 *Properties of the Ideal Epitaxial Configurations* fcc{111}/fcc{111}

A) $r = 1$, $\theta = 0^\circ$, *substrate*: (1 0); *overgrowth*: (1 0)

Structure Factors: $F^0 = -1/2$ $F = 1 - \Delta/2$

Epitaxial Strength: $-\frac{3}{2}(A_{10}-2A_{11}+A_{20}+A_{12}+A_{21}-2A_{22}+A_{13}+A_{31}+A_{40})$
$+ \frac{3}{4}\Delta(A_{10}+4A_{11}+A_{20}+A_{12}+A_{21}+4A_{22}+A_{13}+A_{31}+A_{40})$

Misfit Accommodation:

Surface: <2 1> ∥ <2 1> *Crystal*: $\langle\bar{2}\ 1\ 1\rangle \parallel \langle\bar{2}\ 1\ 1\rangle$

B) $r = 2/\sqrt{3} = 1.1547$, $\theta = 30^\circ$, *substrate*: (1 1); *overgrowth*: (2 0)

Structure Factors: $F^0 = 1$ $F = 1 + \Delta$

Epitaxial Strength: $3(1+\Delta)(A_{11}+A_{22})$

Misfit Accommodation:

Surface: <1 1> ∥ <2 1> *Crystal*: $\langle\bar{1}\ 0\ 1\rangle \parallel \langle\bar{2}\ 1\ 1\rangle$

C) $r = \sqrt{7}/2 = 1.3229$, $\theta = 30^\circ$, *substrate*: (2 0); *overgrowth*: (1 2)

Structure Factors: $F^0 = -1/2$ $F = 1 - \Delta/2$

Epitaxial Strength: $-\frac{3}{2}(1-\frac{\Delta}{2})(A_{20}+A_{40})$

Misfit Accommodation:

Surface: <2 1> ∥ <4 5> *Crystal*: $\langle\bar{2}\ 1\ 1\rangle \parallel \langle\bar{4}\ \bar{1}\ 5\rangle$

D) $r = 3/\sqrt{7} = 1.1339$, $\theta = 19.11^\circ$, *substrate*: (1 2); *overgrowth*: (0 3)

Structure Factors: $F^0 = -1/2$ $F = 1 - \Delta/2$

Epitaxial Strength: $-\frac{3}{2}(1-\frac{\Delta}{2})A_{12}$

Misfit Accommodation:

Surface: <4 5> ∥ <1 2> *Crystal*: $\langle\bar{4}\ \bar{1}\ 5\rangle \parallel \langle\bar{1}\ \bar{1}\ 2\rangle$

E) $r = \sqrt{12/13} = 0.9608$, $\theta = 16.10^\circ$, *substrate*: (1 3); *overgrowth*: (2 2)

Structure Factors: $F^0 = -1/2$ $F = 1 - \Delta/2$

Epitaxial Strength: $-\frac{3}{2}(1-\frac{\Delta}{2})A_{13}$

Misfit Accommodation:

Surface: <5 7> ∥ <1 1> *Crystal*: $\langle\bar{5}\ \bar{2}\ 7\rangle \parallel \langle\bar{1}\ 0\ 1\rangle$

F) $r = 4/\sqrt{13} = 1.1094$, $\theta = 13.90^\circ$, *substrate*: (1 3); *overgrowth*: (0 4)

Structure Factors: $F^0 = -1/2$ $F = 1 - \Delta/2$

Epitaxial Strength: $-\frac{3}{2}(1-\frac{\Delta}{2})A_{13}$

Misfit Accommodation:

Surface: <5 7> ∥ <1 2> *Crystal*: $\langle\bar{5}\ \bar{2}\ 7\rangle \parallel \langle\bar{1}\ \bar{1}\ 2\rangle$

bcc{110}/fcc{111} epitaxial system

The rigid model parameters appropriate to this system are listed in Table 3.4. The selection of ideal configurations from the reciprocal space construction is illustrated in Figures 3.5 while the results are summarized in Tables 3.5 and 3.6.

Table 3.6(a) presents the ideal configurations which match the fundamental Fourier sublattice, while matching with the second order sublattice is listed in Table 3.6(b). In figure 3.6 some configurations are shown in reciprocal space after the overgrowth has been scaled and rotated to coincidence.

With regard to Table 3.6, it should be noted that the epitaxial strengths show only the dominant contribution from the quotient functions which peak as pairs, ie. both p and q are integer. In actual fact in the fcc{111}/fcc{111} system all the pairs $\mathcal{F}Q^1_p$, $\mathcal{F}Q^1_q$ in a given level peaked simultaneously. In this bcc{110}/fcc{111} system only a single pair peaks. However single quotients do peak if one of p or q are integer. These terms cause striations of weak minima in the Misfit energy - r,θ diagrams (see figure 3.3), which radiate from the energy wells. However a single quotient has an order of magnitude of 2M+1, considerably weaker than (2M+1)X(2N+1) if both peak in a large system.

The NW^1, KS^1, KS^2 and NW^2 (*A*, *B*, *D*, and *E*) systems have been described by van der Merwe (1982), for the complementary system with bcc{110} as substrate. The first three configurations occur as a result of matching with the fundamental Fourier sublattice. The second Nishiyama-Wassermann orientation, although rotated through to the same angle as NW^1 in fact arises from matching with the second order sublattice h=1,k=1 . NW^2 is a scaled and rotated second order version of *C* in Table 3.5 . The scale factor $1/\sqrt{3}$ arises from the smaller lattice parameter of this sublattice, as can be seen in Chapter 2, Table 2.2.

Table 3.4 *Parameters for the* bcc{110}/fcc{111} *epitaxial system.*

Substrate Lattice

$\mathbf{a}_1 = \frac{1}{2}\langle\bar{1}\ 1\ 0\rangle a_o$ $\qquad$ $\mathbf{a}_2 = \frac{1}{2}\langle 0\ \bar{1}\ 1\rangle a_o$

$|\mathbf{a}_1| = |\mathbf{a}_2| = a = \frac{a_o}{\sqrt{2}} = a_{nn}$ *,where* a_o *is the cubic lattice parameter.* $\qquad \alpha = 120^\circ$

Position of minimum: $x_0 = \frac{2}{3}$, $y_0 = \frac{1}{3}$

Position of the substrate stacking fault peaks: (basis effect)

$$x^+ = \frac{1}{3} \quad , \quad y^+ = \frac{2}{3}$$

Structure Factor:

$$[1+F^+(h,k)] = 1 + \Delta e^{-i2\pi(hx^+ + ky^+)} = 1 + \Delta e^{-i2\pi(h+2k)/3}$$

$$= \begin{cases} 1+\Delta & (h+2k)=3m \\ 1-\Delta Z^2 & (h+2k)=2n\neq 3m \\ 1-\Delta Z^1 & \text{otherwise} \end{cases}$$

where $\mathrm{Re}(Z^1) = \mathrm{Re}(\frac{1}{2}-i\frac{\sqrt{3}}{2}) = \frac{1}{2}$ *and* $\mathrm{Re}(Z^2) = \mathrm{Re}(\frac{1}{2}+i\frac{\sqrt{3}}{2}) = \frac{1}{2}$ *with* m,n *integer.*

Island Lattice

$\mathbf{b}_1 = \langle\bar{1}\ 1\ 0\rangle b_o$ $\qquad$ $\mathbf{b}_2 = \langle 0\ 0\ 1\rangle b_o$

$b_{nn} = \frac{\sqrt{3}}{2} b_o$, *where* b_o *is the cubic lattice parameter*

$b_1 = |\mathbf{b}_1| = \sqrt{2}\, b_o = \sqrt{8/3}\, b_{nn}$, $\beta = 90^\circ$

$b_2 = |\mathbf{b}_2| = b_o = \frac{2}{\sqrt{3}} b_{nn}$,

Basis atom positions: $x_b^+ = \frac{1}{2}$, $y_b^+ = \frac{1}{2}$

$\kappa = 1$ *(lattice and basis atoms are of one type)*

Structure factor:

$$[1+F^+(p,q)] = 1+\kappa e^{i2\pi(px_b^+ + qy_b^+)} = 1+e^{i\pi(p+q)} = \begin{cases} 2 & p+q \text{ even} \\ 0 & p+q \text{ odd} \end{cases}$$

Table 3.4 *Parameters for the* bcc{110}/fcc{111} *epitaxial system. (Continued)*

Transformation parameters

Scale relationships:

$$r = b_{nn}/a_{nn} = \frac{\sqrt{3}}{2} b_0/a = \sqrt{3/2}\, b_0/a_0$$

$$r_{11} = b_1/a_1 = \sqrt{2}\, b_0/a = \sqrt{8/3}\, r \quad ,$$

$$r_{12} = b_1/a_2 = r_{11} = \sqrt{8/3}\, r$$

$$r_{21} = b_2/a_1 = b_0/a = \frac{2}{\sqrt{3}} r \quad , \quad r_{22} = b_2/a_2 = r_{21} = \frac{2}{\sqrt{3}} r$$

Angular relationships:

$$c_\theta = \sin(\alpha-\theta)/\sin\alpha = 2\cos(30-\theta)/\sqrt{3} \ ,$$

$$s_\theta = \sin\theta/\sin\alpha = 2\sin\theta/\sqrt{3}$$

$$s_{\theta\beta} = \sin(\alpha-\beta-\theta)/\sin\alpha = 2\sin(30-\theta)/\sqrt{3} \ ,$$

$$c_{\theta\beta} = \sin(\beta+\theta)/\sin\alpha = 2\cos\theta/\sqrt{3}$$

$$D_\theta = \sin(\beta+\theta)/\sin\beta = \cos\theta$$

$$T_\theta = -\sin\theta/\sin\beta = -\sin\theta$$

$$T_{\theta\alpha} = \sin(\beta-\alpha+\theta)/\sin\beta = \sin(\theta-30)$$

$$D_{\theta\alpha} = \sin(\alpha-\theta)/\sin\beta = \cos(\theta-30)$$

Other orientations which can be related to lower order Fourier sublattices are *F*, and *E*, by scaling by $2/\sqrt{3}$ and rotating by 30°, to provide higher order versions of the Kurdjumov-Sachs configuration *B*, and the Nishiyama-Wassermann configuration *A*.

This illustrates the fact that if the configurations of the fundamental sublattice are known, other configurations, involving higher order Fourier sublattices can be deduced with ease.

The epitaxial strengths as defined here are negative quantities. Clearly this implies that the second order coefficient A_{11} must be negative for epitaxy with this sublattice to occur, if the island remains centred at $x_0=2/3$, $y_0 = 1/3$, or the island will

translate to optimize the structure factor F^{o}. The conditions in Chapter 2, Table 2.3 allow greater freedom to the negative range of this coefficient. The stacking fault substrate parameter Δ actually assists the tendency to epitaxy with this Fourier sublattice. If $-A_{11} > (A_{10}+A_{20})(1 - \Delta/2)/2(1+\Delta)$, the second order Fourier sublattice will have a greater epitaxial strength than the Fundamental order. For non-ideal systems with $r \simeq .9$, both NW^{2} and KS^{1} and KS^{2} systems may then occur with equal probability.

These remarks do not apply to *local* strain however, as the *strongest* Fourier terms, giving the strongest local gradients, even if they do not contribute significantly to the overall (homogeneous) deformation, are most important here.

Table 3.5 *Lower order Ideal Epitaxial Orientations ov-bcc{110}/fcc{111}-sub*

Matched vectors in reciprocal space				*Parallel Surface lattice*				*Directions Crystallo-graphic*		*Geometric Parameters*		
fcc		*bcc*		*fcc*		*bcc*		*fcc*	*bcc*	r		*Type*
h	k	p	q	k	$\bar{h}$	q	$\bar{p}$			(b_{nn}/a_{nn})	θ°	
A) 1	0	2	0	0	$\bar{1}$	0	$\bar{2}$	<0 1 $\bar{1}$>	<0 0 $\bar{1}$>	1.0607	30	NW^{1}
B) $\bar{1}$	1	$\bar{1}$	1	1	1	1	1	<$\bar{1}$ 0 1>	<$\bar{1}$ 1 1>	0.9186	24.74	KS^{1}
C) 0	1	0	2	1	0	2	0	<$\bar{1}$ 1 0>	<$\bar{1}$ 1 0>	1.5	0	
D)		1	1			1	$\bar{1}$	<$\bar{1}$ 1 0>	<$\bar{1}$ 1 $\bar{1}$>	0.9186	35.26	KS^{2}
E) 1	1	0	2	1	$\bar{1}$	2	0	<$\bar{1}$ 2 $\bar{1}$>	<$\bar{1}$ 1 0>	0.8660	30	NW^{2}
F)		2	2			2	$\bar{2}$	<$\bar{1}$ 2 $\bar{1}$>	<$\bar{1}$ 1 $\bar{1}$>	1.0607	5.26	KS^{3}
G)		3	1			1	$\bar{3}$	<$\bar{1}$ 2 $\bar{1}$>	<$\bar{1}$ 1 $\bar{3}$>	1.0155	34.76	
H)		4	0			0	$\bar{4}$	<$\bar{1}$ 2 $\bar{1}$>	<0 0 $\bar{1}$>	1.2247	60	NW^{3}
I) 2	0	3	1	0	$\bar{2}$	1	$\bar{3}$	<0 $\bar{1}$ 1>	<$\bar{1}$ 1 $\bar{3}$>	0.8795	4.76	

Table 3.6(a) *Properties of the Ideal Epitaxial Configurations*
ov-bcc{110}/fcc{111}-sub
Fundamental

A) $r = 3/\sqrt{8} = 1.0607$, $\theta = 30^\circ$, *substrate*: (1 0) ; *overgrowth*: (2 0)

Structure Factors: $F^0 = -1/2$ $F_{10} = 1 - \Delta/2$ $F^{20} = 2$

Epitaxial Strength: $-(1-\frac{\Delta}{2})(A_{10} + A_{20})$

Misfit Accommodation:

Surface: $\langle 2\ 1\rangle \parallel \langle 1\ 0\rangle$ *Crystal*: $\langle \bar{2}\ 1\ 1\rangle \parallel \langle \bar{1}\ 1\ 0\rangle$

B) $r = \sqrt{27/32} = 0.9186$, $\theta = 24.74^\circ$, *substrate*: $(\bar{1}\ 1)$; *overgrowth*: $(\bar{1}\ 1)$

Structure Factors: $F^0 = -1/2$ $F_{10} = 1 - \Delta/2$ $F^{11} = 2$

Epitaxial Strength: $-(1-\frac{\Delta}{2})(A_{10} + A_{20})$

Misfit Accommodation: (*In order substrate* $\parallel$ *overgrowth*)

Surface: $\langle \bar{1}\ 1\rangle \parallel \langle \bar{1}\ 2\rangle$ *Crystal*: $\langle 1\ \bar{2}\ 1\rangle \parallel \langle 1\ \bar{1}\ 2\rangle$

C) $r = 1.5$, $\theta = 0^\circ$, *substrate*: (0 1) ; *overgrowth*: (0 2)

Structure Factors: $F^0 = -1/2$ $F_{01} = 1 - \Delta/2$ $F^{02} = 2$

Epitaxial Strength: $-(1-\frac{\Delta}{2})(A_{10} + A_{20})$

Misfit Accommodation:

Surface: $\langle 1\ 2\rangle \parallel \langle 0\ 2\rangle$ *Crystal*: $\langle \bar{1}\ \bar{1}\ 2\rangle \parallel \langle 0\ 0\ 1\rangle$

D) $r = \sqrt{27/32} = 0.9186$, $\theta = 35.26^\circ$, *substrate*: (0 1) ;
overgrowth: (1 1)

Structure Factors: $F^0 = -1/2$ $F_{01} = 1 - \Delta/2$ $F^{11} = 2$

Epitaxial Strength: $-(1-\frac{\Delta}{2})(A_{10} + A_{20})$

Misfit Accommodation:

Surface: $\langle 1\ 2\rangle \parallel \langle 1\ 2\rangle$ *Crystal*: $\langle \bar{1}\ \bar{1}\ 2\rangle \parallel \langle \bar{1}\ 1\ 2\rangle$

The parallel directions are all listed in the order
Substrate direction $\parallel$ *Overgrowth direction*
Misfit Accommodation directions : (by eqn 35)
substrate $u = 2h+k$, $v = h+2k$
overgrowth $u = p$, $v = 2q$.

Table 3.6(b) *Properties of the Ideal Epitaxial Configurations ov-bcc{110}/fcc{111}/-sub Higher Orders*

E) $r = \sqrt{3}/2 = 0.8660$, $\theta = 30^{\circ}$, *substrate*: (1 1) ; *overgrowth*: (0 2)

Structure Factors: $F^{0} = 1 \quad F_{11} = 1 + \Delta \quad F^{02} = 2$

Epitaxial Strength: $2(1+\Delta)A_{11}$

Misfit Accommodation:

Surface: <1 1> || <0 2> *Crystal*: $\langle\bar{1}\ 0\ 1\rangle \parallel \langle 0\ 0\ 1\rangle$

F) $r = 3/\sqrt{8} = 1.0607$, $\theta = 5.26^{\circ}$, *substrate*: (1 1) ; *overgrowth*: (2 2)

Structure Factors: $F^{0} = 1 \quad F_{11} = 1 + \Delta \quad F^{22} = 2$

Epitaxial Strength: $2(1+\Delta)A_{11}$

Misfit Accommodation:

Surface: <1 1> || <2 4> *Crystal*: $\langle\bar{1}\ 0\ 1\rangle \parallel \langle\bar{1}\ 1\ 2\rangle$

G) $r = \sqrt{33/32} = 1.0155$, $\theta = 34.76^{\circ}$, *substrate*: (1 1) ; *overgrowth*: (3 1)

Structure Factors: $F^{0} = 1 \quad F = 1 + \Delta \quad F^{31} = 2$

Epitaxial Strength: $2(1+\Delta)A_{11}$

Misfit Accommodation:

Surface: <1 1> || <3 2> *Crystal*: $\langle\bar{1}\ 0\ 1\rangle \parallel \langle\bar{3}\ 1\ 2\rangle$

H) $r = \sqrt{3/2} = 1.2247$, $\theta = 60^{\circ}$, *substrate*: (1 1) ; *overgrowth*: (4 0)

Structure Factors: $F^{0} = 1 \quad F = 1 + \Delta \quad F^{40} = 2$

Epitaxial Strength: $2(1+\Delta)A_{11}$

Misfit Accommodation:

Surface: <1 1> || <0 4> *Crystal*: $\langle\bar{1}\ 0\ 1\rangle \parallel \langle 0\ 0\ 1\rangle$

I) $r = \sqrt{99/128} = 0.8795$, $\theta = 4.76^{\circ}$, *substrate*: (2 0) ; *overgrowth*: (3 1)

Structure Factors: $F^{0} = -1/2 \quad F = 1 - \Delta/2 \quad F^{31} = 2$

Epitaxial Strength: $-(1-\frac{\Delta}{2})A_{20}$

Misfit Accommodation:

Surface: <2 1> || <0 4> *Crystal*: $\langle\bar{2}\ 1\ 1\rangle \parallel \langle 0\ 0\ 1\rangle$

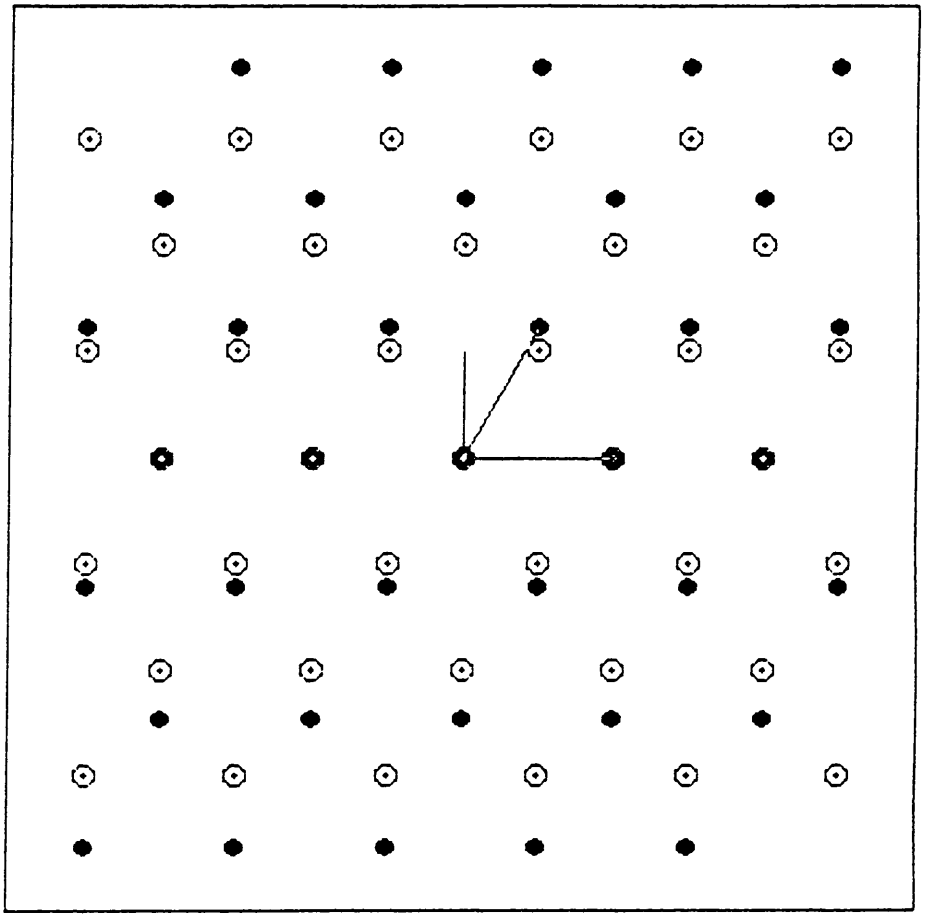

Figure 3.6(a) Superposed substrate and overgrowth reciprocal lattices for the ideal Nishiyama-Wassermann configuration $r = b_{nn}/a_{nn} = 1.06066 \quad \theta = 30^{o}$.

Solid circles : substrate points
Open circles : overgrowth points
Centred solid circles : coinciding overgrowth and substrate points

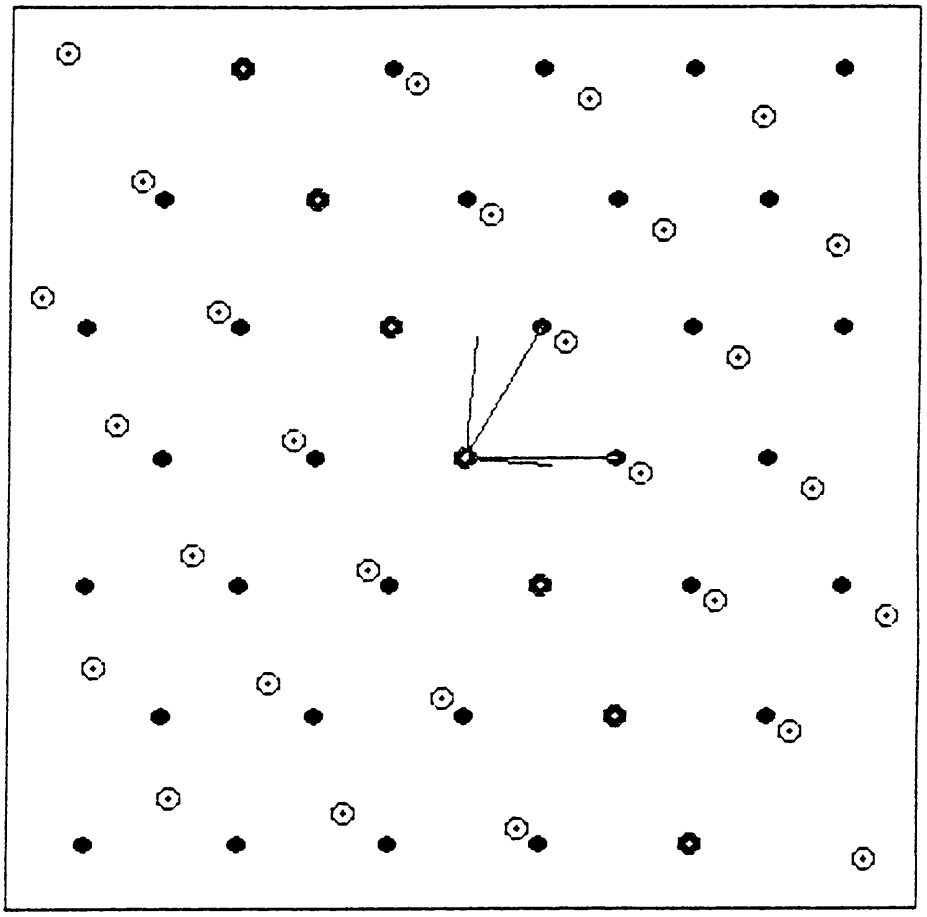

Figure 3.6(b) Superposed substrate and overgrowth reciprocal lattices for the ideal Kurdjumov-Sachs configuration

$r = b_{nn}/a_{nn} = 0.91856 \quad \theta = 24.74^{o}$.

3.5 DISCUSSION

The depth of the misfit energy minimum for each Fourier harmonic is directly dependent on the magnitude of the Fourier coefficient V_{hk}, together with the structure factors F^{o}, F_{hk}, and F^{pq}, (eqns 26, 36 and 37, also Chapter 2, eqns 2.8). As this determines the epitaxial strength, (Tables 3.3 and 3.6), it is evident that the most dominant terms in the Fourier expansion give rise to the important epitaxial configurations. Because, as discussed in Chapter 2, the Fourier coefficients decrease with increasing order, the lower order epitaxial configurations may be expected to predominate. A non-ideally matched lower order configuration may be more important, once strain of the system is allowed, than an ideally matched higher order configuration. This is because the effect of strain may be expected to widen the range of the epitaxial configuration, at a cost of some strain energy, while the higher order exact configuration may provide very little gain in misfit energy because of a small Fourier coefficient. This is the subject of the investigations of Chapter 4.

The ideal epitaxial configurations have been shown to be due to the matching of the row spacings and orientations of atomic rows in the overgrowth and the substrate, or seen in reciprocal space, the matching of the reciprocal space wave vectors associated with these rows (eqn 31). With the model used here, the periodic interaction potential arose from the substrate only. However, it must be true that while the overgrowth atoms experience a periodic substrate potential, defined in terms of the reciprocal lattice vectors of the substrate (Chapter 2), that the substrate atoms likewise experience a periodic potential which may be defined in terms of the overgrowth reciprocal lattice vectors (Van der Merwe 1982). It would be more proper therefore, to define the epitaxial strength not only in terms of the substrate Fourier coefficients V_{hk}, but also include the overgrowth Fourier coefficients, V^{pq} (and the required structure factors). While the epitaxial strength could be given as $F^{o}F_{hk}F^{pq}V_{hk}$ for the present, substrate only approach, it

could be defined as

$$\tfrac{1}{2}(W_a V_{hk} + W^b V^{pq}) F^o F_{hk} F^{pq} \ ,$$

where W_a and W^b are relative energy amplitudes for the substrate and overgrowth amplitudes respectively, and $[h\ k]_a^*$ and $[p\ q]_b^*$ are the reciprocal lattice vectors which match. The factor ½ was included because the interactions between a specific pair of atoms would be included twice if the misfit energy was calculated separately for the two systems and simply added.

Of immediate relevance, is the observation that the Fourier harmonics in the substrate expansion which do not have wave vectors close to those selected by the row-matching criterion in a particular epitaxial system, do not influence the *overall* distortion, contributing only to the total energy as an approximately constant term, the "plateau" value. Correspondingly, only Fourier terms relevant to a particular matching range of r-values, need to be included when relative (qualitative) behaviour near to such orientations is studied. The rigid or row-matching criteria are then an easy and direct aid to the selection of relevant terms in the Fourier expansions.

The *Ideal Epitaxial Configurations* listed in Tables 3.2, 3, 5 and 6 have been obtained from the reciprocal lattice construction (section 3.3), which was used here in idealized form for an *infinite* overgrowth. As was pointed out when the construction was first described, the effect of the overgrowth island size is to widen the misfit energy wells. Correspondingly, the reciprocal lattice point associated with the overgrowth reciprocal lattice vector $[p\ q]_b^*$, has a fine structure associated with it. Instead of being a mathematical point, the smaller the size of the island, the more the point becomes a disc, with secondary circles surrounding it, for a circular island. Essentially the matching criteria are weakened with decreasing crystal size. *Ideal* configurations are therefore correctly defined for infinite overgrowths and substrate. The effect of crystal size on the misfit energy behaviour is also illustrated in figure 3.3.

The reciprocal lattice is the collection of wave vectors which describe the periodicity of the crystal, and shows the wave vectors which have non-zero Fourier amplitudes in a Fourier transform of the crystal. Similarly, the widening of the central energy minimum at an Ideal Configuration with decreasing crystal size is the behaviour expected from the Fourier transform of the crystal as a whole, a circular or rectangular step function. This is analogous to the optical diffraction pattern associated with a single circular, or rectangular hole. Where the reciprocal lattice maps the expected diffraction pattern of a perfectly periodic crystal, the fine structure of each point is the diffraction pattern of the overall finite crystal.

It is therefore possible in principle to use the reciprocal lattice construction also for given finite islands, by detailing the fine structure for each point, but the qualitative, or even quantitative behaviour of the depth of the secondary minima is probably more easily obtained directly from the energy behaviour itself.

Essentially the matching requirements of the smaller islands are less exactly defined than for larger islands, as can be seen for the smallest island in the figure 3.3, where the deep, central, energy wells are enlarged and close to overlapping. Systems not exactly ideal may be found therefore in almost any orientation in the early stages of growth.

Tempering this uncertainty is the simultaneous weakening of the rigidity assumption for small systems. Some of these small islands may be expected to be capable of growing pseudomorphically (matching exactly to the substrate), not taken into account in the rigid deliberations of this chapter. Any discussion of very small systems in terms of a rigid model must be considered highly speculative - further discussions of size effects must include the effect of strain or deformation of the overgrowth, and the associated energies.

3.6 CONCLUSION

In this chapter the van der Merwe - Reiss epitaxial model has been extended to enable the study of the interface of general crystal structures. By introducing structure factors (eqns 26, 36 and 37) both in the overgrowth and substrate systems through the definition of basis effects, such as non-lattice atoms or stacking fault corrections, one is not bound to a representation in terms of primitive surface unit cells. The way these structure factors appear in the misfit energy expressions means that they can be precalculated for infinite systems.

Their effect is to change the importance of the reciprocal lattice points, removing some in the same way as happens in diffraction theory.

The generalized misfit energy expressions have been analyzed (section 3.2), and the key behaviour is that the misfit energy is essentially a constant average or plateau value except when the overgrowth and substrate match, in so-called *Ideal Epitaxial Configurations*, which define sharp delta-function like localized minima in the misfit energy. It has been seen that these minima occur whenever a reciprocal lattice displacement vector of the overgrowth exactly matches a substrate reciprocal lattice vector, in magnitude and direction. As structure factors have been included, these matched reciprocal lattice vectors mean that rows of atoms in the overgrowth and the substrate match in spacing in the direction perpendicular to the atomic rows, and in direction along the rows. The atomic rows are therefore parallel and equally spaced.

To exploit these results as a predictive and interpretive tool a geometric construction analogous to that of Ewald has been designed (section 3.3), and from this the criteria for matching differing structures have been derived, and specifically applied to the bcc{110}/fcc{111} epitaxial system. This was successful in showing the known Nishiyama-Wassermann and Kurdjumov-Sachs epitaxial

configurations (section 3.4, Tables 3.5 and 3.6) as has been done with the basic model by Van der Merwe (1982). The reciprocal lattice discussion illuminated the type of matching actually achieved by these configurations, and has shown several other higher order possible epitaxial configurations.

The major success must be seen in the general applicability and ease of use of the reciprocal lattice formulation of the epitaxial criteria, and its energetic basis as related to the Fourier form of the adatom-substrate interaction potential. Also treatable in the reciprocal lattice formulation is the effect of crystal size, within, of course, the assumption of a rigid overgrowth and substrate.

The extension of the formulation to the prediction of the actual strains to achieve row-matching epitaxy for non-ideal systems, and also the two-dimensionally coherent or pseudomorphic phase for incommensurate structures will be carried out in the next chapter, again allied to energy considerations.

CHAPTER 4

MISFIT STRAIN EPITAXY

The epitaxial model of the previous chapter is modified to allow the overgrowth to strain homogeneously in order to minimize the total interfacial energy, defined here as the sum of the misfit (disregistry) and elastic strain energies. These strains are calculated both by direct numerical minimization of the total interfacial energy and from the reciprocal lattice formulation.

The effect of the anisotropy is explicitly examined by modifying the elastic constants in such a way that the averaged isotropic constants do not change.

The pseudomorphic (2DC) phase for the incommensurate bcc{110} and fcc{111} overgrowth - substrate system is studied in this context, and a key difference between the Kurdjumov-Sachs (KS) and Nishiyama-Wassermann (NW) epitaxial configurations is highlighted. Namely that the pseudomorphic phase cannot be achieved from the KS orientation, (without rotation) but can be attained from the NW orientation.

The effect of anisotropy on the orientational angle of the KS configuration for the systems which do not conform exactly to the ideal lattice parameter is discussed.

Phase diagrams of the stable configurations for systems between the KS and NW lattice ratios are given, and discussed in terms of the effect of anisotropy ratio.

CHAPTER 4

MISFIT STRAIN EPITAXY

In the previous chapter, epitaxial systems were modelled with both the overgrowth and the substrate rigid. *Ideal Epitaxial Configurations*, defined as the scale and orientation relationships for which the *Misfit energy* between the two crystals on either side of the interface is a minimum, were shown to satisfy geometric row-matching criteria exactly for infinite epitaxial systems. The depths of the minima at ideal configurations relative to the overall plateau values provide measures of the tendency to epitaxy of real systems, particularly those with lattice parameters close to the ideal values for row matching.

Real systems which must deform to achieve row-matching cannot be analyzed simply in terms of the rigid model only, however. The minimum energy criterion must be generalized as the minimization of the total interfacial energy consisting of both strain and misfit energies (Kenty 1974).

In this chapter, the substrate is considered rigid and infinite, but the normally finite overgrowth island is allowed to deform in response to the interfacial forces. The strain is limited to homogeneous or position-independent strain, subject to the harmonic model, and is described in terms of linear elasticity theory. This model was developed by van der Merwe (1980,1982) who has applied it to several systems.

Physically, the homogeneous strain model describes misfit accommodation by misfit strain. Systems which require misfit dislocations or a mixture of dislocations and misfit strain have periodic variations of strain fields associated with the dislocations. There are areas of almost coherent matching between substrate and overlayer, alternating with narrow regions of severe misfit. These cases are studied in the next chapter with a *finite*

element approximation based essentially on a Rayleigh-Ritz variational method. The geometric properties of the dislocations, their Burgers vectors, line sense and spacing are also determined from the reciprocal lattice in the next chapter.

In this chapter, the modifications to the unit cell of the overlayer, and consequently to the interfacial misfit energy, which arise from homogeneous strain are derived. Expressions for the strain energy for isotropic and anisotropic elastic constants are given, and the dimensionless *configurational parameter*, ℓ , originally introduced for one-dimensional systems by Frank and van der Merwe (1949) and extended to two-dimensional systems by van der Merwe (1980) is defined to suit the present considerations. The strain which minimizes the total interfacial energy expressed as the sum of the misfit and strain energies, is obtained by direct numerical minimization of the total interfacial energy for several overgrowth-substrate configurations, including some which are predicted to be ideal from the rigid model.

The reciprocal lattice formulation is used to predict strains and rotations which are needed to achieve row-matching for non-ideal systems. The rotation, the change of shape of the unit cell and the necessary general strains for two-dimensional or coherent matching are calculated with the reciprocal lattice model and are compared with those obtained by direct numerical minimization of the total interfacial energy.

With all the preceding considerations the effect of anisotropy is explicitly examined. Sets of modified elastic constants are used which have different anisotropy ratios but yield the same isotropic constants when averaged.

The homogeneous strain model is applied to the bcc{110}/fcc{111} system with the former in the overgrowth position, as a refinement to the purely rigid model of Chapter 3. In particular, the systems with nearest neighbour ratio r between those of the *ideal*

epitaxial configurations, the Nishiyama-Wassermann and Kurdjumov-Sachs configurations, (Refer to Chapter 3 section 3.4) and their relationship to the completely coherent configuration will be studied more closely.

4.1 THE EPITAXIAL MODEL

The epitaxial system is modelled as an island of elastic material with embedded atoms interacting with a rigid substrate. The interaction with the substrate is through the interfacial atoms interacting with the adatom-substrate potential, introduced earlier in Chapter 2 and applied with the rigid model in Chapter 3.

The potential follows the symmetry of the substrate, and its unit cell is described by two vectors $\mathbf{a}_1$ and $\mathbf{a}_2$ with length a_1 and a_2 respectively. These vectors have an angle α between them.

In the case of the fcc{111} substrate the vectors are

$$\mathbf{a}_1 = \tfrac{1}{2}\langle \bar{1}\ 1\ 0\rangle a_o \quad \text{and} \quad \mathbf{a}_2 = \tfrac{1}{2}\langle 0\ \bar{1}\ 1\rangle a_o \ , \tag{1a}$$

where a_o is the conventional cubic lattice parameter. The nearest neighbour distance is

$$a_{nn} = a_1 = a_2 \ . \tag{1b}$$

Refer to Chapter 2, Table 2.1 and Chapter 3, Table 3.4 for more details of the geometric parameters.

Unless otherwise specified, the adatom-substrate interaction potential is that of Chapter 2, eqn 2.51.

4.2 THE OVERGROWTH ISLAND

The distribution of the atoms

The overgrowth island is formed from 2M+1 unit cells in the $\mathbf{b}_1$-direction and 2N+1 in the $\mathbf{b}_2$-direction, embedded in an elastic material. The unit cell contains two atoms, one at the lattice and

the other at the centred position, as described fully in Chapter 3, section 3.2.

To ensure mirror symmetry in the analytically simplest manner, the basis atoms are added to the lower and left edges. The elastic continuum is allowed to extend half a unit cell width beyond the last row of (basis) atoms around the outer edge. This is convenient for the implementation of boundary conditions in the finite element (local strain) model of the next chapter.

The form of the island is illustrated in *Figure* 4.1.

The interaction among the atoms within the overgrowth is assumed to be adequately (Van der Merwe 1980, Stoop *e.a.* 1982) described by the *harmonic approximation* (Ashcroft *e.a.* 1975, ch 22, Born *e.a.* 1954). The surroundings, and the substrate in particular, interact with the discrete atomic mesh which forms the island.

4.3 INTERFACIAL ENERGIES AND OVERGROWTH ELASTIC PROPERTIES

Minimum interfacial energy principle

The epitaxial configurations which will occur in real systems are assumed to be those which minimize the total interfacial energy which is defined as:

$$\textit{Interfacial Energy} \equiv \textit{Strain Energy} + \textit{Misfit Energy}. \quad (2$$

The relative values of the strain and misfit energies have a major influence on the degree to which the misfit energy - due to the disregistry of the overgrowth and substrate lattices - is minimized when the total energy is a minimum.

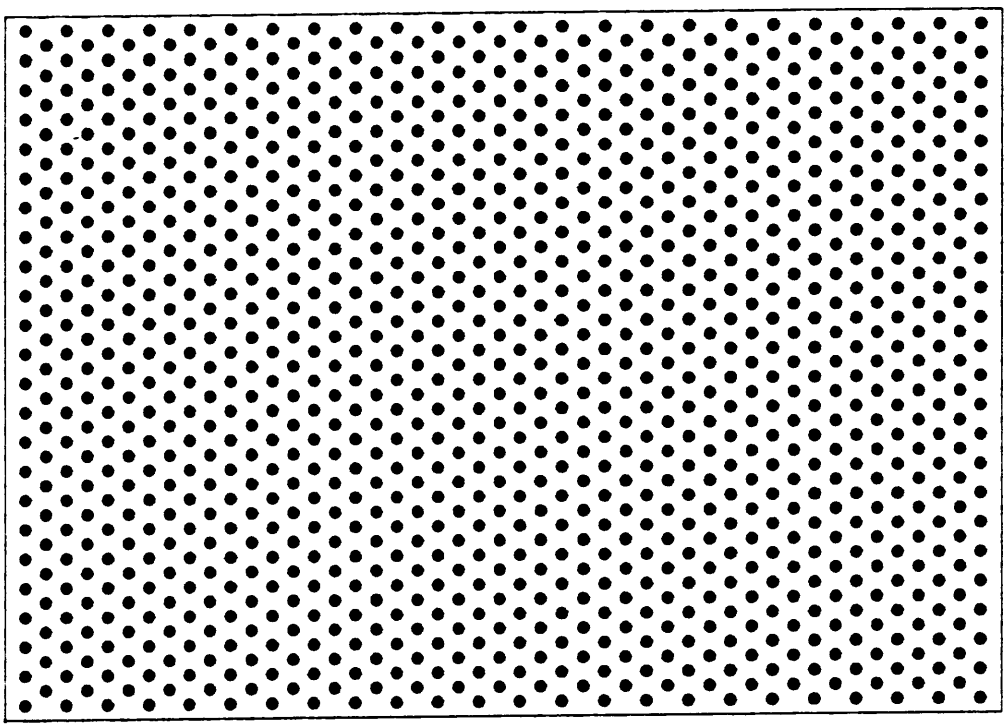

Figure 4.1 The bcc{110} overgrowth island. M=N=11

In contrast to Figure 3.2, the edge is added to indicate the extent of the elastic material beyond the last row of atoms.

Elastic Strain

The strain is expressed in terms of the strain tensor defined in the usual manner:

Let the displacement at a point with coordinates x_1, x_2 and x_3 (relative to some fixed *cartesian* coordinate system) have the components u_1, u_2 and u_3. The components of the strain tensor are then:

$$\varepsilon_{ij} = \frac{1}{2}\left[\frac{\partial u_i}{\partial x_j} + \frac{\partial u_j}{\partial x_i}\right] \quad , \; i,j = 1,2 \text{ or } 3. \qquad (3a$$

Conventionally, the shear strains are related to the strain components as

$$\gamma_{ij} = 2\,\varepsilon_{ij} \; , \qquad (3b$$

with $i \neq j$.

In the case of a thin sheet, simplifications including the introduction of *plane-stress* boundary conditions and the reduction to a two-dimensional description is possible. It is natural to choose the coordinate axes so that the elastic sheet is parallel to the x-y plane.

The simplifying assumptions are:

The stress components σ_{33}, σ_{31}, and σ_{32} normal to the overlayer vanish, and the tangential strains ε_{11}, ε_{22} and γ_{12} and displacements u_1 and u_2 are assumed to be independent of the normal coordinate x_3. (A further constraint $u_3 = 0$ at $x_3 = 0$, which implies that the island remains planar, may be adopted in addition.)

Timoschenko and Goodier (1970 art 20) give the appropriate form of Hooke's law for an *isotropic* elastic continuum which, when written in terms of the shear modulus, μ, and the Poisson ratio, ν, takes

the form:

$$\boldsymbol{\sigma} = \begin{bmatrix} \sigma_x \\ \sigma_y \\ \sigma_{xy} \end{bmatrix} = \mathbf{D} \cdot \boldsymbol{\varepsilon} = \begin{bmatrix} D_{11} & D_{12} & 0 \\ D_{12} & D_{22} & 0 \\ 0 & 0 & D_{33} \end{bmatrix} \begin{bmatrix} \varepsilon_x \\ \varepsilon_y \\ \gamma_{xy} \end{bmatrix} \qquad (4a$$

with

$$D_{11} = D_{22} = 2\mu/(1-\nu),$$

$$D_{12} = 2\mu\nu/(1-\nu) \quad \text{and} \quad D_{33} = \mu \; . \qquad (4b$$

Anisotropic materials may be approximated by an isotropic material by calculating these constants as the Voigt average values (Hirth and Lothe 1968,ch 13) from tabulated anisotropic constants. Alternatively, the anisotropy may be retained in an anisotropic elastic matrix D. More will be said about this in the discussion of the anisotropic model below.

The notation for the two-dimensional problem has been simplified, so that

$$\sigma_x \equiv \sigma_{11} \; , \quad \sigma_y \equiv \sigma_{22} \; , \quad \sigma_{xy} \equiv \sigma_{12}$$

and

$$\varepsilon_x \equiv \varepsilon_{11} \; , \quad \varepsilon_y \equiv \varepsilon_{22} \; , \quad \gamma_{xy} \equiv \gamma_{12} \; . \qquad (5$$

Misfit Energy as a function of Strain

As the island strains homogeneously, every segment of the island, and in particular any unit cell, undergoes the same strain. The misfit energy of a strained island therefore corresponds to that of an overgrowth made up in the same way as the unstrained island, but with a modified unit cell. All that needs to be calculated for a particular state of strain is the effect this has on the dimensions and shape of the unit cell, and hence on the transformation parameters. The expression for the misfit energy is unchanged in form, but is expressed in terms of these strain-modified transformation parameters. [See figures 4.3-5 (b) and (d)(iii).]

The unstrained overgrowth unit cell is characterized by the basis vectors $\mathbf{b}_1$ and $\mathbf{b}_2$, with lengths b_1 and b_2 respectively, and an angle β between them. After strain, the unit cell has vectors $\mathbf{b}_1'$ and $\mathbf{b}_2'$, with lengths b_1' and b_2' and angle β'. Also $\mathbf{b}_1'$ will have rotated through an angle $\delta\theta$ with respect to $\mathbf{b}_1$. These parameters may be calculated from the strain.

In order to express the strain uniquely, it is convenient to choose cartesian coordinates with the x_1-axis parallel to the $\mathbf{b}_1$ basis vector. If the strains are ε_x, ε_y, and γ_{xy} then the point x_1, x_2 in the island is displaced to x_1', x_2' which is (Kelly and Groves 1973)

$$\begin{bmatrix} x_1' \\ x_2' \end{bmatrix} = \begin{bmatrix} 1+\varepsilon_x & \tfrac{1}{2}\gamma_{xy} \\ \tfrac{1}{2}\gamma_{xy} & 1+\varepsilon_y \end{bmatrix} \begin{bmatrix} x_1 \\ x_2 \end{bmatrix} \qquad (6$$

The coordinates of the basis vectors of the strained cell follow from this so that the basis vectors become

$$\mathbf{b}_1' = b_1 \begin{bmatrix} 1+\varepsilon_x \\ \tfrac{1}{2}\gamma_{xy} \end{bmatrix} \quad \text{and} \quad \mathbf{b}_2' = b_2 \begin{bmatrix} (1+\varepsilon_x)\cos\beta + \tfrac{1}{2}\gamma_{xy}\sin\beta \\ \tfrac{1}{2}\gamma_{xy}\cos\beta + (1+\varepsilon_y)\sin\beta \end{bmatrix} . \qquad (7$$

Manipulation of these vector expressions yield the unit cell parameters. The sides of the unit cells are:

$$b_1' = b_1[(1+\varepsilon_x)^2 + \tfrac{1}{4}\gamma_{xy}^2]^{\frac{1}{2}}$$

$$\text{and,} \quad b_2' = b_2\{[(1+\varepsilon_x)\cos\beta + \tfrac{1}{2}\gamma_{xy}\sin\beta]^2 + [\tfrac{1}{2}\gamma_{xy}\cos\beta + (1+\varepsilon_y)\sin\beta]^2\}^{\frac{1}{2}} \qquad (8$$

while the angles follow from

$$b_1'b_2'\cos\beta' = \mathbf{b}_1'\cdot\mathbf{b}_2' = b_1b_2\{(1+\varepsilon_x)[(1+\varepsilon_x)\cos\beta + \tfrac{1}{2}\gamma_{xy}\sin\beta] + \tfrac{1}{2}\gamma_{xy}[\tfrac{1}{2}\gamma_{xy}\cos\beta + (1+\varepsilon_y)\sin\beta]\} \qquad (9a$$

for β', where the sense of the angle is given by the vector cross product of $\mathbf{b}_1'$ and $\mathbf{b}_2'$,

and

$$\theta' = \theta + \delta\theta = \theta \pm \arccos\left\{\frac{1+\varepsilon_x}{[(1+\varepsilon_x)^2 + \tfrac{1}{4}\gamma_{xy}^2]^{\frac{1}{2}}}\right\} \quad , \qquad (9b$$

where the sign is positive if $\gamma_{xy} \geq 0$ and negative otherwise.

In all these expressions the components of the wave vector $[h\ k]^*$ in the reciprocal lattice of the strained crystal are given as

$$p' = hr'_{11}c'_\theta + kr'_{12}s'_\theta$$

and

$$q' = hr'_{21}s'_{\theta\beta} + kr'_{22}c'_{\theta\beta} \qquad (10a$$

where the primed transformation parameters have the same form as for the unstrained system, (Chapter 3, eqns 3.6, 8 and 12) but are expressed in terms of the primed unit cell parameters,:

$$r'_{11} = b'_1/a_1 \quad , \quad r'_{12} = b'_1/a_2 \ ,$$
$$r'_{21} = b'_2/a_1 \quad , \quad r'_{22} = b'_2/a_2 \ , \qquad (10b$$

while,

$$c'_\theta = \sin(\alpha-\theta')/\sin\alpha \quad , \quad s'_\theta = \sin\theta'/\sin\alpha$$

and

$$s'_{\theta\beta} = \sin(\alpha-\theta'-\beta')/\sin\alpha \quad , \quad c'_{\theta\beta} = \sin(\theta'+\beta')/\sin\alpha \ . \qquad (10c$$

Hence, per interfacial atom, the misfit energy is (Chapter 3 eqn 3.27) :

$$\varepsilon_{mis} = \sum_{h,k} V_{hk}F^0\left\{(1+F^+)\frac{\sin\pi(2M+1)p'}{\sin\pi p'}\cdot\frac{\sin\pi(2N+1)q'}{\sin\pi q'} + \right.$$
$$\left. + F^+G'(M,N)\right\}_{hk} \ . \qquad (11a$$

As introduced in chapter 3 (eqns 3.26,29,30 and 37) the structure factors are:

$$F^0 = e^{i2\pi\gamma_0} = e^{iq\cdot r_0} \qquad (11b$$

for the lattice atom, and

$$[1 + F^+(p',q')]_{hk} = [1 + \kappa\, e^{i2\pi(p'x_b^+ + q'y_b^+)}]_{hk} \ , \qquad (11c$$

due to the basis atom in the unit cell, and the term:

$$G'(M,N)_{hk}=\left\{e^{-i2\pi[(M+1)p'+(N+1)q']}\left[e^{i2\pi(M+1)p'}\frac{\sin\pi(2M+1)p'}{\sin\pi p'}\right.\right.$$
$$\left.\left.+\ e^{i2\pi(N+1)q'}\ \frac{\sin\pi(2N+1)q'}{\sin\pi q'}+1\right]\right\}_{hk} \qquad (11d$$

corrects for the basis atoms at the edges.

Strain Energy (Isotropic case)

The strain energy per unit volume, w is

$$w = \frac{1}{2}\,\sigma^{T}\cdot\varepsilon = \frac{1}{2}\,(D_{11}\,\varepsilon_x^2 + D_{22}\,\varepsilon_y^2 + 2D_{12}\,\varepsilon_x\varepsilon_y + D_{33}\,\gamma_{xy}^2)\ , \qquad (12$$

with constants as in equation 4b.

This expression (for an essentially unbounded island) leads to a definition of the *configurational parameter*, ℓ (van der Merwe 1973, 1980).

Integrating over the volume of the overgrowth and dividing by the number of overgrowth atoms in the interface, the strain energy per interfacial atom becomes:

$$\mathcal{E}_{el}^{\infty} = W\,\ell^2\,r^2\,(\,\varepsilon_x^2 + \varepsilon_y^2 + 2P\,\varepsilon_x\varepsilon_y + R\,\gamma_{xy}^2)\ . \qquad (13a$$

Introduced here are the quantities

$$P = \nu/Wr^2 \quad \text{and} \quad R = (1-\nu)/Wr^2\ , \qquad (13b$$

and the parameter

$$\ell^2 = \frac{\mu\,\Omega}{(1-\nu)W\,r^2}\ . \qquad (14$$

ℓ^2 is the *configurational parameter*, W is the energy calibration factor specific to the adatom-substrate interaction potential and is a measure of the strength of the overgrowth-substrate interaction, and r is the nearest neighbour ratio of the unstrained overgrowth and substrate systems. Ω is the volume per *interfacial* atom in the unstrained overgrowth, and is

Ω = *thickness of the overgrowth* x *area of primitive cell*. (15a

The primitive cell referred to is an interfacial surface unit cell of the unstrained overgrowth and contains exactly one interfacial atom.

This definition accommodates an overgrowth thicker than just one monolayer, and makes it possible to compare overlayers of any thickness in a single phase diagram, which gives the epitaxial configuration as a function of ℓ and r.

For a monolayer of bcc{110} material, the atomic volume is

$$\Omega = b_0/\sqrt{2} \times \frac{1}{2}\sqrt{2}\, b_0^2 = 4\, b_{nn}^3/\sqrt{27}\,, \qquad (15b$$

where b_0 is the cubic lattice parameter of the conventional bcc unit cell, and b_{nn} is the distance between nearest neighbour lattice points.

The configurational parameter ℓ relates the factors which contribute significantly to the epitaxy of crystalline systems. It contains

(*i*) measure of the maximum possible gain in misfit energy (per interfacial atom) as the amplitude W of the adatom-substrate interaction potential,

(*ii*) the energy cost during a unit strain (also per interfacial atom), as the quantity $\mu\Omega/(1-\nu)$, and implicitly contains the thickness of the overgrowth in Ω, as well as

(*iii*) a measure of the deformation necessary to achieve coherency, as the nearest-neighbour ratio $r = b_{nn}/a_{nn}$.

For the bounded island considered here, the elastic strain energy per interfacial atom is modified slightly, because of the excess of material introduced for the boundary treatment, and is correspondingly slightly larger. It is [figure 4.4(c), (d)(iii)]

$$\varepsilon_{el} = \varepsilon_{el}^{\infty}\, \Omega^B/\Omega \qquad (16$$

with Ω^B, the mean volume of an interfacial atom for the bounded island, which is

$$\Omega^B = 8b_{nn}^3/\sqrt{27} \times \frac{(2M+1)(2N+1)+(2M+1)+(2N+1)+1}{2(2M+1)(2N+1)+(2M+1)+(2N+1)+1} \cdot \qquad (17$$

It is convenient to keep the definition of ℓ^2 independent of the island size and dependent on the isotropic constants. The anisotropy ratio and ℓ^2 together characterize epitaxial systems. Real systems of like crystals growing on one another have ℓ about 5 (van der Merwe 1982). Here for the purpose of the phase diagram, values ranging from about 2 to about 16 will be considered.

Strain Energy (Anisotropic case)

Real bcc metals are generally anisotropic. Anisotropy ratios, defined as (Hirth and Lothe 1968 Ch 2)

$$A = 2c_{44}/(c_{11}-c_{12}) \qquad (18$$

range in value from 0.69 for Cr to 8.15 for Na while Tungsten is isotropic with $A = 1$. It is therefore appropriate to consider the effect of the anisotropy on the modes assumed by the epitaxial system to minimize the misfit. The constants c_{11}, c_{12} and c_{44} are the as-tabulated stiffness constants (in the conventional contracted notation) of the materials expressed in the conventional cubic axes associated with the lattices.

To this end, the anisotropy must be expressed in some way independent of the isotropic elastic constants, so that the effect of anisotropy alone may be examined. Isotropic constants of a prototype material are first calculated, and, while keeping them unchanged, new elastic constants are calculated for each required anisotropy ratio.

Once these modified anisotropic constants have been calculated, they are expressed in terms of the coordinate system appropriate to the description of the strain. The tensor transformation from the cubic axes to the local cartesian coordinates is applied below.

Modification of elastic constants to specific anisotropies

Isotropic elastic constants are suitably defined in terms of an averaging process, (Hirth *e.a.* 1978 Ch 13) in which the effect of a unit strain is related to the energy over the entire sphere of the directions in 3-dimensions. Applied to the stiffness constants, the *Voigt* averages are expressable in terms of the anisotropy factor, (Hirth *e.a.* eqns 13.26,27)

$$\begin{aligned} \mathcal{H} &= 2c_{44} + c_{12} - c_{11} \\ &= (A-1)(c_{11}-c_{12}) \ . \end{aligned} \qquad (19$$

The Voigt average isotropic constants are:

$$\mu = c_{44} - \mathcal{H}/5 \quad , \quad \lambda = c_{12} - \mathcal{H}/5 \ ,$$

$$\text{with,} \quad \lambda+2\mu = c_{11} + 2\mathcal{H}/5 \quad \text{and} \quad \nu = \lambda/2(\mu+\lambda) \ , \qquad (20$$

where μ is the shear modulus, λ is the Lamé constant, and ν is Poisson's ratio.

Once these isotropic constants have been calculated for the prototype material, it is a simple matter to invert the expressions and calculate new stiffness constants according to the required anisotropy. The modified anisotropy factor H, may be calculated in terms of the isotropic constants and the anisotropy ratio A, so that

$$H = 10(A-1)\mu/(3A+2) \ . \qquad (21$$

The modified stiffness constants follow as

$$c_{11} = (\lambda+2\mu)-2H/5 \quad , \quad c_{12} = \lambda + H/5 \quad \text{and} \quad c_{44} = \mu + H/5 \ . \qquad (22$$

The Voigt average isotropic constants of these modified stiffness constants will be the same as those of the original prototype material.

Table 4.1, relates the constants of the prototype material, bcc-Fe, to the modified constants for several anisotropies. In the actual numerical calculations of the deformable overgrowths, anisotropy values of A = ½, 1 and 5 were used. Fe was chosen largely because it came closest to a good 'average' material, if the stiffness constants of several bcc materials were simply averaged. Similar modification of the elastic constants of bcc-Fe have been performed by Heinisch and Sines (1976), but with the added restriction that the Cauché relations had to be satisfied.

Table 4.1 *Modified elastic stiffness constants of* bcc-Fe

	Anisotropy ratio (A)	*Factor* (H)†	*stiffness constants* † c_{11}	c_{12}	c_{44}
	0.5	-1.24	3.427	0.961	0.616
	1.0	0.0	2.934	1.208	0.863
	2.0	1.08	2.503	1.424	1.079
‡	2.35	1.29	2.42	1.465	1.12
	5.0	2.03	2.122	1.614	1.269
	8.0	2.32	2.005	1.673	1.328

The isotropic constants of bcc-Fe *are* λ=1.208†, μ=0.863†, ν=0.292

† *all* x 10^{12} *dyne* cm^{-2}

‡ *unmodified* bcc-Fe *from Hirth and Lothe* (1968).

Transformation of the elastic constants to local coordinates

The cartesian axes most suited to the description of strain in the bcc{110} overgrowth material have unit vectors $\mathbf{e}_1$, $\mathbf{e}_2$, $\mathbf{e}_3$ parallel to the $\langle\bar{1}\ 1\ 0\rangle$, $\langle 0\ 0\ 1\rangle$ and $\langle 1\ 1\ 0\rangle$ directions, which correspond to $\mathbf{b}_1$, $\mathbf{b}_2$ and a normal vector, respectively. The transformation from cartesian coordinates coinciding with the cubic axes of the crystal to these local cartesian coordinates is most easily accomplished by the rotation (Euler angles - Goldstein 1950 art 4.4) φ_e=135° about the $\langle 0\ 0\ 1\rangle$ crystallographic direction, followed by a rotation θ_e=90° about the (rotated) $\langle 1\ 0\ 0\rangle$ axis.

(The third Euler angle, Ψ_e, is zero.) The transformation matrix for these rotations is then

$$(t_{ij}) = \begin{bmatrix} -1/\sqrt{2} & 1/\sqrt{2} & 0 \\ 0 & 0 & 1 \\ 1/\sqrt{2} & 1/\sqrt{2} & 0 \end{bmatrix} . \qquad (23$$

The transformation rule follows the law for 4'th rank tensors,

$$C_{mn} = C_{ijkl} = \sum_{g,h,p,q} t_{ig} t_{jh} c_{ghpq} t_{kp} t_{lq} , \qquad (24$$

where (C_{ijkl}) are the transformed elastic constants in full tensor notation, while (C_{mn}) are in the conventional contracted notation.

The effort of the transformation may be reduced by taking the symmetry properties of the final coordinate system into account. Waterman (1959) has presented a systematic method which gives the final form of the elasticity matrix from these symmetry properties.

For the local axes chosen here, the matrix of elastic constants has the sparse form:

$$\begin{bmatrix} C_{11} & C_{12} & C_{13} & 0 & 0 & 0 \\ C_{12} & C_{22} & C_{13} & 0 & 0 & 0 \\ C_{13} & C_{12} & C_{11} & 0 & 0 & 0 \\ 0 & 0 & 0 & C_{44} & 0 & 0 \\ 0 & 0 & 0 & 0 & C_{55} & 0 \\ 0 & 0 & 0 & 0 & 0 & C_{44} \end{bmatrix} . \qquad (25$$

Thus one needs to compute only C_{11}, C_{12}, C_{13}, C_{22}, C_{44} and C_{55} from the transformation equation.

Table 4.2 lists these unique transformed constants in terms of the cubic stiffness constants.

Table 4.2 *Anisotropic stiffness constants expressed in local* bcc{110} *coordinates.*

$C_{11} = \frac{1}{2}(c_{11} + c_{12} + 2c_{44})$	$C_{12} = c_{12}$
$C_{13} = \frac{1}{2}(c_{11} + c_{12} - 2c_{44})$	$C_{22} = c_{11}$
$C_{44} = c_{44}$	$C_{55} = \frac{1}{2}(c_{11}-c_{12})$

Plane Stress Boundary conditions

The plane stress conditions are imposed to reduce the problem to two dimensions, i.e $\sigma_{33} = 0$ and $\sigma_{3i} = \sigma_{i3} = 0$ for $i \neq 3$. This immediately implies that $\gamma_{3i} = \gamma_{i3} = 0$, while $C_{13}\varepsilon_{11} + C_{12}\varepsilon_{22} + C_{11}\varepsilon_{33} = \sigma_{33} = 0$. Eliminating ε_{33}, and again simplifying the notation to 2-dimensional form, Hookes law reduces to

$$\boldsymbol{\sigma} = \begin{bmatrix}\sigma_x \\ \sigma_y \\ \sigma_{xy}\end{bmatrix} = \mathbf{D}\cdot\boldsymbol{\varepsilon} = (D_{ij})\varepsilon_x$$

$$= \begin{bmatrix}(C_{11}^2-C_{13}^2)/C_{11} & (C_{11}C_{12}-C_{12}C_{13})/C_{11} & 0 \\ (C_{11}C_{12}-C_{12}C_{13})/C_{11} & (C_{11}C_{22}-C_{12}^2)/C_{11} & 0 \\ 0 & 0 & C_{44}\end{bmatrix}\begin{bmatrix}\varepsilon_x \\ \varepsilon_y \\ \gamma_{xy}\end{bmatrix} . \quad (26$$

In this equation, $\mathbf{D}$ is the elastic matrix for the two-dimensional anisotropic plane stress problem, with the required degree of anisotropy. This elastic matrix has the same sparse form as the isotropic plane stress matrix, so the strain energy per atom becomes

$$\mathcal{E}_{el} = \frac{1}{2}(D_{11}\varepsilon_x^2 + D_{22}\varepsilon_y^2 + 2D_{12}\varepsilon_x\varepsilon_y + D_{33}\gamma_{xy}^2)\Omega^b . \quad (27$$

The configurational parameter ℓ^2 is still defined in terms of the isotropic constants. This means that two dimensionless parameters

define an overgrowth-substrate pair, the unique configurational parameter, and the anisotropy ratio A. (In fact it may be argued that the Poisson ratio ν which appears in the definition of ℓ should also be quoted separately, but as its value varies very little, and is usually about 0.3, its contribution is less than that of the other two. As it is included in ℓ its effect is implicitly taken into account.)

4.4 PREDICTION OF STRAINS FROM THE RECIPROCAL LATTICE

(Refer to Chapter 3, section 3.3 for the original rigid derivation)

Exact row-matching has been shown to be a necessary condition for a misfit energy minimum to occur for rigid systems. This was characterized by the condition that an overgrowth reciprocal lattice translation vector must coincide with a substrate reciprocal lattice vector. Reciprocal lattice matching may be used to predict not only the necessary orientations and nearest neighbour ratios for row-matching for ideal systems, but also the strains and rotations needed if the overgrowth is non-ideal but flexible. These strains naturally depend on the elastic properties derived above.

Two strain mechanisms are particularly simple for one-dimensional row matching. The first changes the size of the unit cell without changing its shape, and is best described as *isotropic* homogeneous strain.

The second uses the elastic constants, and strains to achieve coincidence of the overgrowth and substrate wave vectors, but in such a way that the strain energy is a minimum.

A special case which follows from the second situation, is that in which the overgrowth has been rotated so that the wave vectors share the same direction, but must strain to achieve equality of length. It follows that the minimum energy requirement causes the

Poisson effect to predominate. Physically, the problem is reduced to a one-dimensional matching case, in which the misfit energy can be reduced to a minimum by strain in one direction, but is not influenced at all by strain in the orthogonal direction, and minimum energy strain yields the Poisson effect.

Match achieved by isotropic strain

Isotropic homogeneous strain retains the shape of the overgrowth, but changes its dimensions by a scale factor in order to achieve row matching.

Row matching (Chapter 3 eqn 3.31, 39) is achieved by coincidence of the overgrowth reciprocal lattice vector $\mathbf{q}^{pq}$ with a substrate reciprocal lattice vector $\mathbf{q}_{hk}$, so that

$$\mathbf{q}^{pq} = \mathbf{q}_{hk} \quad . \tag{28}$$

To achieve this coincidence, the overgrowth rotates through an angle given by

$$\cos \phi_r = \mathbf{q}_{hk} \cdot \mathbf{q}^{pq} / [|\mathbf{q}_{hk}| \cdot |\mathbf{q}^{pq}|] \quad , \tag{29}$$

and must accommodate a misfit in the common direction, given crystallographically by the wave vectors, of (eqn 3.34)

$$f_{hk}^{pq} = \frac{|\mathbf{q}_{hk}|}{|\mathbf{q}^{pq}|} - 1 \quad . \tag{30}$$

Again, the sense of the angle is determined from the vector cross-product of the two vectors.

If r' is the nearest neighbour ratio which produces row-matching, and an epitaxial system has the ratio r, then the required isotropic strain is

$$\varepsilon_x = \varepsilon_y = \frac{r'}{r} - 1 = \frac{|\mathbf{q}^{pq}|}{|\mathbf{q}_{hk}|} - 1 \tag{31}$$

without shear.

As this change of overall dimensions is isotropic the cartesian coordinates in which the strains are described may be in any orientation.

Although easy to calculate, as it is independent of elastic constants, isotropic strain is of limited value as non-isotropic strain will have lower strain energy. The only exception is the special case in which the overgrowth and substrate have the same structure and complete pseudomorphism can be achieved by isotropic strain alone.

Strain which minimizes the interfacial energy

The interfacial energy consists of two contributions, namely the misfit energy, given by the adatom-substrate interaction potential as summed over the interfacial overgrowth atoms, and the energy due to the strain of the overgrowth. It follows from the rigid model that the misfit energy is a minimum when the overgrowth reciprocal lattice vector $\mathbf{q}^{pq}$ representing a particular set of rows of atoms, coincides with a substrate reciprocal lattice vector $\mathbf{q}_{hk}$. This energy minimum has a depth given by the value of the Fourier coefficient V_{hk} corresponding to the substrate vector $\mathbf{q}_{hk}$. Off-ideal systems which must strain to achieve this coincidence of wave vectors, will achieve exactly the same minimum value of misfit energy. The strain which will actually occur, will minimize the elastic strain energy, independently of the misfit energy.

Therefore, the strain must satisfy the constraint relation

$$\mathbf{q}^{pq} = \mathbf{q}_{hk}$$

which minimizes the misfit energy, and is subject to the requirement of minimum strain energy to achieve this coincidence.

As the two contributions to the energy are minimized separately and simultaneously, the interfacial energy is a minimum.

As before, the cartesian coordinates in which the strains are expressed have the unit vectors $\mathbf{e}_x$ parallel to $\mathbf{b}_1$, with $\mathbf{e}_y$ perpendicular.

In order to express the governing equation in terms of strain it is necessary to investigate the effect of strain on the reciprocal lattice in particular and reciprocal space in general.

The effect of strain on reciprocal space

A homogeneous strain of direct space can be described as a linear transformation, (Kelly and Groves 1973, ch 5)

$$\mathbf{X} = \begin{bmatrix} X \\ Y \end{bmatrix} = \begin{bmatrix} \alpha_x & \tfrac{1}{2}\gamma_{xy} \\ \tfrac{1}{2}\gamma_{xy} & \alpha_y \end{bmatrix} \cdot \begin{bmatrix} x \\ y \end{bmatrix} = \mathbf{A} \cdot \mathbf{x} \ , \qquad (32$$

where $\alpha_x = 1+\varepsilon_x$, $\alpha_y = 1+\varepsilon_y$ and γ_{xy} is the shear, and $\mathbf{x}$ is the initial position of a point in the space, and $\mathbf{X}$ its final position after strain.

The effect of the strains ε_x , ε_y and γ_{xy} on the reciprocal lattice can be determined from the effect this transformation has on the cartesian unit vectors of the direct and reciprocal spaces.

Consider the unit vectors before strain, $\mathbf{e}_x$, $\mathbf{e}_y$ and $\mathbf{e}_z$ in direct space, and

$$\mathbf{e}_x^* = \mathbf{e}_y \times \mathbf{e}_z / |\mathbf{e}_x \times \mathbf{e}_y| = \mathbf{e}_x \ , \qquad (33$$
$$\mathbf{e}_y^* = \mathbf{e}_z \times \mathbf{e}_x / |\mathbf{e}_x \times \mathbf{e}_y| = \mathbf{e}_y \ ,$$

and $\mathbf{e}_z^* = \mathbf{e}_z$ in reciprocal space.

After strain, the unit vectors become,

$$\mathbf{E}_x = \alpha_x \mathbf{e}_x + \tfrac{1}{2}\gamma_{xy}\mathbf{e}_y \ , \qquad (34a$$
$$\mathbf{E}_y = \tfrac{1}{2}\gamma_{xy}\mathbf{e}_x + \alpha_y \mathbf{e}_y \ ,$$

and $\mathbf{E}_z = \mathbf{e}_z$ in direct space,

and

$$\mathbf{E}_x^* = (\alpha_y \mathbf{e}_x - \tfrac{1}{2}\gamma_{xy}\mathbf{e}_y)/(\alpha_x\alpha_y - \tfrac{1}{4}\gamma_{xy}^2) \ , \qquad (34b$$
$$\mathbf{E}_y^* = (-\tfrac{1}{2}\gamma_{xy}\mathbf{e}_x + \alpha_x \mathbf{e}_y)/(\alpha_x\alpha_y - \tfrac{1}{4}\gamma_{xy}^2) \ ,$$

and $\mathbf{E}_z^* = \mathbf{e}_z$ in reciprocal space.

The resulting linear transformation in reciprocal space is therefore given by the transformation matrix $\mathbf{A}^*$, which is

$$\mathbf{A}^* = \frac{1}{(\alpha_x\alpha_y - \frac{1}{4}\gamma_{xy}^2)} \begin{bmatrix} \alpha_y & -\tfrac{1}{2}\gamma_{xy} \\ -\tfrac{1}{2}\gamma_{xy} & \alpha_x \end{bmatrix} \equiv \begin{bmatrix} \alpha_x^* & \tfrac{1}{2}\gamma_{xy}^* \\ \tfrac{1}{2}\gamma_{xy}^* & \alpha_y^* \end{bmatrix} = \mathbf{A}^{-1} \ . \qquad (35$$

Determination of the strains

The constraint equation may now be expressed in terms of the coordinates of the wave vectors expressed in terms of the cartesian coordinate system, and the transformation matrices as:

$$\mathbf{q}_{hk} = \begin{bmatrix} Q_x \\ Q_y \end{bmatrix} = \begin{bmatrix} \alpha_x^* & \tfrac{1}{2}\gamma_{xy}^* \\ \tfrac{1}{2}\gamma_{xy}^* & \alpha_y^* \end{bmatrix} \cdot \begin{bmatrix} q_x \\ q_y \end{bmatrix} = \mathbf{A}^* \cdot \mathbf{q}^{pq} \ . \qquad (36$$

The components q_x and q_y are the cartesian coordinates of the overgrowth reciprocal lattice vector before the overgrowth is strained, and the components Q_x and Q_y are the cartesian coordinates of the substrate reciprocal lattice vector with which the overgrowth vector must coincide after strain, both expressed in terms of the unit vectors $\mathbf{e}_x$ and $\mathbf{e}_y$.

These constraint equations may be expressed in terms of the direct space transformation parameters, and solved for two of the strain components, most naturally the normal strains.

Then

$$Q_x = (\alpha_y q_x - \tfrac{1}{2}\gamma_{xy} q_y)/(\alpha_x\alpha_y - \tfrac{1}{4}\gamma_{xy}^2) \ , \qquad (37a$$

and $$Q_y = (-\tfrac{1}{2}\gamma_{xy}q_x + \alpha_x q_y)/(\alpha_x\alpha_y - \tfrac{1}{4}\gamma_{xy}^2) \quad . \qquad (37b$$

In addition, the shear strain is determined from the condition of the minimum elastic strain energy,

$$\frac{d\mathcal{E}_{el}}{\Omega_b} = [D_{11}\alpha_x-(D_{11}+D_{12})]d\alpha_x + [D_{22}\alpha_y-(D_{22}+D_{12})]d\alpha_y + D_{33}\gamma_{xy}d\gamma_{xy} + D_{12}\alpha_y d\alpha_x + D_{12}\alpha_x d\alpha_y = 0 \quad . \qquad (38$$

The constraint equations have the solutions

$$\alpha_x = (q_x - Q_y\tfrac{1}{2}\gamma_{xy})/Q_x = 1 + \varepsilon_x \qquad (39a$$

and

$$\alpha_y = (q_y - Q_x\tfrac{1}{2}\gamma_{xy})/Q_y = 1 + \varepsilon_y \quad .$$

Substituting for α_x, α_y, $d\alpha_x$ and $d\alpha_y$ to express this in terms of γ_{xy} only, and substituting these into the extremum condition yields γ_{xy} as

$$\tfrac{1}{2}\gamma_{xy} = \frac{\frac{(q_x-Q_x)}{Q_x}\left[D_{11}\frac{Q_y}{Q_x} + D_{12}\frac{Q_x}{Q_y}\right] + \frac{(q_y-Q_y)}{Q_y}\left[D_{22}\frac{Q_x}{Q_y} + D_{12}\frac{Q_y}{Q_x}\right]}{D_{11}\left[\frac{Q_y}{Q_x}\right]^2 + D_{22}\left[\frac{Q_x}{Q_y}\right]^2 + 2D_{12} + 4D_{33}} \quad . \qquad (39b$$

Substituting this back into α_x and α_y completes the solution.

The quantities $(q_x-Q_x)/Q_x$ and $(q_y-Q_y)/Q_y$ are in fact Eulerian strains in the reciprocal space.(Sokolnikoff 1956, Ch1)

This solution is for the most general case, in which the vectors $\mathbf{q}^{pq}$ and $\mathbf{q}_{hk}$ are brought into coincidence by strain of the overgrowth alone, without rotation. Any rotation of the overgrowth must be carried out before the vectors are expressed in terms the common cartesian coordinates, and the remaining misfit of the system is accommodated by this calculated strain.

Special Case solutions

Several cases in which this solution provides indeterminate answers, or none at all must be treated separately. They are generally speaking the cases in which Q_x and Q_y singly or together are zero.

(i) $q_y \neq 0$, $Q_y = 0$:
Here $\alpha_x = q_x/Q_x$, $\gamma_{xy} = 0$, but $\alpha_y = \infty$,
which means that in this case misfit cannot be accommodated by strain alone from the existing orientation.

(ii) $q_x \neq 0$, $Q_x = 0$:
The case is similar to *(i)*, with $\alpha_y = q_y/Q_y$ and $\alpha_x = \infty$.

(iii) Poisson cases:
$q_y = Q_y = 0$:
The constraint equations have the solution
$\alpha_x = q_x/Q_x$, and $\gamma_{xy} = 0$.
The energy minimization equation then has to be solved for α_y, from which
$(\alpha_y - 1)D_{22} = -D_{12}(\alpha_x - 1)$,
so that the strain follows directly as

$$\varepsilon_y = -\frac{D_{12}}{D_{22}}\varepsilon_x .$$

The similar result $\varepsilon_y = q_y/Q_y$ and $\varepsilon_x = -\frac{D_{12}}{D_{11}}\varepsilon_y$ follows when $q_x = Q_x = 0$.

Although these special solutions apply only to the particular set of axes which yield these conditions directly, the Poisson case in fact always occurs when the two wave vectors have been rotated to the same direction. The general solution provides the correct answers, and the Poisson effect is evident when the strains are expressed in principal axes.

(iv) $q_y = Q_y$ and $q_x = Q_x$:
This is the trivial case in which no strain at all is needed,

and $\alpha_x = \alpha_y = 1$, and $\gamma_{xy} = 0$. This case and the case in which only one of the components is the same follows directly from the general solution.

Of the special cases, clearly the Poisson case is physically the most useful, while (i) and (ii), and situations close to these, indicate when rotation must preceed the strain if any interfacial energy reduction is to be achieved.

The preceding analysis is particularly useful both because the strains and therefore the energies are available in closed form, and also the anisotropy appears only in the elastic constants themselves, and does not influence the form of these equations. The inclusion of anisotropy therefore adds no complications.

4.5 TWO-DIMENSIONAL COHERENCE FROM THE RECIPROCAL LATTICE

The Transition from 1-dimensional to 2-dimensional match

The form of the unit cell, and its orientation, which produces a 2-dimensional match may be deduced from the condition that *two* substrate reciprocal lattice vectors $[h\ k]^*$ and $[H\ K]^*$, say, are also lattice vectors in the overgrowth reciprocal lattice. Matching the overgrowth reciprocal lattice vectors $[p\ q]_b^*$, *and* $[P\ Q]_b^*$ respectively to the substrate vectors, requires the *simultaneous* satisfaction of the equations: (from eqns 10 and 28)

$$\begin{aligned} p &= hr'_{11}c'_\theta + kr'_{12}s'_\theta \ , \\ q &= hr'_{21}s'_{\theta\beta} + kr'_{22}c'_{\theta\beta} \end{aligned} \qquad (40a$$

and

$$\begin{aligned} P &= Hr'_{11}c'_\theta + Kr'_{12}s'_\theta \ , \\ Q &= Hr'_{21}s'_{\theta\beta} + Kr'_{22}c'_{\theta\beta} \ . \end{aligned} \qquad (40b$$

The explicit form of the transformation constants, leads to the

angles :

$$\cot\theta' = \frac{pK-Pk}{Ph-pH}\cdot\frac{a_1}{a_2\sin\alpha} + \cot\alpha \qquad (41a$$

and $$\cot(\beta'+\theta') = \frac{qK-Qk}{Qh-qH}\cdot\frac{a_1}{a_2\sin\alpha} + \cot\alpha \qquad (41b$$

and unit cell parameters,

$$b_1' = \begin{cases} \dfrac{Ph-pH}{hK-Hk}\cdot\dfrac{a_2\sin\alpha}{\sin\theta'} & , \textit{for} \quad \sin\theta' \neq 0 \\ \dfrac{pK-Pk}{hK-Hk}\,a_1 & \textit{for} \quad \sin\theta' = 0 \end{cases} \qquad (42a$$

and,
$$b_2' = \begin{cases} \dfrac{Qh-qH}{hK-Hk}\cdot\dfrac{a_2\sin\alpha}{\sin(\beta'+\theta')} & , \textit{for} \quad \sin(\beta+\theta) \neq 0 \\ \dfrac{qK-Qk}{hK-Hk}\,a_1 & \textit{for} \quad \sin(\beta+\theta) = 0 \end{cases} \qquad (42b$$

.

The unit cell parameters for 2-dimensional matching, b_1',b_2',β' and the orientation angle θ' of $\mathbf{b}_1'$ wrt $\mathbf{a}_1$ are given by these equations. If the overgrowth does not satisfy these conditions, the strains and rotation needed may be calculated for homogeneous strain.

A rotation followed by strain is a linear transformation, and with both the initial and final coordinates of the overgrowth unit vectors expressed in a space lattice fixed in the substrate lattice, this transformation may be formulated in closed form. Expressed in a cartesian coordinate system with the x_1-axis parallel to the $\mathbf{b}_1$ axis before the transformation, the matrix is (compare egn 32):

$$\mathbf{A} = \begin{bmatrix} a_{11} & a_{12} \\ a_{21} & a_{22} \end{bmatrix} = \begin{bmatrix} \dfrac{b_1'}{b_1}\cos\delta\theta & -\dfrac{b_1'}{b_1}\cdot\cos\delta\theta\cdot\cot\beta+\dfrac{b_2'}{b_2}\cdot\dfrac{\cos(\beta'+\delta\theta)}{\sin\beta} \\ \dfrac{b_1'}{b_1}\sin\delta\theta & -\dfrac{b_1'}{b_1}\cdot\sin\delta\theta\cdot\cot\beta+\dfrac{b_2'}{b_2}\cdot\dfrac{\sin(\beta'+\delta\theta)}{\sin\beta} \end{bmatrix}, \qquad (43$$

with $\delta\theta = \theta'-\theta$.

If the overgrowth is allowed to rotate first, and the strain is expressed in coordinate axes fixed in the overgrowth, the angle of rotation and the strain can be separated from the linear transformation matrix.

In terms of these components, the *angle of rotation* ϕ is given by:

$$\tan \phi = \frac{a_{21}-a_{12}}{a_{11}-a_{22}} \qquad (44$$

The strains are then

$$\varepsilon_x = a_{11}\cos \phi + a_{21}\sin \phi - 1 \ , \qquad (45a$$
$$\varepsilon_y = a_{22}\cos \phi - a_{12}\sin \phi - 1 \ ,$$

and

$$\tfrac{1}{2}\gamma_{xy} = a_{12}\cos \phi + a_{22}\sin \phi = a_{21}\cos \phi - a_{11}\sin \phi \ . \qquad (45b$$

These and all the foregoing strains may be expressed in any rotated coordinate system for convenience of interpretation or comparison. This will be done during a discussion of the results below. The appropriate standard transformation (Sokolnikoff 1956 ch1) is given as eqn A27 in Appendix A.

4.6 RESULTS

Two complementary techniques for calculating homogeneous strains which achieve the minimization of total interfacial energy have been described.

The first method involves the direct numerical minimization of the interfacial energy (section 4.3 eqns 2, 11, 13, 16 and 27) yielding the appropriate strains from a given *fixed* orientation. The energy is minimized subject to the strains only, there is therefore *no rotation* of the island to achieve the energy minima.

With the second method, the strains which minimize the elastic strain energy are determined analytically from the reciprocal lattice (section 4.4 eqns 28, 39). This is based on the observation that once one-dimensional matching is achieved, the misfit energy is very nearly the same, regardless of the initial orientation of the island. This is in fact confirmed by the numerical method, as discussed below.

The results of the numerical method are presented graphically in figure 4.2 for the initial (rigid i.e. unstrained island) misfit energy. The interfacial, misfit and strain energies for optimally strained cases, with two values of the energy parameter W, namely 0.4 eV and 0.9 eV follow. A set of diagrams for each of the three values of the anisotropy ratio, ½, 1 and 5, are given as figures 4.3, 4.4 and 4.5 respectively, illustrating the effect of anisotropy rather vividly.

A set of three phase diagrams in figure 4.6 (p 180), corresponding to the three values of the anisotropy illustrate these effects in another way. These phase diagrams present the energy minimizing (and therefore stable) modes of misfit accommodation, and therefore implicitly, the orientation, related to nearest neighbour ratio and Van der Merwe configurational parameter ℓ. Very evident is the effect of anisotropy on the extent of the 2-dimensionally coherent (or pseudomorphic) phase. This is discussed further below.

The selected cases of 1-dimensional strain in the Nishiyama-Wassermann and Kurdjumov-Sachs orientations, as well as the strains for 2-dimensional coherent matching (section 4.5 eqns 44 and 45) are given in Table 4.3, as derived directly from the reciprocal lattice. The strains of the equivalent cases for the finite island calculated by direct minimization are given for comparison in Table 4.4. The island is that of figure 4.1, with M=11=N.

Not immediately evident from Table 4.3 is the achievement of the pseudomorphic (2DC) configuration. In the section just preceding

these results, the achievement of two-dimensional coherency from a given one-dimensional configuration was discussed. Solving the appropriate equations for an initial NW configuration, at the ideal angle, θ_{NW} , which becomes 2DC, yields the strains given in Table 4.3 (a), and requires no rotation, that is $\phi = 0$. However if the initial orientation is θ_{KS}, or any other than an exact θ_{NW}, θ, say, a rotation $\phi = \theta_{NW}-\theta$ is necessary. The strains are then necessarily the same as in the first case. For an initial KS orientation a rotation of $\phi \simeq 5.26^{\circ}$ is necessary. Studying Table 4.4 shows that in no case in which the orientation was other than θ_{NW} was 2DC coherency achieved, confirming these reciprocal lattice arguments.

The comparison shows that there is excellent agreement between the reciprocal lattice predictions and the finite island, best agreement being achieved close to exact configurations. The effect of secondary mininima arising from the finite nature of the island are illustrated by the data of Table 4.4.

A demonstration that the optimal angle between the $\mathbf{b}_1$ and $\mathbf{a}_1$ vectors changes with anisotropy ratio is given in Table 4.5, calculated from the reciprocal lattice, while the same effect is also evident from the diagrams 4.3 to 4.5. This has implications for the orientations which are actually observed in real systems, as variations as large as about three degrees in the relative orientation about the Kurdjumov-Sachs configuration are introduced. This is discussed below with more detail.

Table 4.3 (a) Strains which achieve coherency from several orientations calculated from the reciprocal lattice of an infinite overgrowth. (With Geometric Extremes)

Anisotropy Ratio	$\theta^{\ddagger}$	$r^{\dagger}$	ε_x	ε_y	γ_{xy}	*Mode*
½,1,5	θ_{NW}	r_{NW}	0	0	0	NW
½	"	1	0.06066	-0.00825	0	"
1	"	"	0.06066	-0.01769	0	"
5	"	"	0.06066	-0.06133	0	"
½	"	r_{KS}	0.15470	-0.02104	0	"
1	"	"	0.15470	-0.04512	0	"
5	"	"	0.15470	-0.15640	0	"
½,1,5	θ_2	r_{NW}	0	-0.18350	0	2DC
"	"	1	0.06066	-0.13397	0	"
"	"	r_{KS}	0.15470	-0.05719	0	"
½	θ_{KS}	r_{NW}	0.05559 (-0.00760	-0.13397 -0.07079	0 -0.17873)†	KS
1	"	"	0.03907 (-0.01861	-0.13397 -0.07629	0 -0.16315)†	"
5	"	"	0.02332 (-0.02911	-0.13397 -0.08154	0 -0.14830)†	"
½	θ_{KS}	1	0.03379 (-0.00462	-0.08144 -0.04303	0 -0.10864)†	"
1	"	"	0.02375 (-0.01131	-0.08144 -0.04638	0 0.09918)†	"
5	"	"	0.01418 (-0.01770	-0.08144 -0.04957	0 -0.09015)†	"
½,1,5	"	r_{KS}	0	0	0	"

The strains are in principle coordinates unless otherwise indicated. In the NW *and* 2DC *modes, the cartesian axes have* $\mathbf{e}_x \| \mathbf{b}_1$, *while* $\mathbf{e}_x$ *makes an angle* $\tan^{-1}(1/\sqrt{2})$ *with* $\mathbf{b}_1$ *in the* KS *mode.*

†*These strains are given in the* NW *axes.*

$^{\ddagger}\theta_{NW} = 30^{\circ} = \theta_2$, $\theta_{KS} = 60^{\circ} - \tan^{-1}(1/\sqrt{2}) = 24.7356^{\circ} = 24^{\circ}\ 44'$

$^{\dagger}r_{NW} = 3/\sqrt{8} = 1.06066$, $r_{KS} = \sqrt{27/32} = 0.918559$

Table 4.3 (b) *Coherency strains calculated from the reciprocal lattice of an infinite overgrowth. (Orientational Extremes)*

Anisotropy Ratio	θ ‡	r !	ε_x	ε_y	γ_{xy}	*Mode*
½	θ_{NW}	r_{NW}	0.07917	-0.15711	0.09142	KS
1	"	"	0.06451	-0.16200	0.07449	"
5	"	"	0.05562	-0.16496	0.06422	"
½	"	1	0.08131	-0.12709	0.02384	"
1	"	"	0.07032	-0.13075	0.01115	"
5	"	"	0.06465	-0.13264	0.00461	"
½	"	r_{KS}	0.08462	-0.08055	-0.08092	"
1	"	"	0.07933	-0.08232	-0.08703	"
5	"	"	0.07866	-0.08254	-0.08781	"
½	θ_{KS}	r_{NW}	-0.08052 (0.01265	0.08470 -0.00847	-0.08082 † -0.18272) †	NW
1	"	"	-0.08232 (0.01259	0.07933 -0.01558	-0.08703 † -0.18141) †	"
5	"	"	-0.08954 (0.01235	0.05765 -0.04424	-0.11206 † -0.17613) †	"
½	θ_{KS}	1	-0.04206 (0.07350	0.09856 -0.01700	-0.14571 † -0.18115) †	"
1	"	"	-0.04624 (0.07336	0.08604 -0.03356	-0.16017 † -0.17810) †	"
5	"	"	-0.06400 (0.07276	0.03275 -0.10401	-0.22170 † -0.16511) †	"
½	θ_{KS}	r_{KS}	0.01756 (0.16783	0.12004 -0.03022	-0.24629 † -0.17871) †	"
1	"	"	0.00970 (0.16756	0.09644 -0.06143	-0.27355 † -0.17296) †	"
5	"	"	-0.02440 (0.16641	-0.00585 -0.19667	-0.39166 † -0.14804) †	"

The strains are expressed in cartesian axes which have $\mathbf{e}_x \| \mathbf{b}_1$ *at* θ_{NW} *while* $\mathbf{e}_x$ *is at* $\tan^{-1}(1/\sqrt{2})$ *to* $\mathbf{b}_1$ *at* θ_{KS}.

† *These strains are given in the* NW *axes.*

‡ $\theta_{NW} = 30^\circ = \theta_2$, $\theta_{KS} = 60^\circ - \tan^{-1}(1/\sqrt{2}) = 24.7356^\circ$

! $r_{NW} = 3/\sqrt{8} = 1.06066$, $r_{KS} = \sqrt{27/32} = 0.918559$

Table 4.4 (a) *Strains obtained by numerical minimization of the Total Interfacial Energy for the Finite Island,* M = N = 11. *Anisotropy Ratio* = ½

A = ½	ε_x	ε_y	γ_{xy}	W	Mode†
$\theta = \theta_{NW} = 30^\circ$					(Refer to Fig 4.3)
$r' = r_{NW}$	0.00006	-0.1827	0	6.0 eV	2DC
	0.00007	-0.02436	0	0.9 eV	NW
	0.00014	-0.02053	0	0.4 eV	NW
	0.00019	-0.00736	0	0.1 eV	NW
$r' = 1$	0.06061	-0.1333	0	6.0 eV	2DC
	0.06031	-0.1297	0	0.9 eV	2DC
	0.05889	-0.03680	0	0.4 eV	NW+~KS
	0.00337	-0.00124	0	0.1 eV	IC
$r' = r_{KS}$	0.1544	-0.05697	0	6.0 eV	2DC
	0.1529	-0.05575	0	0.9 eV	2DC
	0.1506	-0.05402	0	0.4 eV	2DC
	0.0033	-0.00045	0	0.1 eV	IC
$\theta = \theta_{KS} = 60\text{-}\tan^{-1}(1/\sqrt{2}) = 24^\circ 44'$					
$r' = r_{NW}$	-0.07839	0.08901	-0.07460	6.0 eV	NW
	-0.07737	0.08085	-0.07737	0.9 eV	NW
	-0.01116	0.01377	-0.01319	0.4 eV	~NW
	-0.00667	0.00598	-0.00557	0.1 eV	IC
$r' = 1$	0.04344	-0.08117	-0.00012	6.0 eV	KS
	0.04039	-0.07938	-0.00080	0.9 eV	KS
	0.03723	-0.07674	-0.00207	0.4 eV	KS
	-0.00030	-0.00151	-0.00118	0.1 eV	IC
$r' = r_{KS}$	-0.00283	-0.00003	-0.00021	6.0 eV	KS
	-0.00175	-0.00001	-0.00018	0.9 eV	KS
	-0.00111	-0.00003	0	0.4 eV	KS
	-0.00038	-0.00002	-0.00011	0.1 eV	KS

The strains are in the coordinates used in Table 4.3.

(Axes at 0° for θ_{NW} *and at approx 35.26° for* θ_{KS}*)*

† $r_{NW} = 3/\sqrt{8} = 1.06066$, $r_{KS} = \sqrt{27/32} = 0.918559$

† NW : *Nishiyama-Wassermann;* KS : *Kurdjumov-Sachs;* IC : *incoherent;*
2DC : *2-dimensionally coherent (pseudomorphic);*
~NW, ~KS *low-order secondary minima,* ~*NW,* ~*KS high-order secondaries*

Table 4.4 (b) *Strains obtained by numerical minimization of the Total Interfacial Energy for the Finite Island, M = N = 11. Anisotropy Ratio = 1*

A = 1	ε_x	ε_y	γ_{xy}	W	Mode†
$\theta = \theta_{NW} = 30^\circ$					(Refer to Fig 4.4)
$r' = r_{NW}$	0.00010	-0.18284	0	6.0 eV	2DC
	0.00013	-0.02509	0	0.9 eV	NW
	0.00025	-0.02195	0	0.4 eV	NW
	0.00041	-0.00997	0	0.1 eV	NW
$r' = 1$	0.06062	-0.1335	0	6.0 eV	2DC
	0.06036	-0.1309	0	0.9 eV	2DC
	0.05860	-0.03958	0	0.4 eV	NW+~KS
	0.00324	-0.00183	0	0.1 eV	IC
$r' = r_{KS}$	0.1544	-0.05713	0	6.0 eV	2DC
	0.1525	-0.05679	0	0.9 eV	2DC
	-0.00497	-0.00087	0	0.4 eV	IC
	-0.0033	-0.00075	0	0.1 eV	IC
$\theta = \theta_{KS} = 60\text{-}\tan^{-1}(1/\sqrt{2}) = 24^\circ 44'$					
$r' = r_{NW}$	-0.07860	0.08791	-0.07572	6.0 eV	NW
	-0.07744	0.07748	-0.08024	0.9 eV	NW
	-0.01050	0.01281	-0.01404	0.4 eV	~NW
	-0.00543	0.00513	-0.00602	0.1 eV	IC
$r' = 1$	0.04242	-0.08112	0	6.0 eV	KS
	0.03467	-0.07915	-0.00090	0.9 eV	KS
	0.02537	-0.07603	-0.00250	0.4 eV	KS
	-0.00016	-0.00138	-0.00133	0.1 eV	IC
$r' = r_{KS}$	-0.00273	-0	0	6.0 eV	KS
	-0.00156	-0.00002	0	0.9 eV	KS
	-0.00095	0	-0.00016	0.4 eV	KS
	-0.00030	0	-0.00114	0.1 eV	KS

The strains are in the coordinates used in Table 4.3.
(Axes at 0° for θ_{NW} and at approx 35.26° for θ_{KS})

$'r_{NW} = 3/\sqrt{8} = 1.06066$, $r_{KS} = \sqrt{27/32} = 0.918559$

† NW : *Nishiyama-Wassermann*; KS : *Kurdjumov-Sachs*; IC : *incoherent*; 2DC : *2-dimensionally coherent (pseudomorphic)*;
~NW, ~KS *low-order secondary minima*, ~*NW*, ~*KS high-order secondaries*

Table 4.4 (c) *Strains obtained by numerical minimization of the Total Interfacial Energy for the Finite Island,* M = N = 11. *Anisotropy Ratio* = 5

A = 5	ε_x	ε_y	γ_{xy}	W	Mode†
$\theta = \theta_{NW} = 30^\circ$					(Refer to Fig 4.5)
$r' = r_{NW}$	0.00018	-0.1832	0	6.0 eV	2DC
	0.00117	-0.1832	0	0.9 eV	2DC
	0.00050	-0.02463	0	0.4 eV	NW
	0.00124	-0.01723	0	0.1 eV	NW
$r' = 1$	0.06065	-0.1338	0	6.0 eV	2DC
	0.06061	-0.1329	0	0.9 eV	2DC
	0.06052	-0.1317	0	0.4 eV	2DC
	0.00352	-0.00432	0	0.1 eV	IC
$r' = r_{KS}$	0.1543	-0.05745	0	6.0 eV	2DC
	0.1521	-0.05882	0	0.9 eV	2DC
	0.0363	-0.05238	0	0.4 eV	NW⁴
	0.0032	-0.00256	0	0.1 eV	IC
$\theta = \theta_{KS} = 60\text{-}\tan^{-1}(1/\sqrt{2}) = 24^\circ 44'$					
$r' = r_{NW}$	-0.07940	0.08480	-0.07911	6.0 eV	NW
	-0.07931	0.06699	-0.09115	0.9 eV	NW
	-0.00981	0.01083	-0.01695	0.4 eV	~NW
	-0.00423	0.00422	-0.00885	0.1 eV	IC
$r' = 1$	0.04082	-0.08111	-0.00012	6.0 eV	KS
	0.00888	-0.07862	-0.00130	0.9 eV	KS
	0.01078	-0.07509	-0.00312	0.4 eV	KS
	-0.00005	0.00126	-0.00203	0.1 eV	IC
$r' = r_{KS}$	-0.00264	-0.00003	-0.00021	6.0 eV	KS
	-0.00135	-0.00002	-0.00018	0.9 eV	KS
	-0.00078	-0.00001	-0.00016	0.4 eV	KS
	-0.00023	0	-0.00013	0.1 eV	KS

The strains are in the coordinates used in Table 4.3.
(Axes at 0° for θ_{NW} and at approx 35.26° for θ_{KS})

' $r_{NW} = 3/\sqrt{8} = 1.06066$, $r_{KS} = \sqrt{27/32} = 0.918559$

† NW : *Nishiyama-Wassermann;* KS : *Kurdjumov-Sachs;* IC : *incoherent;*
2DC : *2-dimensionally coherent (pseudomorphic);*
~NW, ~KS *low-order secondary minima,* ~NW, ~KS *high-order secondaries*
NW⁴ : *The reciprocal lattice vectors* $[\bar{1}\ 2]^*_a$ *and* $[0\ 2]^*_b$ *are matched*

Table 4.5 *Table of Total Interfacial and Elastic Strain energies as a function of Anisotropy. This demonstrates the deviation from the ideal orientation at the Kurdjumov-Sachs configuration for non-ideal systems.* (W = 0.9eV)

Anisotropy Ratio	$\theta = 24.2^\circ$	$\theta = \theta_{KS}$ †	$\theta = 26^\circ$	*Type of Energy*
r = 0.95	*Energies per interfacial atom* (eV)			
½	0.28654	0.28719	0.29619	*Total energy*
	0.00757	0.00773	0.01714	*Strain energy*
1	0.28888	0.28804	0.29237	*Total energy*
	0.00983	0.00868	0.01390	*Strain energy*
5	0.29248	0.28919	0.28442	*Total energy*
	0.01320	0.00981	0.00649	*Strain energy*
r = 0.96				
½	0.29269	0.29445	0.30507	*Total energy*
	0.01286	0.01381	0.02467	*Strain energy*
1	0.29591	0.29556	0.29994	*Total energy*
	0.01619	0.01527	0.02058	*Strain energy*
5	0.30084	0.29706	0.28995	*Total energy*
	0.02104	0.01697	0.01154	*Strain energy*

† $\theta_{KS} = 60^\circ - \tan^{-1}(1/\sqrt{2})$ *is the orientation of the ideal Kurdjumov-Sachs configuration.*

Clearly $A < 1 \Rightarrow \theta'_{KS} - \theta_{NW} > 5.26^\circ$; $A \simeq 1 \Rightarrow \theta'_{KS} - \theta_{NW} \simeq 5.26^\circ$;

$A > 1 \Rightarrow \theta'_{KS} - \theta_{NW} < 5.26^\circ$, *for* $r > r_{KS}$, *is suggested.*

where θ'_{KS} *is the optimal angle at a given ratio and Anisotropy,*

$\theta_{NW} = 30^\circ$ *is the Ideal Nishiyama-Wassermann orientation*

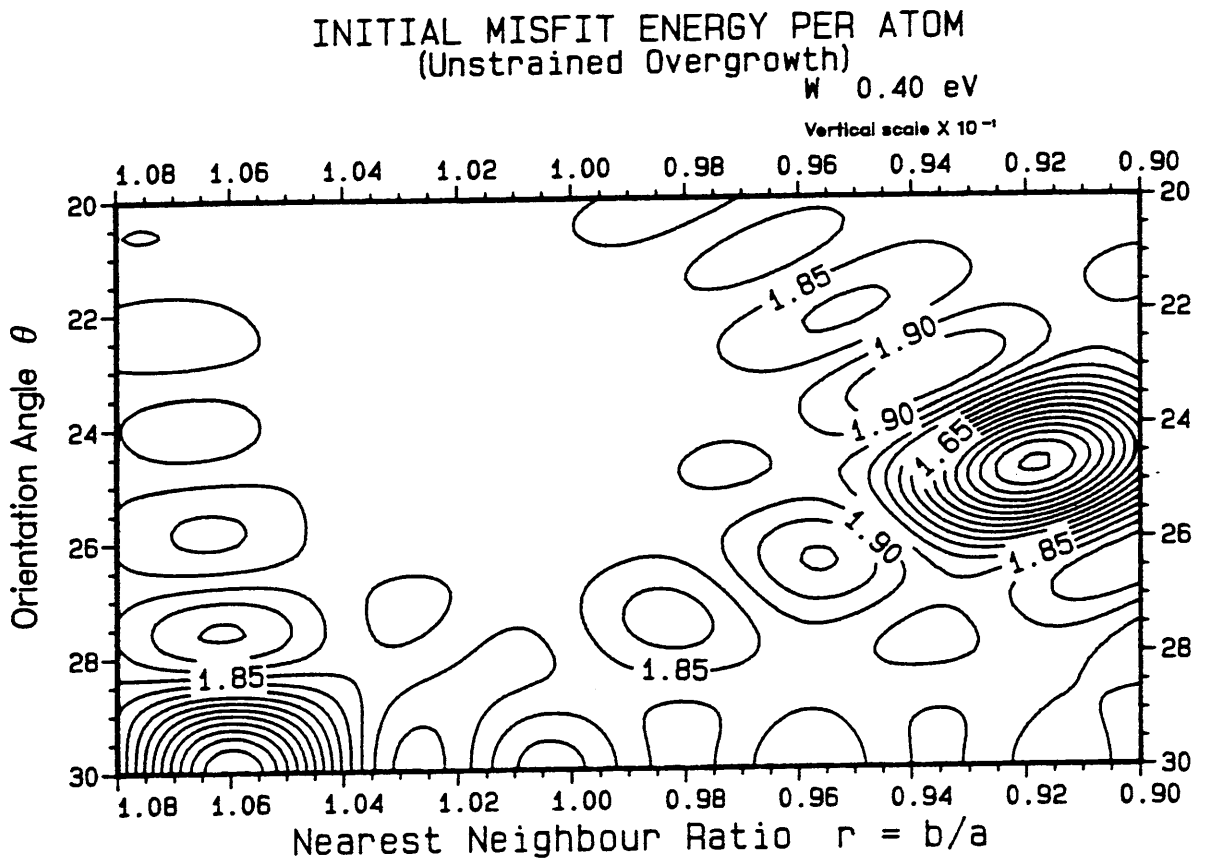

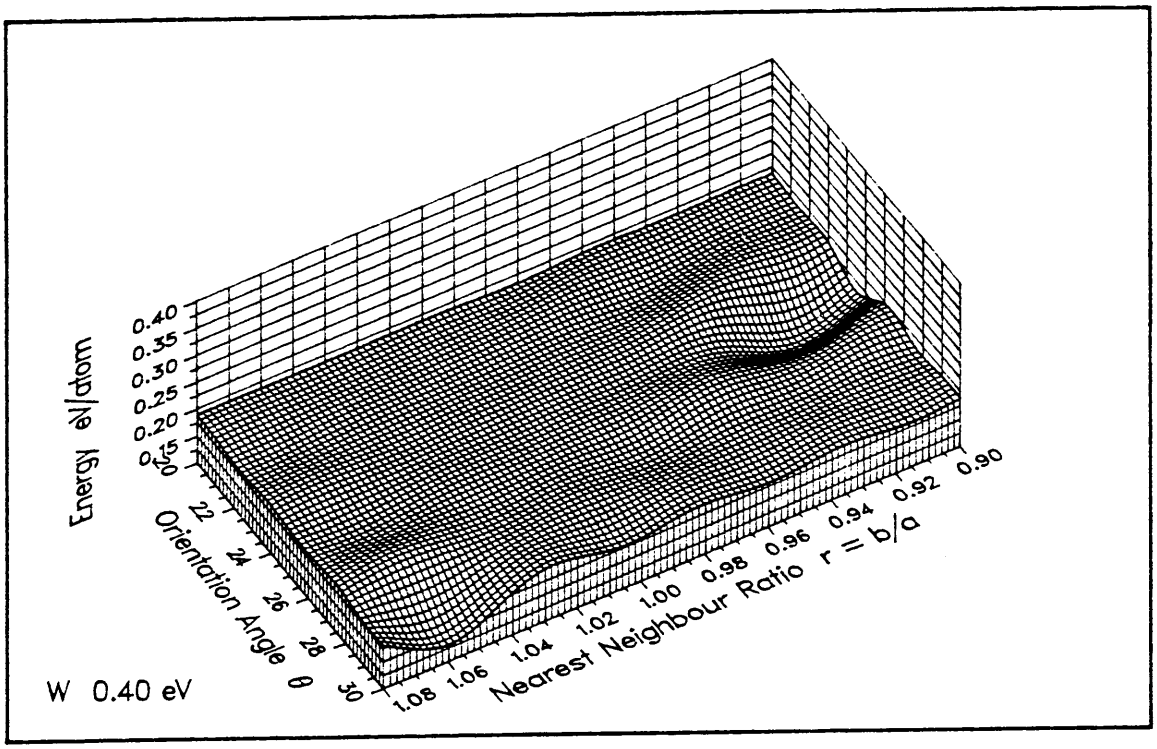

Figure 4.2 Misfit energy of the rigid island of Figure 4.1. Refer to Chapter 3 eqn. 3.27. W = 0.4 eV with the potential Chapter 2 eqn. 2.51.

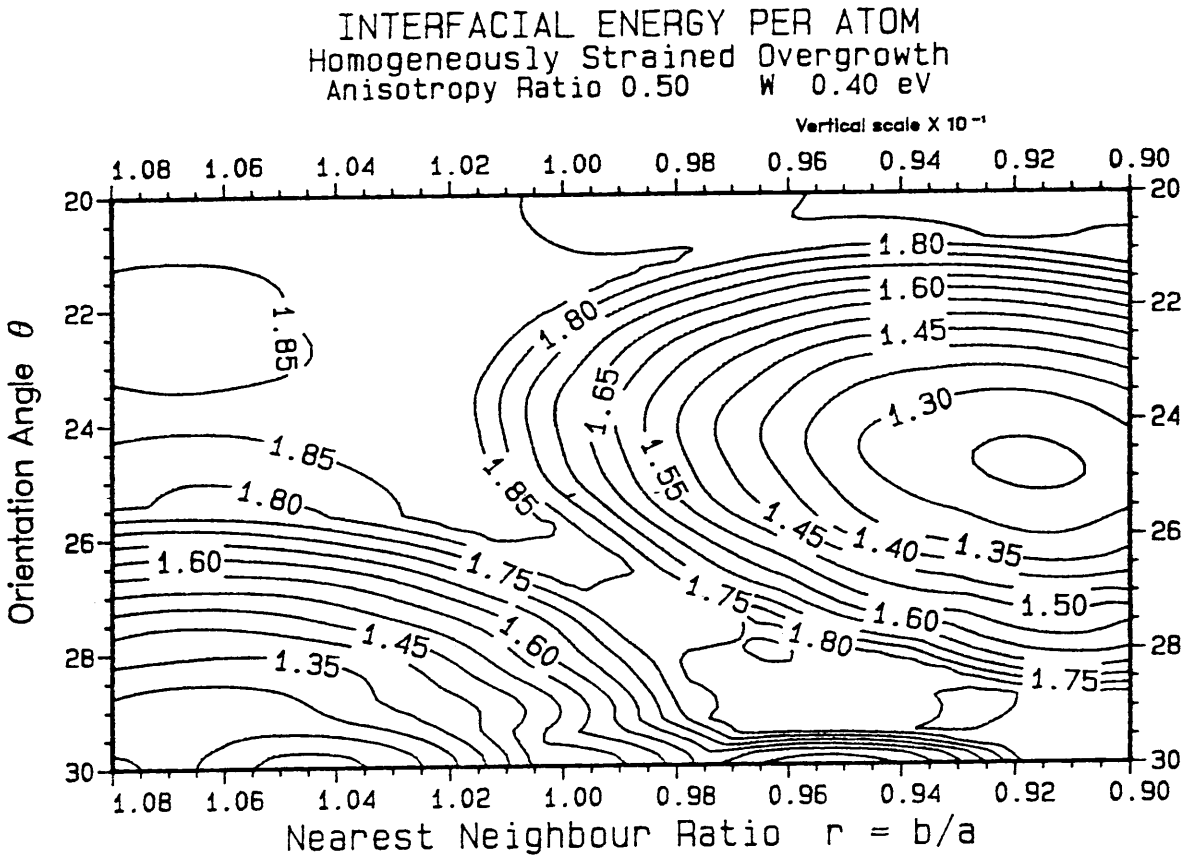

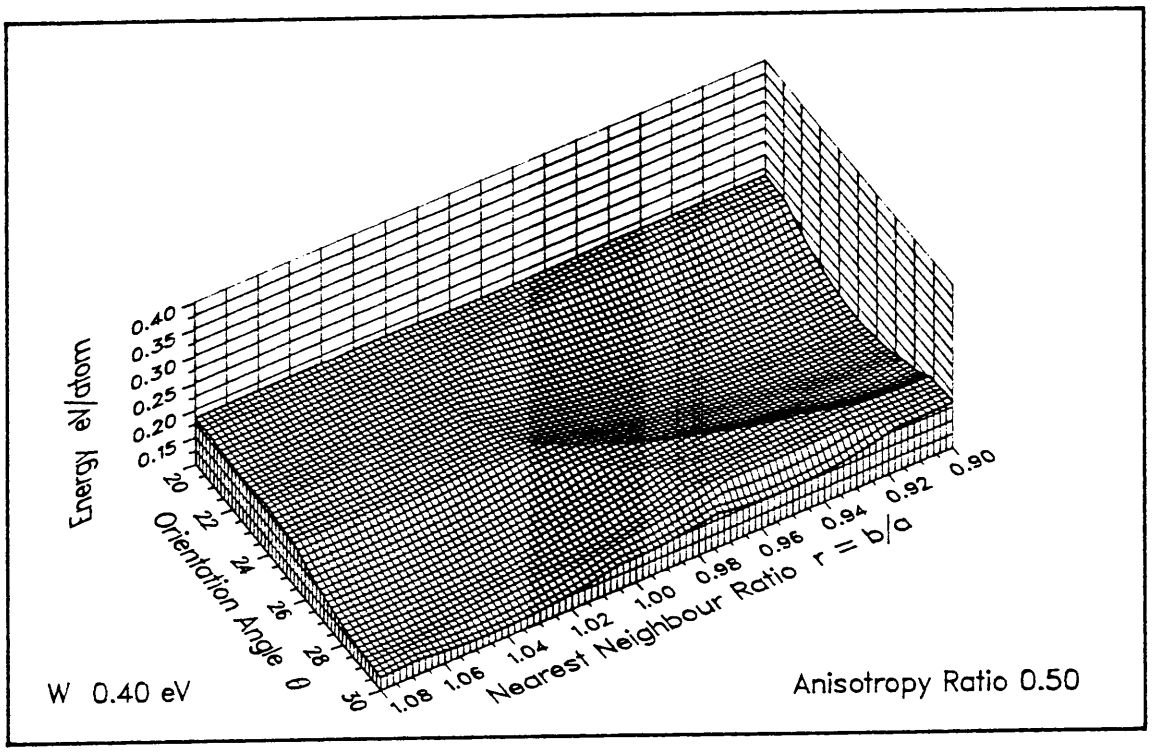

Figure 4.3(a) Interfacial energy after misfit strain W = 0.4 eV A = ½

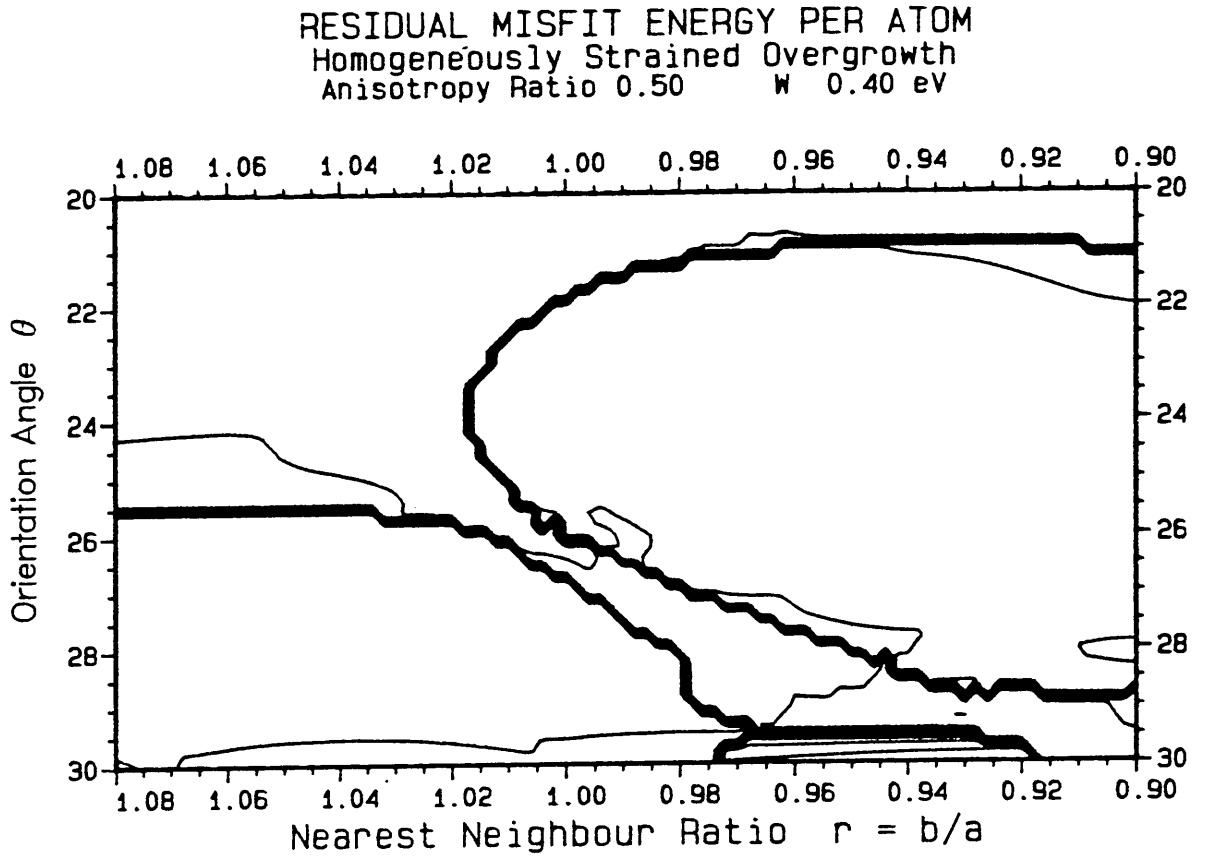

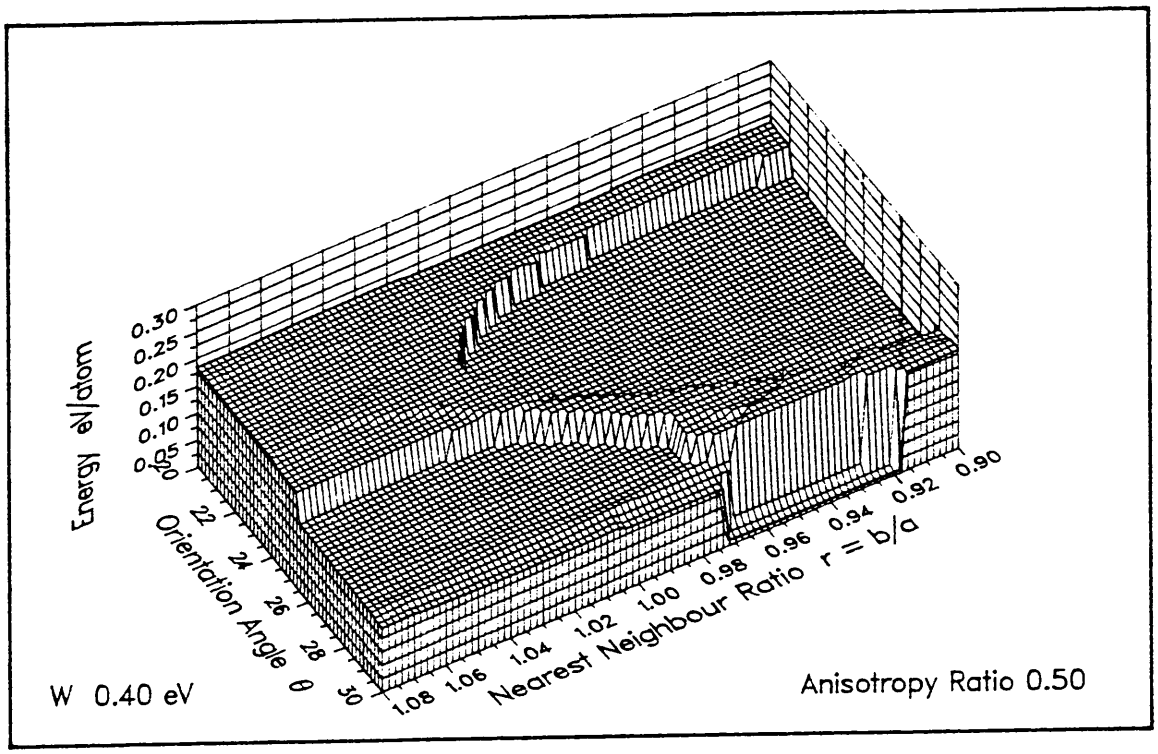

Figure 4.3(b) Residual misfit energy after misfit strain. W = 0.4 eV A = $\frac{1}{2}$.

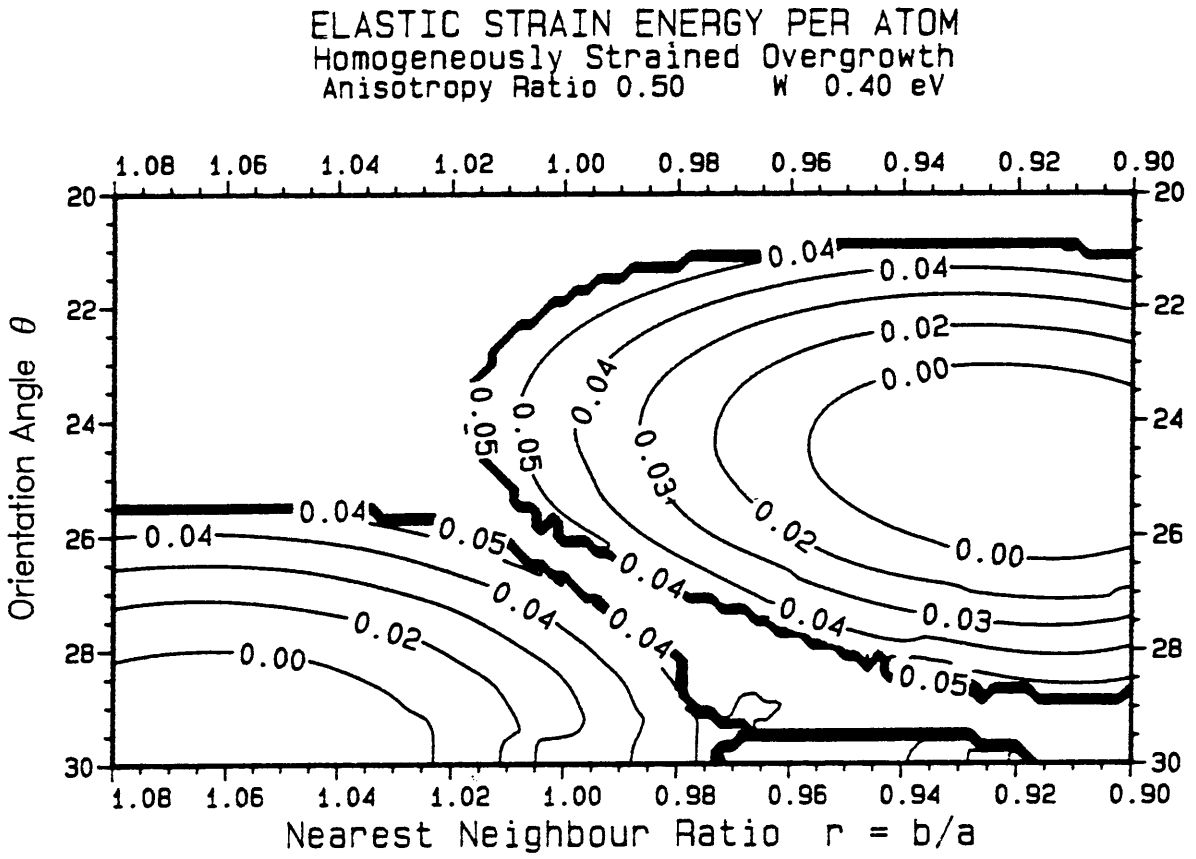

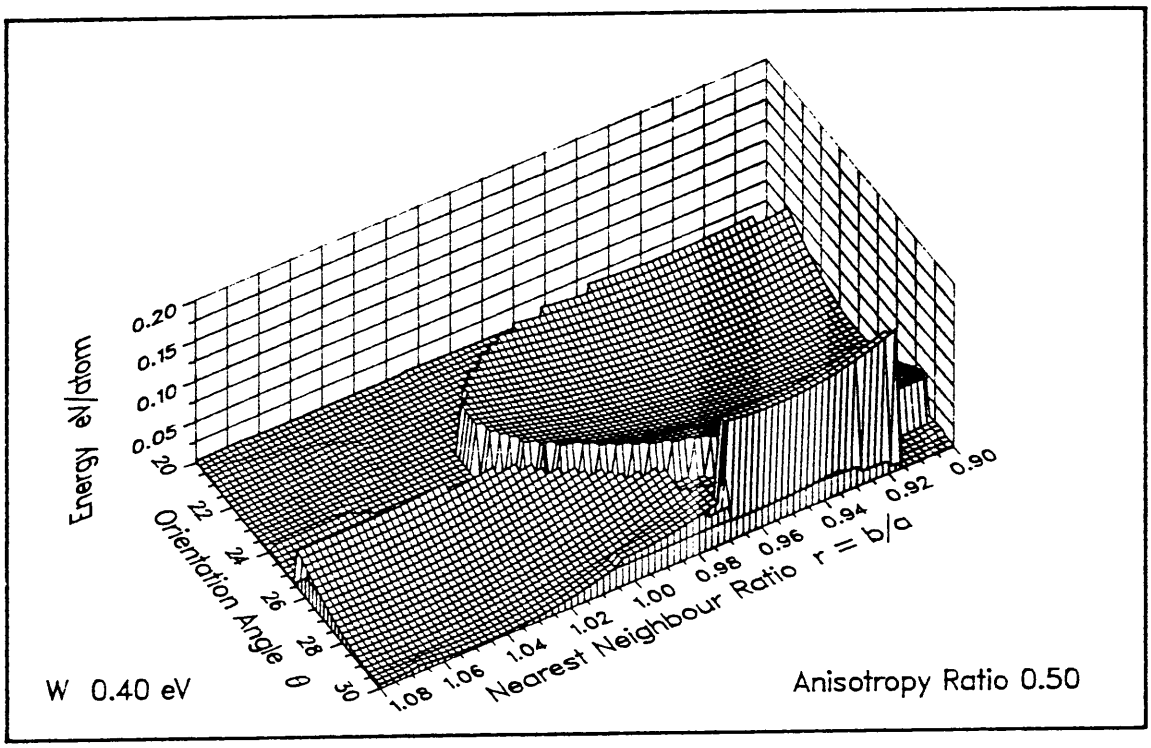

Figure 4.3(c) Misfit strain energy. W = 0.4 eV A = $\frac{1}{2}$.

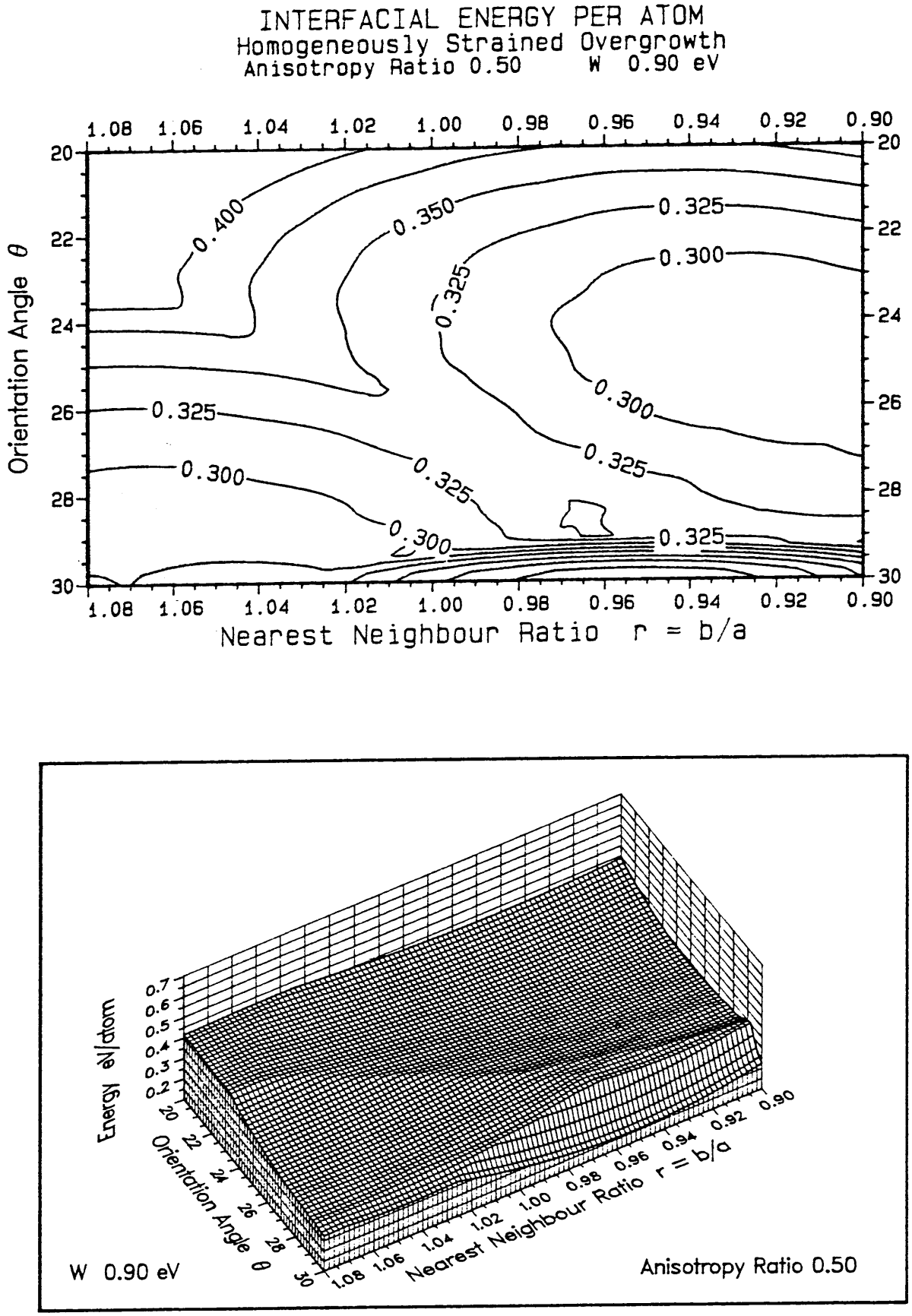

Figure 4.3(d)(i) Interfacial energy after misfit strain W = 0.9 eV
A = $\frac{1}{2}$ (equivalent of Figure 4.3(a))

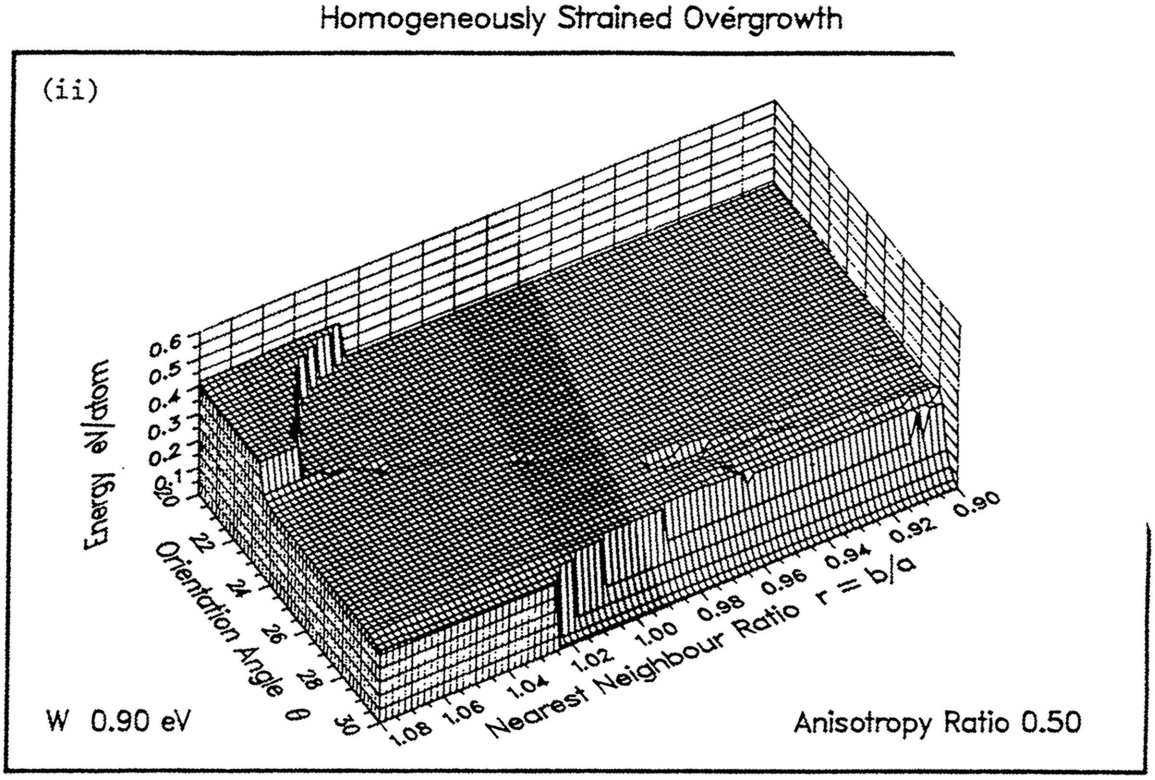

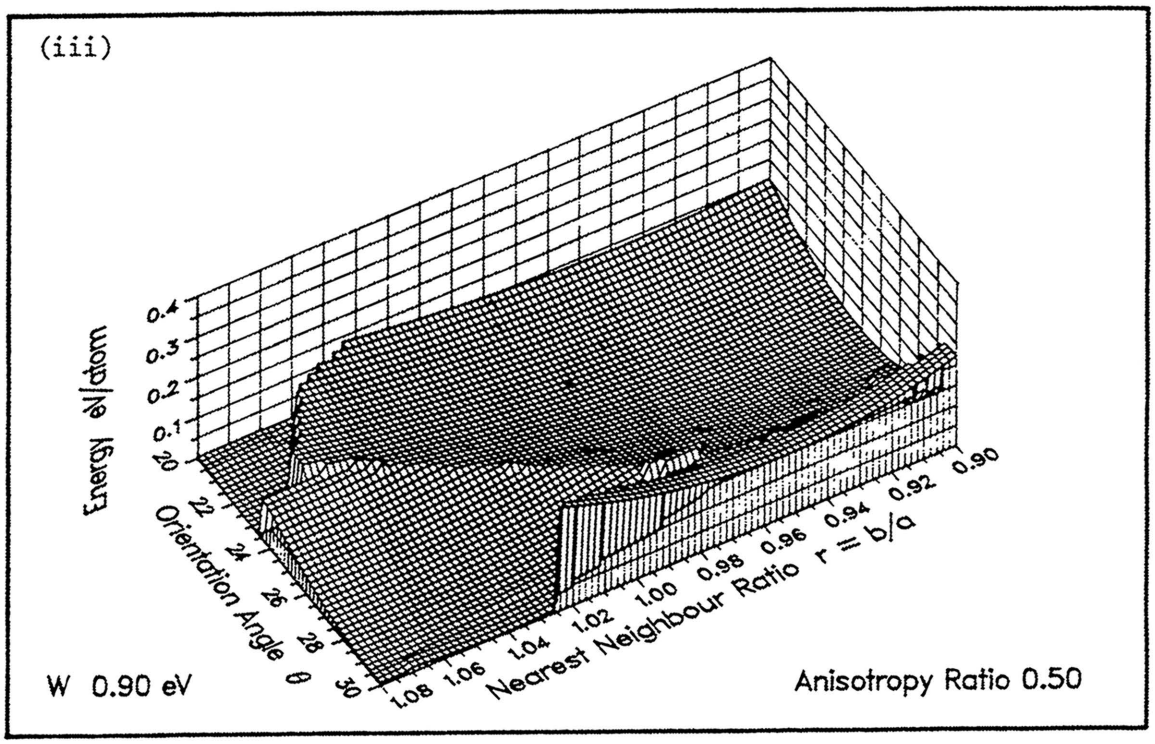

Figure 4.3(d) (ii) Residual misfit energy after misfit strain W = 0.9 eV
A = ½ (equivalent of Figure 4.3(b))

(iii) Misfit strain energy, (equivalent of Figure 4.3(c)).

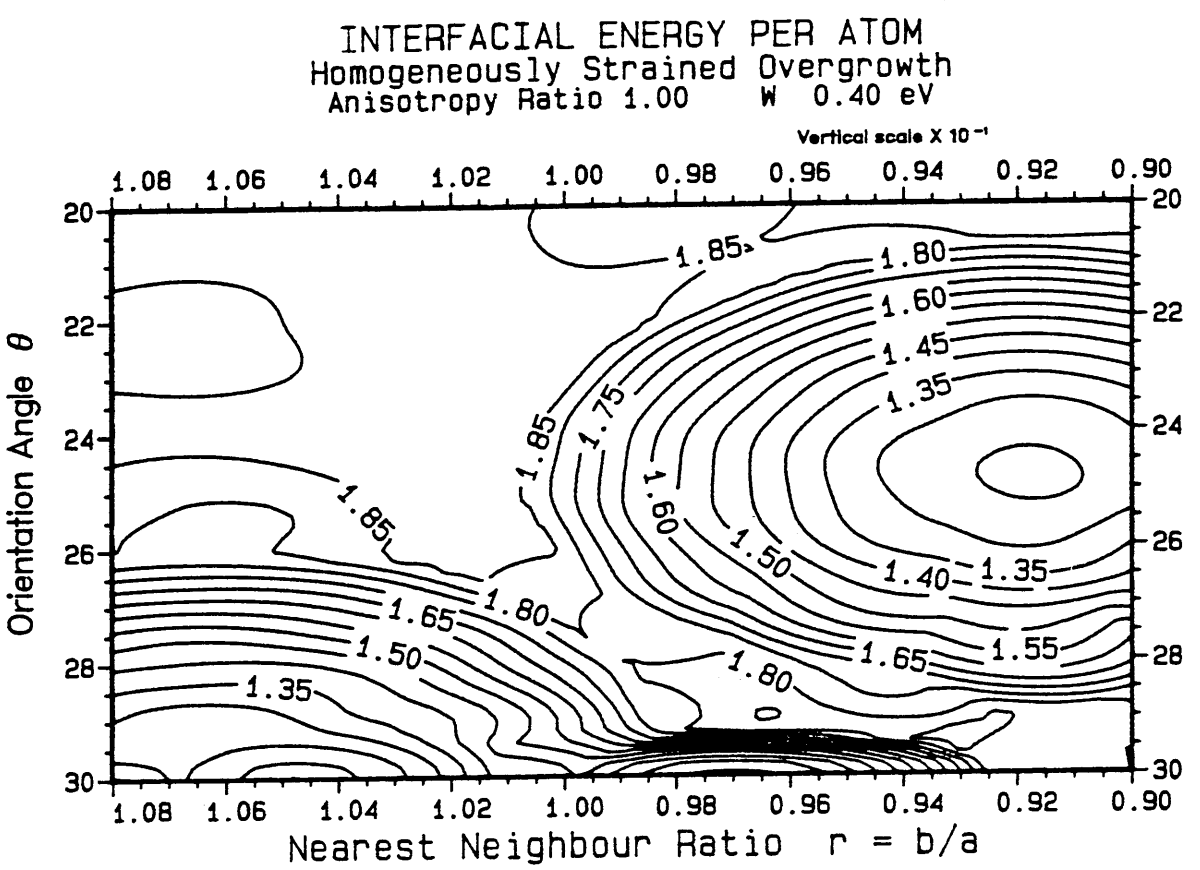

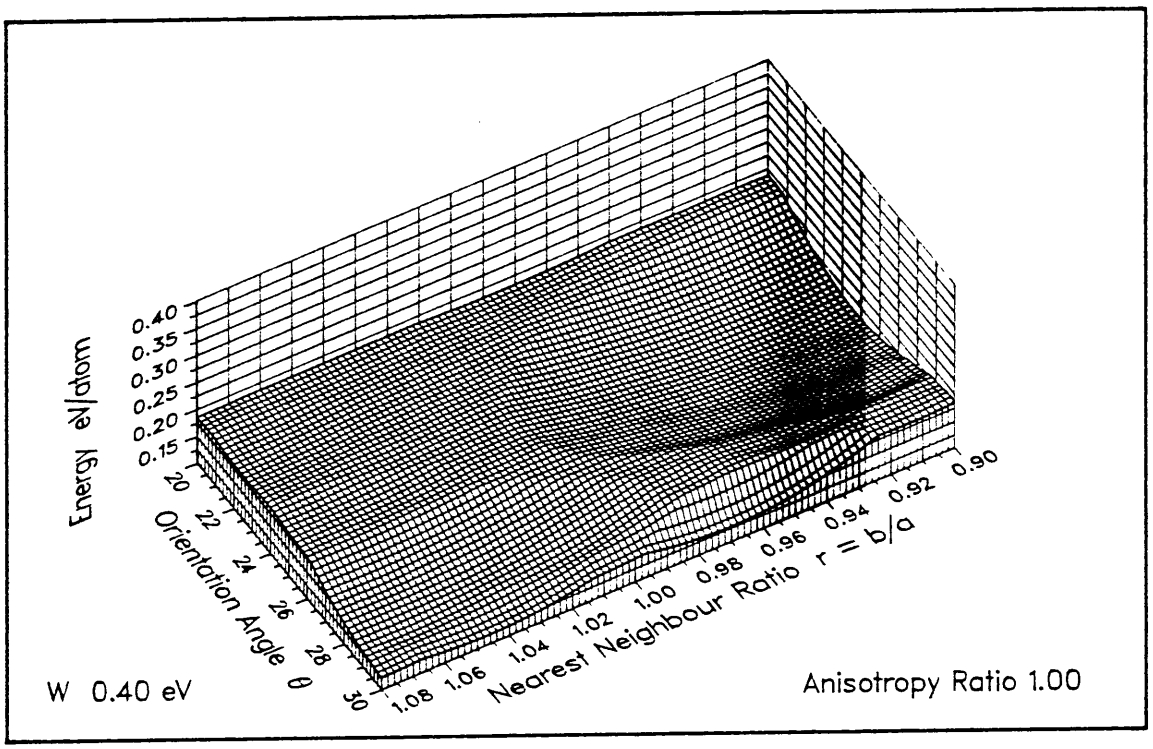

Figure 4.4(a) Interfacial energy after misfit strain W = 0.4 eV A = 1

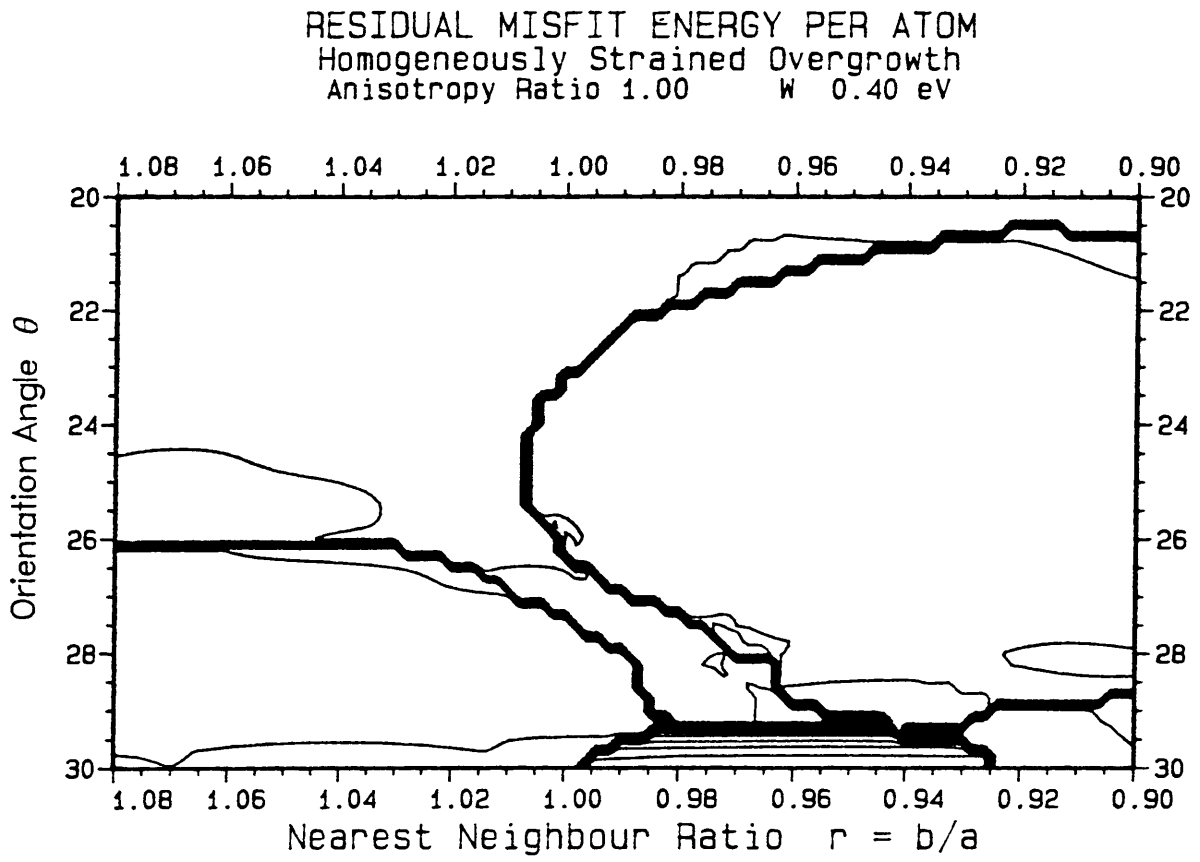

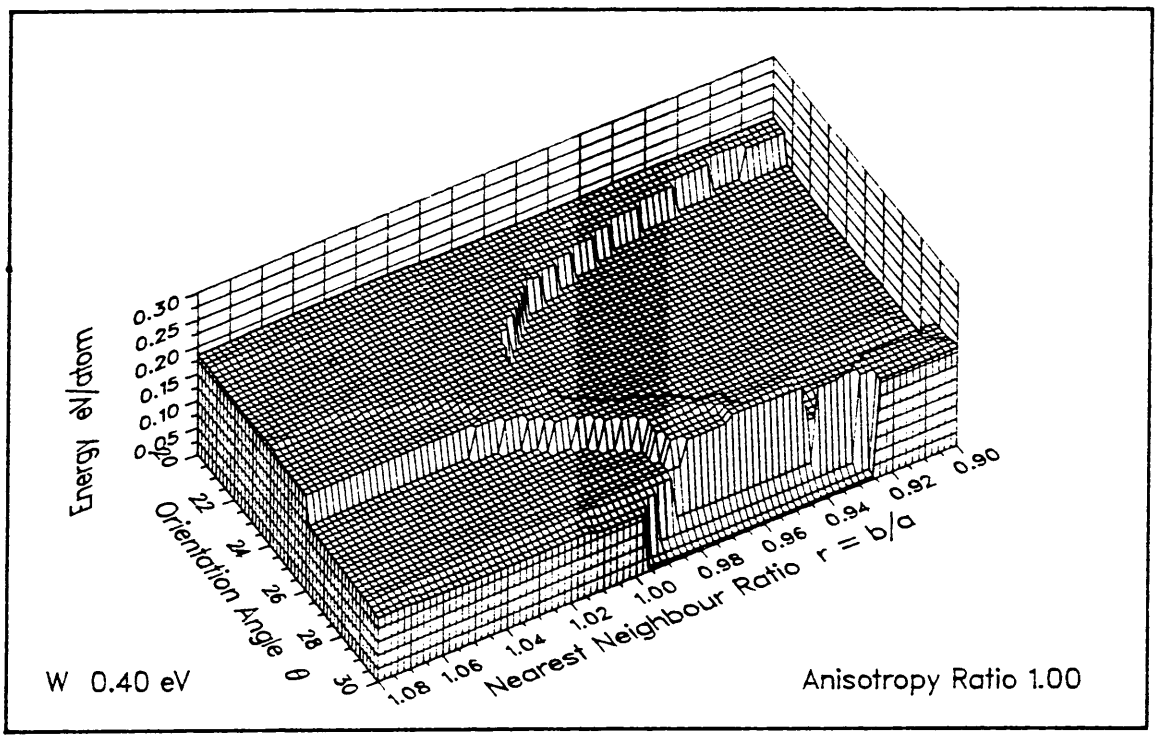

Figure 4.4(b) Residual misfit energy after misfit strain W = 0.4 eV A = 1

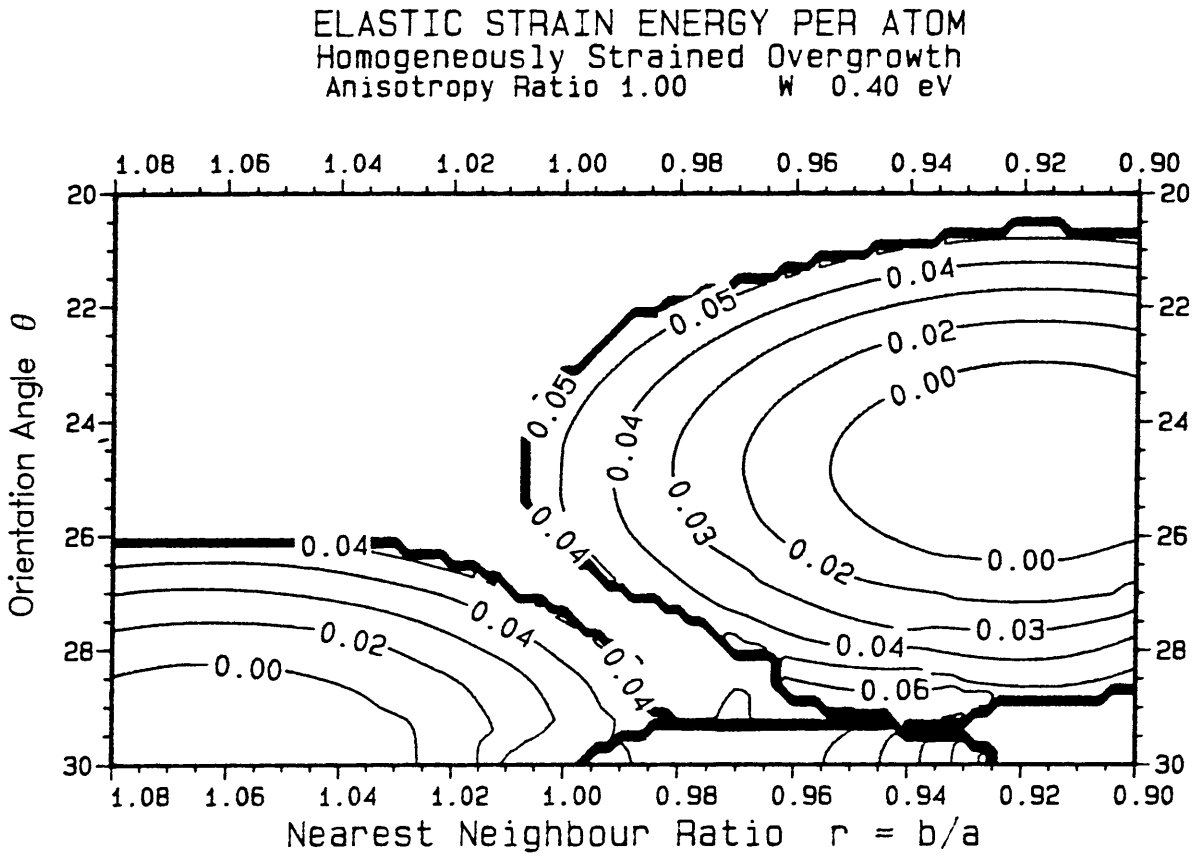

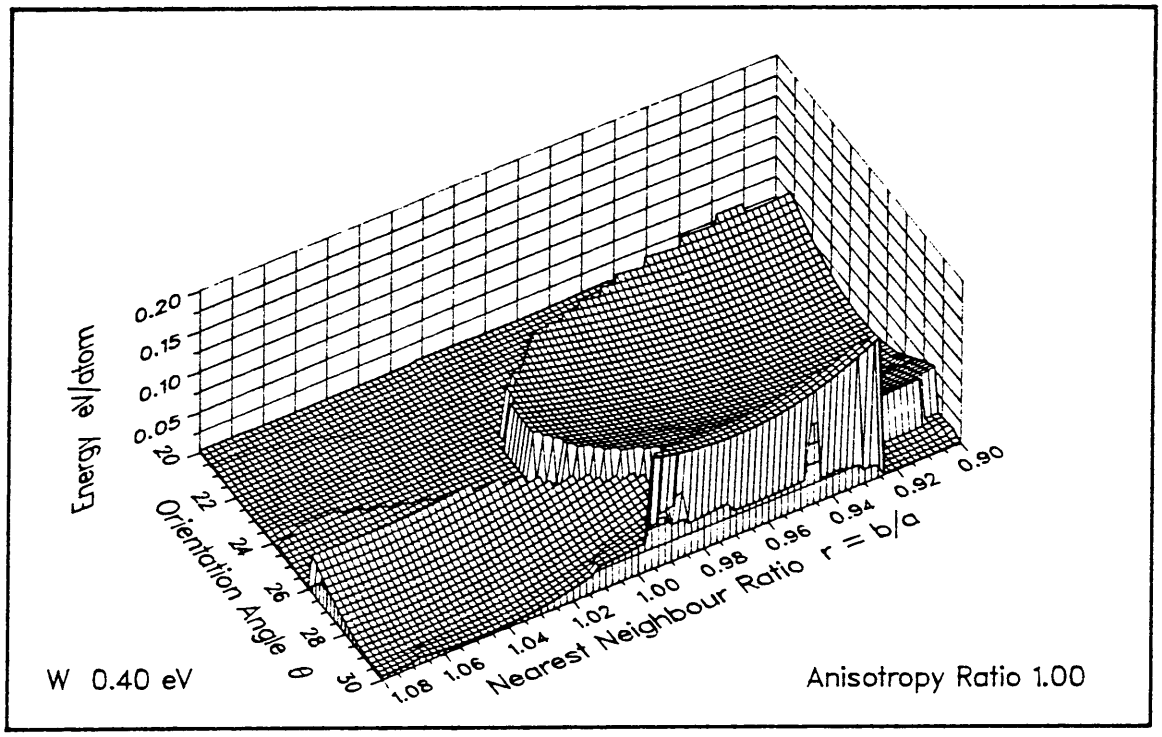

Figure 4.4(c) Misfit strain energy W = 0.4 eV A = 1

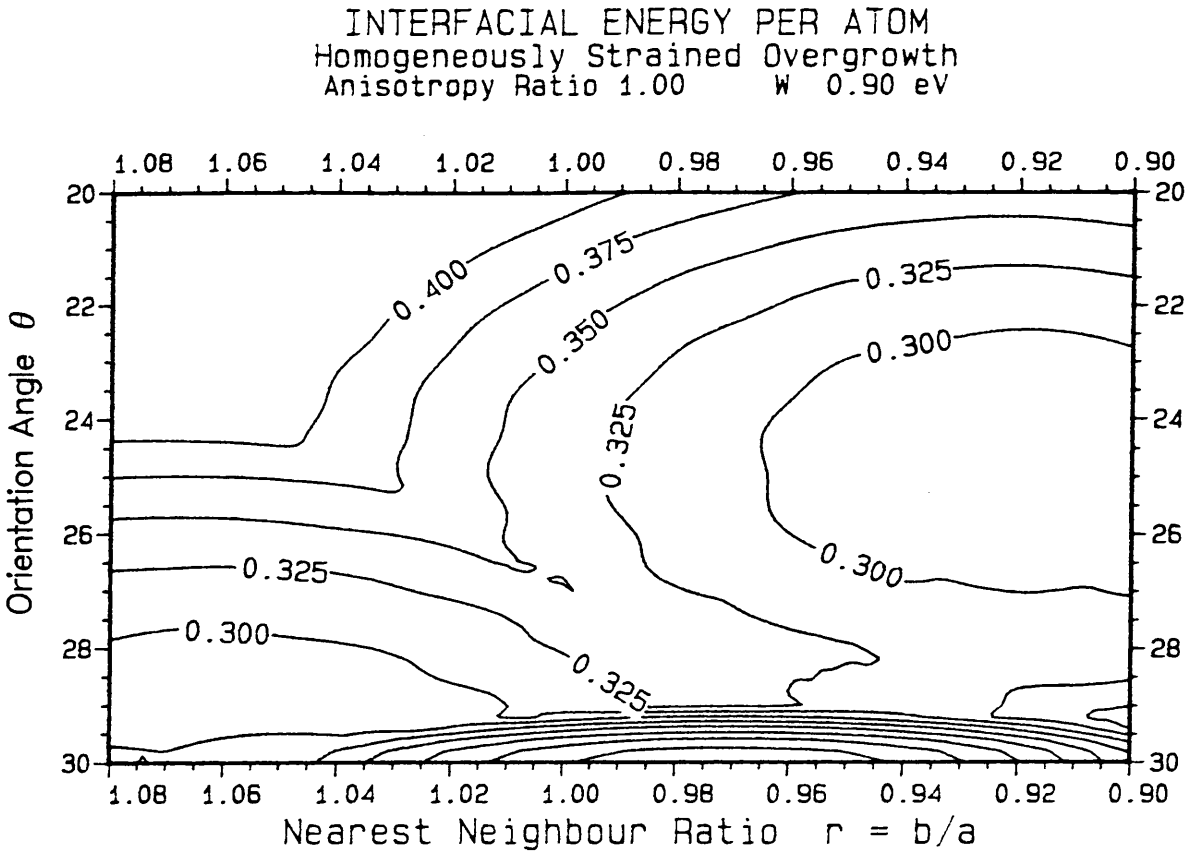

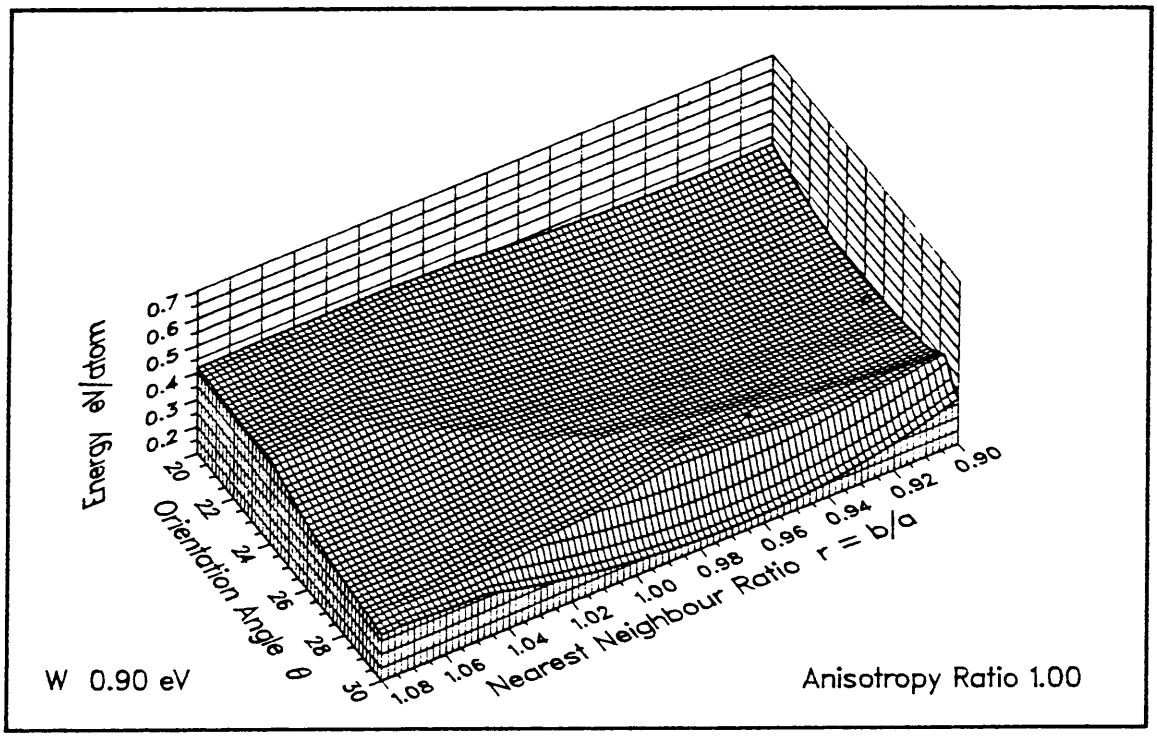

Figure 4.4(d)(i) Interfacial energy after misfit strain W = 0.9 eV A = 1 (equivalent of Figure 4.4(a))

Homogeneously Strained Overgrowth

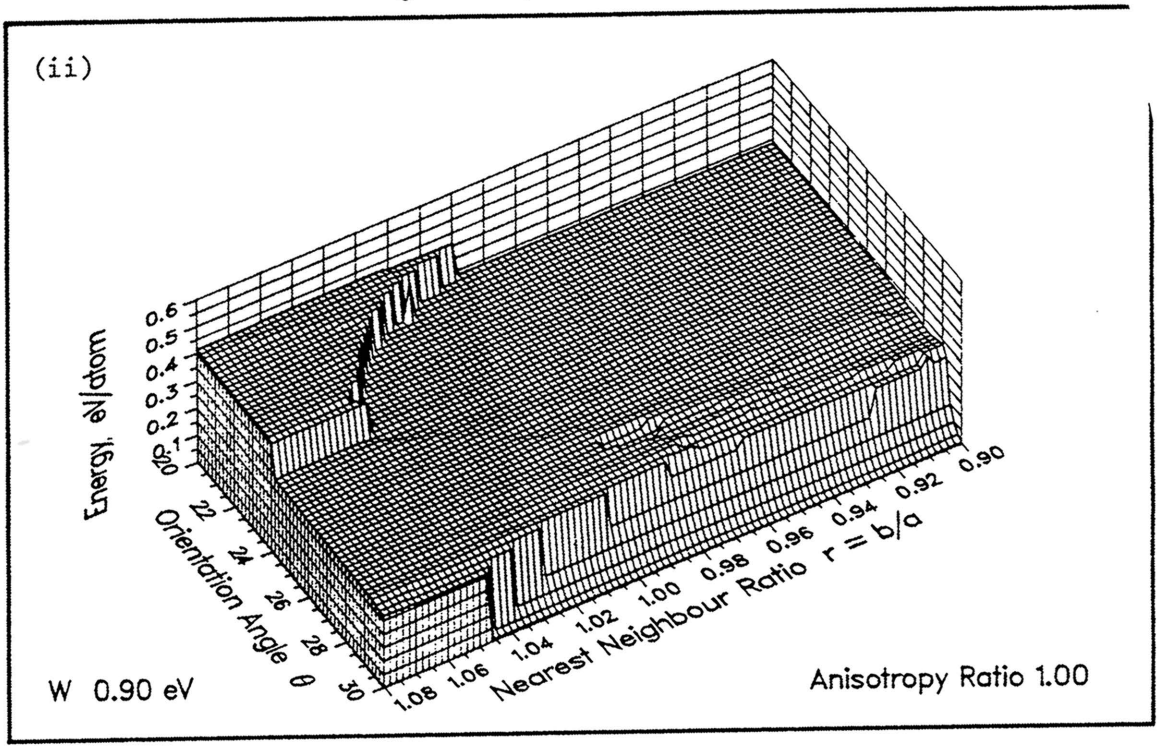

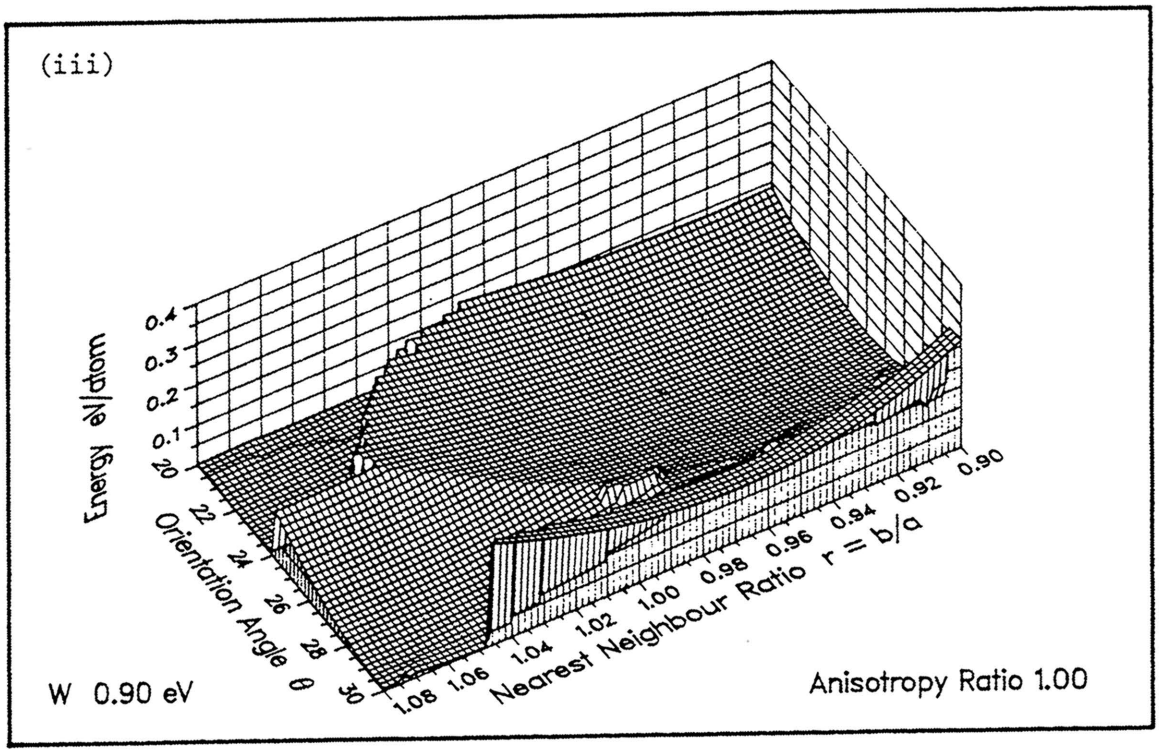

Figure 4.4(d) (ii) Residual misfit energy after misfit strain W = 0.9 eV A = 1 (equivalent of Figure 4.4(b))

(iii) Misfit strain energy (equivalent of Figure 4.4(c))

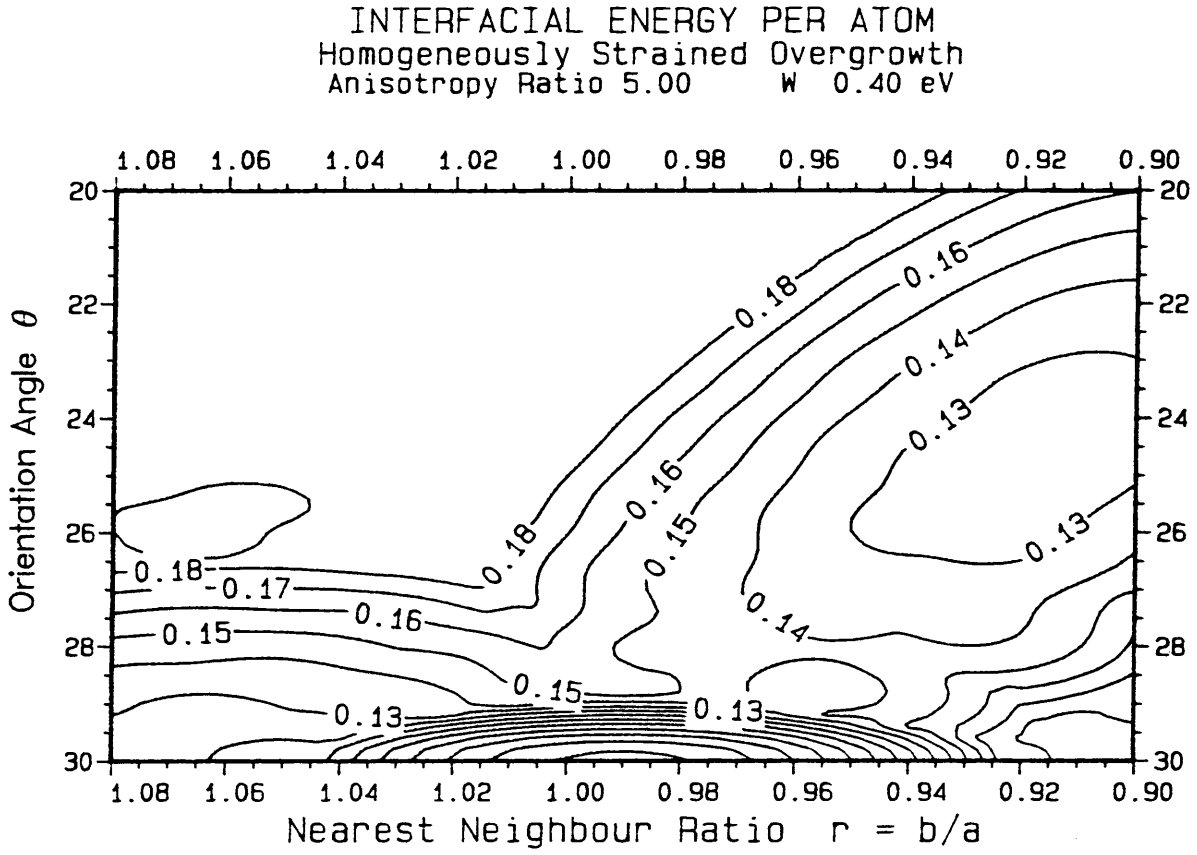

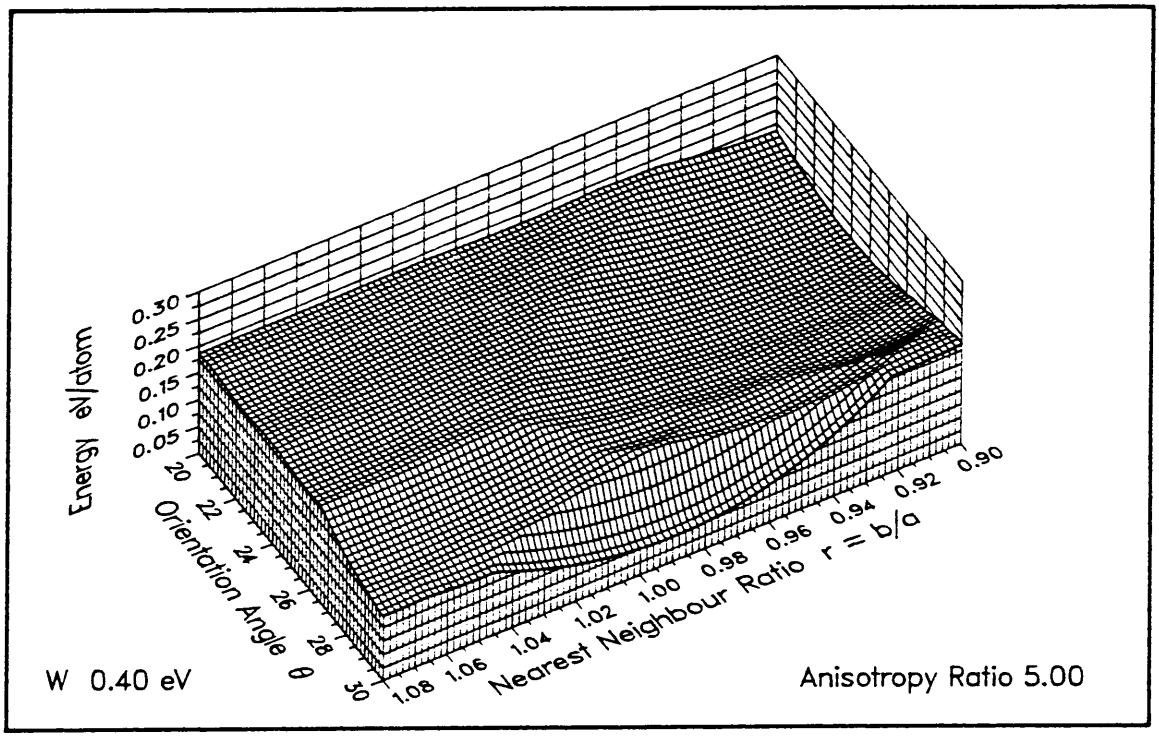

Figure 4.5(a) Interfacial energy after misfit strain W = 0.4 eV A = 5

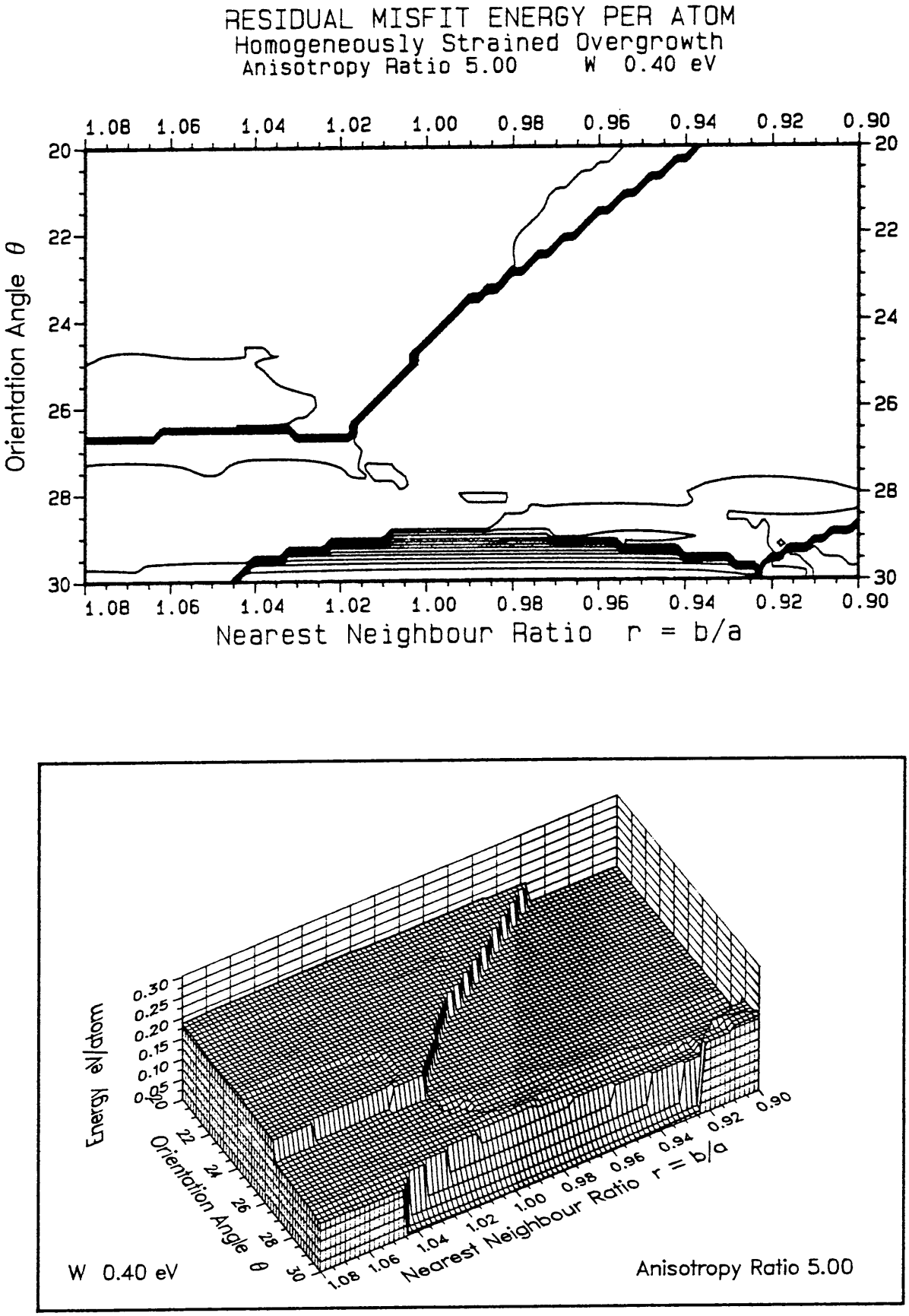

Figure 4.5(b) Residual misfit energy after misfit strain W = ¾.4 eV
A = 5

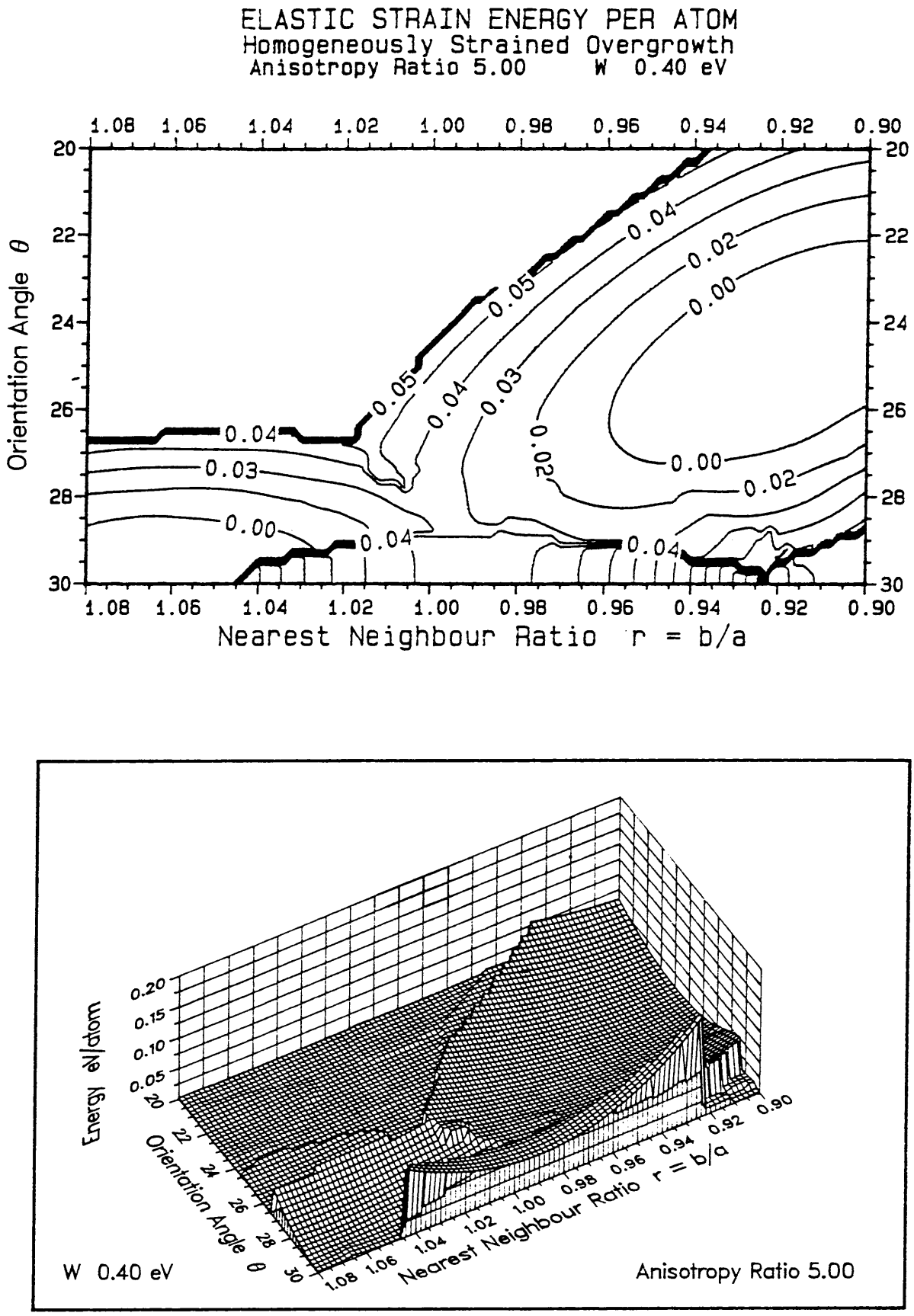

Figure 4.5(c) Misfit strain energy W = 0.4 eV A = 5

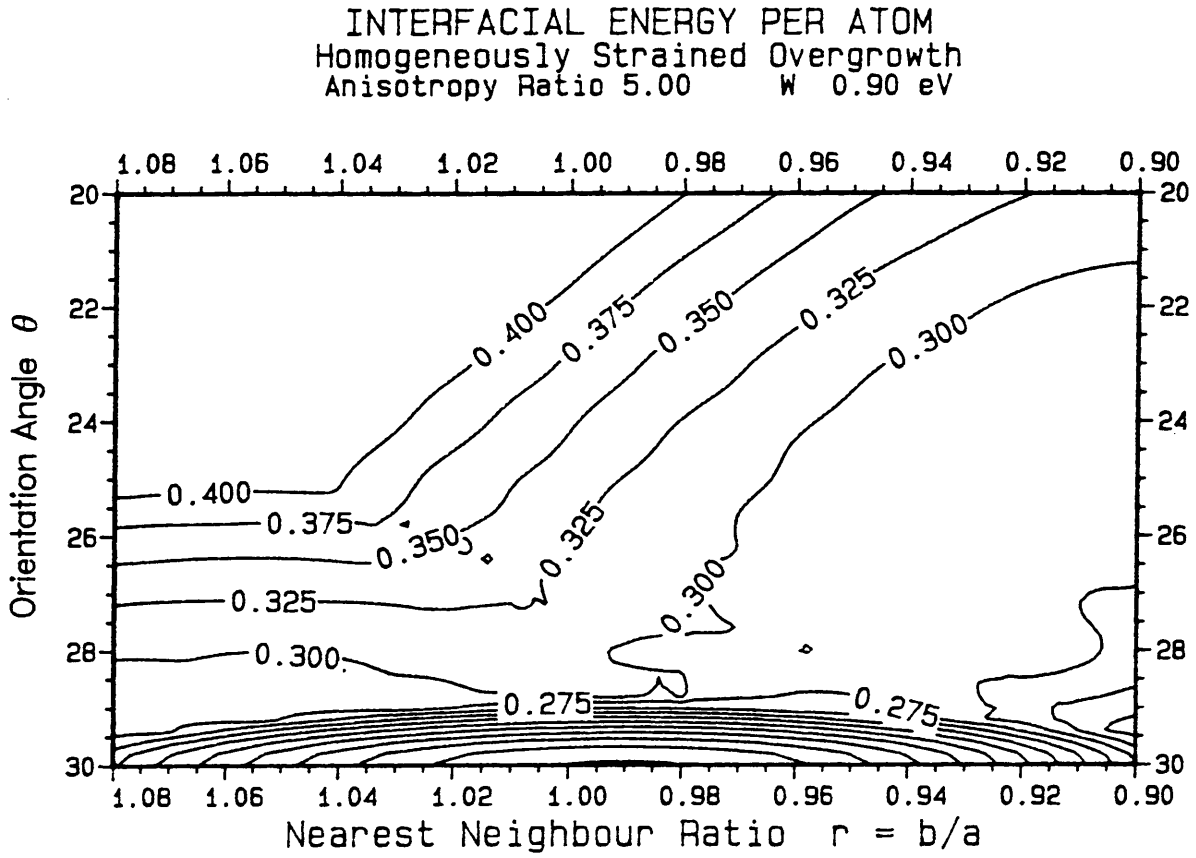

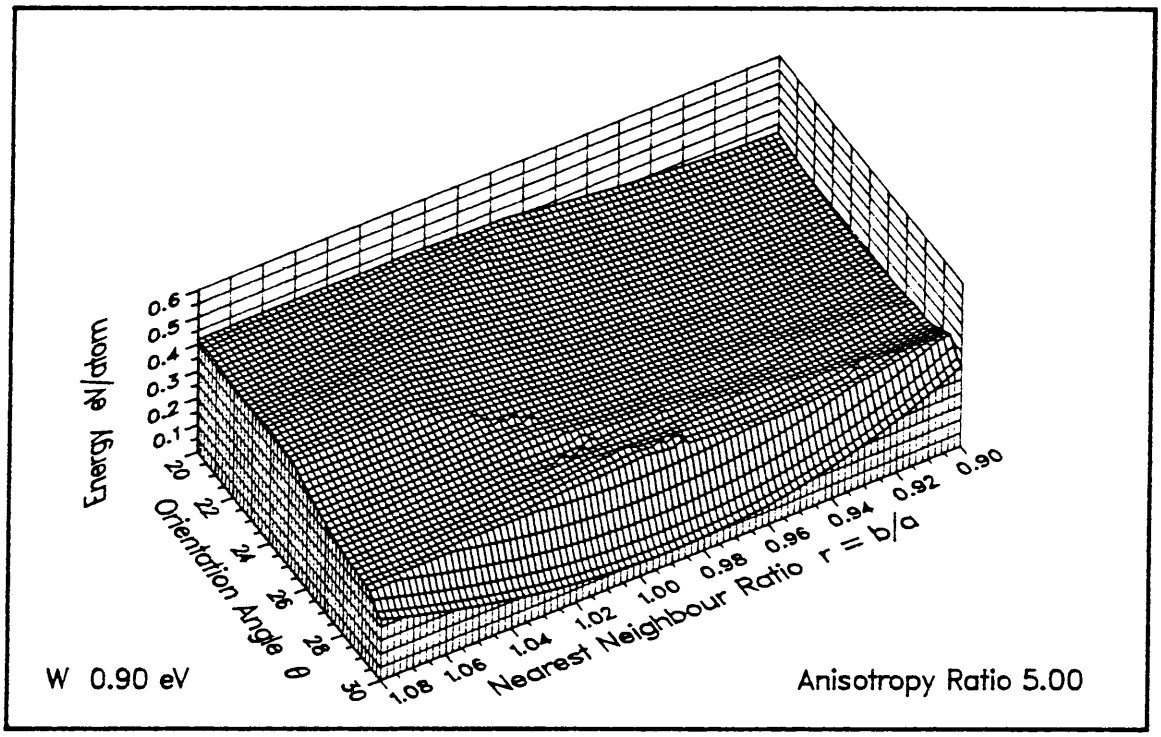

Figure 4,5(d)(i) Interfacial energy after misfit strain W = 0.9 eV A = 5 (equivalent of Figure 4.5(a))

Homogeneously Strained Overgrowth

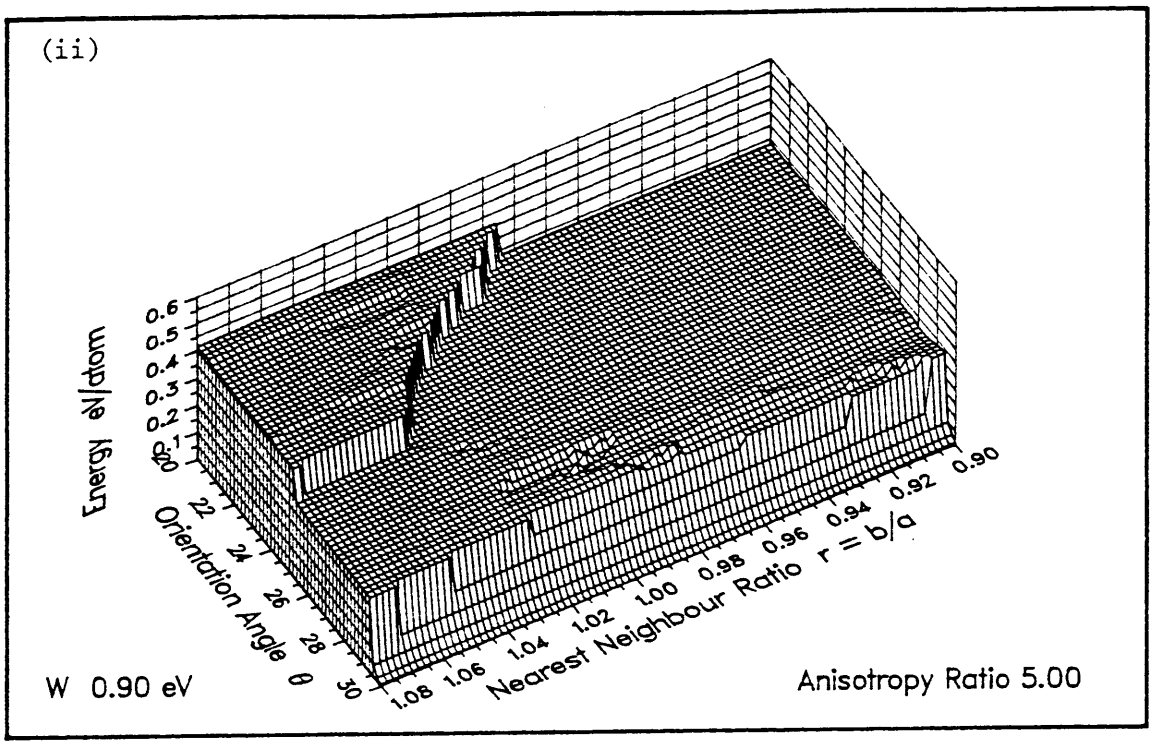

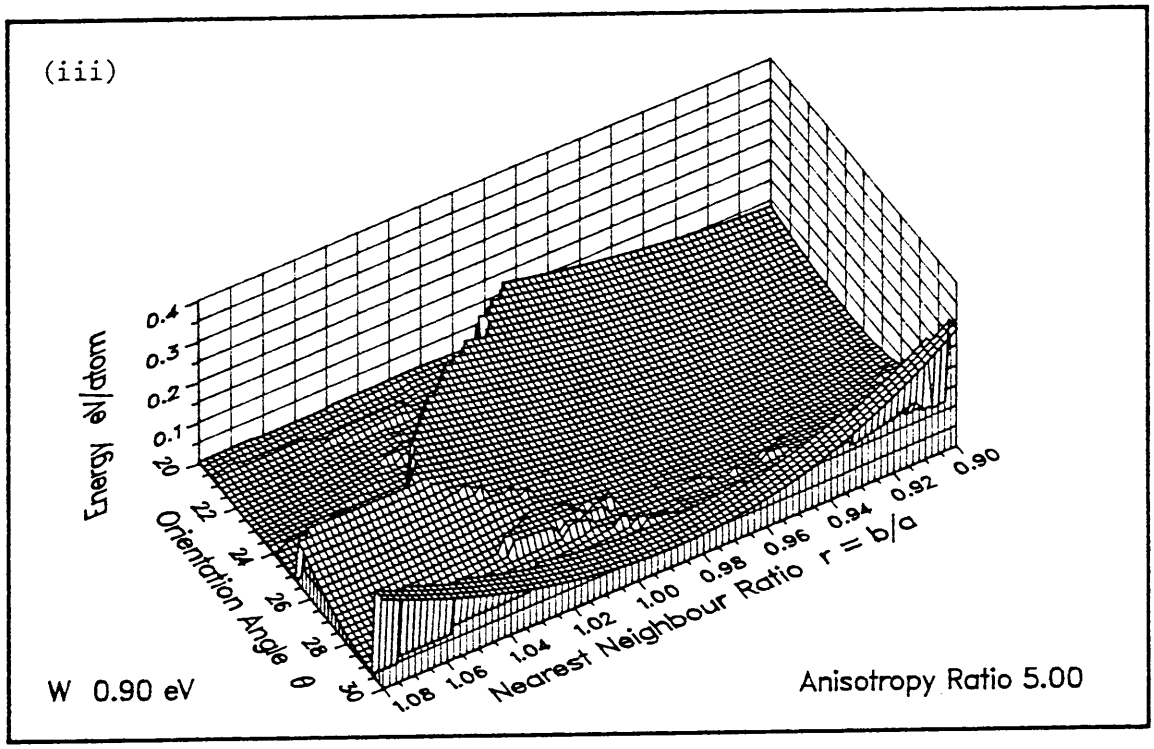

Figure 4.5(d) (ii) Residual misfit energy after misfit strain W = 0.9 eV A = 5 (equivalent of Figure 4.5(b))

(iii) Misfit strain energy (equivalent of Figure 4.5(c))

4.7 DISCUSSION

The results show several characteristics of the introduction of homgeneous *misfit* strain. When the energy diagrams, figures 4.2-5, are compared, it is obvious for example that the two-dimensionally coherent (pseudomorphic) configuration which does not appear in the rigid island energy diagrams produces a definite energy minimum about $r \simeq 1.0$, although its exact location and extent depends on the anisotropy ratio. Further, the misfit strain considerably expands the width of the minima about the rigid Ideal Epitaxial orientations. The misfit strain also introduces a smoothing of the secondary minima, which in many cases are engulfed by the central minimum.

Coherency

The achievement of coherency introduces steps in the residual misfit energy value, [Figures 4.3(b) - 5(b)] so that several plateaux are evident. Firstly the Incoherent Configurations (IC) have the highest residual misfit energies, although this incoherence in the finite monolayer overgrowth may include very high order matching. High order matching possibilities with the secondary minima produce slightly lowered plateau regions.

The greatest reductions in misfit energy occur with the achievement of 1-dimensional coherency, in the Kurdjumov-Sachs (KS) and Nishiyama-Wassermann (NW) configurations and for the 2-dimensional coherent (2DC) phase. The one-dimensionally coherent phases have plateau values of misfit energy essentially indistinguishable in value as the $\{1\ 0\}^*$ substrate wave vectors are matched in both cases. With the inclusion of the overgrowth Fourier potential terms into the misfit energy as discussed in Chapter 3, particularly for thicker overgrowths, some differentiation will be expected. The 2DC phase causes a reduction in misfit energy to essentially zero for an infinite monolayer, and close to zero for finite islands,

because of the finite width of the central energy minimum. This configuration occurs essentially in systems which have nearest neighbour ratios and elastic constants, nearly (but not exactly) favourable to both KS and NW, or strong binding of overgrowth to substrate (large W or small ℓ, less than about 5) as may be seen from the phase diagrams of Figure 4.6, and the energy diagrams themselves.

The pseudomorphic configuration occurs only at the Nishiyama-Wassermann orientation, primarily because in addition to shear the accommodation required to match both NW and KS wave vector pairs simultaneously requires a rotation through $\theta_{NW}-\theta_{KS} \simeq 5.26^{\circ}$ to the NW orientation, as the reciprocal lattice calculation shows.

This has implications for systems which are initially poorly oriented, (because of the width of the minima), and take on the pseudomorphic configuration in an early growth stage. As the overgrowth thickens, ℓ increases, and for systems which energetically favour KS, the transition to KS may be expected to occur (Bauer *e.a.* 1986, also Kuk *e.a.* 1983, Jesser *e.a.* 1979). However an activation energy may be required to re-orient to the KS orientation as suggested by Bruce and Jaeger (1977, 1978). Hence, a spread of angles about the ideal KS orientation may be observed in practice, and possibly some NW orientation, if sufficient energy for re-orientation is unavailable. Schlenk and Bauer (1980) have reported LEED observations on complementary fcc{111} overgrowth, bcc{110} substrate systems which exhibit orientational effects explainable by such non-equilibrium speculations.

This reorientation during the two-dimensional to one-dimensional transition will not occur for a 2DC to NW transition, as rotation is not necessary.

As the lateral size of the overgrowth island influences the width of the central energy maximum, and the depth of secondary minima, the growth mode (Bauer *e.a.* 1972, Bauer 1982, Yagi *e.a.* 1976, Vook 1982) may be expected to play a rôle in the orientational epitaxy. Monolayers, or islands of large lateral extent, may be expected to behave differently to many small, three-dimensional islands.

The smaller thick (ℓ large) islands of Volmer-Weber mode may not be expected to attain the 2DC mode, except for strong binding (ℓ reduced) and perhaps large anisotropy ratios, suggested by the third diagram of figure 4.6. As they grow laterally, they will either settle at secondary orientations, or if close to ideal KS or NW, will rotate to the optimal orientation relatively freely, given a sufficiently low density of islands.

Systems with Frank-Van der Merwe (monolayer by monolayer) or Stranski-Krastanov growth modes, may be expected to exhibit the initial pseudomorphic phase (for ℓ small enough) and, with thickening, the transition to one-dimensional coherency, dependent on the ratio r.

The tendency to re-orient to the exact orientation is reduced by the marked shallowness of the minima around the minimum energy configuration in the presence of misfit strain. This tends to support the prediction that if re-orientation is expected, the result will not be perfect orientation, particularly for non-ideal values of r.

Complicating the effect is the effect of the elastic constants, which most certainly can be expected to be different from bulk constants for thin overgrowths. This has been shown by calculations of the variation of these constants with crystal size, carried out by Auret and Van der Merwe (1974,1975). Without this complication however, is the more direct effect of the anisotropy of the elastic constants. Particular emphasis has been placed in the results on the effect of the anisotropy.

Anisotropy

The effect of the anisotropy ratio has been examined and the results are illustrated in figures 4.3 to 5 and with the phase diagram of figure 4.6. As already mentioned, the energy well about the KS configuration minimum is skewed, so that the optimal orientation with misfit strain deviates somewhat from the ideal. This applies particularly to systems with nearest neighbour ratios quite different from the ideal value. In the example given in Table 4.5, the ratio r = 0.95 with anisotropy ratio ½ has lower energy at 24.2° than at the ideal θ_{KS} orientation, while with anisotropy 5, the 26° orientation has lower energy. It is this effect which increases the extent of the pseudomorphic minimum in the direction of decreasing nearest neighbour ratio, as the KS orientation is brought closer to the NW orientation by increased anisotropy.

The change in KS angle illustrated here is around 2°, which is not insignificant.

The realness of this effect is not doubted, although other methods of modifying the elastic constants, to those of Table 4.1 may very well yield a difference in numerical detail of the extent of the effect. It appears reasonable to conclude that

$$A < 1 \Rightarrow \theta'_{KS}-\theta_{NW} > \theta_{KS}-\theta_{NW} \simeq 5.26^\circ,$$

$$A > 1 \Rightarrow \theta'_{KS}-\theta_{NW} < \theta_{KS}-\theta_{NW} \simeq 5.26^\circ,$$

and $A \simeq 1 \Rightarrow \theta'_{KS} \simeq \theta_{KS}$, when $r > r_{KS}$. The inequality between the angles changes direction when $r < r_{KS}$.

(The inequality is introduced in this third equation because of a small deviation from the ideal angle which also occurs in the isotropic case as detailed examination of the data shows. This is probably due to the finite nature of the island and θ_{KS} is defined of course for an infinite island.)

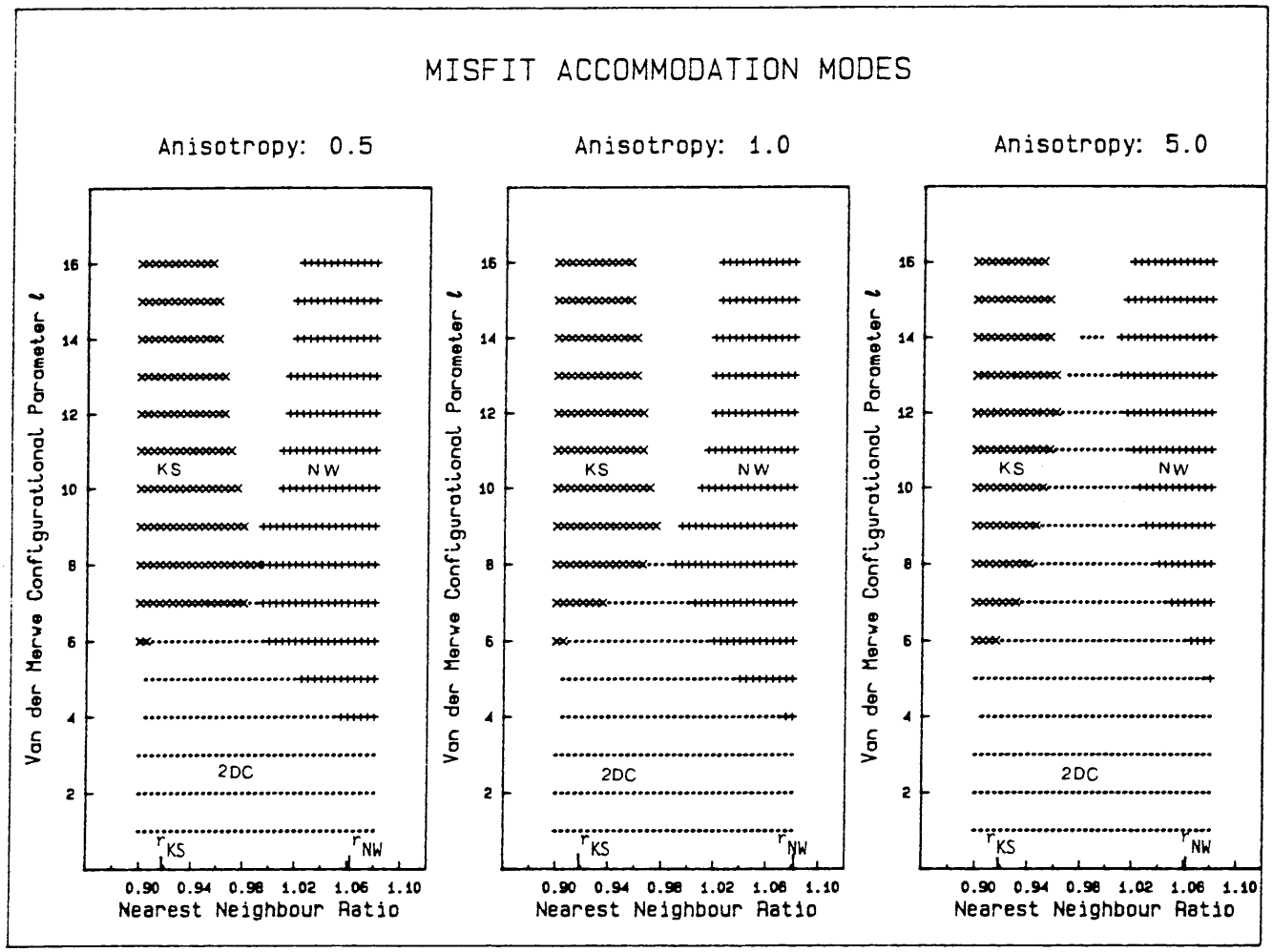

Figure 4.6 Phase diagrams showing the stable configurations

xxxx Kurdjumov-Sachs

++++ Nishiyama-Wassermann

.... 2-dimensionally coherent (pseudomorphic)

Also apparent in the detail of the phase diagrams, is the possibilty of a transition from the 2DC phase directly to an incoherent phase when the anisotropy is large, near a nearest neighbour ratio of 1. The reality of this feature however, may depend on the Poisson Ratio, which in all these diagrams was constant, or on the fact that the KS orientation in the calculations was taken as θ_{KS} and not the optimal angle, which, may differ by the 2° discussed above. The NW angle however does not change with anisotropy, and here there is also a gap in the transition from 2DC which tends to support the existence of this gap. Further detailed modelling of this effect, however small, is left to a more specific study of systems with severe anisotropy.

Reciprocal lattice data

The strains predicted from the reciprocal lattice data agree well with the finite island data for cases close to the ideal configurations. The occurrence of secondary minima in the finite island energy behaviour introduces configurations which have not been considered in the infinite island case. The reciprocal formulation however does prove a useful tool in interpretation of finite data, and the identification of the accommodation modes.

Table 4.3, shows the strains necessary to achieve the exact coherency associated with the infinite island. Several cases do not occur in the direct energy minimization, because strains are too large in some of these. With small ℓ values, however, some rather extreme configurations, with nearest neighbour ratio close to one of the ideal configurations, and oriented in the other ideal (Table 4.3 b) do occur. These cases occur at the larger values of W, with $r = r_{NW}$ and $\theta = \theta_{KS}$, in table 4.4 (a)-(c) for all anisotropy ratios. The strains compare well with the equivalent cases of Table 4.3 (b), in which the accommodation mode is in fact NW, in spite of the θ_{KS} orientation.

Interestingly, the other extreme, $r = r_{KS}$ and $\theta = \theta_{NW}$ does not result in a one-dimensionally coherent configuration, (Table 4.4)

but rather in 2DC mode. This illustrates once more the fundamental difference between the KS orientation, and the NW orientation, namely that 2DC is possible only from the NW orientation. From the KS orientation, a rotation is necessary before 2DC can be achieved.

4.8 CONCLUSION

In this chapter the importance of strain in the orientational epitaxy of monolayer overgrowths was quite clearly demonstrated. In particular the pseudomorphic phase cannot be achieved without strain in the incommensurate overgrowth-substrate system, of which the bcc{110}/fcc{111} system is an example.

The fundamental difference between the Kurdjumov-Sachs and the Nishiyama-Wassermann one-dimensional coherent configurations has been highlighted by both approaches used here. Namely the fact that two-dimensional coherency cannot be achieved without rotation from the KS orientation, or indeed from any orientation other than the NW orientation.

Another important result is the deviation from the geometrically predicted orientation of the Kurdjumov-Sachs configuration when the system is not isotropic. It was shown directly that the optimal orientation may change by as much as 3°, for systems which have nearest neighbour ratios not ideal KS, when the anisotropy ratio approaches 5.

An important development in this chapter has been the extension of the reciprocal space analysis of the properties of epitaxy to allow the prediction of misfit strains (which minimize the strain energy).

The essential equivalence for large systems of the direct energy minimization, undertaken numerically, and the reciprocal lattice approach which is essentially analytical has been aptly demonstrated.

In conclusion one may indicate that the original derivation of the reciprocal space formulation with the rigid model did allow the inclusion of secondary circles in the reciprocal space due to the size of the finite island. This property has not been used here, as the direct minimization showed these effects adequately.

The next step, after the inclusion of *Misfit Strain*, the main thrust of this chapter, is necessarily a discussion of the effect of local and periodically repeating variations in the strain fields, particularly in the directions other than those in which misfit strain alone has improved matching. Where dimensional misfit remains, misfit dislocations of the edge type are expected, while in orientational misfits these misorientations can be expected to result in arrays of screw dislocations. These cases are studied in the next chapter, in both the reciprocal space formulation and by direct energy minimization for finite systems, by introducing more degrees of freedom, so accommodating local variations of the strain.

CHAPTER 5

LOCAL STRAIN AND MISFIT DISLOCATIONS

The restrictions of the previous model are further reduced, as the overgrowth is allowed to relax differentially with position. This allows the relaxation associated with interfacial misfit dislocations.

The local strain fields are obtained from a numerical Finite Element model, a variational technique related to the Rayleigh-Ritz variational method, which is derived essentially from first principles.

The reciprocal space formulation is further extended to allow the description of the full interfacial structure, from misfit vernier to misfit dislocations. The spacing, Burgers vectors, orientation, and line sense of misfit dislocations in a general misfitting interface are derived from the reciprocal lattice, and applied to the bcc{110}-fcc{111} system.

The interpretation of the positions of the interfacial atoms is carried out in detail with these tools, and correlated with the energy behaviour. The inherent difference between the Kurdjumov-Sachs and the Nishiyama-Wassermann configurations is once more illustrated, this time from the structural details of the interface. The structural effects of relaxation about higher order epitaxial configurations are illustrated.

The effect of anisotropy is also considered explicitly.

CHAPTER 5

LOCAL STRAIN AND MISFIT DISLOCATIONS

Ideal epitaxial configurations which minimize interfacial misfit energy have been defined and predicted with a model in which both the overgrowth and substrate are assumed rigid. In an improved model, the island was allowed to strain homogeneously and the *strain* energy was included in the interfacial energy. Epitaxy was predicted to occur when the interfacial energy consisting of both misfit and strain energies was minimized.

In the model considered in this chapter the overall - misfit - strain predicted from the homogeneous model is kept, but, additionally, local relaxation of the overgrowth is allowed, to further reduce the interfacial energy.

This local relaxation is associated with misfit dislocations. The reciprocal lattice formulation developed in Chapter 3 (section 3.3) and extended to strained cases in Chapter 4 (sections 4.4 and 4.5) is extended further to enable the description of the interfacial misfit dislocation structure of completely general misfitting interfaces. Their spacing, Burgers vectors and line sense are all derivable from the reciprocal space maps of the overgrowth and substrate crystals.

The actual relaxation process is modelled with a Finite Element description. The island being modelled is allowed to strain homogeneously to minimize total interfacial energy, then kept to this misfit strain and boundary orientation, but allowed to relax internally.

The finite element formulation is preferred to the finite difference approaches which have been applied by several authors in the study of epitaxy, (Snyman *e.a.* 1975, Snyman *e.a.* 1980, Stoop *e.a.* 1982 c) as general computer programs which may be used for a variety of situations are easier to write, and boundary conditions easier to implement, with the former.

As with the homogeneous strain model, the atom-atom interaction within the island is again assumed to lie within the harmonic approximation, and the island is treated as an elastic continuum which deforms in response to externally applied forces arising from its interaction with the substrate.

5.1 BROAD DESCRIPTION OF THE FINITE ELEMENT MODEL

In the finite element approach the continuous function which describes the behaviour of a continuum system is replaced with a piecewise continuous approximation in terms of simpler functions defined over small sections. The initially infinite number of degrees of freedom of the continuum is reduced to a finite number in this manner, as each small section or element only has as many degrees of freedom as there are unknown coefficients in the approximating functions. The parameters of the piecewise continuous function are adjusted until a potential energy, in the case of an elasticity problem, is minimized. Equivalently, equilibrium based on this energy minimization may be sought directly in terms of a force balance equation. The approach clearly has many aspects in common with variational methods, and when the governing continuous function is the displacement of the continuum, and strain and interaction energy are minimized together, the method in fact corresponds with the Rayleigh-Ritz variational method.

Steps in the finite element description

The finite element method is applied in several steps. These are:

1. *Subdivision (Discretization)*

   The continuum is divided into finite regions of simple shape known as elements. These elements interact with their surroundings only through selected points, called nodes, which usually lie on the element boundaries. The number of nodes in

each element determines the order of an interpolating polynomial describing the displacement. The behaviour of the elements is expressed in terms of the behaviour of the nodes, and, in this case, the nodal displacements are the parameters which determine the overall approximation, and are therefore the sought unknown quantities.

Characteristically, a relationship of the form

$$\mathbf{f}^e = \mathbf{k}^e \cdot \mathbf{u}^e \qquad (1$$

is obtained for each element. (The superscripted "e" indicates element equations referring to a particular "e-th" element or to distinguish element equations from the overall "system" equations where confusion may arise.) Here $\mathbf{u}^e$ is a column matrix of values of the displacements at the nodes. In a system governed by linear elasticity, the element stiffness matrix $\mathbf{k}^e$ is independent of $\mathbf{u}^e$. The $\mathbf{f}^e$ are the loads applied externally to the element. As used here, the loads arise from the overgrowth-substrate interaction. In general these will change as the element deforms, which means that the system of equations is non-linear.

2. *Assembly*

The element equations are combined into a much larger system of simultaneous equations governing the entire continuum. These equations have a similar form to the element equations, as

$$\mathbf{f} = \mathbf{k} \cdot \mathbf{u} \qquad (2$$

where the matrices refer to the values at all the nodes of the discretized system.

In practice the system stiffness matrix $\mathbf{k}$ is symmetric, sparse, banded and positive definite (See Davies 1980, pp 135-136 for an example) for all the systems modelled here, which considerably simplifies the numerical solution of the equations.

3. *Insertion of Boundary Conditions*

The rigid body motions, rotation and translation, must be prevented, or the governing equations will be singular. As in the homogeneous model, the central atom, which will be chosen to coincide with a node, is held in a potential minimum. The displacement components of the boundary atoms are restricted in such a way that the average strain is equal to the homogeneous strain. This also prevents rigid body rotations. The load and stiffness matrices are altered by the inclusion of boundary conditions, but the equations retain their form and become:

$$\mathbf{K}^{B}\cdot\mathbf{U} = \mathbf{F}^{B} \quad , \qquad (3$$

where, at the same time, the matrices have been expressed in dimensionless form. The superscripted "B" indicates that boundary conditions have been implemented.

4. *Atomic Structure dependent quantities*

The actual values of the force terms arise from the details of the distribution of atoms in the island together with the substrate potential. Also dependent on these are other quantities expressed in absolute units, specifically the residual misfit and elastic strain energies. These effects are included after the finite element equations have been set up, but necessarily during the solution stage.

5. *Solution*

The final step is the numerical solution of the system equations. The methods used are described in appendix B.

The finite element model is now developed step by step as outlined in this broad description.

5.2 DISCRETIZATION OF THE OVERGROWTH ISLAND

The overgrowth island is modelled as a continuum in which the atoms are embedded. The displacement of the continuum,

$$\mathbf{u} = (u_x(x,y), u_y(x,y)) \qquad (4$$

is approximated *piecewise* by polynomials defined on the elements. The order of these interpolating polynomials depends on the size, shape and number of nodes in the elements, while the coefficients are determined by the values of the displacement function at the nodes.

The displacements of the atoms are given by the values of the continuous displacement function at their (undisplaced) positions. The overgrowth-substrate interaction is through the adatom-substrate potential, which results in forces which are applied to the continuum at the atom sites. As these forces are combined to equivalent forces acting only through the nodes of the elements it is advantageous, but not essential, if the distribution of the nodes and atoms coincide to a large extent. Considerations of symmetry make some choices of element shape more natural than others.

Choice and description of the elements

Four of the five two-dimensional Bravais lattices (Strozier 1975, Kittel 1966 Ch1) have a mirror line in the plane. These lattices may all be divided into rectangular unit cells, while only the remaining oblique lattice must be sectioned with triangles. Because rectangles retain the mirror symmetry of so many lattices and have the advantage of a simpler formulation, rectangular elements are used, particularly as they are suited to the bcc{110} symmetry.

However, although the lattices have at least mirror symmetry, many space groups do not, so that rectangular unit cells are generally not primitive, and atoms will occur at positions other than at the corners of the rectangles. In order to accommodate such atoms, a second-order interpolating polynomial is used. This provides a considerable improvement on a linear interpolating scheme, and allows coarser discretization (Iverson 1969) with some reduction in computational effort, or alternatively an effective increase in the size of the island. This gain is achieved because a second order displacement function allows the strain to vary bi-linearly across an element, an improvement on the constant strain approximation which results from a linear interpolation. A further increase in the order however, increases the computational costs, but with less gain in accuracy, so that a rectangular element with second order interpolating function is optimal.

A well-known standard element of this type, the *bi-quadratic Lagrangian* element, was actually used. A small rectangular island of bcc{110} material, divided in this fashion is shown in figure 5.1.

The Bi-Quadratic Lagrange Element

The rectangular element has nine nodes, one at each corner, at each of the midside positions, and at the centre. The positions of the nodes, and a numbering scheme are shown in figure 5.2. Within the element the values of the interpolated function, in this case the displacement components u_x and u_y are expressed in terms of their values at the nodes.

The interpolation is most suitably expressed in terms of a local coordinate system (ξ,η) parallel to the sides of the rectangle with origin at the central node. ξ and η range from -1 to +1 from edge to edge.

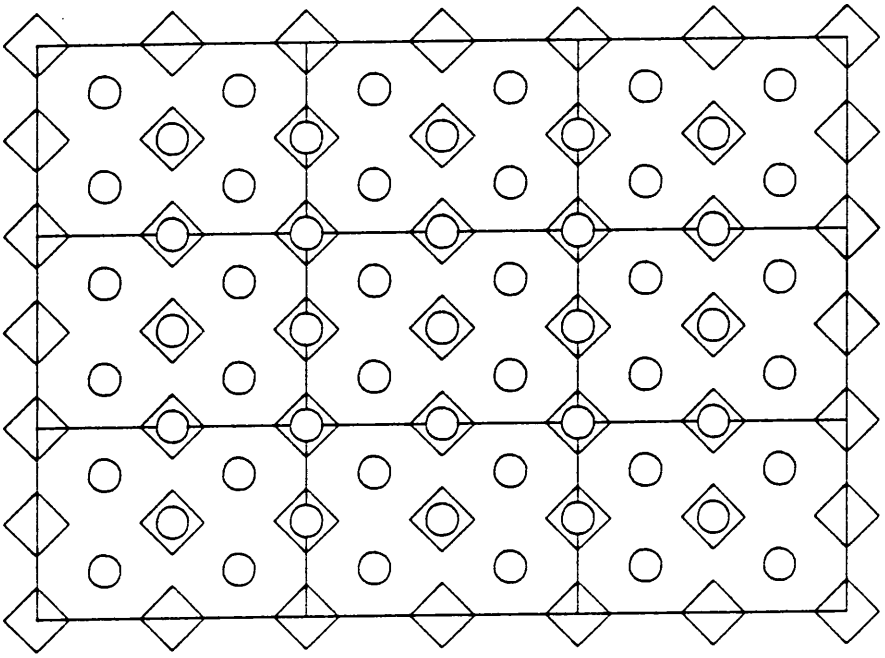

Figure 5.1 Small island sectioned into biquadratic Lagrange finite elements

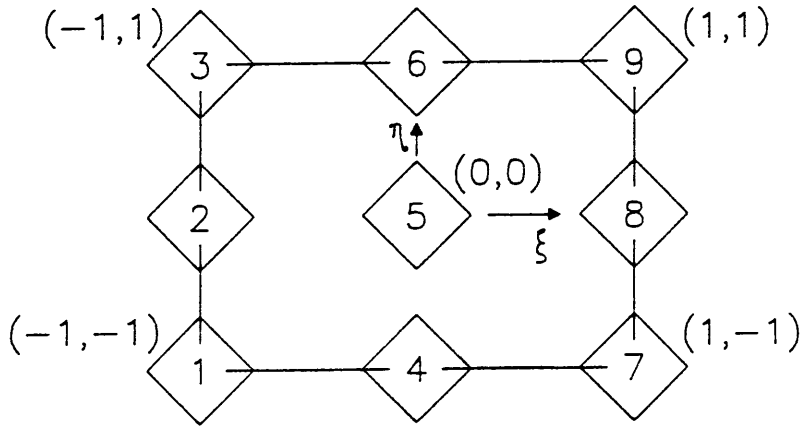

Figure 5.2 Biquadratic Lagrange element showing the element node numbers and local coordinates ξ and η

The function $u_x(\xi,\eta)$ may be expressed as

$$u_x(\xi,\eta) = \alpha_0 + \alpha_1\xi + \alpha_2\xi^2 + \alpha_3\xi\eta + \alpha_4\xi\eta^2 + \alpha_5\xi^2\eta + \alpha_6\xi^2\eta^2 + \alpha_7\eta + \alpha_8\eta^2. \qquad (5$$

At the nodes the values of u_x are given as

$$\begin{aligned}
u_x^1 &= \alpha_0 - \alpha_1 + \alpha_2 + \alpha_3 - \alpha_4 - \alpha_5 + \alpha_6 - \alpha_7 + \alpha_8 \qquad (6\\
u_x^2 &= \alpha_0 - \alpha_1 + \alpha_2\\
u_x^3 &= \alpha_0 - \alpha_1 + \alpha_2 - \alpha_3 - \alpha_4 + \alpha_5 + \alpha_6 + \alpha_7 + \alpha_8\\
u_x^4 &= \alpha_0 - \alpha_7 + \alpha_8\\
u_x^5 &= \alpha_0\\
u_x^6 &= \alpha_0 + \alpha_7 + \alpha_8\\
u_x^7 &= \alpha_0 + \alpha_1 + \alpha_2 - \alpha_3 + \alpha_4 - \alpha_5 + \alpha_6 - \alpha_7 + \alpha_8\\
u_x^8 &= \alpha_0 + \alpha_1 + \alpha_2\\
u_x^9 &= \alpha_0 + \alpha_1 + \alpha_2 + \alpha_3 + \alpha_4 + \alpha_5 + \alpha_6 + \alpha_7 + \alpha_8 \ ,
\end{aligned}$$

where the superscripts refer to the node numbers defined in figure 5.2.

Equivalent to the polynomial approximation is the truncated Taylor expansion

$$u_x(\xi,\eta) = \left(1+H\frac{\partial}{\partial\xi}+\frac{H^2}{2}\frac{\partial^2}{\partial\xi^2}\right)\left(1+K\frac{\partial}{\partial\eta}+\frac{K^2}{2}\frac{\partial^2}{\partial\eta^2}\right)u_x(\xi,\eta)\Big|_{\xi=0,\eta=0} \qquad (7$$

with $H|_{\xi=0} = \xi$, and $K|_{\eta=0} = \eta$.

The coefficients α_0 to α_9 may be expressed in terms of the nodal values and also in terms of the coefficients of the Taylor expansion as

$$\begin{aligned}
\alpha_0 &= u_x^5 = u_x(0,0) \ , \qquad (8\\
\alpha_1 &= \tfrac{1}{2}(u_x^6-u_x^4) = \frac{\partial}{\partial\xi}u_x \ ,\\
\alpha_2 &= \tfrac{1}{2}(u_x^6-2u_x^5+u_x^4) = \tfrac{1}{2}\frac{\partial^2}{\partial\xi^2}u_x \ ,\\
\alpha_3 &= \tfrac{1}{4}[(u_x^9-u_x^7)-(u_x^3-u_x^1)] = \frac{\partial^2}{\partial\xi\partial\eta}u_x \ ,
\end{aligned}$$

$$\alpha_4 = \tfrac{1}{4}[(u_x^9-2u_x^8+u_x^7)-(u_x^3-2u_x^2+u_x^1)] = \tfrac{1}{2}\frac{\partial^3}{\partial\xi\partial\eta^2}u_x \quad ,$$

$$\alpha_5 = \tfrac{1}{4}[(u_x^9-2u_x^6+u_x^3)-(u_x^7-2u_x^4+u_x^1)] = \tfrac{1}{2}\frac{\partial^3}{\partial\xi^2\partial\eta}u_x \quad ,$$

$$\alpha_6 = \tfrac{1}{4}[(u_x^9-2u_x^8+u_x^7)-2(u_x^6-2u_x^5+u_x^4)+(u_x^3-2u_x^2+u_x^1)] = \tfrac{1}{4}\frac{\partial^4}{\partial\xi^2\partial\eta^2}u_x \quad ,$$

$$\alpha_7 = \tfrac{1}{2}(u_x^6-u_x^4) = \frac{\partial}{\partial\eta}u_x \quad ,$$

$$\alpha_8 = \tfrac{1}{2}(u_x^6-2u_x^5+u_x^4) = \tfrac{1}{2}\frac{\partial^2}{\partial\eta^2}u_x \quad ,$$

where the coefficients have been identified with the finite difference approximations to the derivatives as calculated at the centre of the element, where $\xi=\eta=0$.

By substituting these expressions into the polynomial expansion, and collecting terms in the nodal values u_x^s, the function $u_x(\xi,\eta)$ may be expressed as a product of matrices of functions independent of u_x - but characteristic of the *element*, and nodal values. Hence,

$$u_x(\xi,\eta) = [N_1(\xi,\eta) \quad N_2(\xi,\eta) \ \ldots \ \ldots \ N_9(\xi,\eta)]\begin{bmatrix} u_x^1 \\ u_x^2 \\ \cdot\cdot \\ \cdot\cdot \\ u_x^9 \end{bmatrix} \quad , \qquad (9$$

where the $N_s(\xi,\eta)$ are the *shape functions*, (also known as weight functions) and are given in full in Table 5.1.

The second component of the displacement vector, and indeed *any* continuous function may be expressed in terms of the same shape functions and the appropriate nodal values (Zienkiewicz 1971, Norrie *e.a.* 1973).

Table 5.1 *Shape functions,* $N_s(\xi,\eta)$*, of the Bi-Quadratic Lagrangian Element.*

$N_1 = \frac{1}{4}(\xi^2-\xi)(\eta^2-\eta)$	$N_2 = \frac{1}{2}(\xi^2-\xi)(1-\eta^2)$	$N_3 = \frac{1}{4}(\xi^2-\xi)(\eta^2+\eta)$
$N_4 = \frac{1}{2}(1-\xi^2)(\eta^2-\eta)$	$N_5 = (1-\xi^2)(1-\eta^2)$	$N_6 = \frac{1}{2}(1-\xi^2)(\eta^2+\eta)$
$N_7 = \frac{1}{4}(\xi^2+\xi)(\eta^2-\eta)$	$N_8 = \frac{1}{2}(\xi^2+\xi)(1-\eta^2)$	$N_9 = \frac{1}{4}(\xi^2+\xi)(\eta^2+\eta)$

from: Davies, A.J., (1980) , ch 5 p198.

It is convenient to combine the equations in such a way that the x- and y-components alternate in the column matrix for the displacement, as:

$$\mathbf{u} = \begin{bmatrix} u_x \\ u_y \end{bmatrix} = \left[\begin{array}{cc|cc|c|cc|c} N_1 & 0 & N_2 & 0 & \cdots & N_s & 0 & \cdots \\ 0 & N_1 & 0 & N_2 & \cdots & 0 & N_s & \cdots \end{array}\right] \begin{bmatrix} u_x^1 \\ u_y^1 \\ u_x^2 \\ u_y^2 \\ \vdots \\ u_x^s \\ u_y^s \\ \vdots \end{bmatrix}$$

$$= [\mathbf{N}_1 \ \mathbf{N}_2 \ \cdots \ \mathbf{N}_s \ \cdots] \begin{bmatrix} \mathbf{u}^1 \\ \mathbf{u}^2 \\ \vdots \\ \mathbf{u}^s \\ \vdots \end{bmatrix} = [\mathbf{N}_s] \cdot [\mathbf{u}^s] \ , \qquad (10$$

where, as before, the index s refers to the node number in the element, and $\mathbf{u}^s$ refers to the displacement vector of node s. The submatrix $\mathbf{N}_s$ is a matrix of shape functions appropriate to the degrees of freedom of the node s.

Here, and subsequently, matrices are indicated by using bold letters, or by listing a general element between brackets, e.g.: $\mathbf{A} = [A_s]$. A matrix which has been partitioned into submatrices is written as $[\mathbf{A}_s]$, i.e. a matrix consisting of submatrices. As

applied above, $[\mathbf{N}_s]$ is a matrix which has been partitioned into the submatrices of shape functions

$$\mathbf{N}_s = \begin{bmatrix} N_s & 0 \\ 0 & N_s \end{bmatrix} , \tag{11a}$$

and $[\mathbf{u}^s]$ has been partitioned into submatrices of the vector components

$$\mathbf{u}^s = \begin{bmatrix} u_x^s \\ u_y^s \end{bmatrix} . \tag{11b}$$

Elasticity : Strain, Stress and Hookes's Law

The strain is defined as usual in terms of the displacement function, and may be written in matrix form as

$$\boldsymbol{\varepsilon} = \begin{bmatrix} \varepsilon_x \\ \varepsilon_y \\ \gamma_{xy} \end{bmatrix} = \begin{bmatrix} \frac{\partial}{\partial x} & 0 \\ 0 & \frac{\partial}{\partial y} \\ \frac{\partial}{\partial y} & \frac{\partial}{\partial x} \end{bmatrix} \begin{bmatrix} u_x \\ u_y \end{bmatrix} . \tag{12}$$

Expressed in terms of the nodal values, with $\mathbf{u} = [\mathbf{N}_s] \cdot [\mathbf{u}^s]$, (eqn 10) the strain is

$$\boldsymbol{\varepsilon} = [\mathbf{B}_s][\mathbf{u}^s] \tag{13}$$

where $[\mathbf{B}_s]$ is a matrix of submatrices of the form

$$\mathbf{B}_s = \begin{bmatrix} N_{s,x} & 0 \\ 0 & N_{s,y} \\ N_{s,y} & N_{s,x} \end{bmatrix} , \tag{14}$$

with $N_{s,x} = \partial N_s / \partial x$ etc., the partial derivatives of the shape functions. The shape functions are expressed explicitly in terms of local coordinates ξ and η, but differentiated in terms of the absolute coordinates x and y. With the ξ and η axes parallel to the x and y axes however, the transformation has a Jacobian of

simple form, where

$$\frac{h_x}{2}\, d\xi = dx, \quad \text{and} \quad \frac{h_y}{2}\, d\eta = dy \ . \qquad (15$$

Here h_x and h_y are the horizontal and vertical dimensions of the rectangular element respectively as shown in figure 5.2. The derivatives of the shape functions are listed in Table 5.2.

The stress follows in matrix form from Hooke's law and a matrix of elastic constants $\mathbf{D}$ as

$$\sigma = \mathbf{D}\cdot\varepsilon = \mathbf{D}\cdot[\mathbf{B}_s]\cdot[u^s] \ . \qquad (16$$

The matrix $\mathbf{D}$ of elastic constants satisfying plane stress conditions is the same as that used in the homogeneous strain model of the previous chapter.

Table 5.2 *Derivatives of the Shape functions.*

Node No s	$N_{s,x}$	$N_{s,y}$
1	$\frac{1}{2}(2\xi-1)(\eta^2-\eta)/h_x$	$\frac{1}{2}(\xi^2-\xi)(2\eta-1)/h_y$
2	$(2\xi-1)(1-\eta^2)/h_x$	$-2(\xi^2-\xi)\eta/h_y$
3	$\frac{1}{2}(2\xi-1)(\eta^2+\eta)/h_x$	$\frac{1}{2}(\xi^2-\xi)(2\eta+1)/h_y$
4	$-2\xi(\eta^2-\eta)/h_x$	$(1-\xi^2)(2\eta-1)/h_y$
5	$-4\xi(1-\eta^2)/h_x$	$-4(1-\xi^2)\eta/h_y$
6	$-2\xi(\eta^2+\eta)/h_x$	$(1-\xi^2)(2\eta+1)/h_y$
7	$\frac{1}{2}(2\xi+1)(\eta^2-\eta)/h_x$	$\frac{1}{2}(\xi^2+\xi)(2\eta-1)/h_y$
8	$(2\xi+1)(1-\eta^2)/h_x$	$-2(\xi^2+\xi)\eta/h_y$
9	$\frac{1}{2}(2\xi+1)(\eta^2+\eta)/h_x$	$\frac{1}{2}(\xi^2+\xi)(2\eta+1)/h_y$

Element Equilibrium Equations

The element will strain to accommodate external loads until at equilibrium the loads and stress forces balance. In the context of the epitaxial model, the overgrowth will strain until the forces arising from its interaction with the substrate are balanced.

Before discussing the force-balance governing the entire elastic continuum, it is useful to derive the equilibrium equations between the strain of a single element and a distributed force field applied to the element. This force field may be a distribution of body, surface or line tractions, but all result in essentially the same equation.

Consider an applied force distribution, $\mathbf{p}(x,y)$, which will be assumed to be a body-force field.

In order to derive the equilibrium equations, the principle of virtual work is invoked. Allow the elastic material to undergo a virtual displacement field

$$d\mathbf{v} = [\mathbf{N}_s]\cdot[d\mathbf{v}^s], \tag{17a}$$

with the virtual strain

$$d\boldsymbol{\varepsilon}_v = [\mathbf{B}_s]\cdot[d\mathbf{v}^s] \ . \tag{17b}$$

The virtual work density due to the internal stress field is then

$$w_\sigma = d\boldsymbol{\varepsilon}_v^T\cdot\boldsymbol{\sigma} \ . \tag{18a}$$

(The superscripted "T" indicates the transposed matrix as usual.)

The virtual work done on the element is obtained by integration over the volume domain $\mathfrak{D}_e$ of the element, and is:

$$\begin{aligned} W_\sigma &= \int_{\mathfrak{D}_e} d\boldsymbol{\varepsilon}_v^T\cdot\boldsymbol{\sigma}\ d\mathfrak{D}_e = \int_{\mathfrak{D}_e}\{[\mathbf{B}_s,]\cdot[d\mathbf{v}^{s'}]\}^T\cdot\boldsymbol{\sigma}\ d\mathfrak{D}_e \\ &= [d\mathbf{v}^{s'}]^T\cdot\int_{\mathfrak{D}_e}[\mathbf{B}_s,]^T\cdot\mathbf{D}\cdot[\mathbf{B}_s]\cdot[\mathbf{u}^s]\ d\mathfrak{D}_e \ . \end{aligned} \tag{18b}$$

The virtual work due to the distributed body-force $\mathbf{p}(x,y)$ is

$$\begin{aligned} W_p &= \int_{\mathfrak{D}_e} d\mathbf{v}^T\cdot\mathbf{p}\ d\mathfrak{D}_e = \int_{\mathfrak{D}_e}\{[\mathbf{N}_s,]\cdot[d\mathbf{v}^{s'}]\}^T\cdot\mathbf{p}\ d\mathfrak{D}_e \\ &= [d\mathbf{v}^{s'}]^T\cdot\int_{\mathfrak{D}_e}[\mathbf{N}_s,]^T\cdot\mathbf{p}\ d\mathfrak{D}_e \ . \end{aligned} \tag{18c}$$

Now, the total work done by the virtual displacement must be zero, so that $W_\sigma - W_p = 0$, and, since the virtual displacement is arbitrary, the multipliers must be equal. Therefore,

$$\{\int_{\mathfrak{D}_e} [B_{s,}]^T \cdot D \cdot [B_s]\, d\mathfrak{D}_e\} \cdot [u^s] = \int_{\mathfrak{D}_e} [N_{s,}]^T \cdot p\, d\mathfrak{D}_e \ . \qquad (19a$$

With the substitutions,

$$\int_{\mathfrak{D}_e} [B_{s,}]^T \cdot D \cdot [B_s]\, d\mathfrak{D}_e \equiv [k_{s,s}]^e, \qquad (19b$$

known as the *element stiffness matrix*, and

$$\int_{\mathfrak{D}_e} [N_{s,}]^T \cdot p\, d\mathfrak{D}_e \equiv [F_{s,}]^e, \qquad (19c$$

the equilibrium equation is written as

$$[k_{s,s}]^e \cdot [u^s]^e = [F_{s,}]^e \ . \qquad (20$$

In this equation, the superscripted "e" has been introduced to emphasize that these matrices refer to *element* properties. The $[F_{s,}]^e$ are interpretable as forces applied at the nodes, which cause strain and do (virtual) work equivalent to that of the load distribution $p(x,y)$.

Although body forces were considered here, equivalent nodal loads could have been derived for *any* distributed load type, with an appropriately chosen domain. Body forces were chosen in particular, because the monolayer overgrowth-substrate interaction will be modelled as expressions of this type.

Explicit calculation of the element stiffness matrices

The overgrowth island is modelled as a thin slice of elastic material, and, as in the homogeneous strain model, the material is assumed to be thin enough to allow plane stress boundary conditions, with **D** the appropriate matrix of elastic constants. This matrix was calculated in the previous chapter for several values of the anisotropy ratio A.

Consider the e'th element, with constant thickness t_e, area $\mathcal{D}^2_e$ and volume $\mathcal{D}_e = t_e\mathcal{D}^2_e$. The element stiffness matrix is given by

$$[k_{s',s}]^e = \left[\int_{\mathcal{D}_e} [B_{s',}]^T \cdot \mathbf{D} \cdot [B_s] \, d\mathcal{D}_e \right]^e$$

$$= \frac{\mu}{(1-\nu)} t_e \left[\int_{\mathcal{D}^2_e} [B_{s',}]^T \cdot \mathbf{D}' \cdot [B_s] \, d\mathcal{D}^2_e \right]^e$$

$$\equiv \frac{\mu}{(1-\nu)} t_e \left[\int_{\mathcal{D}^2_e} [P_{mn}]_{s',s} \, d\mathcal{D}^2_e \right]^e$$

$$\equiv \frac{\mu}{(1-\nu)} t_e \, [K_{s',s}]^e \qquad (21$$

where $\mathbf{D}' = \mathbf{D}(1-\nu)/\mu$ is a matrix of dimensionless elastic constants. The elastic constants μ and ν are isotropic constants, the shear modulus and Poisson ratio respectively, derived from the anisotropic constants by Voigt-averaging (Chapter 4, eqn 20, Hirth *e.a.* 1968, Ch 13), and have been described more fully in the discussion on the homogeneous strain model of the foregoing chapter. Also, the matrix $[K_{s',s}]^e$ is dimensionless, as will be shown below.

The integrand has been written as the 2X2 submatrix $[P_{mn}]_{s',s}$, which, given explicitly, is:

$$[P_{mn}]_{s',s} = \begin{bmatrix} N_{s',x} & 0 & N_{s',y} \\ 0 & N_{s',y} & N_{s',x} \end{bmatrix} \cdot \begin{bmatrix} D'_{11} & D'_{12} & D'_{13} \\ D'_{21} & D'_{22} & D'_{23} \\ D'_{31} & D'_{32} & D'_{33} \end{bmatrix} \cdot \begin{bmatrix} N_{s,x} & 0 \\ 0 & N_{s,y} \\ N_{s,y} & N_{s,x} \end{bmatrix} . \qquad (22a$$

Expanding this matrix product the entries of $[P_{mn}]_{s',s}$ are

$$P_{11} = D'_{11}N_{s',x}N_{s,x} + D'_{13}N_{s',x}N_{s,y} + D'_{31}N_{s',y}N_{s,x} + D'_{33}N_{s',y}N_{s,y}$$

$$P_{12} = D'_{12}N_{s',x}N_{s,y} + D'_{13}N_{s',x}N_{s,x} + D'_{32}N_{s',y}N_{s,y} + D'_{33}N_{s',y}N_{s,x}$$

$$P_{21} = D'_{21}N_{s',y}N_{s,x} + D'_{23}N_{s',y}N_{s,y} + D'_{31}N_{s',x}N_{s,x} + D'_{33}N_{s',x}N_{s,y}$$

$$P_{22} = D'_{22}N_{s',y}N_{s,y} + D'_{23}N_{s',y}N_{s,x} + D'_{32}N_{s',x}N_{s,y} + D'_{33}N_{s',x}N_{s,x} \qquad (22b$$

Clearly, the elements of the stiffness matrix all contain sums of terms of the form

$$I_{s'i,sj} = \int_{\mathfrak{D}_e^2} N_{s',i}\, N_{s,j}\, dx\, dy \qquad (23$$

where $,i$ and $,j$ refer to the partial derivatives with respect to x or y as given in Table 5.2 .

As is evident from Table 5.2, all the shape function derivatives may be written as $f_{si}(\xi,\eta)/h_y$, so that the integrals are

$$I_{s'i,sj} = \int_{h_x h_y} \int f_{s'i}(\xi,\eta)/h_y \; f_{sj}(\xi,\eta)/h_y \; dx\, dy$$

$$= \int_{-1}^{+1} \int_{-1}^{+1} f_{s'i}(\xi,\eta)\; f_{sj}(\xi,\eta)\; d\xi\, d\eta/(4h_{21}) \quad , \qquad (24$$

with $h_{21}=h_y/h_x$, the ratio of the sides of the element.

These integrals are dependent only on the shape and nodes of the individual elements, as only the local coordinates ξ and η appear, and may therefore be pre-calculated. With nine nodes per element and two displacement components per node, there are 18X18 such integrals and, because of symmetry, 171 are unique.

As all these integrals are of simple form and there are so many of them, listing them all analytically is not worthwhile. Rather, these integrals are calculated numerically at the actual modelling stage. The Gauss-Legendre numerical quadrature technique is particularly suited to this purpose, and an implementation of this standard technique from the IMSL (1980) package of programs was used.

As a consequence of the form of the integrals, $[\mathbf{K}_{s',s}]^e$ is dimensionless and freely scalable. A scalable stiffness matrix for the entire structure will be assembled from this matrix in a manner consistent with the equilibrium conditions satisfied by the overgrowth-substrate system as a whole.

Only the form of the overgrowth island needs to be known in advance, but its dimensions in absolute terms are inserted at a final calculation stage. The process of assembling a system stiffness matrix needs to be carried out only once for a particular overgrowth.

This allows a wide range of substrate types to be matched with a given overgrowth.

5.3 SYSTEM EQUILIBRIUM EQUATIONS - THE ASSEMBLY OF SYSTEM MATRICES

The equations governing the entire system of elements and therefore the entire overgrowth are derived by invoking the principle of virtual work for quantities constructed from the element definitions. The relationship between these global and element quantities lead directly to a method of constructing the governing equations in matrix form from the element matrices. This is usually termed the assembly stage.

Equilibrium equations for the entire region

By defining shape functions for the entire system of elements from the element shape functions, the principle of virtual work may be invoked in the same way and equilibrium relations of the same form as the element equations derived.

Apply some ordering scheme to all the nodes of the overgrowth so that the displacements may be expressed in a single column matrix, $[u_S]$, where the upper-case index S refers to the overall node-numbering scheme. (The actual numbering scheme used is summarized in table 5.3 below.)

In terms of all the nodes then, the displacement may be expressed as (from eqn 9, 10 ,11)

$$u(x,y) = [N_S] \cdot [u_S] \qquad (25$$

where

$$N_S = \begin{cases} N_s^e(\xi,\eta) & \text{if } x,y \text{ lies at } \xi,\eta \text{ in an element e and where the node S has number s in the element.} \\ 0 & \text{if point } x,y \text{ is not within the element.} \end{cases}$$

Applying the definition of strain, the matrix $[B_S]$, is similarly defined in terms of the element matrix $[B_s]^e$. The principle of virtual work may then be applied to the entire overgrowth. Following an analysis formally the same as for the single element (eqns 19, 20), the system equilibrium relation follows as

$$[k_{S'S}] \cdot [u_S] = \left[\int_{Vol} [B_{S'}]^T \cdot D \cdot [B_S] \, dVol \right] \cdot [u_S] = [F_{S'}] \quad . \quad (26$$

The integral is taken over the entire overgrowth. Here $[k_{S'S}]$ is the *system stiffness* matrix. From the relationship between the element and the system matrices, it may be seen that

$$[k_{S'S}] = \sum_{e=1}^{L} [k_{s's}]^e \quad , \quad (27$$

and

$$[F_S] = \sum_{e=1}^{L} [F_s]^e \quad , \quad (28$$

where the nodes S and S' in terms of the overall numbering system, are the nodes s and s' in the e'th element.

In these last equations, the element matrices are first expanded to full size by writing their entries into a zero matrix of the same size as the full system matrix, with the appropriate transformation from element to system numbering scheme. These matrices may then be added in true matrix algebraic fashion to obtain the system matrix (Davies 1980 ch 4.6). Alternatively, the addition may be performed entry by entry, appropriately renumbered, directly into the larger matrix.

The system nodal force matrix is similarly constructed by adding the nodal force contributions from the distributed forces in each element. A point force applied at a node is added only once.

These system equations are valid for elements which ensure displacement continuity (Zienkiewicz 1971) which is satisfied by the Lagrange elements.

Assembly of the system matrices

The individual element matrices are combined to a single matrix describing the elastic properties of the overgrowth. This process of constructing the system matrix from the element matrices is known as the *assembly* stage of the finite element model.

Key to the construction of the system stiffness matrix is an optimal numbering scheme applicable to the nodes. Only the nodes in a particular element have non-zero contributions to the system stiffness matrix, and as a result the system matrix can be constructed as a band matrix, which saves computer storage and allows the treatment of relatively large islands. An inefficient numbering scheme would tend to increase the bandwidth and reduce the advantages of the formulation.

Global node numbering scheme

In previous models, the island has been constructed as a rectangular array of atoms and this arrangement is kept here. As the nodes of the finite element model do not *necessarily* coincide with atoms in the island the discretization of the continuum is discussed first. The specific atomic positions are relevant only when the nodal loads are actually calculated.

The island is sectioned into several rectangular finite elements, each with 3 nodes to a side. This implies that the rectangular

island must have an odd number of nodes per side. Consider therefore an island with M columns of nodes repeated parallel to the $\mathbf{b}_1$ direction each with N nodes lying along the $\mathbf{b}_2$ direction. Both M and N are odd, and there are $M \times N$ nodes in the island. Each node has two degrees of freedom, so that the system matrix is of order $(2 \times M \times N)$.

The position of a node lying in the m'th row and n'th column is conveniently given by a number pair (m,n). Naturally enough, with $(1,1)$, the first node, and (M,N), the node at the diagonally opposite corner of the island, a unique single number may be asigned to each node with the formula

$$\text{Node-no} \equiv S = (m-1) \times N + n \quad , \qquad (\textit{while} \quad N \leq M) \; . \qquad (29$$

This numbering system is illustrated in figure 5.3. Essentially, the nodes are numbered along columns in the $\mathbf{b}_2$ direction, starting in the bottom left corner until the upper border is reached, and then continuing from the bottom edge to the top again. This scheme is optimal for the rectangular island while the number, N, of nodes in a column is less than or the same as the number, M, in each row.

As was mentioned before, it is convenient to alternate degrees of freedom in the displacement matrix, so that the x-degree of freedom of node number S is listed at position $S_x = 2S-1$, while the y-degree of freedom is listed at $S_y = 2S$.

Assembly of the stiffness and load matrices

The system stiffness matrix is constructed from the stiffness matrix of each of the elements by mapping the element freedom numbers from each element into the global numbering scheme and adding the $K^e_{s_i,s_j}$ entry in the element matrix to the corresponding

entry K_{S_i,S_j} in the system matrix, where in both cases i and j have the values x and y as appropriate.

A systematic method of including all the nodes in this reassignment can be achieved by renumbering the nodes element-by-element. Every node with both the column, m, and row, n, positions odd, and not lying on the upper or right hand borders (so that $m<M$ and $n<N$), will have an element with nine nodes associated with it. This node will be the first vertex node in the element. This is illustrated in figure 5.3 and in detail in figure 5.4. The mapping from element node numbering to node coordinate to global node number is given in Table 5.3, which also shows how the degrees of freedom are numbered.

Table 5.3 *Mapping of node numbers from element to global numbering schemes.*

ELEMENT NUMBERING			*Node*	*GLOBAL NUMBERING*		
Node	*Freedom No*		*Co-*	*Node No*	*Freedom No*	
No s	s_x	s_y	*ordinates*	S	S_x	S_y
1	1	2	m,n	$(m-1)N+n$	$2(m-1)N+2n-1$	$2(m-1)N+2n$
2	3	4	$m,n+1$	$(m-1)N+n+1$	$2(m-1)N+2n+1$	$2(m-1)N+2n+2$
3	5	6	$m,n+2$	$(m-1)N+n+2$	$2(m-1)N+2n+3$	$2(m-1)N+2n+4$
4	7	8	$m+1,n$	$mN+n$	$2(mN+n)-1$	$2(mN+n)$
5	9	10	$m+1,n+1$	$mN+n+1$	$2(mN+n)+1$	$2(mN+n)+2$
6	11	12	$m+1,n+2$	$mN+n+2$	$2(mN+n)+3$	$2(mN+N)+4$
7	13	14	$m+2,n$	$(m+1)N+n$	$2(m+1)N+2n-1$	$2(m+1)N+2n$
8	15	16	$m+2,n+1$	$(m+1)N+n+1$	$2(m+1)N+2n+1$	$2(m+1)N+2n+2$
9	17	18	$m+2,n+2$	$(m+1)N+n+2$	$2(m+1)N+2n+3$	$3(m+1)N+2n+4$

Applying this renumbering scheme element by element, the element stiffness matrix entries may be added to the appropriate positions in the initially empty system stiffness matrix. The element nodal load vectors may be combined to a system load matrix in the same way.

The essential properties of symmetry of the element stiffness matrix are carried through to the system matrix. Also, if the dimensionless stiffness matrices are used at the assembly stage, a dimensionless and freely scalable system matrix is constructed.

The system equations for the force balance is then of the same form as that for the elements, and is

$$\frac{\mu}{(1-\nu)} t_e b_2 [\mathbf{K}_{S',S}] \cdot [\mathbf{U}_S] = \frac{W}{b_2} [\mathbf{F}_{S'}] \ , \qquad (30$$

where the nodal displacement and force matrices have been made dimensionless by the replacement of $[\mathbf{u}_S]$ by $b_2[\mathbf{U}_S]$ and $[\mathbf{F}_S]$ by $\frac{W}{b_2}[\mathbf{F}_{S'}]$. W is the energy calibration factor of the adatom-substrate interaction potential already introduced in earlier models. Now W/b_2 has the units of force and $[\mathbf{F}_{S'}]$ is dimensionless.

In the case of the bcc{110} island considered here, the volume of an overgrowth primitive cell is $\Omega = \frac{1}{2} t_e b_1 b_2 = t_e b_2^2/\sqrt{2}$. The system equation may therefore be rewritten in terms of the van der Merwe configurational parameter,

$$\ell^2 = \frac{\mu \ \Omega}{(1-\nu) W r^2} \ , \qquad (31$$

introduced with the homogeneous strain model (Chapter 4 eqn 4.14), to read

$$[\mathbf{K}_{S',S}] \cdot [\mathbf{U}_S] = [\mathbf{F}_S]/(\sqrt{2} r^2 \ell^2) \ . \qquad (32$$

This system of non-linear equations is completely dimensionless, and depends only on the nearest neighbour ratio, the configurational parameter, and the dimensionless stiffness, displacement and nodal force matrices. Additionally, the left hand side depends only on the finite element discretization and properties of the continuum forming the overgrowth, while the right hand side depends on the atomic structure of the overgrowth and the substrate, and contains all overgrowth-substrate interaction terms.

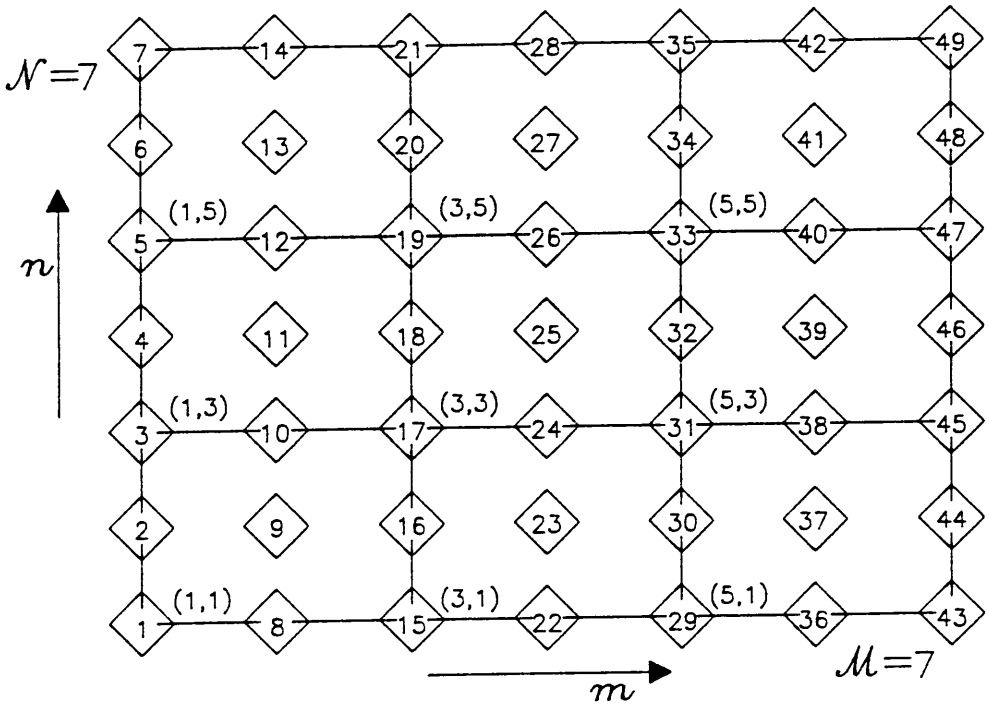

Figure 5.3 Global node numbering scheme for the example island of Figure 5.1

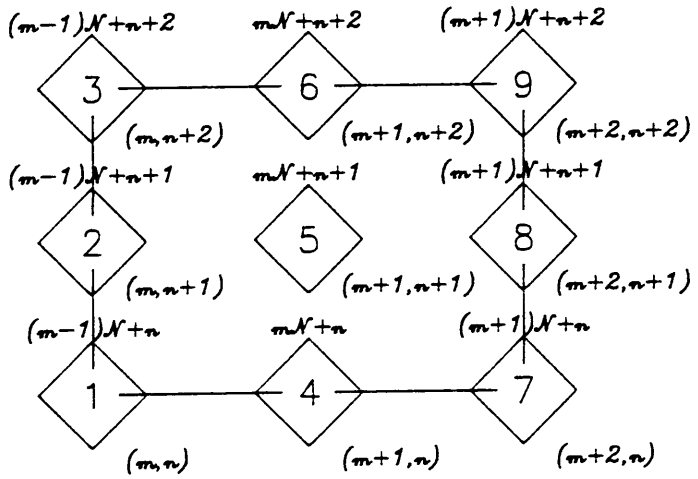

Figure 5.4 Detail of node numbering schemes for a single element with the corner node (m,n)

5.4 THE INSERTION OF BOUNDARY CONDITIONS

The boundary conditions chosen have to serve a two-fold purpose:

Firstly to prevent rigid body motion of the overgrowth in its own coordinate system, which means that free translation and rotation of the island must be prevented. If this is not implemented the matrix $[\mathbf{K}_{S',S}]$ (eqn 32) is singular - its determinant is zero and the matrix not invertible - and the system equations are not soluble.

Secondly, to provide physically reasonable restrictions to the problem in order to facilitate interpretation.

In this case the boundary conditions required for the physical restrictions are sufficient to satisfy the singularity condition as well.

As was mentioned in the introduction to the model, the boundary conditions used are implemented specifically to allow the study of the effect of *local* strain on the reduction of interfacial misfit after the island has strained homogeneously - in a variety of fixed orientations. This is most easily achieved by forcing the displacement of the edges of the island to correspond to an average strain which matches the homogeneous strain. Therefore, the required boundary conditions are of the Dirichlet type.

At the same time, the description must be consistent with a large island so that interfacial atomic arrangements, such as misfit dislocations, can be recognized.

By choosing a zero average strain, the misfit will be accommodated by interfacial misfit dislocations only (Bauer and Van der Merwe 1986). A non-zero average strain can be used to describe both a mixture of misfit dislocations and misfit strain accommodation, as well as the case of pure misfit strain.

Naturally, for purposes of comparison, the island used throughout this study must be used again, namely a symmetrical island with a boundary of elastic material. (This island was of course chosen originally because it is sufficiently easy to implement.)

The fixed average strain boundary conditions

The island is illustrated in figure 4.1 in the discussion on the homogeneous strain model, and the boundary conditions are schematically illustrated in figure 5.5.

The x-degrees of freedom of the nodes on the left and right boundaries are restricted so that the x-displacement of these nodes corresponds to the required homogeneous strain ε_x and any shear component γ_{xy}. The y-degrees of freedom of these atoms are, however, left free. In a similar fashion the y-degrees of freedom of the upper and lower boundaries are restricted to the required homogeneous strain ε_y and the shear, if any. Both restrictions are applied to the corner nodes, which also keeps the average shear of the island the same as the homogeneous shear γ_{xy}.

The form of the island and the type of boundary condition allows the island to represent an overgrowth material which is not free to rotate without cost in elastic strain energy - much like an island in contact with other islands on the substrate. (As different orientations are examined however, tendencies to rotation are seen as lowered energy in different orientations). This effect can only be studied with such a local strain model, as the interior of the island is allowed to rotate towards the more optimal orientation, while the boundary is prevented from rotating.

In addition, as the orientation has been defined in terms of the rotation of the overgrowth island about the central atom of the island, the central node, which in the implementation will also coincide with the central atom, is not allowed to displace. This is not considered a severe restriction, as this atom will usually be placed in a substrate minimum energy position. For a sufficiently

large island, such points are either bound to occur anyway, or the local strain will allow the neighbouring atoms to very nearly take up their optimal positions with only a relatively small energy cost. Both the preceding rigid and homogeneous strain models have explicitly assumed this configuration.

Implementation

The unbounded problem has been given (eqn 32) as

$$[\mathbf{K}_{S,S}]\cdot[\mathbf{U}_S] = [\mathbf{F}_S]/(\sqrt{2}r^2\ell^2) \ .$$

The Dirichlet boundary conditions may be collectively expressed in the form

$$U_{n_i} = \alpha_{n_i} \ , \quad i = 1,2 \ .. \ N_F \ , \qquad (33$$

where N_F , is the number of degrees of freedom which are restricted and α_{n_i} is the prescribed displacement of the i^{th} restricted degree of freedom, which has the freedom number n_i in the global numbering scheme. As pointed out during the design of this numbering scheme, each entry $\mathbf{U}_S$ in the system displacement matrix $[\mathbf{U}_S]$ is a 2-member column submatrix with entries U_{S_x} and U_{S_y}. These correspond with entries U_{2S-1} and U_{2S} in the unpartitioned $2MN$-dimensional system displacement matrix. Here there are $M\times N$ nodes in the finite element discretization, with $2\times M\times N$ degrees of freedom in total. It is useful to refer to the table 5.3 in this context.

Expand the unbounded system equation, as follows

$$\begin{bmatrix} K_{11}U_1 + \ldots + K_{1n_1}U_{n_1} + \ldots + K_{1n_i}U_{n_i} + \ldots \\ \ldots \\ K_{n_1 1}U_1 + \ldots + K_{n_1 n_1}U_{n_1} + \ldots + K_{n_1 n_i}U_{n_i} + \ldots \\ \ldots \\ K_{n_i 1}U_1 + \ldots + K_{n_i n_1}U_{n_1} + \ldots + K_{n_i n_i}U_{n_i} + \ldots \\ \ldots \end{bmatrix} = \mathcal{C} \begin{bmatrix} F_1 \\ \ldots \\ F_{n_1} \\ \ldots \\ F_{n_i} \\ \ldots \end{bmatrix} , \quad (32'$$

where $\mathcal{C} = (\sqrt{2}r^2\ell^2)^{-1}$.

One may incorporate the prescribed displacements without changing the number of equations - which is necessary if general equation solving techniques are used. This is done by replacing the appropriate row in the system equation with the freedom-displacement entry in the correct column and zero's elsewhere. And further, replace all references to the prescribed freedom and also the force entry with the prescribed displacement.

$$\begin{bmatrix} K_{11}U_1 + \ldots + K_{1n_1}\alpha_{n_1} + \ldots + K_{1n_i}\alpha_{n_i} + \ldots \\ \ldots \\ 0 + \ldots + U_{n_1} + \ldots + 0 + \ldots \\ \ldots \\ 0 + \ldots + 0 + \ldots + U_{n_i} + \ldots \\ \ldots \end{bmatrix} = \begin{bmatrix} \mathcal{C}F_1 \\ \ldots \\ \alpha_{n_1} \\ \ldots \\ \alpha_{n_i} \\ \ldots \end{bmatrix}$$

These equations may be brought to their final form by subtracting all the entries containing the prescribed displacements, i.e. terms of the same form as $K_{1n_i}\alpha_{n_i}$ from both sides of the equation, and

then writing them as a matrix product once more as

$$\begin{bmatrix} K_{11} & \cdots & 0 & \cdots & 0 & \cdots \\ \cdots & \cdots & \cdots & \cdots & \cdots & \cdots \\ 0 & \cdots & 1 & \cdots & 0 & \cdots \\ \cdots & \cdots & \cdots & \cdots & \cdots & \cdots \\ 0 & \cdots & 0 & \cdots & 1 & \cdots \\ \cdots & \cdots & \cdots & \cdots & \cdots & \cdots \end{bmatrix} \cdot \begin{bmatrix} U_1 \\ \cdots \\ U_{n_1} \\ \cdots \\ U_{n_i} \\ \cdots \end{bmatrix} = \begin{bmatrix} \zeta F_1 - \sum_{i=1}^{N_F} K_{1n_i} \alpha_{n_i} \\ \cdots \\ \alpha_{n_1} \\ \cdots \\ \alpha_{n_i} \\ \cdots \end{bmatrix} . \qquad (34$$

This matrix equation may be written as

$$[\mathbf{K}_{S',S}]^B \cdot [\mathbf{U}_S] = [\mathbf{F}_{S'}]^B ,$$

or in non-partitioned form,

$$\mathbf{K}^B \cdot \mathbf{U} = \mathbf{F}^B ,$$

and its solution satisfies the boundary conditions. (The superscripted "B" indicates matrices for which the boundary conditions have been implemented. Also the prefactor ζ has been included in $[\mathbf{F}_S]^B \equiv \mathbf{F}^B$ where applicable.)

Clearly, the introduction of Dirichlet boundary conditions in the form of prescribed displacements for some of the degrees of freedom, leads to new system stiffness, $[\mathbf{K}_{S',S}]^B \equiv \mathbf{K}^B$, and force, $\mathbf{F}^B$, matrices.

5.5 QUANTITIES DEPENDENT ON ATOMIC STRUCTURE

Interfacial Energies and Forces

Energies of strain and misfit are calculated once the details of the island atomic structure, the size of the island and the adatom-substrate interaction potential have been specified. While the units of length are scaled with b_2, the y-dimension of the overgrowth atomic lattice unit cell, the number of unit cells and the number of nodes in each direction must be specified. Together

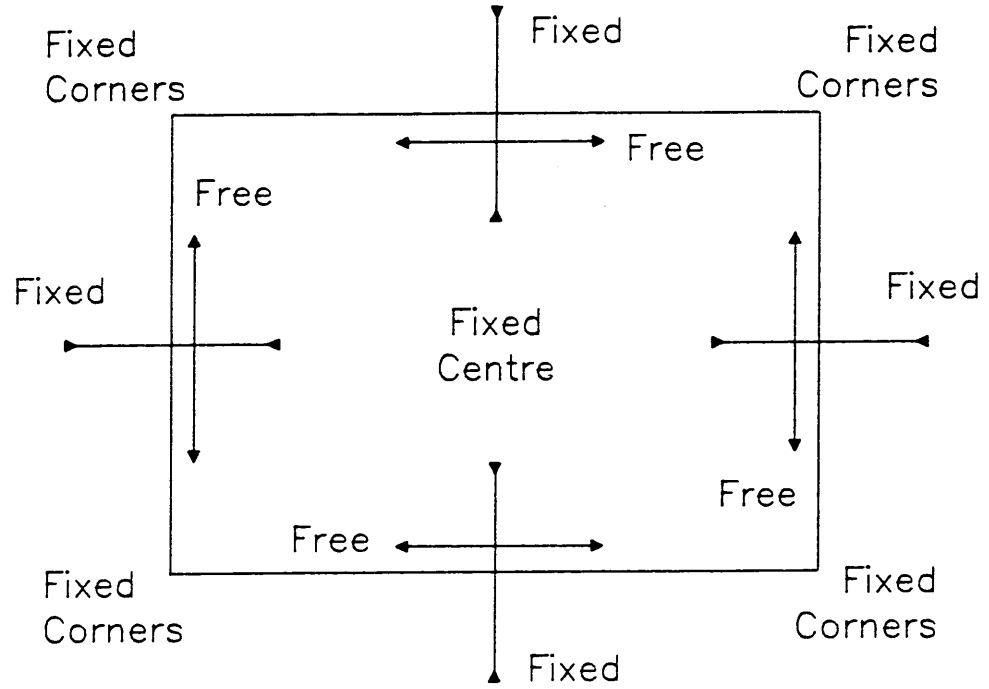

Figure 5.5 Boundary conditions.
Outward arrows indicate free movement of the nodes along the boundary.
Inward arrows indicate fixed degree of freedom perpendicular to the boundary.

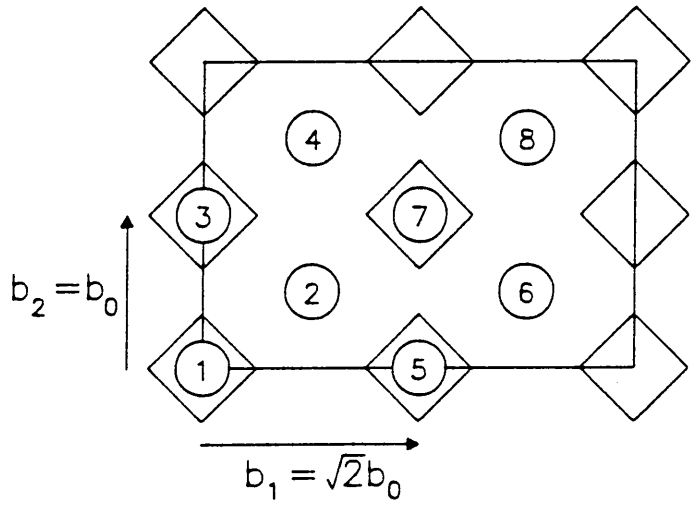

Figure 5.6 Position of the atoms in the element

with the nearest neighbour ratio $r = b_{nn}/a_{nn}$, b_2 also fixes the overgrowth and substrate dimensions.

Positions of the atoms

The atoms are positioned in each finite element in such a way that each atom contributes only once to a particular node. This is achieved by placing atoms in the interior, bottom and left edges of an element, but not at the upper and right edges. This is illustrated in figure 5.6, in which the element numbering scheme for both atoms and nodes is illustrated.

In the case of interior elements, atoms are placed at all the positions shown, so that there are 8 atoms in an interior element. Because of the boundary treatment used here and in the previous chapter, left and lower boundary elements are constructed differently: The atoms 1 and 3 are removed from a left boundary element, the atoms 1 and 5 are removed from a lower boundary element, and 1, 3 and 5 are all removed from the element at the lower left corner.

Bearing the special boundary treatment in mind, the elements are repeated at every second node from bottom to top and left to right in the island. For an island discretized with $M \times N$ nodes there are therefore $(M-1)/2 \times (N-1)/2$ finite elements, which gives a total of

$$G = 2 \times (M-1) \times (N-1) - (M + N) + 3 \qquad (36$$

atoms in the island. With this arrangement, the island is $(M-1)b_1 \times (N-1)b_2$ in size before strain. Because of computer limitations, an island of 625 nodes $(M = N = 25)$ and 1105 atoms is actually used. There are 1250 nodal degrees of freedom, before boundary conditions are taken into account. (In terms of the rigid and homogeneous strain models, M=N=11. (Chapter 3 eqn 28, Chapter 4 eqn 11)

It remains convenient to choose the origin of the island lattice coordinates at the central atom of the island, as in earlier models. The nodes are numbered as described in the global numbering scheme of Table 5.3, and also have indices m,n giving their row and column numbers which range from 1 to M and 1 to N respectively. In terms of their indices, node S is at position

$$X^S_{m,n} = b_1[m-(M-1)/2] = b_2[m-(M-1)/2]/b_{21}$$

and $$Y^S_{m,n} = b_2[n-(N-1)/2] \qquad (37$$

with node number $S = (m-1)N+n$, and $b_{21} = b_2/b_1$.

Starting with $m,n = 1,1$, every node with both m and n odd, but less than M and N respectively, is at the bottom left corner of an element. The absolute positions of atoms corresponding to such a node m,n are tabulated in Table 5.4.

Table 5.4 *Undisplaced Positions* X^{at}, Y^{at} *of the atoms in the element with corner node* m,n .

Atom No (element)	*Absolute Position*	*Atom No (element)*	*Absolute Position*
1	$X^S_{m,n}$, $Y^S_{m,n}$	2	$X^S_{m,n}+\frac{1}{2}b_1$, $Y^S_{m,n}+\frac{1}{2}b_2$
3	$X^S_{m,n}$, $Y^S_{m,n}+b_2$	4	$X^S_{m,n}+\frac{1}{2}b_1$, $Y^S_{m,n}+\frac{3}{2}b_2$
5	$X^S_{m,n}+b_1$, $Y^S_{m,n}$	6	$X^S_{m,n}+\frac{3}{2}b_1$, $Y^S_{m,n}+\frac{1}{2}b_2$
7	$X^S_{m,n}+b_1$, $Y^S_{m,n}+b_2$	8	$X^S_{m,n}+\frac{3}{2}b_1$, $Y^S_{m,n}+\frac{3}{2}b_2$

$X^S_{m,n} = b_1[m-(M-1)/2]$ *and* $Y^S_{m,n} = b_2[n-(N-1)/2]$ *are the coordinates of the first node of an element with global node number* S

It is possible to construct larger islands, using the same number of nodes, simply by increasing the number of atoms assigned to each node, (2 here). For example, with two unit cells assigned to each

node in each direction, there are 8 atoms per node. This accompanies a loss of resolution but may be expected to produce a description still better than a rigid or homogeneous strain model. The generalization to cope with this increase in number of atoms is straightforward.

Atom positions after strain

In response to the interaction of the overgrowth atoms with the substrate, the island undergoes an equilibrium strain as the atoms displace. The displacement function calculated at the original atomic sites gives the displacements of the atoms. These new positions are:

$$[x^{at},y^{at}] = [X^{at}+u_x(X^{at},Y^{at}),Y^{at}+u_y(X^{at},Y^{at})] \ , \qquad (38$$

where X^{at},Y^{at} is the position of the atom "at" in the unstrained island.

In terms of the shape functions and the nodal displacements,

$$\begin{bmatrix} x^{at} \\ y^{at} \end{bmatrix} = \begin{bmatrix} X^{at} \\ Y^{at} \end{bmatrix} + [\cdots \mathbf{N}_s(X^{at},Y^{at}) \cdots] \begin{bmatrix} \vdots \\ \mathbf{u}^s \\ \vdots \end{bmatrix}^e \qquad (39$$

is the displaced position of the atom "at", located in the e^{th} element.

As the vertices of the unit cell coincide with element nodes, the transformation from atomic lattice to global (or absolute) units is

$$x = b_1 x_b \quad \text{and} \quad y = b_2 y_b \ , \qquad (40a$$

with inverse transformation

$$x_b = x/b_1 \quad \text{and} \quad y_b = y/b_2 \ . \qquad (40b$$

Necessarily, the origin of the absolute coordinate system coincides with the atomic lattice coordinate system which continues to be chosen at the central atom of the island.

The transformation from overgrowth lattice coordinates to substrate lattice coordinates, as defined in earlier chapters (Chapter 3 eqn 3.6), and summarized in the Appendix A (eqn A2), is

$$x_a = x_b r_{11} c_\theta + y_b r_{21} s_{\theta\beta} + x_0 \quad ,$$
$$y_a = x_b r_{12} s_\theta + y_b r_{22} c_{\theta\beta} + y_0 \quad . \qquad (41a$$

The transformation parameters have been defined previously. With these transformations, any position in the overgrowth may be expressed in either global or lattice coordinates, and transformed to an equivalent position in terms of the substrate lattice.

For the bcc{110} overgrowth and fcc{111} substrate system considered here, the transformation parameters are given fully in Table 3.4 of the discussion of the rigid model in chapter 3 and may be summarized as:

$$x_0, y_0 = \tfrac{2}{3}, \tfrac{1}{3} \; ; \quad b_2 = 2b_{nn}/\sqrt{3} = b_1/\sqrt{2} \; ; \quad a_1 = a_2 = a_{nn} \qquad (41b$$
$$r_{11} = b_1/a_1 = \sqrt{8/3}r = r_{12} \; ; \quad r_{21} = b_2/a_1 = 2r/\sqrt{3} = r_{22}$$
$$c_\theta = 2\cos(30-\theta)/\sqrt{3} \; ; \quad s_\theta = 2\sin\theta/\sqrt{3}$$
$$s_{\theta\beta} = 2\sin(30-\theta)/\sqrt{3} \; ; \quad c_{\theta\beta} = 2\cos\theta/\sqrt{3} \quad .$$

The orientation angle, θ, is the angle between $\mathbf{b}_1$ and $\mathbf{a}_1$.

Misfit energy

The adatom-substrate potential formulation used in the rigid and homogeneous strain models is retained here. This potential is given as the Fourier expression:

$$V(\mathbf{r}_a) = \sum_{\{\mathbf{q}\}} V_{\mathbf{q}} \, e^{i\mathbf{q}\cdot\mathbf{r}_a} \quad . \qquad (42$$

The set, $\{\mathbf{q}\}$ comprises all reciprocal lattice translation vectors of the substrate lattice, while H normalizes the potential, and W is an energy calibration factor.

As described in Chapter 2, this general expression is simplified by the introduction of symmetry conditions, and truncated to a finite

series which sufficiently reproduces the required properties of the surface. Again, as in Chapter 4 with the homogeneous strain model, row-matching configurations of the bcc{110} overgrowth with first-order terms of the fcc{111} substrate only are studied. The potential series becomes: (Chapter 2 eqns 2.51)

$$\frac{V}{W} = H\Big\{(A_{00} + \Delta B_{00}) + A_{10}[\cos 2\pi x + \cos 2\pi(y-x) + \cos 2\pi y] + \\ + \Delta B_{10}[\sin 2\pi x + \sin 2\pi(y-x) - \sin 2\pi y]\Big\},$$

with $A_{10} = 1$, $B_{10} = \frac{\sqrt{3}}{2}$, $A_{00} = \frac{3}{2}$, $B_{00} = \frac{9}{4}$, and $H^{-1} = \frac{9}{2}(1+\frac{\Delta}{2})$. (43

Δ is the stacking fault parameter used earlier (Chapter 2 eqn 2.7 and section 2.3) and is again chosen as $\Delta = \frac{1}{2}$. Several values of W are used in keeping with a suitable choice of ℓ-values, specifically, systems with W = 0.4 eV, 0.9 eV, 1.5 eV ,3.0 eV and 6.0 eV were studied.

In order to calculate the misfit energy remaining after strain, this interaction potential is summed for all the overgrowth atoms, as displaced, expressed in terms of the substrate lattice coordinates. Hence the misfit energy per atom, between the strained overgrowth and the rigid substrate is:

$$\varepsilon_m = \frac{W}{G}\sum_{at=1}^{G} V(x_a^{at}, y_a^{at})/W \ . \qquad (44$$

Interfacial Forces

The force experienced by each interfacial atom is determined from the gradient of the adatom-substrate potential as seen in the absolute coordinates. These forces which act as point forces at the atom positions, are combined to form a body force field $\mathbf{p}(X^{at}, Y^{at})$ acting on the overgrowth island. From this field, the equivalent nodal loads are calculated and inserted into the equilibrium equations.

The force field which arises from these point forces may be represented as the delta-function distribution

$$\mathbf{p}(x,y) = \sum_{at=1}^{G} \delta(X^{at}-x)\delta(Y^{at}-y)\begin{bmatrix} -V_{,x}[x+u_x(x,y),y+u_y(x,y)] \\ -V_{,y}[x+u_x(x,y),y+u_y(x,y)] \end{bmatrix} , \qquad (45$$

where the derivatives of the potential are taken with respect to the global coordinate system, and u_x and u_y are the displacement components of the point x,y in the unstrained element.

The equivalent nodal loads are calculated from the principle of virtual work as invoked earlier, so that within the e'th element the contribution of the force field to the node "s" is

$$\mathbf{F}_s^e = \int_{\mathfrak{D}_e} \mathbf{N}_s^T \cdot \mathbf{p}\, d\mathfrak{D}_e = \sum_{\substack{\text{atoms} \\ \text{in e}}} \mathbf{N}_s(X^{at},Y^{at})^T \cdot \begin{bmatrix} -V_{,x} \\ -V_{,y} \end{bmatrix}_{x^{at},y^{at}} . \qquad (46$$

This means that while the interaction forces change, the shape function expressions $\mathbf{N}_s(X^{at},Y^{at})$ are pre-calculated as weight factors.

The forces are derived from the potential by partial differentiation in the global coordinates. Several transformations must be included, as the potential is most simply expressed in terms of the substrate coordinates. The Jacobians of the transformations are given as (from eqn 40)

$$J_{b,g} = \begin{bmatrix} \frac{\partial x_b}{\partial x} & \frac{\partial y_b}{\partial x} \\ \frac{\partial x_b}{\partial y} & \frac{\partial y_b}{\partial y} \end{bmatrix} = \begin{bmatrix} 1/b_1 & 0 \\ 0 & 1/b_2 \end{bmatrix} = \frac{1}{b_2}\begin{bmatrix} b_{21} & 0 \\ 0 & 1 \end{bmatrix} , \qquad (47a$$

with $b_{21} = b_2/b_1$ and (from eqn 41)

$$J_{a,b} = \begin{bmatrix} \frac{\partial x_a}{\partial x_b} & \frac{\partial y_a}{\partial x_b} \\ \frac{\partial x_a}{\partial y_b} & \frac{\partial y_a}{\partial y_b} \end{bmatrix} = \begin{bmatrix} r_{11}c_\theta & r_{12}s_\theta \\ r_{21}s_{\theta\beta} & r_{22}c_{\theta\beta} \end{bmatrix} . \qquad (47b$$

Here $J_{b,g}$ is the Jacobian of the transformation from global to lattice overgrowth coordinates, while $J_{a,b}$ relates the overgrowth lattice and substrate lattice coordinates. Hence

$$\begin{bmatrix} -V_{,x} \\ -V_{,y} \end{bmatrix} = J_{b,g} \cdot J_{a,b} \cdot \begin{bmatrix} -\frac{\partial}{\partial x_a} \\ -\frac{\partial}{\partial y_a} \end{bmatrix} V(x_a, y_a) . \qquad (47c$$

The overall substrate coordinates to global overgrowth coordinate transformation therefore has the Jacobian matrix

$$J_{a,g} = J_{b,g} J_{a,b} = \frac{1}{b_2} \begin{bmatrix} r_{11}c_\theta b_{21} & r_{12}s_\theta b_{21} \\ r_{21}s_{\theta\beta} & r_{22}c_{\theta\beta} \end{bmatrix} . \qquad (47d$$

Explicitly, the only quantity carrying a dimension, and dependent on absolute size is the inverse length $1/b_2$. This is the only scaling parameter, and hence $b_2 J_{a,g}$ is dimensionless.

The element nodal load matrix, obtained by combining the force contributions of all the atoms in the element to each of the nodes in a single column matrix $[\mathcal{F}_s]^e$ can be calculated once the substrate-adatom interaction potential has been explicitly differentiated with respect to the substrate lattice coordinates, i.e.

$$[\mathcal{F}_s]^e = \left[\sum_{\substack{\text{atoms} \\ \text{in e}}} \mathbf{N}_s^T(X^{at}, Y^{at}) \cdot J_{a,g} \cdot \begin{bmatrix} -V_{,x_a} \\ -V_{,y_a} \end{bmatrix}_{x_a^{at}, y_a^{at}} \right]$$

$$= \frac{W}{b_2} \left[\sum_{\substack{\text{atoms} \\ \text{in e}}} \mathbf{N}_s^T(X^{at}, Y^{at}) \cdot \{b_2 J_{a,g}\} \cdot \left\{ \frac{1}{W} \begin{bmatrix} -V_{,x_a} \\ -V_{,y_a} \end{bmatrix}_{x_a^{at}, y_a^{at}} \right\} \right]$$

$$= \frac{W}{b_2} [F_s^e] . \qquad (48$$

where $[F_s]^e$ is a column matrix of dimensionless force terms, since the potential terms, V/W are dimensionless.

Just as the element stiffness matrices have to be combined into a single overall (system) matrix, so the element nodal load matrices are assembled into a system nodal load matrix.

Explicit Potential gradient terms

Differentiation of the adatom-substrate potential in terms of the substrate lattice coordinates x_a, y_a is straightforward and yields the expressions: (See Chapter 2 eqn 2.52)

$$\frac{V_{,x_a}}{W} = 2\pi H\left\{-A_{10}[\sin 2\pi x - \sin 2\pi(y-x)] + \Delta B_{10}[\cos 2\pi x - \cos 2\pi(y-x)]\right\}$$

$$\frac{V_{,y_a}}{W} = 2\pi H\left\{-A_{10}[\sin 2\pi(y-x) + \sin 2\pi y] + \Delta B_{10}[\cos 2\pi(y-x) - \cos 2\pi y]\right\} \quad (49$$

with the same sine and cosine terms as in the original energy expression but with reversed rôles.

The calculation of the trigonometric functions is a relatively slow process in a digital computer. This re-use of the function values (when, as usual, both forces and energies are required) and the corresponding saving of computer time is the major reason why this sine formulation for the stacking fault terms is preferred to the displaced potential formulation which contains only cosine terms in the energy, and only sine terms in the forces. Both approaches are described in Chapter 2.

Elastic strain energy

The elastic strain energy density is (compare eqn 18)

$$w = \tfrac{1}{2}\,\sigma^T \cdot \varepsilon = \tfrac{1}{2}\,\varepsilon^T \cdot D \cdot \varepsilon \ , \quad (50$$

since $\mathbf{D}^T = \mathbf{D}$. Expressed in terms of the nodal values for a particular element e this becomes,

$$w^e = \tfrac{1}{2}\left\{\{[B_{s,}]\cdot[u^{s'}]\}^T\cdot\mathbf{D}\cdot[B_s]\cdot[u^s]\right\}^e \quad . \tag{51}$$

Integrating over the volume of the element, and summing over the L elements which make up the entire system and dividing by the number of atoms, G, yields the strain energy per atom as

$$\varepsilon_{el} = \frac{1}{2G}\sum_{e=1}^{L}\left\{[u^{s'}]^T\cdot[k_{s',s}]\cdot[u^s]\right\}^e \quad , \tag{52}$$

in terms of the element stiffness matrix $[k_{s',s}]^e$. Calculated from the dimensionless system matrices the elastic strain energy per atom is:

$$\begin{aligned}\varepsilon_{el} &= \frac{1}{2G}\frac{\mu}{(1-\nu)}t_e b_2^2\,[U_{S,}]^T\cdot[K_{S',S}]\cdot[U_S] \\ &= \frac{W}{\sqrt{2}}\frac{\ell^2 r^2}{G}\,[U_{S,}]^T\cdot[K_{S',S}]\cdot[U_S] \quad ,\end{aligned} \tag{53}$$

where, in the second equation, the volume per interfacial atom for the bcc{110} overgrowth has been included, and the energy expressed in terms of the configurational parameters.

5.6 SOLUTION OF THE EQUILIBRIUM EQUATIONS

The system equilibrium equations are solved numerically using an iteration procedure.

Firstly, the element stiffness matrices are set up and assembled to form the system stiffness matrices, in dimensionless form. Two matrices are produced, one with boundary conditions implemented, and one without. (The first is required in the solution of the equations and the second is used to calculate the strain energy.)

Then, the bounded stiffness matrix is decomposed into upper and lower triangular matrices and because the matrix is symmetric, only the lower triangular matrix is stored, and inverted.

The unbounded and inverted matrices are kept for the solution stages.

Once the particular epitaxial system has been chosen and all parameters specified, initial displacements are calculated, from an average strain consideration, either zero strain, or strain corresponding to the homogeneous strain model. The former corresponds to a model in which misfit accommodation is by local strain only - *viz.* misfit dislocations. The second type allows a mixture of misfit strain and misfit dislocations, as well as cases of pure misfit strain.

From these displacements, the atomic positions and hence the force matrix, with boundary conditions implemented, are calculated.

The equations are then solved for the nodal displacements.

From these displacements, the new positions of the atoms in the substrate coordinate system are calculated, and a new force matrix is constructed. Solution of the governing equations for the new forces leads to new displacements, and so on.

The solution is considered complete, once the changes in total interfacial energy calculated for successive steps has converged to a small enough value.

Because the forces change with displacement, frequently decreasing in fact, the displacements arising from a solution of linear equations at each step are generally too large, and simply iterating as outlined may cause overcorrection at some stage and result in oscillations. The solution technique includes several mechanisms to prevent oscillation and ensure a homogeneous approach to the final solution. These are technical matters described in the Appendix B.

5.7 PREDICTION OF MISFIT DISLOCATION STRUCTURES FROM THE RECIPROCAL LATTICE

Dislocation structures which arise from misfit occurring with or without the existence of misfit strain can also be predicted from the reciprocal lattice. Both in the presence or absence of homogeneous strain, misfit dislocations will be introduced whenever reciprocal lattice vectors in the overgrowth and substrate reciprocal lattices are close, but do not coincide. The more the reciprocal lattice vectors are separated, the closer the dislocations line becomes, and the reduced relaxation leads to a Misfit Vernier, rather than dislocations.

As originally suggested by Frank (1950), the misfit dislocations arise from elastic relaxation about points of lattice coincidence, referred to as Minimum Strain points. This concept has been extended by Bollmann (1970) to the general O-lattice, which allows coincidence points at non-lattice positions, or even coincidence lines or planes. The lattice coincidence occurs when the lattice spacings of overgrowth and substrate are rationally related, while Bollmann's O-lattice applies to the general, non-rational case. Naturally in the presence of *misfit strain*, these coincidence structures apply to the strained lattices. Relaxation occurs about the coincidence lattice arising from the misfit between the strained islands, as long as sufficient energy is available from the interaction between the two crystals to maintain the misfit strain. This is naturally an energy balance problem.

In the reciprocal lattice, structures which arise from the misfit of two lattices can be inferred directly. Whereas both Frank and Bollmann's approaches rely on the direct space, *with all the atoms treated simultaneously, the reciprocal space is a map of the periodicities and their mismatch.* An entire family of atomic rows (in two dimensions) is represented by a point in reciprocal space, as are planes of atoms in three dimensions. The coincidences of

these lines or planes likewise reduce to vector pairs when mapped in the reciprocal space.

Formulation of Misfit

Consider figure 5.7 *c*. Shown are the origins of the reciprocal spaces of the overgrowth and substrate, superimposed and in coincidence. Two vectors are shown, $\mathbf{q}_b$ in the overgrowth reciprocal lattice, and $\mathbf{q}_a$ in the substrate. With these vectors as shown, the two lattices do not match, and therefore the lattice rows perpendicular to each wave vector, with the spacing given by (Chapter 3 eqn 3.33)

$$\lambda_b = \frac{2\pi}{|\mathbf{q}_b|} \quad \text{and} \quad \lambda_a = \frac{2\pi}{|\mathbf{q}_a|} \quad , \qquad (54$$

are in misfit.

The (absolute) *misorientation* between these lattice rows is given by the angle θ, which is obtainable from the scalar product as

$$\cos\theta = \frac{\mathbf{q}_a \cdot \mathbf{q}_b}{|\mathbf{q}_a||\mathbf{q}_b|} \quad . \qquad (55$$

The sense is obtainable from the cross product of these vectors. (Refer to Chapter 3 eqn 3.39.)

Parallel Orientation

In *parallel* orientation, ($\theta = 0$), shown for example in figure 5.7 a, the misfit has conventionally been defined in any of three ways, either as (Chapter 3 eqn 3.38, also Chapter 1 section 1.5)

$$f_{ba} = \frac{\lambda_b - \lambda_a}{\lambda_a} \quad , \quad f_{ba} = \frac{\lambda_b - \lambda_a}{\lambda_b} \quad , \text{ or as } \quad f_{ba} = \frac{\lambda_b - \lambda_a}{\frac{1}{2}(\lambda_a + \lambda_b)} \qquad (56\ a\text{-}c$$

The first definition, introduced by Frank and Van der Merwe (1949), is conventionally used in the case of small misfit between a deformable monolayer overgrowth and rigid substrate.

Misfit Dislocations in Reciprocal Space

a) Edge b) Screw c) Mixed

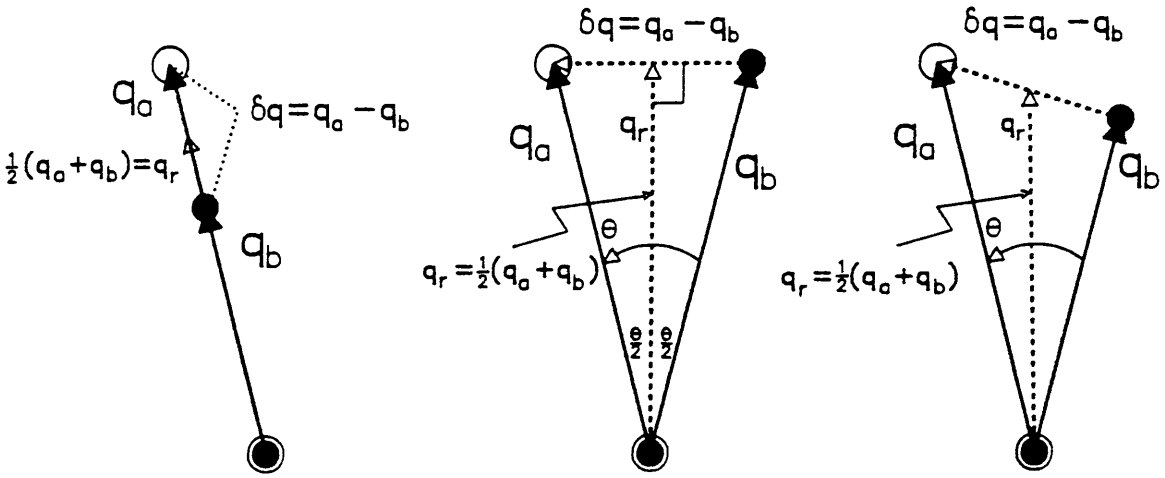

Figure 5.7 Misfit dislocations in reciprocal space.

Solid circles : overgrowth points
Open circles : substrate points

The second definition, used frequently by Matthews (see 1975, 1979) is convenient when both misfit strain and dislocations are present, again usually with a rigid substrate.

The third definition on the other hand, is usually applied to the more general case of equally thick overgrowth and substrate, where both overgrowth and substrate are assumed to be elastically deformable (Van der Merwe 1950, 1963, 1964, Van der Merwe *e.a.* 1975).

Each of the definitions in turn is associated with a natural choice of Burgers vector. In the first definition, the Burgers vector of the misfit dislocation is referred to the rigid substrate spacing, and will have a length λ_a and a direction parallel to the propagation vector of the lattice rows, $\mathbf{q}_a$.

Likewise, in the second definition, the length of the Burgers vector is λ_b, (as strained in the case of misfit strain), in the overgrowth, parallel to the propagation vector $\mathbf{q}_b$.

The third definition on the other hand relates the Burgers vector to a reference lattice with spacing

$$\lambda_r = [\tfrac{1}{2}(\frac{1}{\lambda_a} + \frac{1}{\lambda_b})]^{-1} = \frac{2\lambda_a\lambda_b}{\lambda_a+\lambda_b} , \qquad (57$$

the harmonic mean of the contributing spacings, or one-dimensional lattice parameters. The wave vector of the harmonic mean has the average of the wave vectors, namely

$$\frac{2\pi}{\lambda_r} = \tfrac{1}{2}(\frac{2\pi}{\lambda_a} + \frac{2\pi}{\lambda_b}) . \qquad (58$$

The vernier period of registry, the dislocation spacing, is then given by

$$P\lambda_a = (P+1)\lambda_b = (P+\tfrac{1}{2})\lambda_r , \qquad (59$$

for $\lambda_b < \lambda_a$, where P is an integer if the ratio of spacings λ_a/λ_b is rational. The misfit definition is obtained from the identity

$$\frac{\lambda_r}{P\lambda_a} = \frac{\lambda_b-\lambda_a}{\tfrac{1}{2}(\lambda_a+\lambda_b)} = f_{ab} . \qquad (60$$

The Burgers vector is the length of the harmonic mean, and is parallel to the mean propagation vector

$$\mathbf{q}_r = \tfrac{1}{2}(\mathbf{q}_a + \mathbf{q}_b). \qquad (61$$

To add to the possibilities, the quantity $(\lambda_b - \lambda_a)/\lambda_r$ may also have its uses as a measure of misfit.

Misfit defined in terms of the Reciprocal Lattice

The misfit accomodation, as such, is completely specified by the combination of reciprocal space vectors as presented in figure 5.7, or alternatively by the dislocation spacing (and direction), the Burgers vector, and the respective lattice parameters (and directions). As indicated below, the description of the Burgers vector in the general case of a twist-misfit boundary is most conveniently described in terms of the harmonic mean reference lattice, as was done by Jesser and Kuhlmann-Wilsdorf (1967*b*), although defined in the direct lattice by these authors. However, any of the measures of misfit are useful, as any one may be derived from any other, as long as the directions and lattice parameters are known.

While the above definitions are all useful for one-dimensional misfits, a single definition of misfit in a general case of differing structures is more difficult, as both spatial and angular misfits need to be defined. (See for example Van der Merwe 1980, Stoop *e.a.* 1982.) Clearly a general definition is obtained when both the misorientation, a measure of misfit, and the directions which do not match are given.

As the preceding discussion has been formulated in terms of the harmonic mean, or mean of the propagation vectors of the atomic rows, the extension to a general case is almost natural.

Beat Propagation vector

Referring to figure 5.7 once again, the misorientation between overgrowth and substrate in the reciprocal lattice directions $\mathbf{q}_a$ and $\mathbf{q}_b$ pertinent to the substrate and overgrowth respectively, is clearly the angle θ. The absolute (reciprocal) misfit vector may be defined as the vector

$$\delta\mathbf{q} = \mathbf{q}_b - \mathbf{q}_a \ , \qquad (62$$

from which the beat wavelength, which expresses this difference, may be calculated as

$$\lambda_D = \frac{2\pi}{|\delta\mathbf{q}|} = \frac{2\pi}{(\delta\mathbf{q}\cdot\delta\mathbf{q})^{\frac{1}{2}}} = \frac{2\pi}{[(\mathbf{q}_b-\mathbf{q}_a)\cdot(\mathbf{q}_b-\mathbf{q}_a)]^{\frac{1}{2}}}$$

$$= \frac{2\pi}{(q_b^2+q_a^2-2\mathbf{q}_b\cdot\mathbf{q}_a)^{\frac{1}{2}}} = \frac{1}{(\frac{1}{\lambda_a^2}+\frac{1}{\lambda_b^2}-\frac{2}{\lambda_a\lambda_b}\cos\theta)^{\frac{1}{2}}}$$

$$= \frac{\lambda_a\lambda_b}{(\lambda_b^2+\lambda_a^2-2\lambda_a\lambda_b\cos\theta)^{\frac{1}{2}}} \ . \qquad (63$$

These beats will be observed from vertically above in direct-space as straight-line Moiré fringes spaced with λ_D and perpendicular to the direction $\delta\mathbf{q}$. (See for example Bollmann 1970 ch 5, or Jesser 1973)

The Reference Lattice

The reciprocal lattice vectors $\mathbf{q}_a$ and $\mathbf{q}_b$ each define one-dimensional lattices with primitive direct lattice vectors $\mathbf{v}_a$ and $\mathbf{v}_b$ respectively. Each vector has a length given by the wavelength of $\mathbf{q}_a$ and $\mathbf{q}_b$ respectively, and points in the same directions. Thus

$$\mathbf{v}_a = \lambda_a\mathbf{q}_a/|\mathbf{q}_a| \text{ and } \mathbf{v}_b = \lambda_b\mathbf{q}_b/|\mathbf{q}_b| \ . \qquad (64$$

The accommodation of misfit is expressed in terms of a reference lattice defined as the harmonic mean of the lattice spacings in the directions of $\mathbf{q}_a$ and $\mathbf{q}_b$, as (eqn 61)

$$\mathbf{q}_r = \tfrac{1}{2}(\mathbf{q}_a+\mathbf{q}_b) \ . \qquad (61$$

This direction divides the misorientation angle θ into two angles. Both are equal to $\theta/2$ for a pure twist boundary, (figure 5.7 *b*), but are non-equal in general, as shown in figure 5.7 *c*.

Misfit Dislocation Lines

In terms of misfit dislocation theory, the spacing λ_D is in fact the spacing of misfit dislocation lines, with propagation direction given by the vector $\delta\mathbf{q}$, which is the wave vector of the plane waves which coincide with the dislocation lines.

In analogy with the identification between Miller indices of lattice planes and the reciprocal lattice translation vectors, (Ashcroft *e.a.* 1975, ch 5) the *intercepts* of the dislocation lines are integer multiples of the reciprocals of the components of the vector $\delta\mathbf{q}$ in the crystal coordinates. When $\delta\mathbf{q}$ is expressed in substrate reciprocal lattice coordinates as $[\delta q_1, \delta q_2]_a$, the dislocation lines occur at intercepts

$$(n/\delta q_1)\mathbf{a}_1 \text{ and } (n/\delta q_2)\mathbf{a}_2 \qquad (66a$$

respectively, where n is a positive or negative integer. Similarly, in the overgrowth lattice, with overgrowth reciprocal lattice coordinates $[\delta q_1, \delta q_2]_b$, the lines intercept at

$$(n/\delta q_1)\mathbf{b}_1 \text{ and } (n/\delta q_2)\mathbf{b}_2 \qquad (66b$$

along the $\mathbf{b}_1$ and $\mathbf{b}_2$ direct lattice basis directions. If the first dislocation line is displaced from the origin, naturally this displacement must be added to the intercepts.

The Line sense

The sense of the dislocation line is given by a vector lying in the line, perpendicular to the propagation vector. The direct lattice vector,

$$[\delta q_2 \quad -\delta q_1] \qquad (67$$

is such a vector, as is simple to confirm. (Compare Chapter 3 eqn 35.) This vector is a suitable sense vector.

Burgers vectors

The Burgers vector of the dislocation array follows from the harmonic mean, (Van der Merwe 1950, 1963, Jesser *e.a.* 1967 *b*, Jesser 1973), (eqn 57) as

$$\mathbf{B}_M = \frac{2\pi}{|\mathbf{q}_r|}\cdot\frac{\mathbf{q}_r}{|\mathbf{q}_r|} \quad . \tag{68}$$

(The magnitude of $|\mathbf{q}_r|$ is repeated to emphasize the fact that the magnitude of the Burgers vector follows from the first, while the second is used to generate a unit vector from $\mathbf{q}_r$.) The misfit dislocation arrays are (figure 5.7 *b*)

pure screw when

$$|\mathbf{q}_a| = |\mathbf{q}_b| \Rightarrow \mathbf{q}_r \perp \delta\mathbf{q} \tag{69a}$$

and (figure 5.7 *a*)

pure edge when

$$\mathbf{q}_a \parallel \mathbf{q}_b \Rightarrow \mathbf{q}_r \parallel \delta\mathbf{q} \quad . \tag{69b}$$

All other angular orientations provide misfit dislocations of mixed character. (figure 5.7 c)

The possible alternative choices of Burgers vectors, as substrate vectors of length λ_a parallel to $\mathbf{q}_a$ or overgrowth vector with length λ_b parallel to $\mathbf{q}_b$ do not have this simple relationship between screw and edge character, and both necessitate a partial pre-rotation of the Burgers vector, as is done by Bollmann (1970 ch 12, pp 148-154), (see also later), but in direct space. Naturally a mixed approach, in which the Burgers vector is described in either of the alternative ways, but the edge or screw character is determined from the harmonic mean $\mathbf{q}_r$ is quite useful, particularly for small misorientations where Frank's formula (the direct space formulation of the closure failure, see for example Jesser 1973, Bollmann 1970, Amelinckx, 1979 p420) is convenient.

Twist interfaces rotated through small angles will have only arrays of pure screw dislocations in the interface. Pure misfit interfaces have only misfit dislocations as there is no orientational misfit. These pure cases obviously occur when overgrowth and substrate share the same symmetry.

For general systems, among them *twist-misfit* boundaries or the interface between systems with different structures, orientations and lattice parameters, the general mixed interfacial dislocation arrays may be expected, as well as screw or edge dislocations for some special epitaxial orientations. This will be illustrated by the systems studied here, namely the bcc{110}/fcc{111} interface.

Comparison with Previously known definitions.

General Two-Dimensional Interface

Bollman(1970) (refer to Chapter 1 section 1.3) has studied the general interface problem in direct space, and has specifically used the set of all substrate lattice translation vectors (which he called *b*-space), as the possible Burgers vectors. This is equivalent to the special definition of the misfit in terms of the rigid substrate systems only. From the above discussion, the descriptions are compatible only at small misorientations, when the vector $\mathbf{q}_r \simeq \mathbf{q}_a$, from which Burgers vectors are obtained from the lattice spacing in the direction of $\mathbf{q}_a$. Alternatively, the screw or edge character must be determined independently by calculating the Burgers vector components by applying a rotation matrix compensating for the realignment during the attainment of matching, so that the Burgers vector components are given as

$$\begin{bmatrix} B_1 \\ B_2 \end{bmatrix} = [\mathbf{I}-\mathbf{A}^{-1}]\cdot\mathbf{X} = \begin{bmatrix} 1-\cos\theta & -\sin\theta \\ \sin\theta & 1-\cos\theta \end{bmatrix}\cdot\begin{bmatrix} X_1 \\ X_2 \end{bmatrix}, \qquad (70$$

where $\mathbf{I}$ is the unit matrix and $\mathbf{A}$ is the matrix with which the overgrowth can be generated from the substrate, (rotation only in this special but illustrative case). Here X_1 and X_2 are components of a vector in the overgrowth *direct* lattice which is brought to coincidence with the substrate direct lattice vector with components B_1 and B_2 both expressed in an appropriate cartesian coordinate system. This form of the formula is applicable to a pure twist boundary, but illustrates the complication.

This is also compatible with the definition of misfit in this case as (eqn 56a)

$$f_{ba} = \frac{\lambda_b - \lambda_a}{\lambda_a} \quad ,$$

in a coinciding overgrowth and substrate (pure misfit) direction.

Twist-Misfit Interface

Jesser and Kuhlmann-Wilsdorf (1967*b*) have discussed the geometry of the general *twist-misfit* interface, and gave a direct-space treatment of this interface which is the equivalent of the reciprocal space treatment given here. The geometry in direct space is however extremely difficult to manipulate for all but the special cases discussed by them, where one of the directions of match coincides with a primitive (or in fact cubic) lattice direction. For this case they define the reference lattice spacing with associated Burgers vector magnitude

$$B_M = \frac{2ab}{a+b} \quad , \qquad (71$$

following Van der Merwe (1950, 1963, 1964) and Jesser and Kuhlmann-Wilsdorf (1967*a*). That this Burgers vector in fact coincides with the definition given here can be demonstrated:

Suppose that there is *no misorientation* between the directions $\mathbf{q}_a$ and $\mathbf{q}_b$, i.e. $\mathbf{q}_a \| \mathbf{q}_b$. Then the magnitude of $\mathbf{q}_r$ is

$$q_r = |\mathbf{q}_r| = |\tfrac{1}{2}(\mathbf{q}_a + \mathbf{q}_b)| = 2\pi\tfrac{1}{2}\left(\frac{1}{\lambda_a} + \frac{1}{\lambda_b}\right) = 2\pi\frac{\lambda_a + \lambda_b}{2\lambda_a\lambda_b} \quad . \qquad (72$$

The magnitude of the Burgers vector is then

$$B_M = \frac{2\pi}{|\mathbf{q}_r|} = \frac{2\lambda_a\lambda_b}{\lambda_a + \lambda_b} \quad . \qquad (73$$

This is exactly the same expression as the special one above (eqn 68), when the simple cubic, or closest packed directions are in misfit, and $\lambda_a = a$ and $\lambda_b = b$.

The spacing of the misfit dislocations is given by Jesser and Kuhlmann-Wilsdorf (1967*b*) as

$$\frac{\lambda_a \lambda_b}{(\lambda_a^2 + \lambda_b^2 - 2\lambda_a \lambda_b \cos\theta)^{\frac{1}{2}}} ,$$

which is the wavelength λ_D of the absolute misfit vector $\delta\mathbf{q}$ (eqn 63). In the special cases treated by Jesser and Kuhlmann-Wilsdorf in which two perpendicular arrays of screw or edge misfit dislocations occurred, it was true that one set of dislocation lines is perpendicular to the direct space closure failure ($\mathbf{v}_b - \mathbf{v}_a$), of equivalent vectors, when one was a cubic direction. However this is not general, as follows from the propagation direction $\delta\mathbf{q}$, and the discussion by Jesser (1973).

Jesser (1973) has realized the advantage of describing the Moiré patterns achieved in misfitting systems in reciprocal space, and in fact has identified these with *possible* dislocation arrays (Jesser p71), while Bollmann(1970) has identified them with dislocations directly, subject to a suitable choice of the transformation matrix $\mathbf{A}$. Analyzed in direct space however, the uniqueness of the accommodation of misfit resulting from *nearby* overgrowth and substrate reciprocal lattice points was not previously possible. In fact the development given in Chapter 3 of the Van der Merwe-Reiss rigid model, together with the work of Fletcher and co-workers (Fletcher *e.a.* 1975) and Novaco and McTague (1977) have provided the energetic basis for this identification in *reciprocal* space.

All the dislocation arrays predicted in this fashion may be expected to occur whenever it is energetically favourable for the lattices to relax elastically. Where relaxation is insignificant, as in the case of very large misfits where the 'dislocation' spacing is of the order of a single lattice spacing, the misfit accommodation will occur as a *Misfit Vernier*, again with the same parameters as defined for the dislocation arrays. Clearly nearby wave vectors of very high but different order, will give rise to the *Coincidence Dislocation* arrays described by Matthews (1975).

Thick systems and the discussion of stepped and general grain boundaries require a consideration of the full three-dimensional structure of the reciprocal lattices, instead of just the two-dimensional section applicable for thin films. It may be expected that Burgers vectors (see Matthews 1975 and references therein) not in the interfacial plane can then be derived from the reciprocal space.

5.8 RESULTS

Several systems with bcc{110} islands on fcc{111} substrates characterized by interfacial potential amplitude W which ranged from 0.1 eV to 6eV were studied. The systems with the nearest neighbour ratios ranging in 10 nearly equal steps from 0.9 to 1.08 in the two orientation angles coinciding with the ideal Nishiyama-Wassermann and Kurdjumov-Sachs configurations were examined. All these cases were treated with the elastic constants of Table 4.2 in Chapter 4, for the anisotropy ratios ½, 1 and 5.

The systems were first allowed to reduce their misfit energy by homogeneous strain alone, as described in Chapter 4. The energy reduction was calculated by direct numerical minimization of the total interfacial energy subject to the homogeneous strains ε_x , ε_y and γ_{xy} without allowing rigid body rotation as a whole. This means that the strains recorded in Chapter 4, Table 4.4 were used as the misfit strain energetically favoured by the overgrowths.

The finite element formulation was then applied and the island was allowed a further reduction in interfacial energy by the local relaxation of the overgrowth. Because of the periodic distribution of "Minimum Strain" or O-Lattice points the local strain fields may be expected to be repeated periodically in an infinite monolayer, but this periodicity will be to some extent obscured by the finite island. The island is finite of necessity in the formulation used here as the positional coordinates of each node are free, subject to necessary boundary conditions. Other methods such as Boundary

element techniques with periodic boundary conditions could possibly allow the numerical description of infinite systems.

The islands in every case were discretized into 25X25 Finite element nodes, with finite elements of the biquadratic Lagrange type described in this Chapter. With the interpolation scheme and boundary conditions described here, this meant 1105 atoms in the island, with initially 1250 degrees of freedom, before the inclusion of the boundary conditions.

As before the substrate is assumed rigid.

The results are presented in two ways.

Firstly the energy behaviour is shown in figures 5.8, 9 and 10, for the various anisotropy ratios. The reduction of total interfacial energy with relaxation is evident in the diagrams.

Secondly the interfacial structure after relaxation is shown directly in figure 5.11 as the atom positions are plotted. Four different symbols are used to describe the relationship of the substrate to the overgrowth:

up triangles indicate atoms in the minimum potential energy position of the substrate, while

down triangles (although not appearing in in *these* diagrams) indicate atoms in the secondary, stacking fault position. With the stacking fault parameter $\Delta = 0.5$, these are rare for strong adatom-substrate bonding as determined by W.

Maximum potential energy positions are indicated with a solid circle, and

intermediate positions with *small dots*.

(Necessarily a tolerance was included in the allocation of the symbols, and atoms needed to be located within 1/6 diagonal distance from the maximum or minimum, otherwise they were assumed at a saddle point.)

This representation has much in common to that of Snyman and Snyman (1981) who studied the interface between two hexagonal nets, fcc{111} overgrowth and substrate, using finite difference methods, although they used circles only.

Reciprocal lattice predictions are summarized in Table 5.5 for the systems with interesting (non-pseudomorphic or 2DC) interfacial structures. These correspond particularly to W = 0.4eV, and the misfit strains are those which were summarized in Table 4.4 of the homogeneous strain numerical minimization of Chapter 4.

Table 5.5 lists the wave vectors, each representing a family of atomic rows, which are misoriented or have different spacings, but are close enough to form misfit dislocations, rather than a misfit vernier. (The spacing is more than just one or two wavelengths.) Also only the lowest order wave vectors are considered in this fashion, primarily because the only substrate potential terms included in the interfacial interaction were of low order. Interestingly, the case $r=r_{KS}$ and $\theta=30^{\circ}=\theta_{NW}$, A=5, in fact matches in a high order mode in the Nishiyama-Wassermann angle, as can be seen in the reciprocal space maps of fig 5.12. This system's interfacial structure is particularly rich, and difficult to interpret without the reciprocal space description.

The dislocation lines are described in several ways, but primarily in the (strained) overgrowth crystal coordinates, as this is suitable for interpretation of the interface maps. The spacing is expressed as a multiple of the nearest neighbour distance (as strained), which can be scaled to the interface maps as 1/48 of the entire diagonal. The lines themselves are given by their intersections $1/\delta q_1$ and $1/\delta q_2$ (eqn 66) in terms of the crystal coordinates $\mathbf{b}_1$ and $\mathbf{b}_2$ respectively. Also listed are the components of a vector oriented parallel to the dislocation lines. Forms of representation not listed can be calculated from the transformations of Appendix A, (A1,A2) after first calculating the strained unit cell parameters, as described in Chapter 4 and also listed in the Appendix A (A22-23).

The Burgers vectors associated with the misfit dislocations are also listed. These Burgers vectors are the substrate vectors, and not the reference lattice vectors, as these are suitable for systems with a rigid substrate and small misfits or small misorientations, the cases considered here. The error is small for small angles, as attested to by the success of Frank's formula, which itself does not differentiate between the Burgers vector choices.

The agreement between the predictions of the reciprocal lattice deliberations is excellent, as may be seen by comparing the reciprocal lattice plots of figure 5.12 with the interfacial maps of figure 5.11. Careful examination of the figure 5.11 from rather oblique angles (Directions are indicated in some of the representative diagrams) shows the interfacial screw arrays in the systems such as $r=r_{KS}$, $\theta=\theta_{NW}$, A=1 or 5. The variation between up-triangles and dots seen from above indicate the edge arrays, in systems such as the $r=r_{NW}$, $\theta=\theta_{NW}$ cases. Systems with intersecting screw and edge dislocation arrays of low order show interactions resulting in extended dislocation nodes which appear as groupings of solid circles or dots. These are particularly noticeable in the $r=r_{NW}$, $\theta=\theta_{KS}$ case, which is rich on misfit verniers, and therefore little relaxation to reduce the size of the bad fit regions occurs.

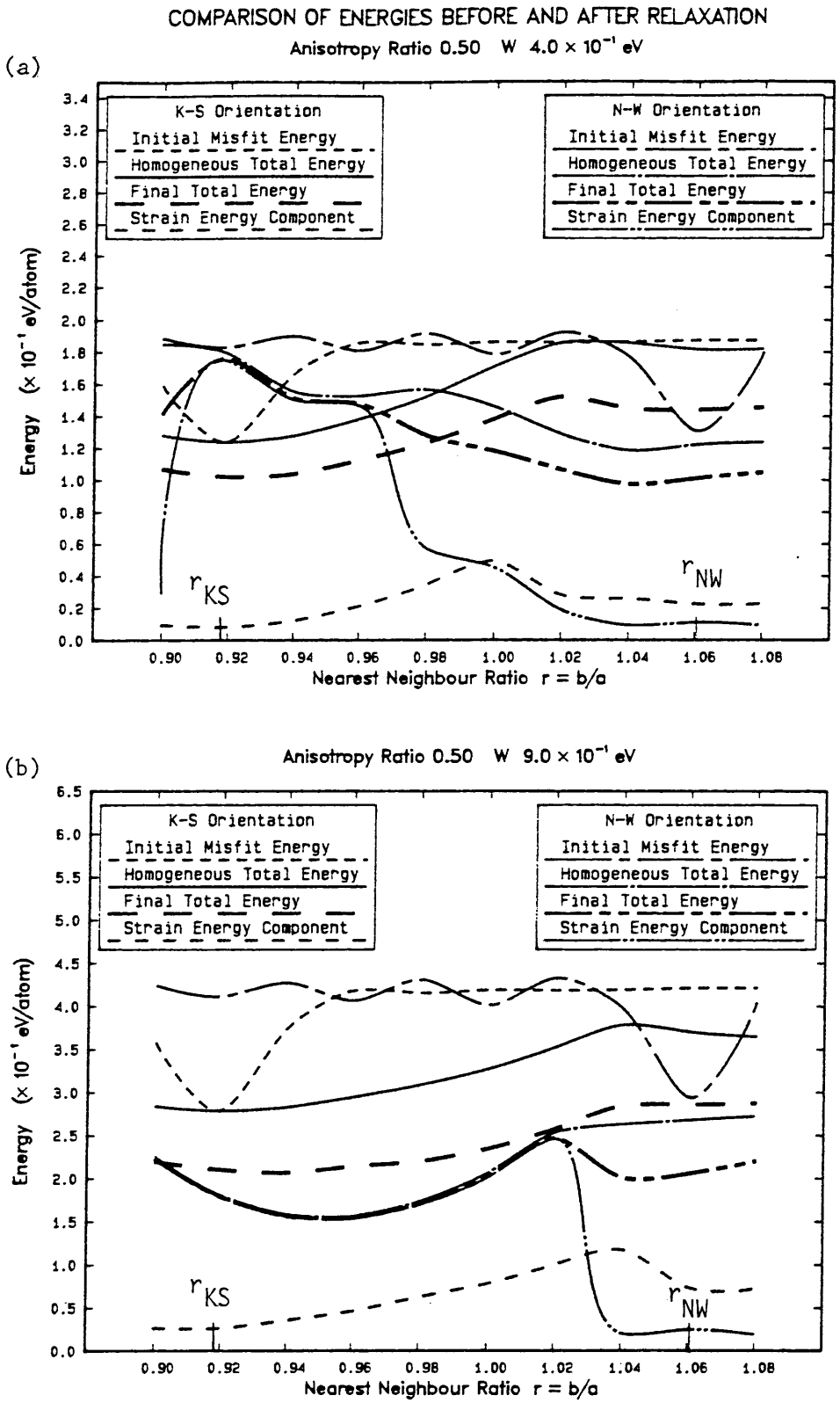

Figure 5.8 Energy diagrams with A = $\frac{1}{2}$

(a) W = 0.4 eV
(b) W = 0.9 eV

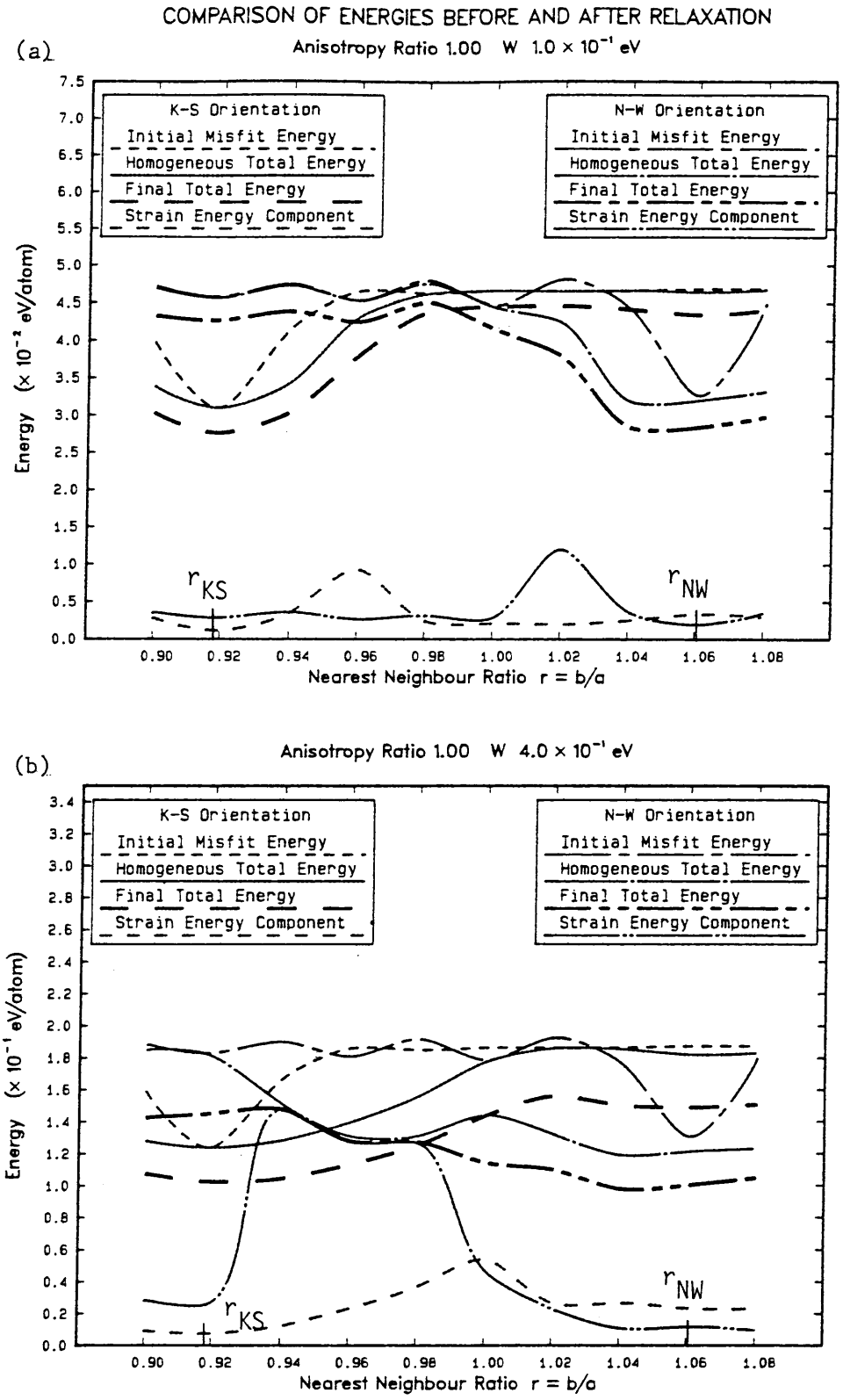

Figure 5.9 Energy diagrams for an isotropic overgrowth, A = 1

(a) W = 0.1 eV
(b) W = 0.4 eV

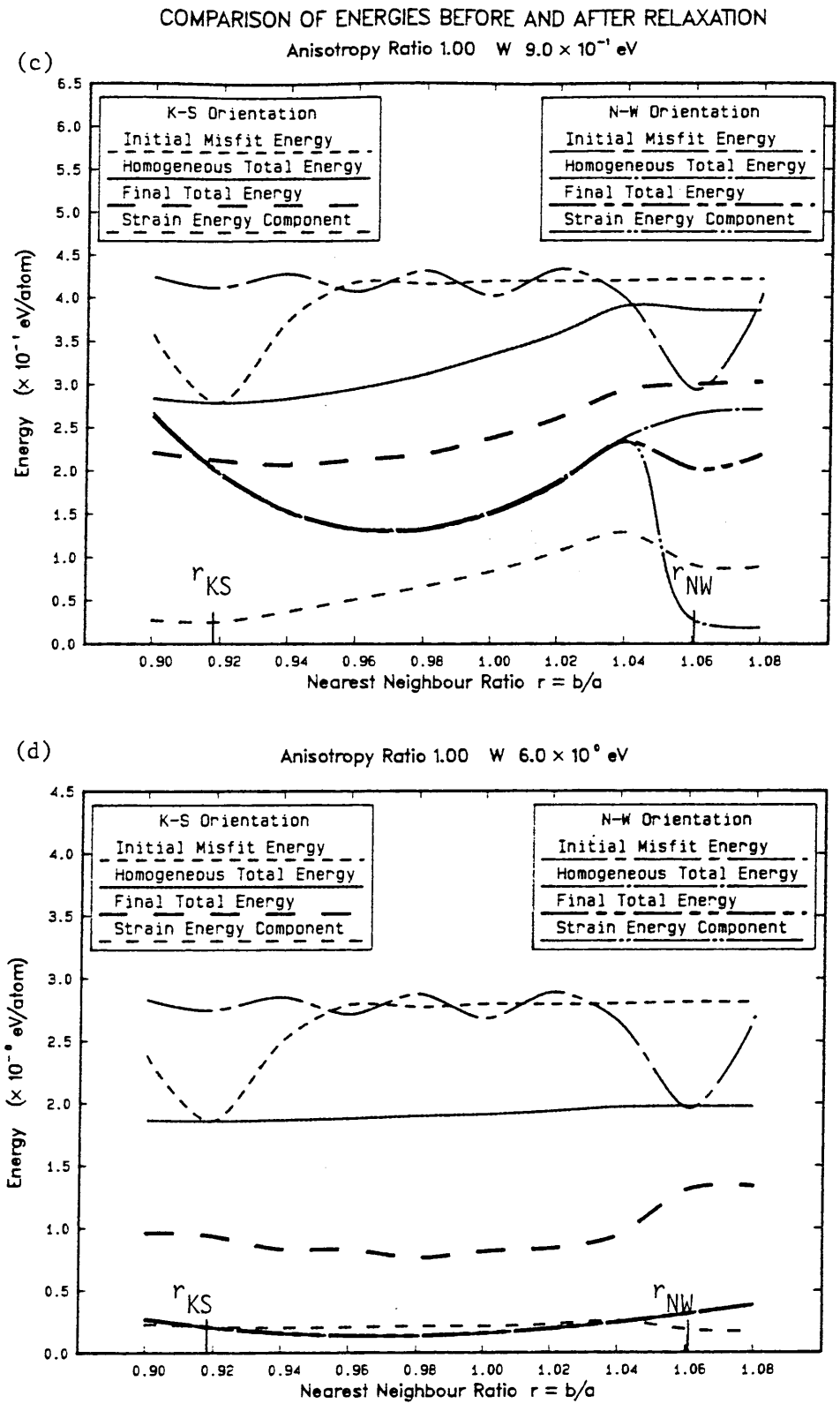

Figure 5.9 Continued. Energy diagrams for an isotropic overgrowth
A = 1

(c) W = 0.9 eV
(d) W = 6 eV

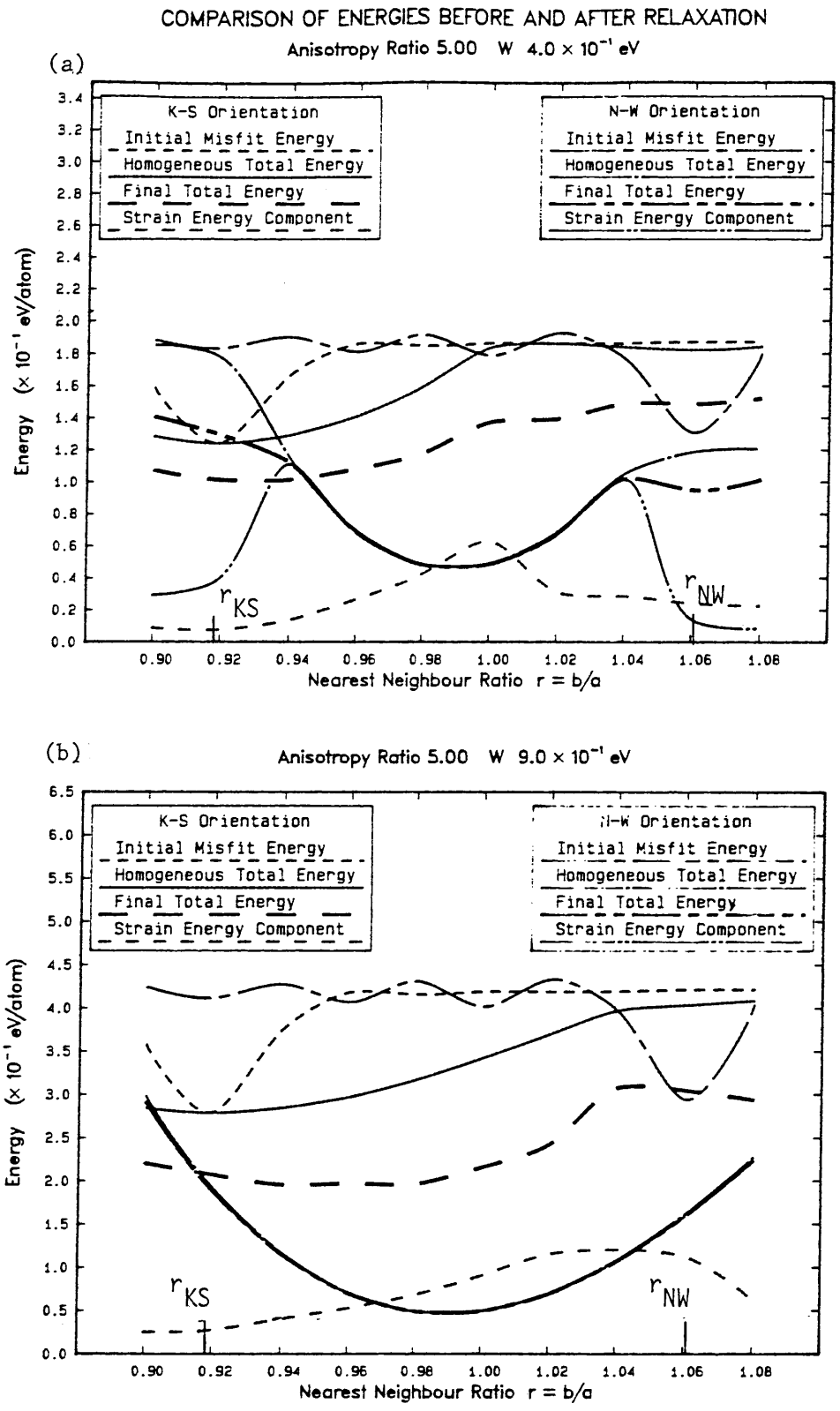

Figure 5.10 Energy diagrams with A = 5

(a) W = 0.4 eV
(b) W = 0.9 eV

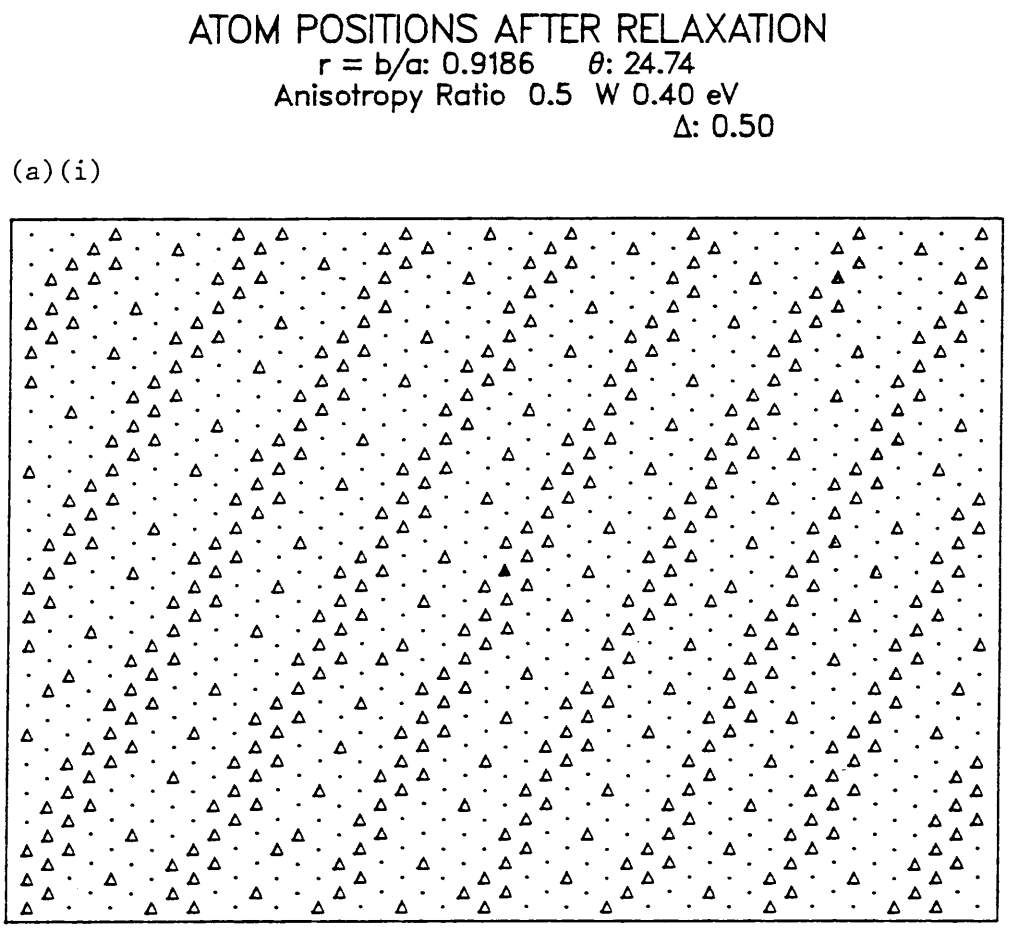

Figure 5.11 Positions of the atoms in the interface after local relaxation calculated with the finite element method. Where applicable, annotation indicates dislocation lines, the numbers are the same as in Table 5.5.
Optimal viewing directions are discussed in the text.

Up triangles : ideal lattice positions
Down triangles : stacking fault position
Solid circle : maximum misfit position
Dots : intermediate (saddle) position
Solid up triangle : indicates the central atom

Figure 5.11(a)(i) Ideal Kurdjumov-Sachs W = 0.4 eV A = ½

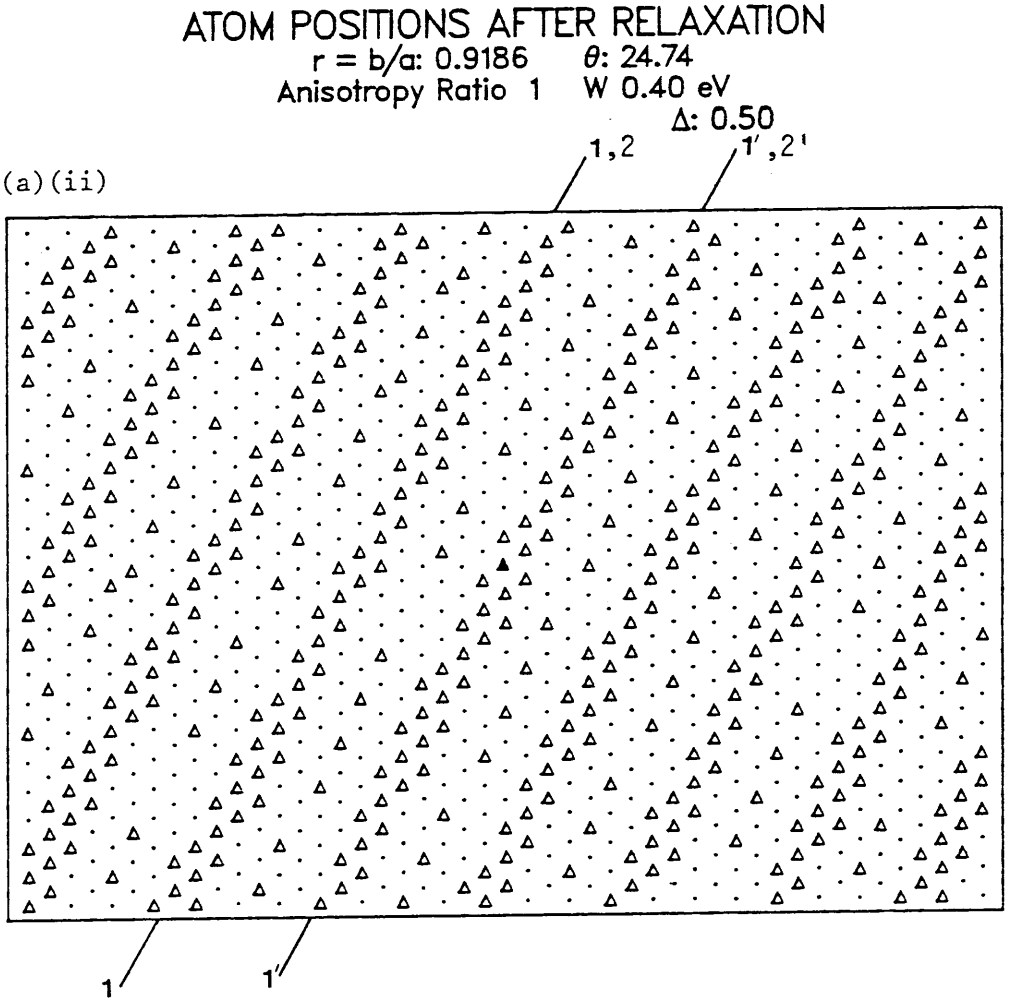

Figure 5.11(a)(ii) Ideal Kurdjumov-Sachs W = 0.4 eV A = 1

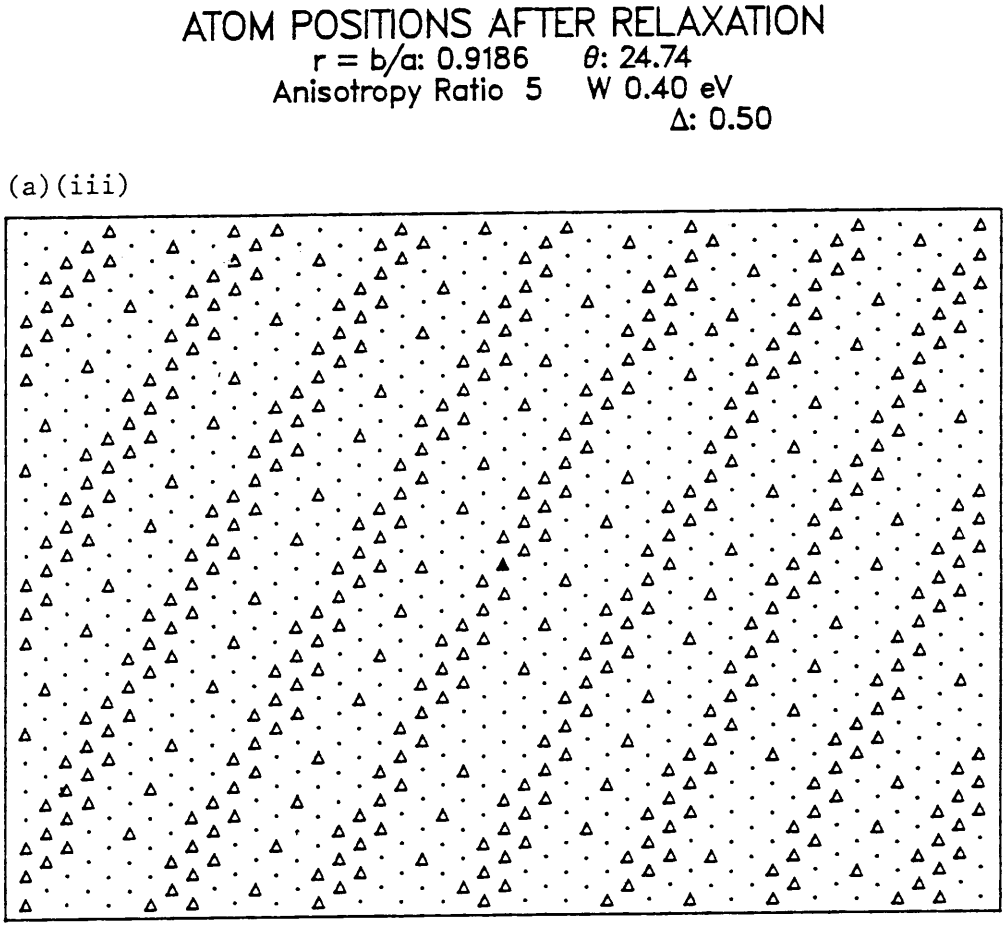

(a)(iii)

Figure 5.11(a)(iii) Ideal Kurdjumov-Sachs W = 0.4 eV A = 5

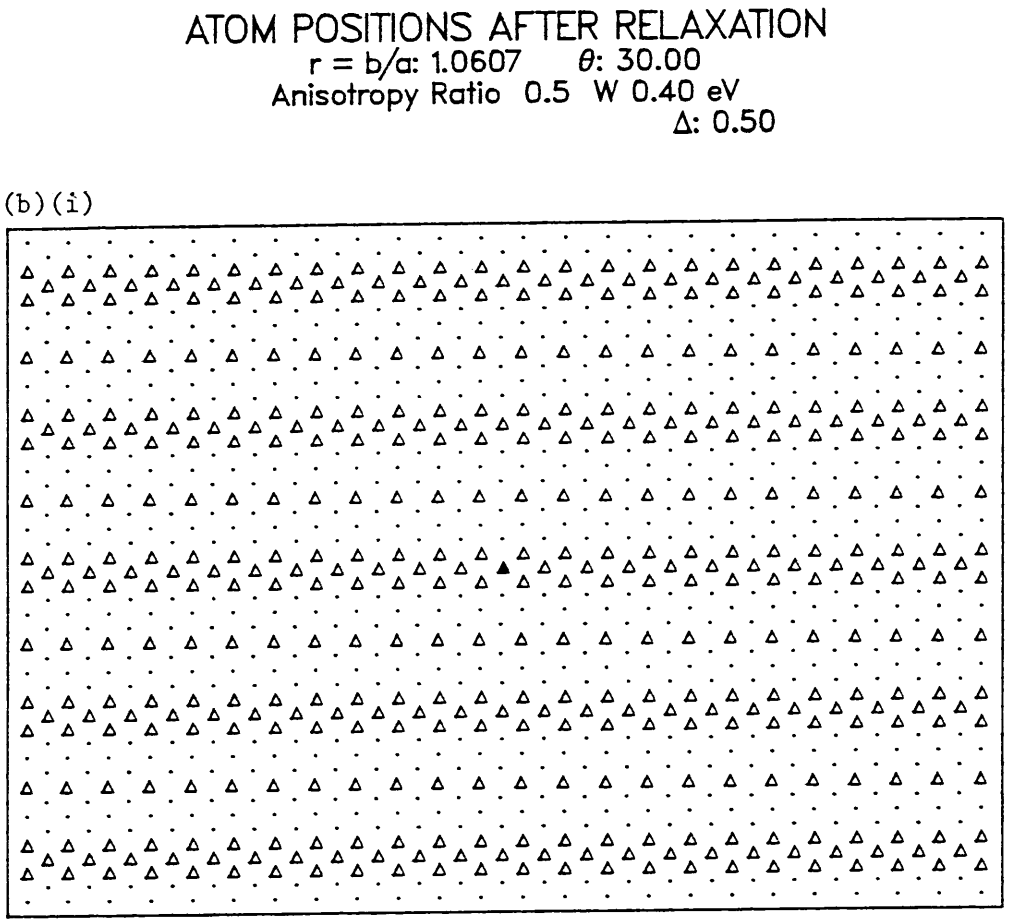

(b)(i)

Figure 5.11(b)(i) Ideal Nishiyama-Wassermann W = 0.4 eV A = $\frac{1}{2}$

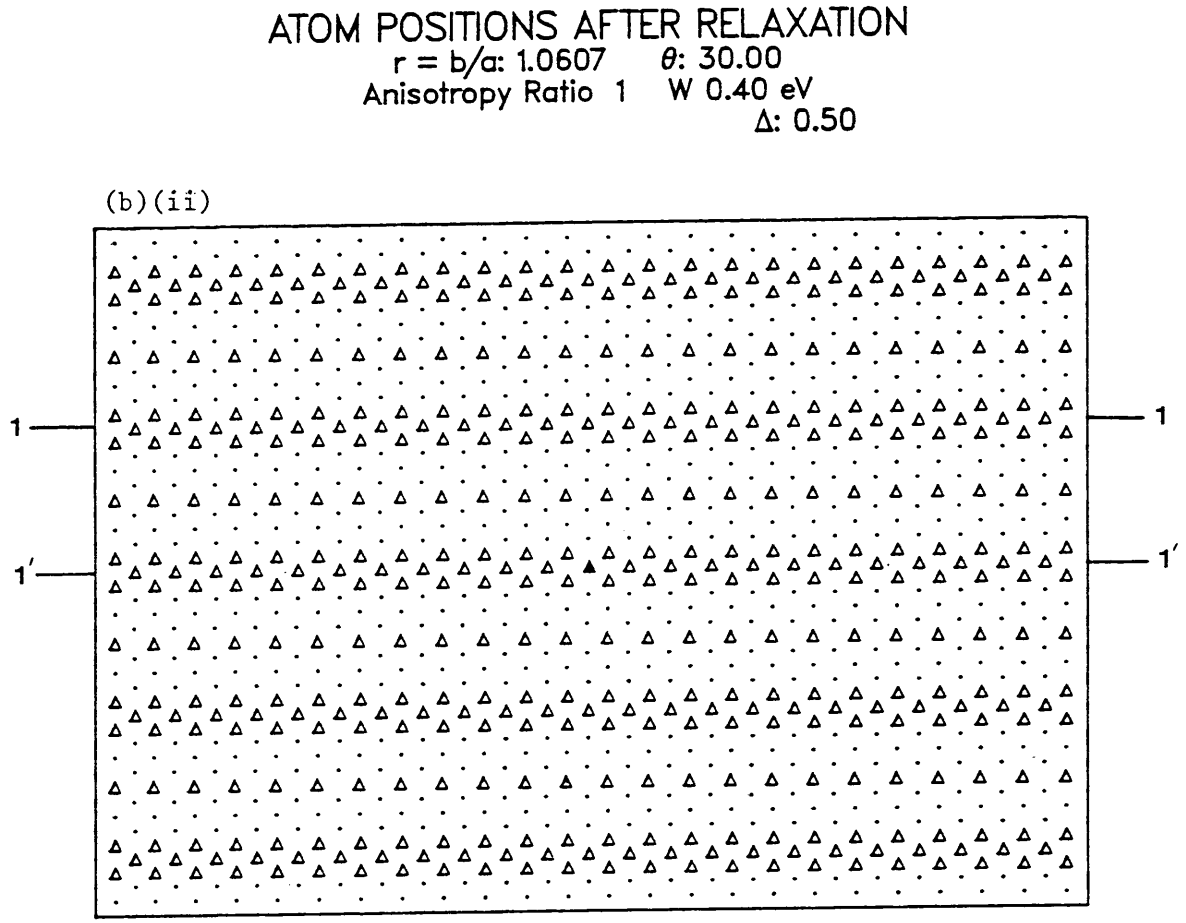

Figure 5.11(b)(ii) Ideal Nishiyama-Wassermann W = 0.4 eV A = 1

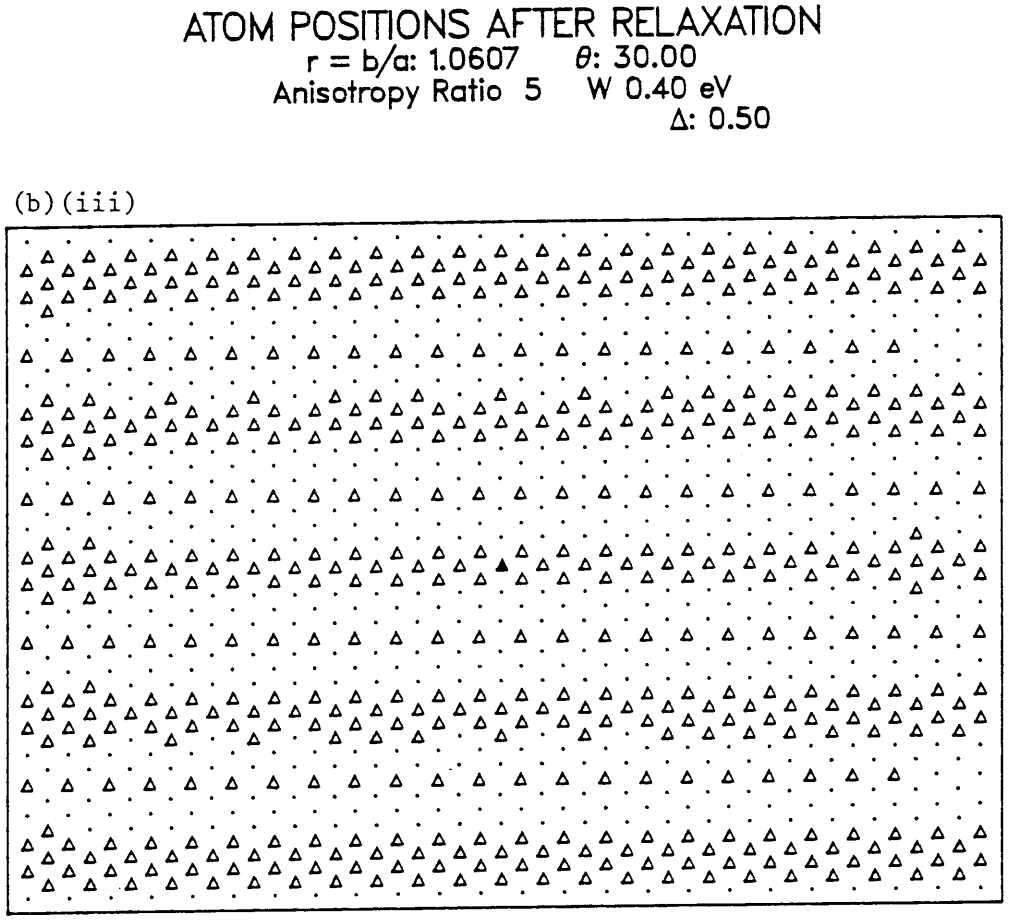

(b)(iii)

Figure 5.11(b)(iii) Ideal Nishiyama-Wassermann W = 0.4 eV A = 5

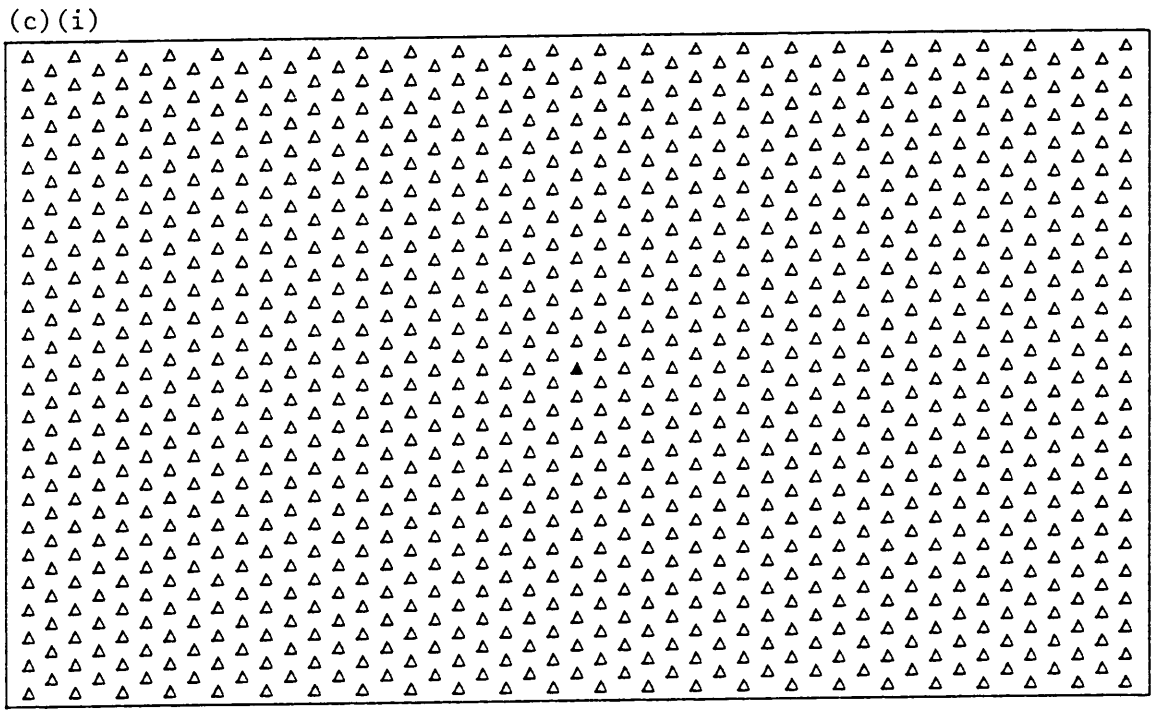

Figure 5.11(c)(i) Extreme Nishiyama-Wassermann W = 0 .4 eV A = $\frac{1}{2}$

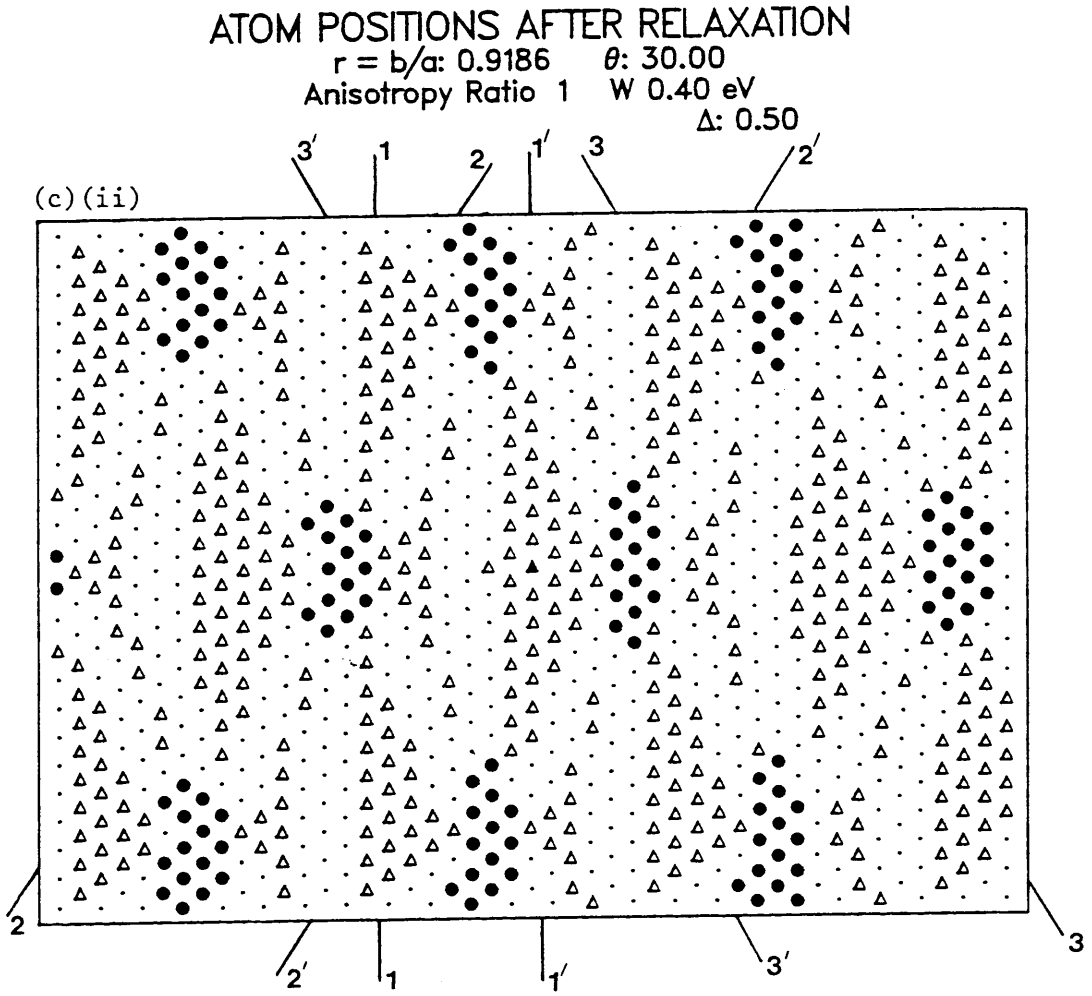

Figure 5.11(c)(ii) Extreme Nishiyama-Wassermann W = 0.4 eV A = 1

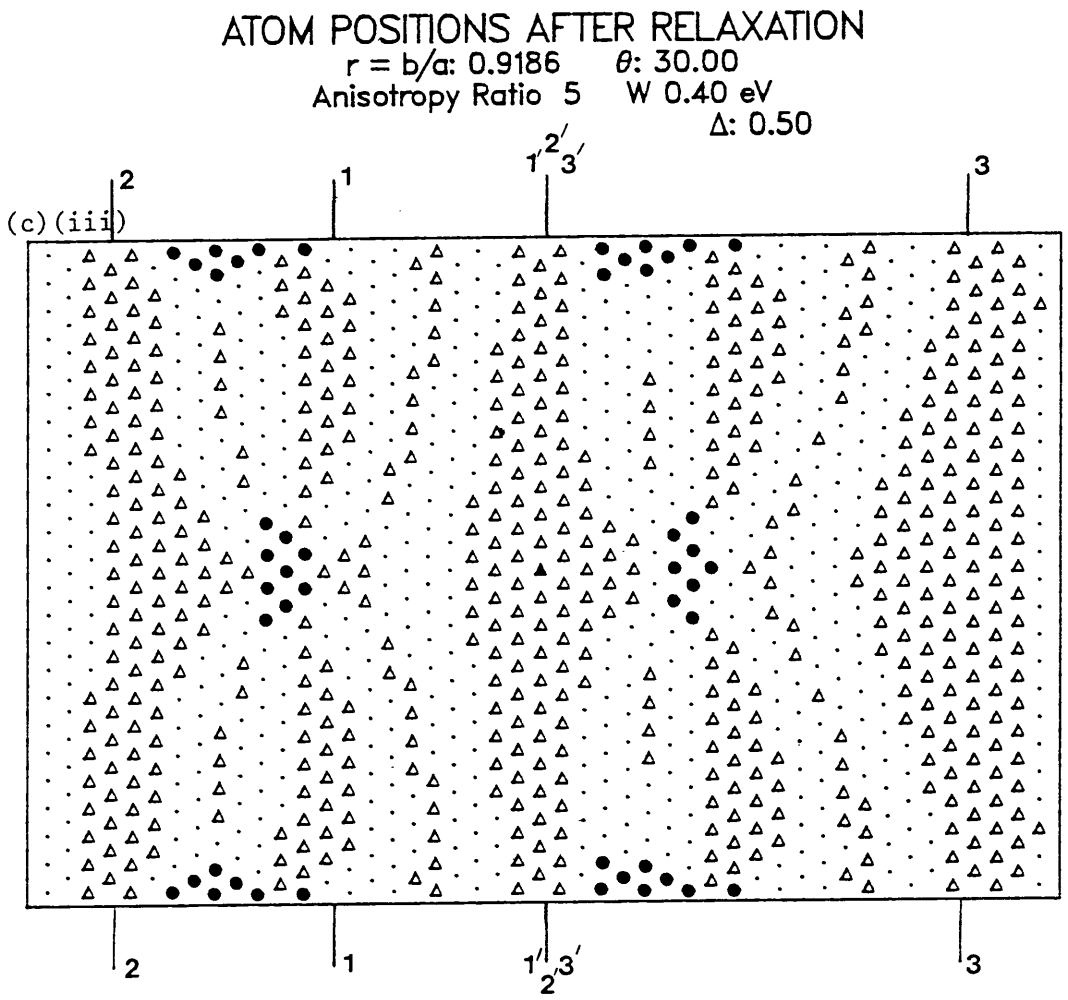

Figure 5.11(c)(iii) Extreme Nishiyama-Wassermann W = 0.4 eV A = 5

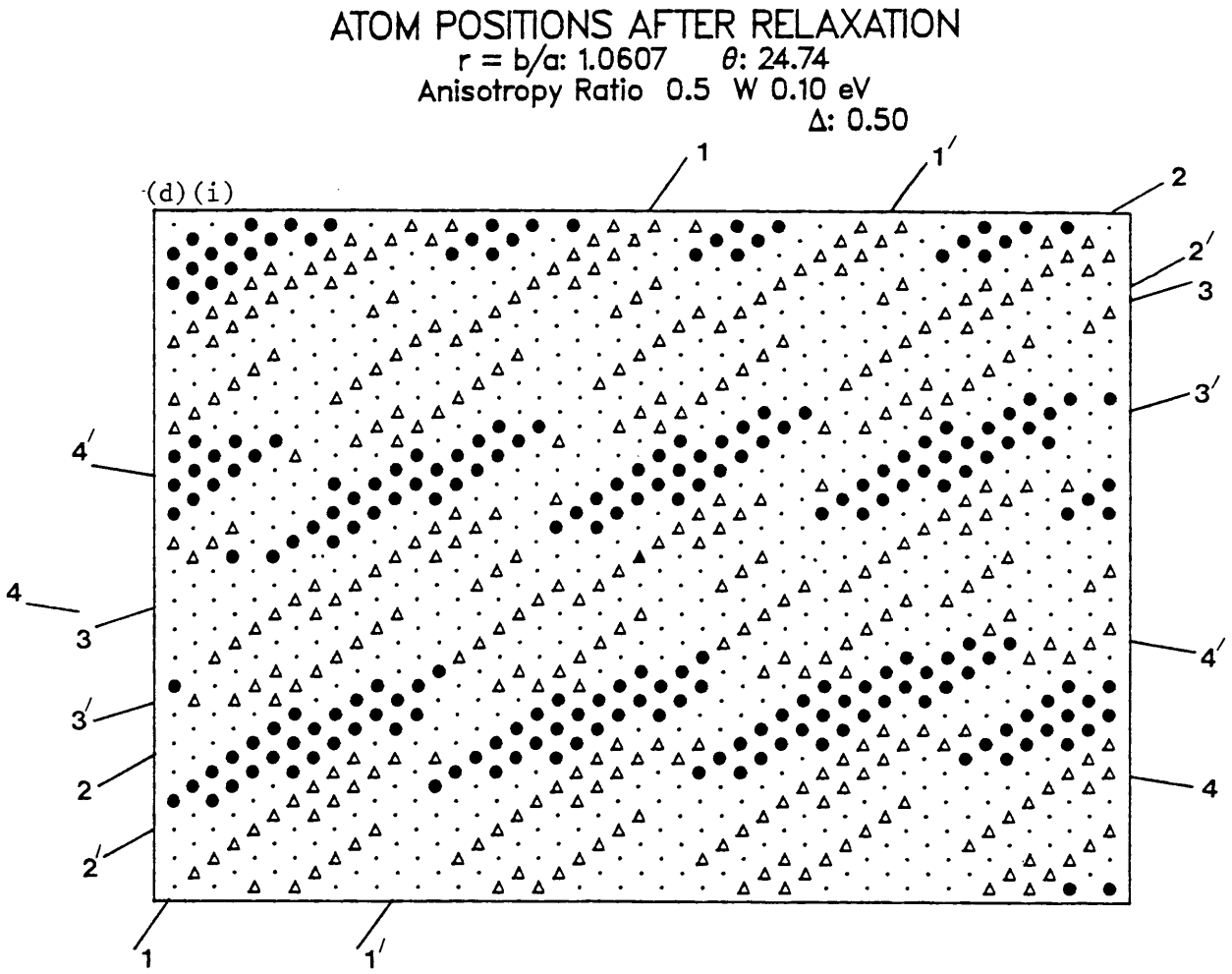

Figure 5.11(d)(i) Extreme Kurdjumov-Sachs W = 0.4 eV A = $\frac{1}{2}$

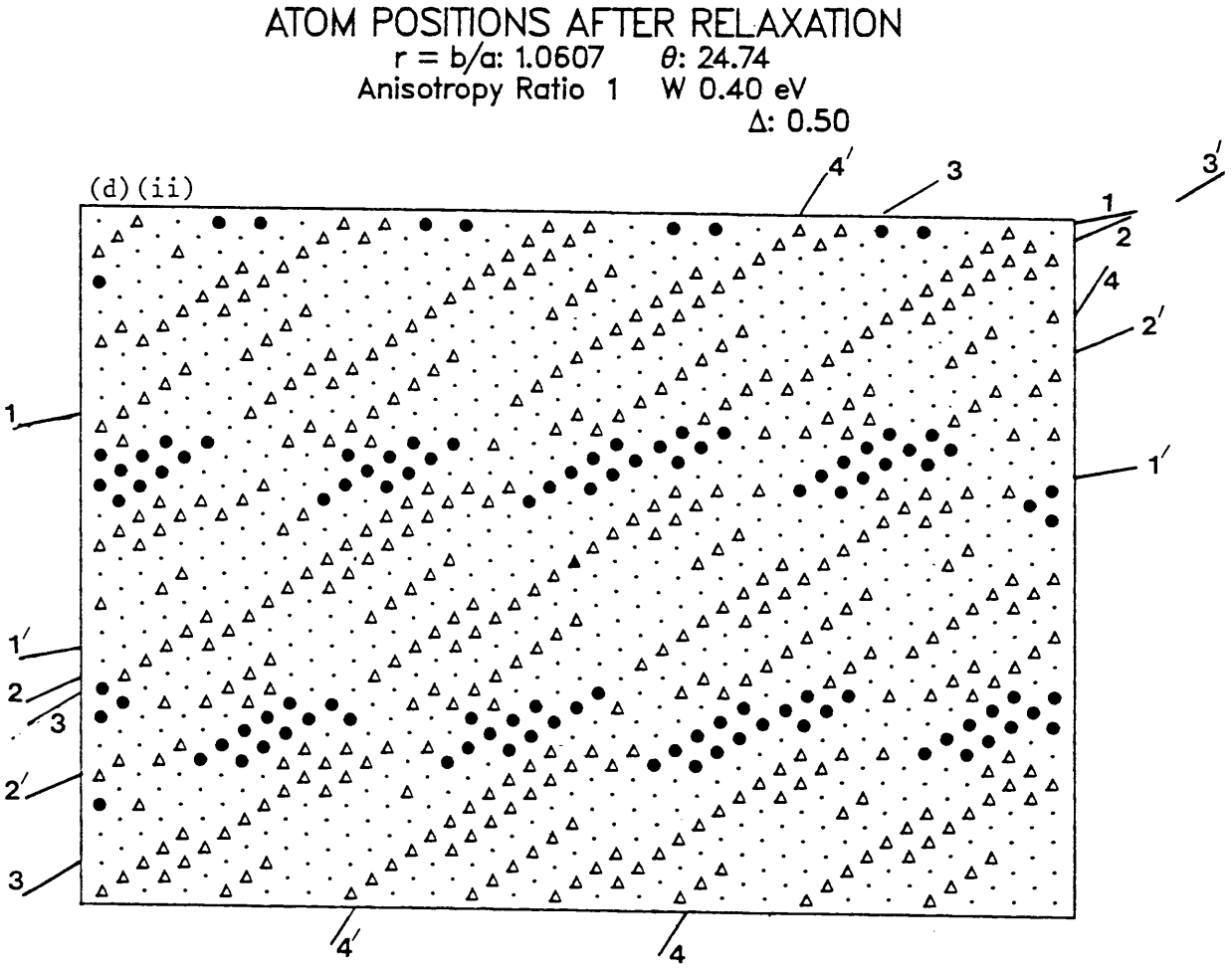

Figure 5.11(d)(ii) Extreme Kurdjumov-Sachs W = 0.4 eV A = 1

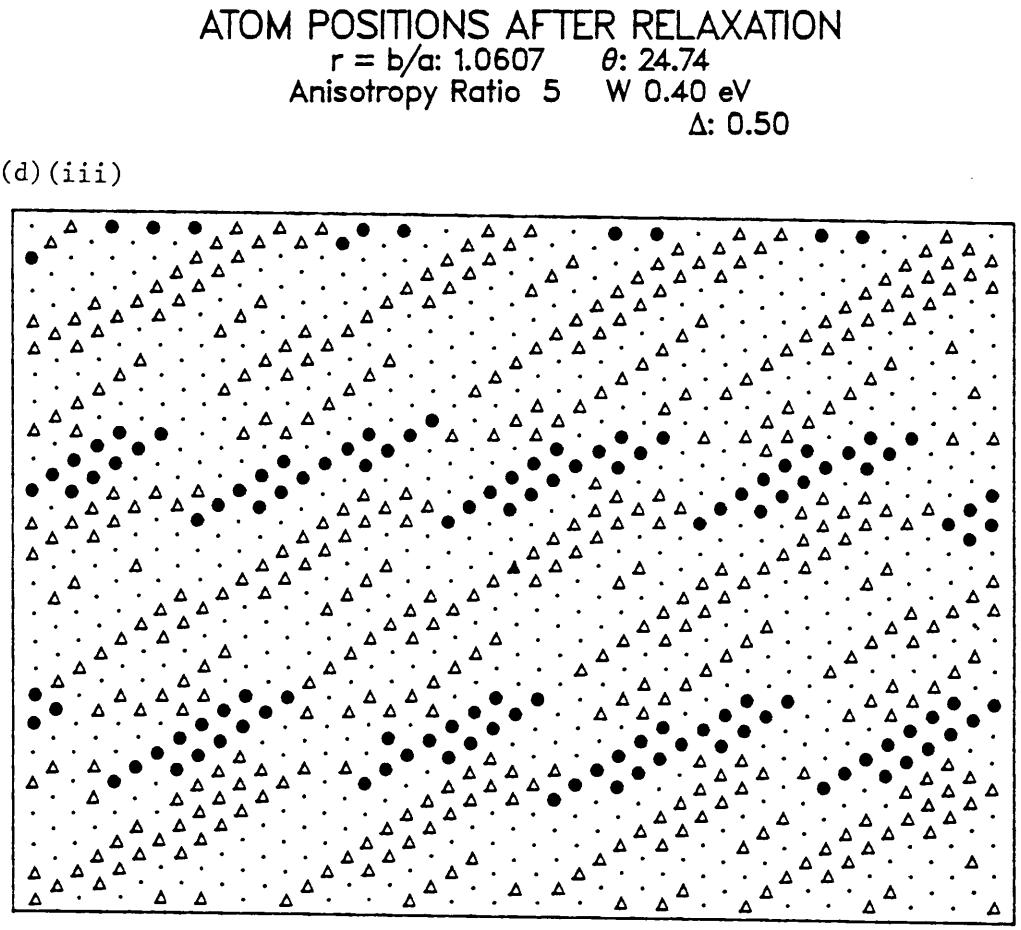

(d)(iii)

Figure 5.11(d)(iii) Extreme Kurdjumov-Sachs W = 0.4 eV A = 5

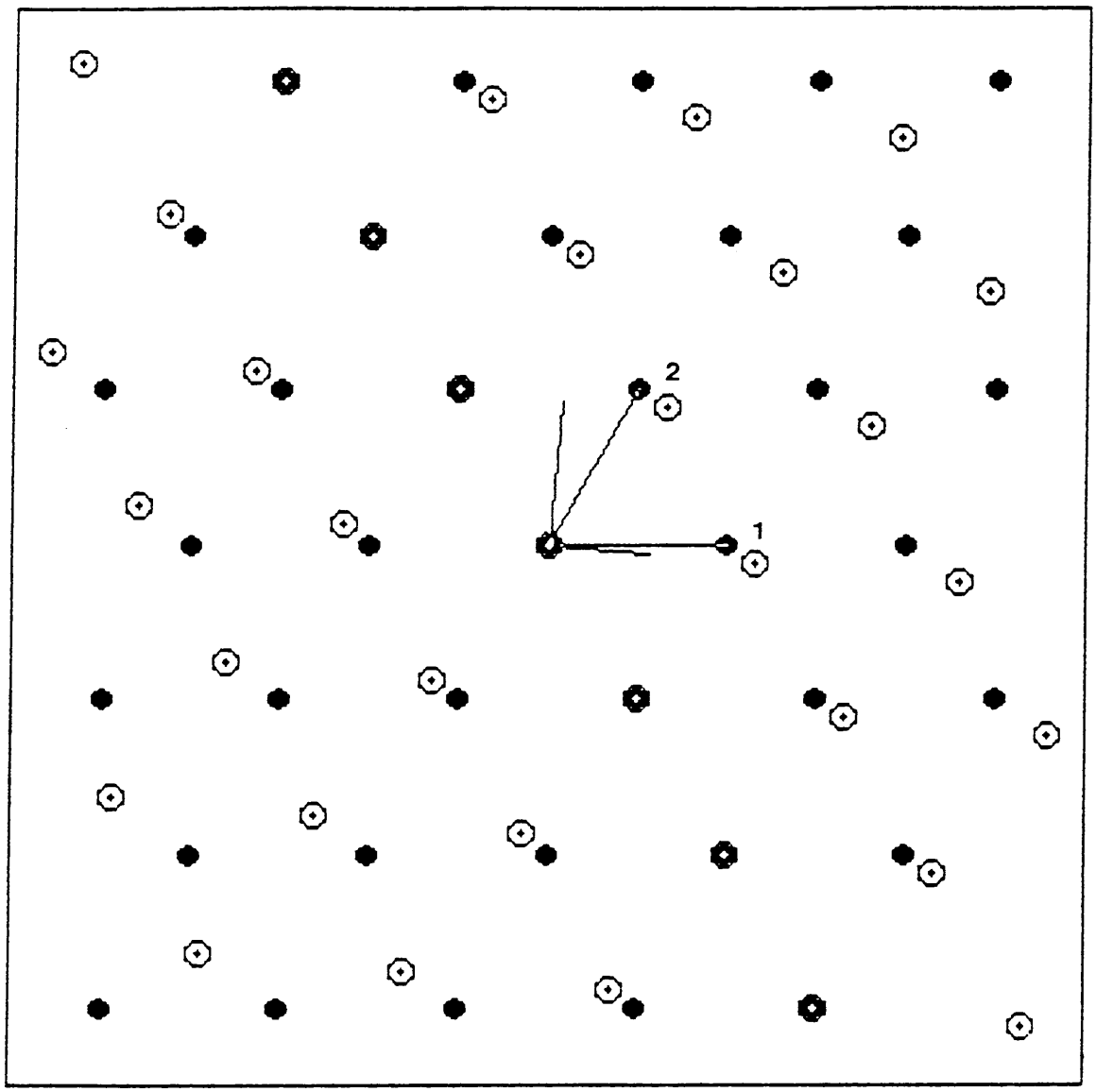

Figure 5.12(a) Reciprocal lattice map of an ideal Kurdjumov-Sachs system. W=0.4eV A=1 (refer to Table 5.5(a))

$r = 0.91856$ $\theta = 24.74^{\circ}$ $\varepsilon_x = -0.00095$ $\varepsilon_y = 0$ $\gamma_{xy} = -0.00016$

Solid circles represent substrate points, open circles represent the overgrowth.

Centred solid circles represent coinciding substrate and overgrowth points.

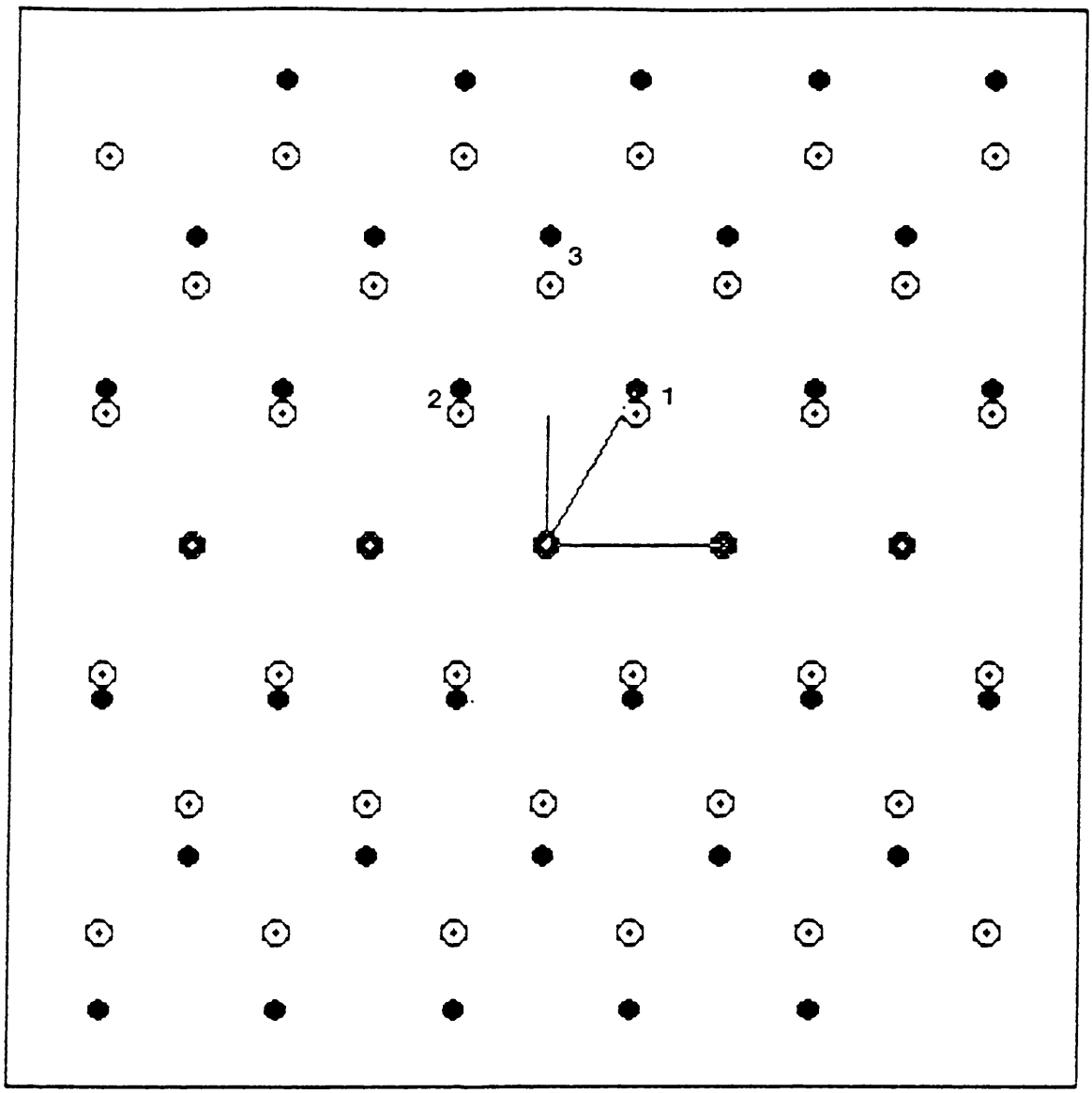

Figure 5.12(b) Reciprocal lattice map of an ideal Nishiyama-Wassermann system. W = 0.4eV A = 1 (refer to Table 5.5(b))

r = 1.06066 $\theta = 30^{o}$ $\varepsilon_x = 0.00025$ $\varepsilon_y = -0.02195$ $\gamma_{xy} = 0$

Symbols as in Figure 5.12(a)

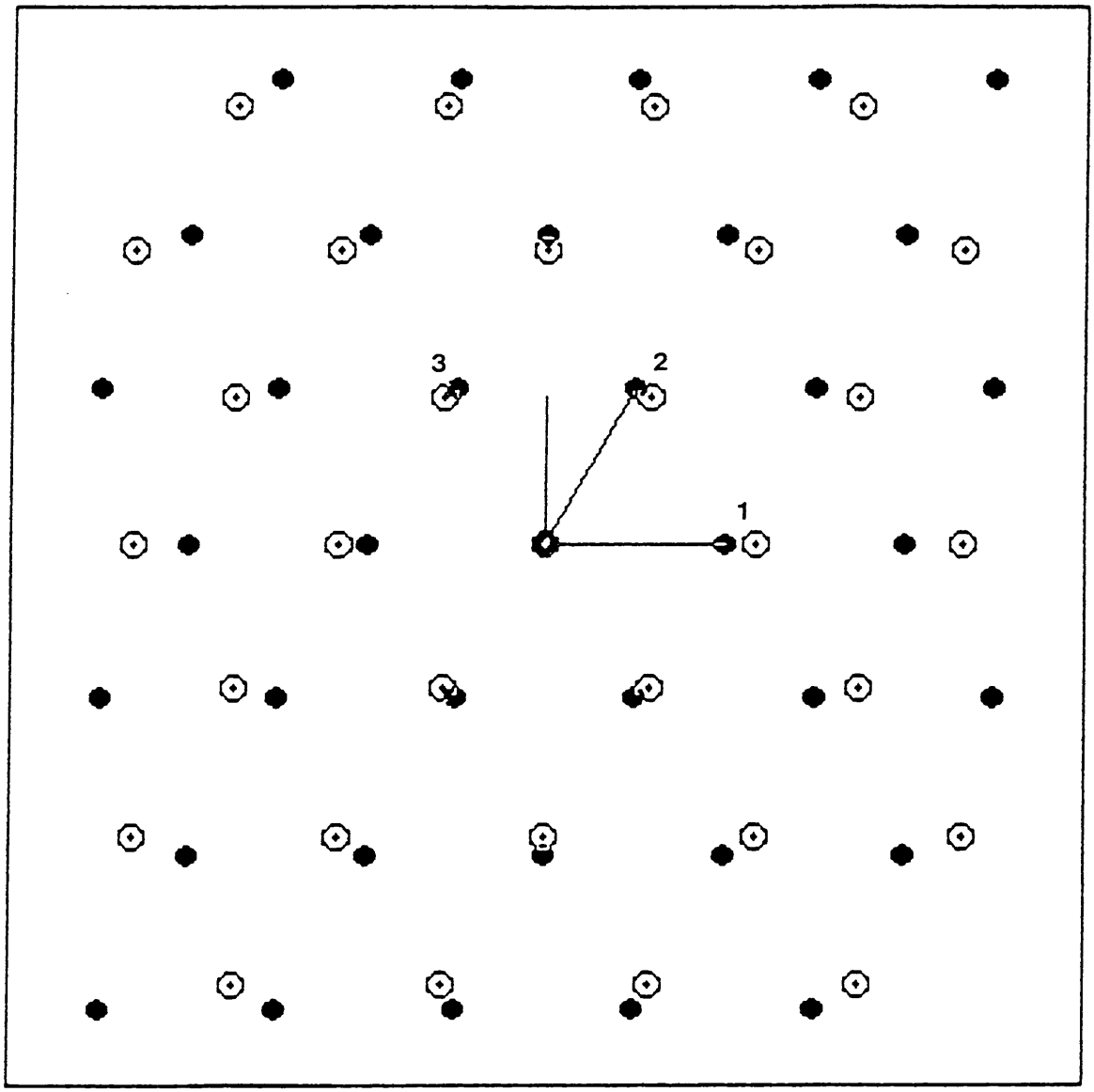

Figure 5.12(c)(ii) Reciprocal lattice map of an extreme system in the Nishiyama-Wassermann orientation. W = 0.4 eV A = 1 (Refer to Table 5.5(c))

r = 0.91856 $\theta = 30^{o}$ $\varepsilon_x = -0.00497$ $\varepsilon_y = -0.00087$ $\gamma_{xy} = 0$

Symbols as in Figure 5.12(a)

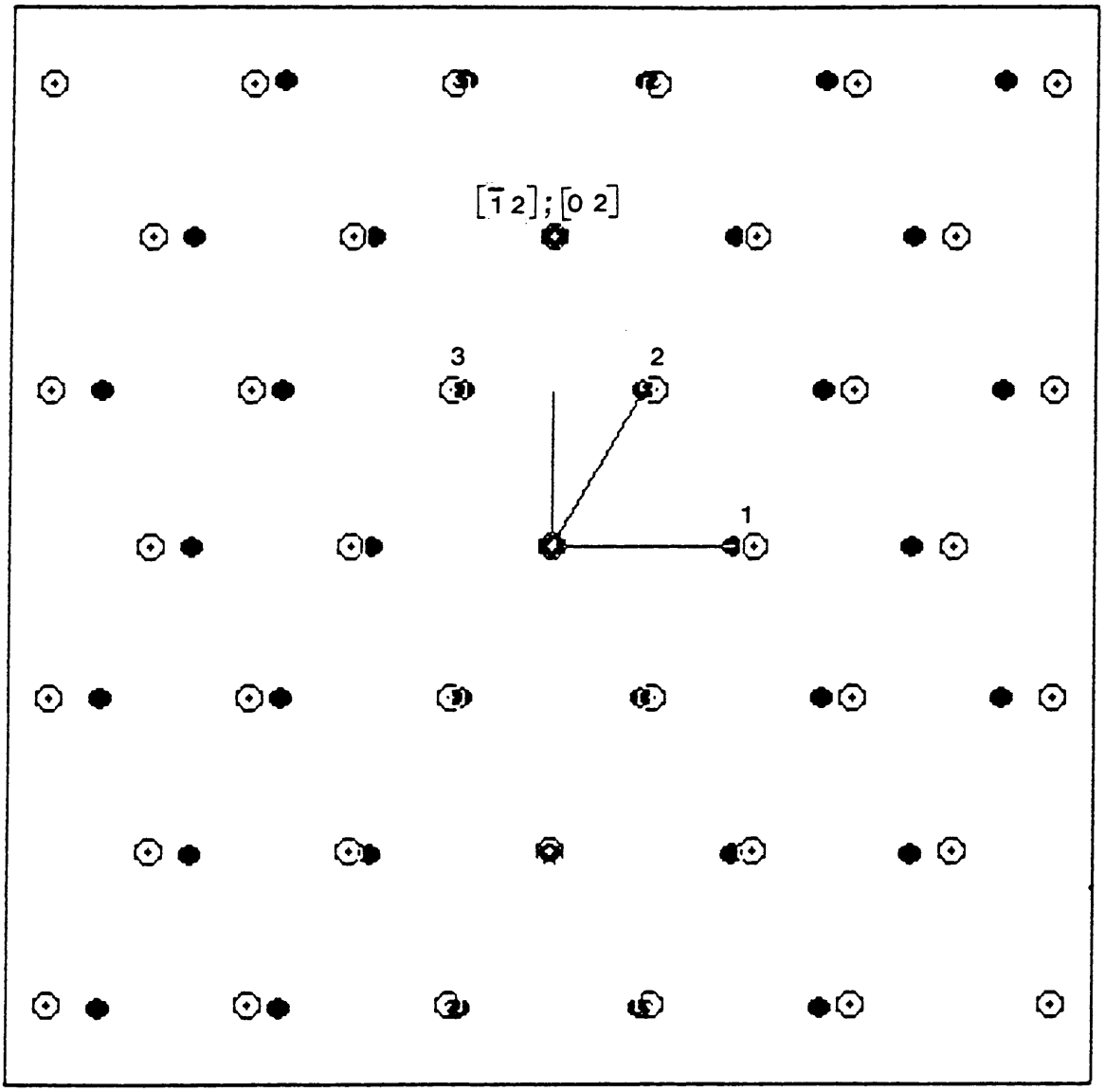

Figure 5.12(c)(iii) Reciprocal lattice map of an extreme system in the Nishiyama-Wassermann orientation. W = 0.4 eV A = 5 (Refer to Table 5.5(c))

r = 0.91856 $\theta = 30^{o}$ $\varepsilon_x = 0.0363$ $\varepsilon_y = -0.05238$ $\gamma_{xy} = 0$

Symbols as in Figure 5.12(a)

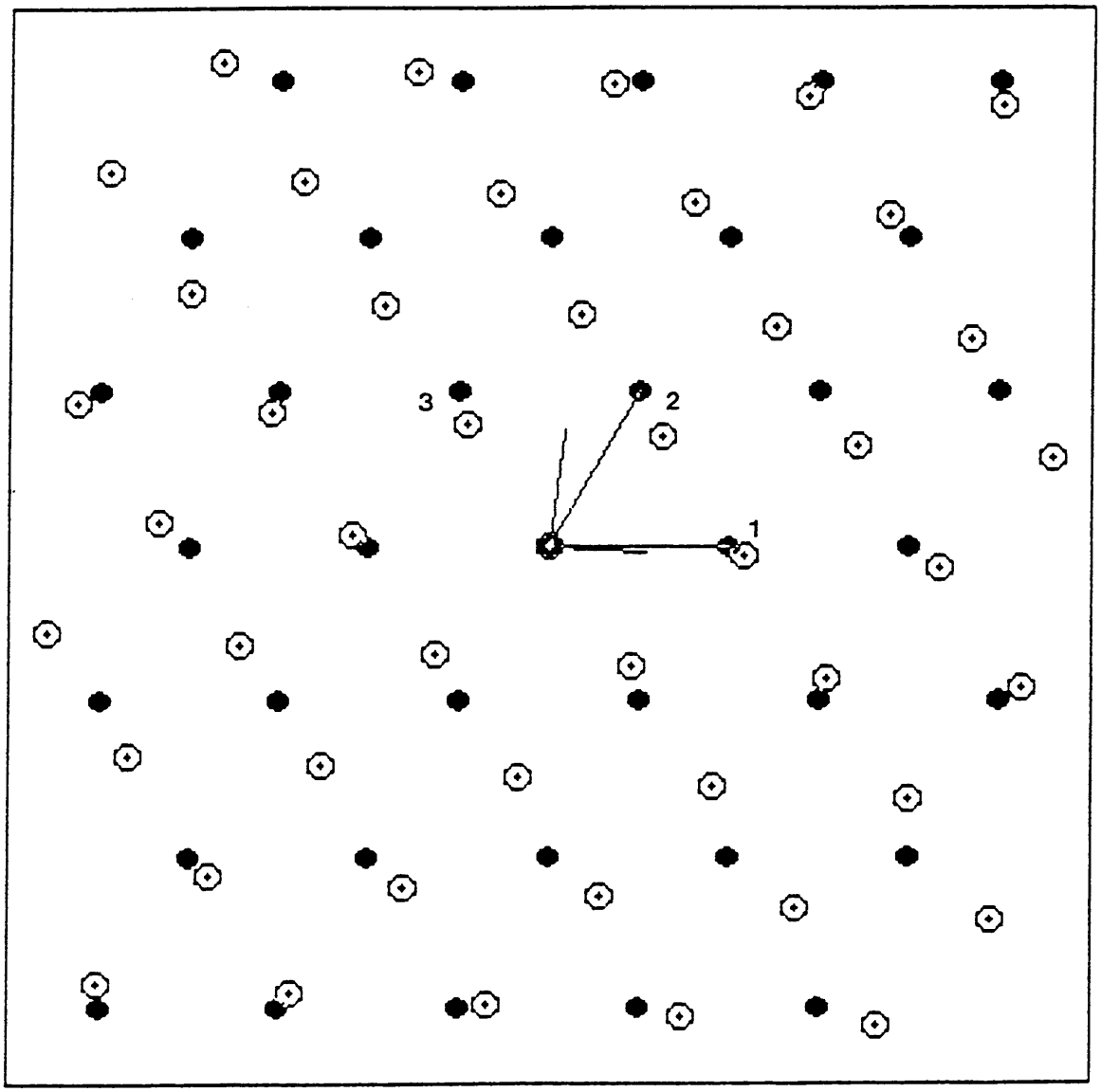

Figure 5.12(d)(i) Reciprocal lattice map of an extreme system in the Kurdjumov-Sachs orientation. W = 0.4 eV A = ½ (Refer to Table 5.5(d)

r = 1.06066 $\theta = 24.74^{o}$ $\varepsilon_x = -0.07839$ $\varepsilon_y = 0.08901$ $\gamma_{xy} = -0.0746$

Symbols as in Figure 5.12(a)

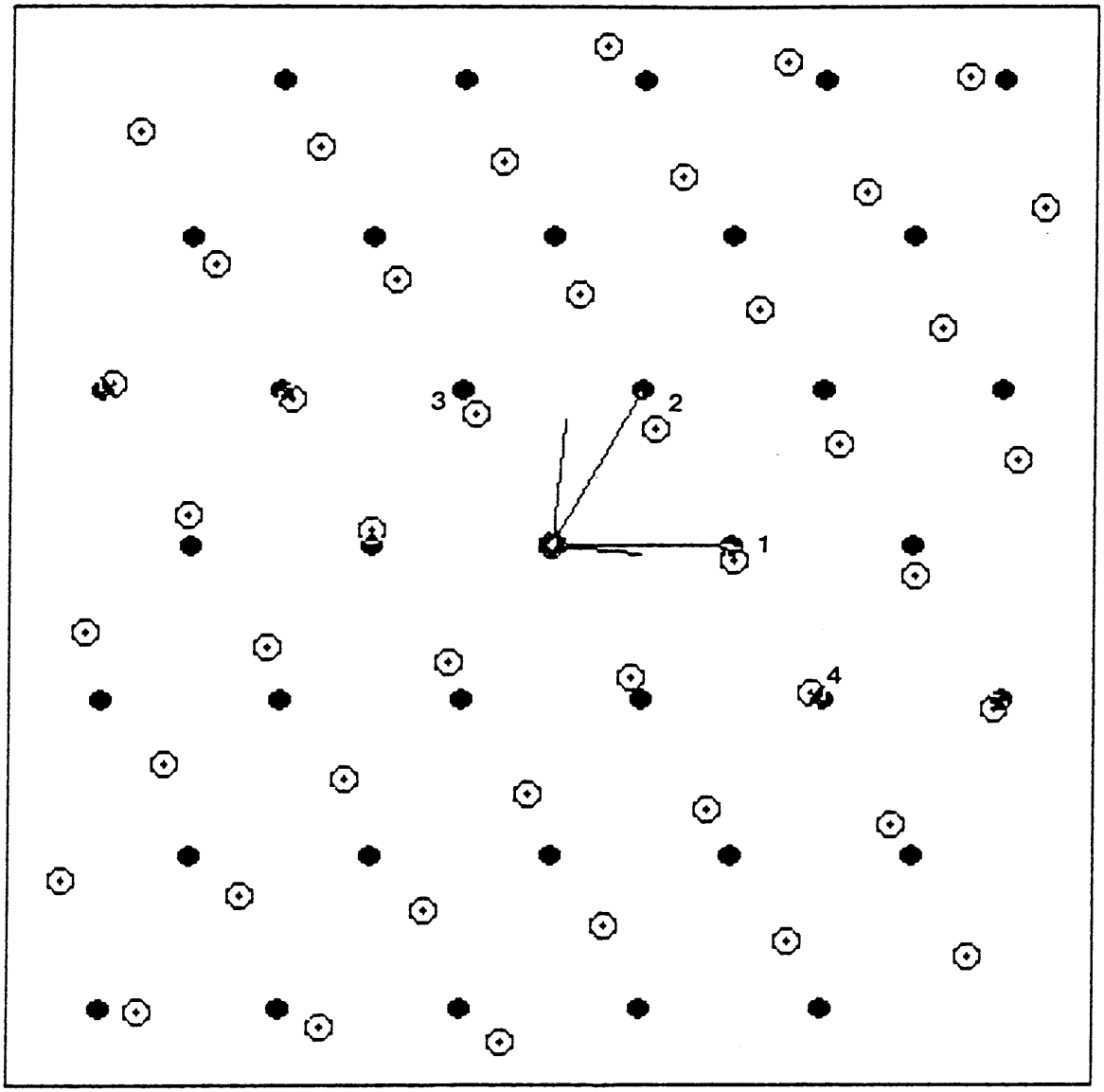

Figure 5.12(d)(ii) Reciprocal lattice map of an extreme system in the Kurdjumov-Sachs orientation. W = 0.4eV A = 1 (Refer to Table 5.5(d))

r = 1.06066 $\theta = 24.74^{o}$ $\varepsilon_x = -0.0105$ $\varepsilon_y = 0.01281$ $\gamma_{xy} = -0.01404$

Symbols as in Figure 5.12(a)

Table 5.5 (a) (Ideal KS) *Reciprocal Space Predictions of the Interfacial Misfit Dislocation structure for several Misfit Strained ov-*bcc(110)/fcc(111)*-sub interfaces.*

$r = r_{KS}$. $\theta = \theta_{KS}$ (*Strain axes at 35.2644°*)

A = 1 *strains:* ε_x = -0.00095 ε_y = 0 γ_{xy} = -0.00016 *KS*

(1) *Misfit type: Substrate* [1 0], *Overgrowth:* [2 0]

δq :	*Substrate*		*Overgrowth:*	
Reciprocal:	-0.2121	0.1223	-0.2769	0.1123
Direct lattice:	-1.2644	0.1365	-0.7747	0.6269

Spacing: $\lambda_D = 2\pi/|\delta q|$: 4.6962 (x a_{nn}) 5.1126 (x b_{nn}) *

Dislocation line: Intercepts: -3.6113 8.9087 (*Overgrowth*)
sense components: 0.11228 0.27691 "

Burgers Vector

1.0	0.5	*length:* 0.8660 (x a_{nn}) (*Substrate*)
0.6061	0.0750	*length:* 0.9428 (x b_{nn}) (*Overgrowth*)

(2) *Misfit type: Substrate* [0 1], *Overgrowth:* [1 1]

δq :	*Substrate*		*Overgrowth:*	
Reciprocal:	-0.2116	0.1223	-0.2761	0.1123
Direct lattice:	-1.2604	0.1385	-0.7723	0.6272

Spacing: $\lambda_D = 2\pi/|\delta q|$: 4.7063 (x a_{nn}) 5.1236 (x b_{nn}) *

Dislocation line: Intercepts: -3.6223 8.9022 (*Overgrowth*)
sense components: 0.11233 0.2761 "

Burgers Vector

0.5	1.0	*length:* 0.8660 (x a_{nn}) (*Substrate*)
0.3030	0.742	*length:* 0.9428 (x b_{nn}) (*Overgrowth*)

In this and the subsequent Tables 5.5, the substrate directions [1 0] and [0 1] refer to the cubic crystal directions ½<$\bar{1}$ 1 0> and ½<0 $\bar{1}$ 1> , respectively. The overgrowth basis vectors are <$\bar{1}$ 1 0> and <0 0 1> respectively. (refer to Chapter 2 Table 2.1, and Chapter 3 Table 3.4)

* b_{nn} distances are approximate in the strained structure

The cases A=½, 5 do not differ significantly

Table 5.5 (b) (Ideal NW) *Reciprocal Space Predictions of the Interfacial Misfit Dislocation structure for several Misfit Strained ov-*bcc(110)/fcc(111)*-sub interfaces.*

$r = r_{NW}$ $\theta = \theta_{NW}$ (*Strain axes at* 0°)

A = 1 *strains:* $\varepsilon_x = 0.00025$ $\varepsilon_y = -0.02195$ $\gamma_{xy} = 0$ *NW*

(1) *Misfit type: Substrate* [0 1], *Overgrowth:* [1 1]

δq :	*Substrate*		*Overgrowth:*	
Reciprocal:	-0.0825	0.1652	0.0002	0.1979
Direct lattice:	0.0010	1.0384	0.0005	0.8664
Spacing: $\lambda_D = 2\pi/\lvert\delta q\rvert$:	6.0540	(x a_{nn})	5.7078	(x b_{nn})

Dislocation line: Intercepts: 4000 5.054 (*Overgrowth*)
sense components: 0.1979 -0.00025 "

Burgers Vector

0.5 1.0 *length:* 0.8660 (x a_{nn}) (*Substrate*)

0.2499 0.6261 *length:* 0.8165 (x b_{nn}) (*Overgrowth*)

(2) *Misfit type: Substrate* [$\bar{1}$ 1], *Overgrowth:* [$\bar{1}$ 1]

δq :	*Substrate*		*Overgrowth:*	
Reciprocal:	-0.0827	0.1652	-0.0002	0.1979
Direct lattice:	-0.0010	1.0373	-0.0005	0.8664
Spacing: $\lambda_D = 2\pi/\lvert\delta q\rvert$:	6.0540	(x a_{nn})	5.7078	(x b_{nn})

Dislocation line: Intercepts: -4000 5.054 (*Overgrowth*)
sense components: 0.1979 0.00025 "

Burgers Vector

-0.5 0.5 *length:* 0.8660 (x a_{nn}) (*Substrate*)

-0.2499 0.626 *length:* 0.8165 (x b_{nn}) (*Overgrowth*)

(3) *Misfit type: Substrate* [$\bar{1}$ 2], *Overgrowth:* [0 2]

δq :	*Substrate*		*Overgrowth:*	
Reciprocal:	-0.1652	0.3304	0	0.3957
Direct lattice:	-0.0000	2.0757	0	1.7328
Spacing: $\lambda_D = 2\pi/\lvert\delta q\rvert$:	3.0270	(x a_{nn})	5.8539	(x b_{nn})

Dislocation line: Intercepts: ∞ 2.527 (*Overgrowth*)
sense components: 0.3957 0 "

Burgers Vector

0 0.5 *length:* 0.5000 (x a_{nn}) (*Substrate*)

0 0.4174 *length:* 0.4714 (x b_{nn}) (*Overgrowth*)

The cases A=½ , 5 are similar

Table 5.5 (c) [Extreme NW] *Reciprocal Space Predictions of the Interfacial Misfit Dislocation structure for several Misfit Strained ov-*bcc(110)/fcc(111)*-sub interfaces.*

$r = r_{KS}$ $\theta = \theta_{NW}$ (*Strain axes at* 0°)

A = 1 *strains:* $\varepsilon_x = -0.00497$ $\varepsilon_y = -0.00087$ $\gamma_{xy} = 0$

(1) *Misfit type: Substrate:* [1 0], *Overgrowth:* [2 0]

δq :	*Substrate*		*Overgrowth:*	
Reciprocal:	-0.1605	0	-0.2766	0
Direct lattice:	-1.3443	-0.6722	-0.7800	0

Spacing: $\lambda_D = 2\pi/|\delta q|$: 5.3969 (x a_{nn}) 5.8754 (x b_{nn})

Dislocation line: Intercepts: -3.616 ∞ (*Overgrowth*)

sense components: 0 0.2766 "

Burgers Vector

1.0 0.5 *length:* 0.8660 (x a_{nn}) (*Substrate*)

0.5802 0 *length:* 0.9428 (x b_{nn}) (*Overgrowth*)

(2) *Misfit type: Substrate* [0 1], *Overgrowth:* [1 1]

δq :	*Substrate*		*Overgrowth:*	
Reciprocal:	-0.1084	0.0564	-0.1383	0.0597
Direct lattice:	-0.6722	0.0181	-0.3900	0.3342

Spacing: $\lambda_D = 2\pi/|\delta q|$: 9.221 (x a_{nn}) 10.04 (x b_{nn})

Dislocation line: Intercepts: -7.232 16.74 (*Overgrowth*)

sense components: 0.0597 0.1383 "

Burgers Vector

0.5 1.0 *length:* 0.8660 (x a_{nn}) (*Substrate*)

0.2901 0.7077 *length:* 0.9428 (x b_{nn}) (*Overgrowth*)

(3) *Misfit type: Substrate* [$\bar{1}$ 1], *Overgrowth:* [$\bar{1}$ 1]

δq :	*Substrate*		*Overgrowth:*	
Reciprocal:	0.0520	0.0564	0.1383	0.0597
Direct lattice:	0.6722	0.6903	0.3900	0.3342

Spacing: $\lambda_D = 2\pi/|\delta q|$: 9.2210 (x a_{nn}) 10.0386 (x b_{nn})

Dislocation line: Intercepts: 7.232 16.74 (*Overgrowth*)

sense components: 0.0597 -0.1383 "

Burgers Vector

-0.5 0.5 *length:* 0.8660 (x a_{nn}) (*Substrate*)

-0.2499 0.626 *length:* 0.8165 (x b_{nn}) (*Overgrowth*)

The case A = ½ is two-dimensionally coherent

Table 5.5 (c) (Extreme NW) (Continued) *Reciprocal Space Predictions of the Interfacial Misfit Dislocation structure for several Misfit Strained ov-*bcc(110)/fcc(111)*-sub interfaces.*

$r = r_{KS}$ $\theta = \theta_{NW}$ (*Strain axes at* 0°)

(*continued*)

A = 5 *strains:* $\varepsilon_x = 0.03630$ $\varepsilon_y = -0.05238$ $\gamma_{xy} = 0$

(1) *Misfit type: Substrate:* [1 0], *Overgrowth:* [2 0]

δq :	*Substrate*		*Overgrowth:*	
Reciprocal:	-0.1143	0	-0.2051	0
Direct lattice:	-0.9572	-0.4786	-0.5333	0

Spacing: $\lambda_D = 2\pi/|\delta q|$: 7.5799 (x a_{nn}) 8.2519 (x b_{nn})

Dislocation line: Intercepts: -4.877 ∞ (*Overgrowth*)

sense components: 0 0.205 "

Burgers Vector

1.0 0.5 *length:* 0.8660 (x a_{nn}) (*Substrate*)

0.5572 0 *length:* 0.9428 (x b_{nn}) (*Overgrowth*)

(2) *Misfit type: Substrate:* [0 1], *Overgrowth:* [1 1]

δq :	*Substrate*		*Overgrowth:*	
Reciprocal:	-0.0597	0.0051	-0.1025	0.0051
Direct lattice:	-0.4787	-0.2074	-0.2666	0.0317

Spacing: $\lambda_D = 2\pi/|\delta q|$: 15.12 (x a_{nn}) 16.46 (x b_{nn})

Dislocation line: Intercepts: -9.753 196 (*Overgrowth*)

sense components: 0.0051 0.1025 "

Burgers Vector

0.5 1.0 *length:* 0.8660 (x a_{nn}) (*Substrate*)

0.2786 0.7462 *length:* 0.9428 (x b_{nn}) (*Overgrowth*)

(3) *Misfit type: Substrate:* [$\bar{1}$ 1], *Overgrowth:* [$\bar{1}$ 1]

δq :	*Substrate*		*Overgrowth:*	
Reciprocal:	0.0546	0.0051	0.1025	0.0051
Direct lattice:	0.4786	0.2712	0.2666	0.0317

Spacing: $\lambda_D = 2\pi/|\delta q|$: 15.12 (x a_{nn}) 16.46 (x b_{nn})

Dislocation line: Intercepts: 9.753 195 (*Overgrowth*)

sense components: 0.0051 -0.1025 "

Burgers Vector

-0.5 0.5 *length:* 0.8660 (x a_{nn}) (*Substrate*)

-0.2786 0.746 *length:* 0.9428 (x b_{nn}) (*Overgrowth*)

The pair [$\bar{1}$ 2] ; [0 2] in the reciprocal lattices are matched by the misfit strain in this case

Table 5.5 (d) [Extreme KS] *Reciprocal Space Predictions of the Interfacial Misfit Dislocation structure for several Misfit Strained ov-*bcc(110)/fcc(111)*-sub interfaces.*

$r = r_{NW}$ $\theta = \theta_{KS}$ (*Strain axes at 35.2644°*)

A = ½ *strains:* $\varepsilon_x = -0.07839$ $\varepsilon_y = 0.08901$ $\gamma_{xy} = -0.0746$

(1) *Misfit type: Substrate:* [1 0], *Overgrowth:* [2 0]

δq :	*Substrate*		*Overgrowth:*	
Reciprocal:	-0.1216	0.0723	-0.1714	0.0888
Direct lattice:	-0.7154	-0.0967	-0.4047	0.2771

Spacing: $\lambda_D = 2\pi/|\delta q|$: 8.1775 (x a_{nn}) 7.7098 (x b_{nn})

Dislocation line: Intercepts: -5.8343 11.26 (*Overgrowth*)
sense components: 0.0888 0.1714 "

Burgers Vector

1.0 0.5 *length:* 0.8660 (x a_{nn}) (*Substrate*)

0.5608 0.0859 *length:* 0.8165 (x b_{nn}) (*Overgrowth*)

(2) *Misfit type: Substrate:* [0 1], *Overgrowth:* [1 1]

δq :	*Substrate*		*Overgrowth:*	
Reciprocal:	-0.2742	0.2913	-0.2965	0.3767
Direct lattice:	-1.0770	1.2919	-0.6507	1.2709

Spacing: $\lambda_D = 2\pi/|\delta q|$: 3.058 (x a_{nn}) 2.884 (x b_{nn})

Dislocation line: Intercepts: -3.373 2.655 (*Overgrowth*)
sense components: 0.3767 0.2965 "

Burgers Vector

0.5 1.0 *length:* 0.8660 (x a_{nn}) (*Substrate*)

0.2804 0.6016 *length:* 0.8165 (x b_{nn}) (*Overgrowth*)

(3) *Misfit type: Substrate:* [$\bar{1}$ 1], *Overgrowth:* [$\bar{1}$ 1]

δq :	*Substrate*		*Overgrowth:*	
Reciprocal:	-0.1527	0.2190	-0.1251	0.2879
Direct lattice:	-0.3616	1.1952	-0.2460	0.9938

Spacing: $\lambda_D = 2\pi/|\delta q|$: 4.4525 (x a_{nn}) 4.1979 (x b_{nn})

Dislocation line: Intercepts: -7.994 3.473 (*Overgrowth*)
sense components: 0.2879 0.1251 "

Burgers Vector

-0.5 0.5 *length:* 0.8660 (x a_{nn}) (*Substrate*)

-0.2804 0.5157 *length:* 0.8165 (x b_{nn}) (*Overgrowth*)

Table 5.5 (d) (Extreme KS) (Continued) *Reciprocal Space Predictions of the Interfacial Misfit Dislocation structure for several Misfit Strained ov-*bcc(110)/fcc(111)*-sub interfaces.*

$r = r_{KS}$ $\theta = \theta_{NW}$ (*Strain axes at 35.2644°*)
(*continued*)
A = 1 *strains:* ε_x =-0.01050 ε_y = 0.01281 γ_{xy} = -0.01404

(1) *Misfit type: Substrate:* [1 0], *Overgrowth:* [2 0]

δq :	*Substrate*		*Overgrowth:*	
Reciprocal:	-0.0566	0.0990	-0.0306	0.1215
Direct lattice:	-0.0590	0.5927	-0.0605	0.4951
Spacing: $\lambda_D=2\pi/\lvert\delta q\rvert$:	10.07	(x a_{nn})	9.4894	(x b_{nn})

Dislocation line: Intercepts: -32.64 8.228 (*Overgrowth*)
sense components: 0.1215 0.0306 "

Burgers Vector

1.0	0.5	*length:* 0.8660 (x a_{nn}) (*Substrate*)
0.5283	0.0690	*length:* 0.8165 (x b_{nn}) (*Overgrowth*)

(2) *Misfit type: Substrate:* [0 1], *Overgrowth:* [1 1]

δq :	*Substrate*		*Overgrowth:*	
Reciprocal:	-0.1961	0.2472	-0.1847	0.2968
Direct lattice:	-0.6075	1.2496	-0.3828	1.2043
Spacing: $\lambda_D=2\pi/\lvert\delta q\rvert$:	3.831	(x a_{nn})	3.612	(x b_{nn})

Dislocation line: Intercepts: -5.415 3.370 (*Overgrowth*)
sense components: 0.2968 0.1847 "

Burgers Vector

0.5	1.0	*length:* 0.8660 (x a_{nn}) (*Substrate*)
0.2641	0.6362	*length:* 0.8165 (x b_{nn}) (*Overgrowth*)

(3) *Misfit type: Substrate:* [$\bar{1}$ 1], *Overgrowth:* [$\bar{1}$ 1]

δq :	*Substrate*		*Overgrowth:*	
Reciprocal:	-0.1396	0.1482	-0.1540	0.1752
Direct lattice:	-0.5485	0.6570	-0.3223	0.7092
Spacing: $\lambda_D=2\pi/\lvert\delta q\rvert$:	6.011	(x a_{nn})	5.667	(x b_{nn})

Dislocation line: Intercepts: -6.492 5.707 (*Overgrowth*)
sense components: 0.1752 0.1540 "

Burgers Vector

-0.5	0.5	*length:* 0.8660 (x a_{nn}) (*Substrate*)
-0.2642	0.5672	*length:* 0.8165 (x b_{nn}) (*Overgrowth*)

The case A = 5 shows similar behaviour

5.9 DISCUSSION

The final interfacial structures are determined by the original orientation, the overall misfit strain and the relaxation around the O-lattice of the *strained* lattice. Obtainable from the reciprocal lattice is the unrelaxed interfacial structure. This information is however very useful, as it does include the dislocation spacings, orientations and their Burgers vectors. In keeping with the premise of Bollmann's (1970) geometrical description, the O-lattice structures remain after local relaxation.

As the exact energy behaviour has not been formulated in terms of the reciprocal lattice, the local relaxation per se is not available from this description. The local relaxation is here determined numerically with the previously described Finite Element formulation, yielding the figures 5.11. The dislocation structure however correlates very well with these relaxed interfacial structures.

Known qualitative aspects of dislocation theory can be used with the reciprocal lattice description. For example it is known (Van der Merwe 1950, 1963, 1980, Frank and Van der Merwe 1949, Van der Merwe and Ball 1975) that a large misfit, with a resulting small spacing between dislocations and hence very little local relaxation results more properly in a Misfit Vernier than misfit dislocations. A distinction is introduced when the areas of good fit are enlarged by local strain compared to the areas of bad fit. In the Misfit Vernier case the bad fit regions are essentially the same size as good fit regions.

From the reciprocal space the qualitative prediction can be made that when the absolute misfit vector magnitude $|\delta\mathbf{q}|$ is large, its wavelength only a few lattice spacings, a Misfit Vernier, with no meaningful relaxation, results. When the absolute misfit vector is very short, with a long wavelength, the accommodation of misfit

will allow significant relaxation and a misfit dislocation array occurs.

The systems which have been presented in the results have been selected to show several of the features occurring in interfaces. Systems which have only pure edge arrays, both vernier and dislocations are illustrated. Also illustrated are systems with interacting arrays of screw and edge dislocations. There are several cases which show complicated mixed arrays, particularly the systems which have strained to matching between high order reciprocal lattice points. Some of these arrays are difficult to interpret without the reciprocal lattice maps and the representative systems are provided with reciprocal lattice plots in figure 5.12.

In the following discussion the reciprocal lattice vectors are indicated with the notation $[h\ k]^*$, and pairs are always listed in the order substrate vector, overgrowth vector, as

$$[h\ k]^* \ ; \ [p\ q]^* \ .$$

Systems Oriented for 1-Dimensionally Ideal Matching

The systems occurring as Ideal Epitaxial Configurations, the Nishiyama-Wassermann and Kurdjumov-Sachs systems, as given in Table 5.5 *a* and *b*, with associated figures 5.11 *a* and *b* and 5.12 *a* and *b* have the simplest interfacial structure for all the anisotropy ratios. In these systems a low-order pair of reciprocal lattice vectors matches, with the resulting row-matching of atomic rows already established for one family of atomic rows. As the bcc{110}/fcc{111} interface presents nearly three-fold symmetry, there are always three possible wave vector pairs which need to be matched. If one pair already matches, the two others are close together and give rise to dislocation arrays.

Ideal Kurdjumov-Sachs

In the Kurdjumov-Sachs system, (a in the Table 5.5 and the figures 5.11 and 5.12), $r=r_{KS}$, $\theta=\theta_{KS}$ the pair $[\bar{1}\ 1]^*$; $[\bar{1}\ 1]^*$ coincides. The pairs $[1\ 0]^*$; $[2\ 0]^*$ and $[0\ 1]^*$; $[1\ 1]^*$ (and others parallel to the direction of $[\bar{1}\ 1]^*$) give rise to dislocations. The first pair has both length and orientational misfit, which is taken up by a mixed misfit dislocation array (1). The second pair, being related by symmetry to $[\bar{1}\ 1]^*$; $[\bar{1}\ 1]^*$, so that both have the same length, has only orientational misfit. This is accommodated by a *pure screw* dislocation array (2). These arrays however have essentially the same dislocation spacing and line sense, as $\delta\mathbf{q}$ is common to both. An array with the propagation vector $\delta\mathbf{q}$ and a combined Burgers vector lying in the substrate direction [1.5 1.5], ($\frac{3}{4}\langle\bar{1}\ 0\ 1\rangle$ in substrate cubic coordinates) may be expected to result. This Burgers vector is at essentially 60° with the propagation vector, so that the screw component, nearly parallel to the $\mathbf{b}_2$- (vertical) direction of the overgrowth, dominates. The spacing of the lines is relatively close however, about 5 nearest neighbour distances, so that little relaxation is expected and the array structure tends to a vernier. The figures 5.11 a (i)-(iii) can be viewed when held obliquely along the diagonal from bottom right to upper left, showing slight kinking of the atomic rows in an upward direction. This shows the little relaxation which does occur.

The structure is not affected qualitatively by anisotropy, as can be seen from the figures, however as an increasing anisotropy ratio softens the material in the cubic <001>-directions, (refer to Table 4.1 in which c_{11} decreases with increasing anisotropy), the relaxation can be seen to increase slightly from (i) to (iii).

Ideal Nishiyama-Wassermann

The interfacial structure of the ideal Nishiyama-Wassermann system is also straight forward. The reciprocal lattice pair $[1\ 0]^*$; $[2\ 0]^*$ match, while the mismatch of the pairs $[0\ 1]^*$; $[1\ 1]^*$ and $[\bar{1}\ 1]^*$; $[\bar{1}\ 1]^*$ is accommodated by mixed dislocations. However, as the dislocation lines are equally spaced and parallel the oppositely directed screw components of the coinciding dislocation arrays cancel, so that only the edge components remain, creating a single pure edge array, with Burgers vector of type [0 1.5] in the substrate coordinates. For the fcc{111} substrate coordinates this corresponds to the Burgers vector $\frac{3}{4}\langle 0\ \bar{1}\ 1\rangle$. Also present, but at a spacing of about 3 nearest neighbour distances, and exactly half of these other pairs, is a misfit vernier arising from the pair $[\bar{1}\ 2]^*$; $[0\ 2]^*$.

Again, as the anisotropy is increased, the stiffness of the $\mathbf{b}_2$-direction is reduced, and there is more relaxation of the overgrowth widening the region of good fit. This can be seen in the progression from figure 5.11 *b* (i) to (iii).

Extremes

Two further systems have been chosen to illustrate some interesting effects, namely the two systems with $r=r_{KS}$, $\theta=\theta_{NW}$ and $r=r_{NW}$, $\theta=\theta_{KS}$.

The $r=r_{KS}$, $\theta=\theta_{NW}$ extreme:

The first system arises if the island has grown in a coherent configuration, but when it thickens cannot rotate to its ideal configuration. The degree of anisotropy very drastically affects the misfit accommodation, and the relative importance of misfit strain and misfit dislocations.

The second is perhaps more esoteric, but does show some interesting features, particularly the difficulty of achieving even local matching, with a resulting dominance of Misfit Vernier over misfit dislocations.

Referring to Table 5.5 *c*, as well as figures 5.11 and 5.12 *c*, the variety of interfacial structures is evident. The case with anisotropy ratio ½ in fact achieves 2D-coherent matching, while the misfit in the isotropic case is accommodated with misfit dislocations, and with anisotropy ratio 5, misfit strain achieves a second order matching pair, $[\bar{1}\ 2]^*$; $[0\ 2]^*$, and misfit dislocations and vernier accommodate the first order pairs.

The isotropic case shows three major dislocation arrays arising from first order pairs.

The mismatch between pair (1), $[1\ 0]^*$; $[2\ 0]^*$ gives rise to an array of edge dislocations (with a spacing of about 6 nearest neighbour distances this array tends to a vernier), with dislocation lines parallel to the $\mathbf{b}_2$ direction. The Burgers vector in substrate coordinates is the type [1 ½], equivalent to $\frac{1}{4}\langle\bar{2}\ 1\ 1\rangle$ in crystal coordinates, and parallel to the $\mathbf{b}_1$-direction in the overgrowth.

Two non-parallel predominantly screw but mixed dislocation arrays arise from the pairs (2), $[0\ 1]^*$; $[1\ 1]^*$ and (3), $[\bar{1}\ 1]^*$; $[\bar{1}\ 1]^*$, one of which normally matches in an ideal Kurdjumov-Sachs orientation. The slight deviation from screw character was introduced by the small misfit strain which allowed a non-exact matching of the high order pair $[\bar{1}\ 2]^*$; $[0\ 2]^*$ pair. As this latter match is not exact, edge dislocations with dislocation lines parallel to $\mathbf{b}_1$ also arise from this pair, but because of the higher order nature, whose potential terms are not represented in the substrate potential (see Chapters 2 and 4) very little relaxation is associated with this array.

The screw arrays (2) and (3) are related by symmetry, and have the same spacing, about 10 nearest neigbour distances. This significant spacing allows considerable relaxation and their effect is evident as very clear kinks in the atomic rows in figure 5.11 *c* (ii). These are most easily seen by looking along the diagonal directions in the diagram. The collections of poor fit evident as the groups of solid circles are extended nodes, bounded by the dislocation lines. The large regions of good fit coincide with intersections of the three good-fit lines.

The configuration with anisotropy ratio 5 [Table 5.5 *c*, figures 5.11 and 5.12 *c* (iii)] is somewhat different, because the less stiff $\mathbf{b}_2$-direction allows the high order pair $[\bar{1}\ 2]^*$; $[0\ 2]^*$ to match with misfit strain. The three first order pairs then lead to three parallel dislocation arrays, parallel to $\mathbf{b}_2$. The pair $[1\ 0]^*$; $[2\ 0]^*$ results in an edge dislocation array, spaced at about 8 nearest neigbour distances, and with Burgers vector [1 ½], in terms of the substrate surface coordinates which is equivalent to the crystallographic vector $\frac{1}{4}\langle\bar{2}\ 1\ 1\rangle$ in the cubic coordinates.

Spaced at twice this interval (thus about 16 nearest neighbour spacings) are the two other mixed arrays from the pairs $[0\ 1]^*$; $[1\ 1]^*$ and $[\bar{1}\ 1]^*$; $[\bar{1}\ 1]$. These arrays are close to parallel to $\mathbf{b}_2$, but as Table 5.5 shows, are not exactly parallel. As a result the screw components do not cancel, although they are the same for the two structures, and their effect can be observed very clearly by looking along the diagonal directions in figure 5.11 *c* (iii). The large dislocation spacings result in large regions of good fit, seen from the grouped triangles, and very small regions of bad fit, seen as the small groups of solid circles. The Burgers vectors are [½ 1], (*i.e.* $\frac{1}{4}\langle\bar{1}\ \bar{1}\ 2\rangle$) and $[\bar{\frac{1}{2}}\ \frac{1}{2}]$ (thus $\frac{1}{4}\langle 1\ \bar{2}\ 1\rangle$).

The $r=r_{NW}$, $\theta=\theta_{KS}$ extreme:

Less affected by the anisotropy, the final system considered is the other extreme, $r=r_{NW}$, $\theta=\theta_{KS}$.

With anisotropy ratio A=½, (Table 5.5 *d*, figures 5.11 and 5.12 *d*, (i)) the first order pairs yield arrays of mixed dislocations (1), (spacing about 8 nearest neighbour distances), a screw vernier (2) (spacing 3 distances), and a closely spaced (about 4 distances), mainly edge array.

The screw component of the edge array (1) from the pair $[1\ 0]^*$; $[2\ 0]^*$, can be observed by looking obliquely in a direction parallel to the $\mathbf{b}_2$- (vertical) direction. The Burgers vector of the array is [1 ½] (correponding to $\frac{1}{4}\langle\bar{2}\ 1\ 1\rangle$). There is no noticable relaxation associated with the screw vernier (2), from the pair $[0\ 1]^*$; $[1\ 1]^*$ with Burgers vector, [½ 1], (*i.e.* $\frac{1}{4}\langle\bar{1}\ \bar{1}\ 2\rangle$). The remaining array is primarily edge, arising from the pair $[\bar{1}\ 1]^*$; $[\bar{1}\ 1]$ with Burgers vector $[\bar{½}\ ½]$ (thus $\frac{1}{4}\langle 1\ \bar{2}\ 1\rangle$). This is still very narrowly spaced, and is essentially a misfit vernier. The large regions of poor fit, (solid circles), rather narrow regions of good fit, (the triangles), in figure 5.11 *d* (i) attest to the little relaxation due to the lack of misfit dislocations.

The isotropic system, which allows strain in the $\mathbf{b}_2$- (cubic) direction more easily than the foregoing case shows more misfit strain, so that the misfit verniers in fact show an increased tendency to dislocations.

The dislocation array arising from pair (1) $[1\ 0]^*$; $[2\ 0]^*$ has become virtually pure screw, and spaced more than 9 nearest neighbour distances apart. Again looking obliquely along $\mathbf{b}_2$ (vertically) in the figure 5.11 (d) (ii), shows the increased kinks

along these atomic rows due to the greater relaxation associated with the dislocations.

The mixed vernier (2) from the pair $[0\ 1]^*$; $[1\ 1]^*$ has slightly increased spacing, (to less than 4 spacings), but essentially remains a vernier.

The array (3), arising from $[\bar{1}\ 1]^*$; $[\bar{1}\ 1]^*$ is essentially pure edge, and increased its spacing to nearly 6 nearest neighbour distances. This is a major improvement, and the wider regions of good fit (triangles) result from this.

Additionally an edge array (4) results from the near matching of the pair $[2\ \bar{1}]^*$; $[3\ \bar{1}]^*$, with a spacing of about 11 nearest neighbour distances. This array has Burgers vector [½ 0], which is $\frac{1}{4}\langle\bar{1}\ 1\ 0\rangle$ in the substrate cubic coordinates. However, because of the absence of adatom-substrate potential terms of this high order, no extensive relaxation from these misfit arrays are easily discernible.

The final system of this type with <u>anisotropy ratio A=5,</u> continues the trend to further improved matching, with nearly unchanged dislocation spacings.

These extreme cases have shown that materials which are close to the Kurdjumov-Sachs ideal ratios can achieve reasonably good matching, with dislocations in the interfaces, when aligned at the Nishiyama-Wassermann orientational angle. The actual interfacial structure, ranging from two-dimensionally coherent to widely spaced dislocation arrays is heavily dependent on the anisotropy ratio. The Nishiyama-Wassermann systems however do not behave favourably in the Kurdjumov-Sachs orientational angle.

Energy behaviour

The energy behaviour of several systems with nearest neighbour ratios ranging from 0.9 to 1.08, which included the exact ideal Kurdjumov-Sachs and ideal Nishiyama-Wassermann ratios, r_{KS} and r_{NW} respectively, were studied. The interaction energy scaling factors (or overall amplitude values) W, ranged from 0.1eV to 6eV and the energy behaviour of all the ratios were examined at the two orientations, exact Kurdjumov-Sachs, $\theta_{KS} \simeq 5.26^{\circ}$, and exact Nishiyama-Wassermann, $\theta_{NW}=30^{\circ}$.

The energy of each of these systems was calculated for a rigid overgrowth, (described in Chapter 3), an overgrowth with homogeneous (misfit) strain which minimized the total interfacial energy, (as in Chapter 4), and finally with local relaxation, effectively allowing misfit dislocations. This final dislocation relaxation was studied numerically with the Finite Element method as described earlier in this chapter.

(Although the minizing strain and energies were calculated for the homogeneoeus strain case as in Chapter 4, the energies were also calculated by the Finite Element expressions as a check on the entire formulation, and were correct within the precision of the computer, so that nearly all significant digits agreed.)

The diagrams, figures 5.8, 9 and 10, referring to anisotropy ratios of ½, 1 and 5 respectively, summarise the changes in interfacial energy as the various misfit accommodation modes are included in the calculations. The special interfaces discussed earlier, and illustrated in figure 5.11, were obtained from these calculations as the minimum energy structures.

It is important to note that the relaxation allowed after the misfit strain was introduced did not allow a rotation of the island, in keeping with the essential restrictions of Chapters 3 and 4, the rigid and misfit strain discussions respectively. Neither was a further average strain allowed, other than a small

relaxation in the boundary region, which was kept empty of atoms. The boundaries of the islands were therefore fixed, (although boundary nodes were allowed to displace *within* the boundary, as shown in figure 5.5).

The diagrams, irrespective of anisotropy ratio, qualitatively show similar behaviour for changes in the overlayer-substrate binding strength, as expressed through W.

Corresponding to the lowest values of the overall amplitude, W=0.1eV, the energy after homogeneous strain is essentially the same as that of the rigid system, except for ratios close to but not equal, to the ideal values, r_{KS} and r_{NW}. This indicates very little misfit strain. The local relaxation in this case introduces a reduction of about 15% from the homogeneous levels. As the final total energy is vastly different from the strain energy, there is no two-dimensional coherency for this weak binding, but some relaxation associated with misfit dislocations does exist. Because of the minor role played by relaxation here, (the strain energy ranges from 10% to 30% of the final energy) only the diagram for the isotropic case is shown here.

With W=0.4eV, all anisotropy ratios show a two-dimensionally coherent phase for the Nishiyama-Wassermann orientation angle near $r=r_{KS}$. The range for this phase tends to increasing r-value with increasing anisotropy ratio. (This phase is recognized by the equality of strain and total energy and corresponding zero misfit energy.) In the one-dimensionally coherent regions (about r_{KS} and r_{NW}) the homogeneous strain tends to widen the energy minimum-wells, increasing the region of exact coherence. In the intermediate region, with neither full two-dimensional nor one-dimensional coherence, local, misfit dislocation strain does reduce the energy from the homogeneous value by about 10%.

When W is increased to 0.9eV the two-dimensionally coherent region (at the $\theta_{NW}=30^{\circ}$ only) grows towards the ratio r_{NW} and already engulfs the r_{KS} ratio. The ratio r_{NW} is two-dimensionally coherent

when the anisotropy ratio is high, but remains one-dimensionally coherent as Nishiyama-Wassermann configuration, for the isotropic case. In the θ_{KS} orientation the decrease in interfacial energy with misfit dislocation strain is about 20% to 30% near the extreme r_{NW} ratio. Clearly at this strong binding energy, the force which tends to decrease the misfit, in spite of the rather close spacing of misfit dislocation arrays, as discussed earlier, results in closely spaced misfit dislocations, whereas at low binding these remain a misfit vernier. This view is suppported by the increase in strain energy associated with this accommodation. The decrease in strain energy arises both because misfit strain is unfavourable at this r_{NW}, θ_{KS} extreme, and the dearth of misfit dislocations. Misfit dislocations lower the energy more away from the the ideal configurations than close to them primarily because misfit strain causes 1-dimensional coherence, and therefore fewer non-coincident pairs of reciprocal lattice points near the ideal ratios.

At the highest value of the binding amplitude, W=6eV, the θ_{NW} orientation angle has become the two-dimensionally coherent phase for the entire range, and all anisotropy ratios. Once again the diagrams are essentially similar. The θ_{KS} orientation, also independent of anisotropy, being unable to achieve two-dimensional coherence, because of the orientational misfit, succeeds in considerably lowering the misfit energy, and the total interfacial energy from the misfit strain case by severe local strain. The interface is in fact saturated with dislocations as can be seen from the flatness of both the total energy and strain energy curves. The energy reduction introduced by the dislocations is about 50% over the misfit strain reduction, while the strain energy is about 25% of the final total energy.

Comparative behaviour between the energies of the θ_{NW} and θ_{KS}-orientations.

With a view to discussing the actual realization of the θ_{KS} orientation and configuration for systems with nearest neighbour ratios close to r_{KS} it is useful to view the diagrams from the highest binding value, equivalent to a low value of the Van der Merwe configuration parameter ℓ (about 1 with W=6eV) and thin or soft overgrowth, to the lowest overall amplitude, corresponding to a high value of ℓ, (about 16 for W=0.1eV) and thick or stiff overgrowth.

Starting with the thin case, ℓ small, the interface is either heavily dislocated if one-dimensionally exactly coherent, or fully two-dimensionally coherent, with the latter case having the lower energy, and is therefore preferred. Naturally, the non-θ_{NW} orientational angle will have a lower energy value, the smaller the deviation from θ_{NW} at very high binding amplitudes. Even at the W=0.9eV case, with ℓ about 4, the θ_{NW} orientation is favoured above the θ_{KS} orientation for all but the ideal r_{KS} system.

As the system thickens, (equivalently here, W becomes less, at about 4eV and ℓ increases), the one-dimensional coherence becomes energetically favoured over the two-dimensionally coherent cases, with the result that the θ_{KS} orientation is less dislocated, and correspondingly more clearly defined, and is favoured energetically. If the constraints on the system are such that reorientation is not possible, the extreme θ_{NW} , r_{KS} interfaces discussed above may be observed, screw and edge dislocations or misfit verniers in the interface. With dislocated structures, it may be expected that diffraction information will show regions associated with the θ_{KS} orientation as well as the θ_{NW} orientation. It can be expected that neither is closely defined.

The final diagrams, W=0.1 eV, ℓ large, show clear preference for the θ_{KS} angle for near θ_{KS} systems.

Although the thickening process has been rather naively related to the increase in ℓ parameter, a thicker crystal has not of course been modelled accurately with the techniques discussed here. The reason is that the plane stress boundary condition on the elastic problem which implies the absence of a strain gradient in the thickness direction of course applies only to a thin system and the forces have been applied to the finite element nodes in two-dimensional fashion. As the overlayer-substrate interaction may be expected to reduce with distance from the interface, this is not representative of any but the thinnest overgrowths, as pointed out by Van der Merwe and Ball (1975).

5.10 CONCLUSION

This chapter ends the progression from rigid model, through misfit or homogeneous strain to the inclusion of misfit dislocations or misfit vernier as factors in the description of epitaxy.

The reciprocal space description which was the natural result of the rigid model and the assumption that epitaxial orientations minimize the interfacial energy, as derived in Chapter 3, was here extended to the description of the interfacial structure. The extension allows the detailed description of the misfit dislocation structure, the spacing of the dislocation arrays and their propagation direction, their line sense and their Burgers vectors. With this of course comes a unique criterion for the screw, edge, or mixed nature of these arrays. Relating the spacing to the qualitative aspects of known dislocation theory, yields the qualitative interpretation facility for a differentiation between Misfit Vernier and Misfit dislocations.

Key to the reciprocal space description are the nearly coinciding reciprocal lattice vectors, $\mathbf{q}_a$ from the substrate and $\mathbf{q}_b$ from the overgrowth. An Ideal Epitaxial Configurations is the scale and orientation for which $\mathbf{q}_a = \mathbf{q}_b$. If this is not possible for a given system, then, naturally depending on available energy and the form

of the adatom-substrate interaction energy, the systems will tend to strain to achieve this coincidence. The homogeneous, misfit strain is calculable from these vectors, and the elastic constants of the crystals concerned, where here the substrate was treated as rigid.

If Misfit strain is insufficient to achieve coincidence of the vectors, or the energy considerations favour some other coincidence, the absolute misfit

$$\delta\mathbf{q} = \mathbf{q}_a - \mathbf{q}_b \ ,$$

or beat wave vector, becomes the propagation vector of the misfit dislocation lines. The wavelength, $\lambda_D = 2\pi/|\delta\mathbf{q}|$, is the spacing of dislocations, while $\delta\mathbf{q}$ is perpendicular to the dislocation lines, so giving their orientation. The components of the beat vector, δq_1 , δq_2 define the line sense of the dislocation array, as components $[\delta q_2 \ , \ -\delta q_1]$, or as intercepts on the lattice directions, $1/\delta q_1$, $1/\delta q_2$, analogous to the construction of the Miller indices of crystallographic planes from the reciprocal lattice vector normal to the plane.

The nature of the dislocations is determined from the reference vector,

$$\mathbf{q}_r = \tfrac{1}{2}(\mathbf{q}_a + \mathbf{q}_b) \ ,$$

which in its turn provides a Burgers vector, in terms of the reference lattice with the vectorial harmonic mean spacing of the two wave vectors. This Burgers vector is given as

$$\mathbf{B}_M = 2\pi \ \mathbf{q}_r/|\mathbf{q}_r|^2 \ .$$

The misfit dislocation array is pure *screw* if $\mathbf{q}_r \perp \delta\mathbf{q}$, and pure *edge* if $\mathbf{q}_r \parallel \delta\mathbf{q}$. Alternative choices of Burgers vector are of course valid when useful and may be chosen as the vectors

$$\mathbf{B}_a = 2\pi \ \mathbf{q}_a/|\mathbf{q}_a|^2 \qquad \text{or} \qquad \mathbf{B}_b = 2\pi \ \mathbf{q}_b/|\mathbf{q}_b|^2 \ ,$$

although neither of these choices provides the nature of the dislocations as conveniently as $\mathbf{B}_M$, which must therefore be considered a *natural* choice.

The qualitative criterion that if the beat wavelength λ_D is only a few atomic spacings, very little relaxation is possible leads to a

distinction between the accommodation of the misfit by Misfit Vernier for short wavelengths, and by Misfit dislocations when this spacing is several atomic spacings.

The periodic distortions associated with misfit dislocations can be observed in diffraction experiments, and this description is compatible with the interpretation of RHEED results obtained by Gradmann (1964) and the more recent LEED results of Gradmann and Waller (1982). These beat wave vectors have been observed directly in the diffraction patterns of the second paper. The correspondence of the reciprocal lattice maps and diffraction patterns should make this description particularly useful in the analysis of experimental systems. Multiple scattering however yields similar diffraction patterns.

This description, together with a detailed map of the reciprocal lattices of the overgrowth and substrate have been applied to the study of the interfacial dislocation structure of the bcc{110}-fcc{111} interface which forms the major model system. The interfacial structure is actually obtained from the Finite Element description which seeks to minimize the total interfacial energy by a force balance across the interface.

This treats the overgrowth as an elastic continuum, and the adatom-substrate interaction as a periodic force field active at the positions of the overgrowth interfacial atoms. The force field arises from the adatom-substrate interaction potential originally expressed as a (truncated) Fourier series. The elastic continuum is discretized into small regions, each containing about 8 atoms, and across which the displacement varies as a bi-quadratic polynomial with 9 constant coefficients.

The two approaches, the energy minimizing, or force balance, numerical Finite Element technique, and the purely structural considerations of the reciprocal lattice approach agree in their structural content, and together form a powerful tool in the

prediction, from energy principles on the one hand, and interpretation on the other hand, of the behaviour and structure of the interface of incommensurate structures.

These methods were applied to the bcc{110}/fcc{111} interface with the bcc island in the overgrowth position. The existence of misfit dislocations or verniers and their nature coexisting with misfit strain could be both predicted and explained consistently in the two descriptions. The effect of the anisotropy of the elastic constants was studied explicitly, and was shown to be considerable, particularly for systems intermediate between the ideal Kurdjumov-Sachs and Nishiyama-Wassermann nearest neighbour ratios.

A speculative discussion on the effect of a thickening overgrowth island, and the transition from an initally preferred Nishiyama-Wassermann orientation, to the situation in which the Kurdjumov-Sachs orientation is preferable was given.

The inherent difference in nature, first introduced in Chapter 4, between the first, which is the same orientation as the pseudomorphic, or two-dimensionally coherent configuration, and the second which differs in orientation by about 5.26° , was extended to include the difference in the interfacial structure between the two configurations. A Kurdjumov-Sachs preferred system ($r \simeq r_{KS}$) can occur in the Nishiyama-Wassermann orientation with misfit dislocations in the interface, associated with lowered misfit energy. However, a Nishiyama-Wassermann system ($r \simeq r_{NW}$) in the Kurdjumov-Sachs orientation is inherently poorly matched, and accomodates the misfit with several misfit verniers particularly in the low order periodicities associated with dominant Fourier terms in the misfit energy. The implication is that while the misfit of materials close to the Kurdjumov-Sachs nearest neighbour ratio can exist with low energy misfit in the Nishiyama-Wassermann orientation, the reverse is not true. It is reasonable therefore to expect systems which show poorly defined Kurdjumov-Sachs

orientations, and possibly the simultaneous existence of some sharp Nishiyama-Wassermann orientations. (Bruce and Jaeger 1978 a,b, Gaigher and van der Berg 1987). Less likely is a poorly defined Nishiyama-Wassermann orientation with sharp Kurdjumov-Sachs orientation.

An overview of the progression from the simplest rigid model to the dislocation treatment of these incommensurate structures is left to the following, concluding chapter.

CHAPTER 6

CONCLUSION

In this concluding chapter the successes achieved with the combined approach of the direct energy minimization and the reciprocal lattice techniques are highlighted.

The development of the reciprocal lattice formulation from an epitaxial criterion for ideal, inherently rigid, epitaxial configurations to a formulation which can predict and describe the accommodation of misfit fully in terms of misfit strain and interfacial misfit dislocations or misfit verniers, where applicable, is briefly summarized.

Some of the results applicable to the epitaxial systems with the three-fold symmetrical substrates considered here are put into context with the general considerations.

The possible application of the reciprocal lattice formulation in three-dimensional rather than surface form concludes the chapter.

CHAPTER 6

CONCLUSION

The preceding chapters have seen the development of a general description of the epitaxy of thin films with any crystalline symmetry on substrates of any crystal symmetry. Energy considerations lead directly to a criterion for the existence of epitaxial configurations in terms the reciprocal lattices of the overgrowth and the substrate crystals.

Ideal Epitaxial Configurations were defined (van der Merwe 1982, Chapter 3 here) as those combinations of lattice parameters or ratio of nearest neighbour distances, and azimuthal orientation, which minimize the misfit energy for rigid overgrowth and substrate, for a given pair of surface structures. Usually the definition refers to infinitely wide overgrowth and substrate. These ideal configurations occur when a pair of reciprocal lattice vectors of the substrate and overgrowth coincide in length and orientation. This criterion is analogous to the Laue criteria in diffraction theory (Busch and Schade 1976), and leads to a geometrical realization as a construction analogous to that of Ewald.

In terms of the construction, as generalized from initially rigid systems, the misfit strain necessary to achieve epitaxial matching, but subject to the constraint of minimum energy, could be derived from the reciprocal lattice, and a simple, closed expression for this homogeneous strain was found. Also derived were the strains and rotations necessary to achieve two-dimensional coherent matching of an elastically deformable overgrowth and rigid substrate. Parallel to the reciprocal lattice description, the strains were also calculated by direct numerical minimization of the total interfacial energy, defined for the purpose as the sum of the misfit and strain energies. The numerical minimization was performed on an overgrowth of finite lateral extent, while the analytical results were obtained for an infinite overgrowth. The effects of the finite nature of the overgrowth island were

emphasized with this parallel approach, by direct comparison of the strains, and the resulting structures as seen in the reciprocal lattice.

The effect of local strain in the further reduction of the interfacial energy was examined by a numerical Finite Element technique, applied to the islands which had been allowed to reduce their energy by misfit strain, if this was favourable. The atomic structure of the interface was obtained directly from the Finite Element analysis. This structure was analyzed in terms of a generalized description of misfit dislocations (or Misfit Vernier) obtained in the reciprocal lattice. The dislocation spacing, direction, line sense and Burgers vectors were all derived analytically and compared to the numerical results, which served to emphasize the power of the reciprocal lattice description by the agreement and ease of use.

Explicitly, the effect of anisotropy of the elastic constants was studied for all the strained cases, and the energy and phase diagrams of Chapter 4, with the energy and structural diagrams of Chapter 5 (figures 4.3-6 and 5.8-12 respectively) illustrate the effects very clearly. The extent of the pseudomorphic phase as a function of the ratio, $r = b_{nn}/a_{nn}$, of nearest neighbour distances of the overgrowth and substrate lattices respectively is influenced strongly by the anisotropy. This phase only occurs at a single orientation, that of the Nishiyama-Wassermann configuration, (Bruce *e.a.* 1977, 1978, Nishiyama 1934, Wassermann 1933), - or its symmetrically equivalent realizations - in the bcc{110}/fcc{111} model system studied here.

Also, the inherent difference in properties of the two dominant configurations of the bcc{110}/fcc{111} model system, namely the Nishiyama-Wassermann and the Kurdjumov-Sachs (Bruce and Jaeger 1977, 1978, Olsen and Jesser 1971, Kurdjumov and Sachs, 1930) orientations were analyzed. These are both configurations in which atomic rows match coherently in a direction perpendicular to the atomic rows, and are thus one-dimensionally coherent configurations. It was found that where misfit is accommodated by

misfit strain, the orientation angle of the Kurdjumov-Sachs configuration for systems which do *not* have the exact nearest neighbour ratio of the ideal configurations is strongly dependent on the elastic constants, and the anisotropy ratio in particular. The magnitude of this deviation from the ideal angle naturally depends on the strength of the binding between the overgrowth and substrate as well, but may be as much as 3° for metal-metal systems with a large anisotropy ratio. The orientational angle for the Nishiyama-Wassermann configuration remains at the ideal angle, θ_{NW}.

Structurally, a large deviation from the optimal Kurdjumov-Sachs angle towards the Nishiyama-Wassermann orientation by systems which normally align as Kurdjumov-Sachs is accommodated by networks of screw and edge *dislocations*, which are widely spaced and allow the development of large regions of good fit. For systems which normally align as Nishiyama-Wassermann, deviation towards the Kurdjumov-Sachs orientation results in the formation of Misfit Verniers, expensive as far as misfit energy is concerned, as regions of good fit remain small. (Chapter 5, Table 5.5, figures 5.11-12)

Also relevant is that the Kurdjumov-Sachs orientation deviates from the pseudomorphic orientation. This means that if a system grew pseudomorphically at first (Matthews and Jesser 1969, Olsen and Jesser 1971), and then as it thickened the optimal one-dimensional coherent configuration was the Kurdjumov-Sachs configuration, the overgrowth needed to rotate to reduce the misorientation. This type of reorientation of thickening films has been observed directly by Olsen and Jesser (1971). That reorientation is necessary, and probably requires an activation energy, (Bruce *e.a.* 1978 *b*) will result in a spread of orientations between the pseudomorphic orientation and the Kurdjumov-Sachs angle. This spread, which reduced when the temperatures were higher, possibly providing the activation energy, has been observed by Gaigher and van der Berg (1987). If the overgrowth is prevented from rotating, the misorientation must be accommodated by screw dislocation or vernier arrays. A system which transforms to the Nishiyama-Wassermann

misorientation must be accommodated by screw dislocation or vernier arrays. A system which transforms to the Nishiyama-Wassermann configuration however, does not have an orientational misfit thereafter, yielding edge dislocation networks if insufficient energy for homogeneous strain is available.

Also possible, but a small effect, is the direct transition from a two-dimensionally coherent phase to an incoherent, dislocated phase without the transition to a one-dimensionally coherent phase. This relies on a large anisotropy ratio, for systems for which neither one-dimensional configuration is ideal, and each is equally distant, energetically. Such a transition can be seen in the phase diagram figure 4.6 *c*. Again, such a system would be found more frequently in the Nishiyama-Wassermann orientation, because its angle is the same as the pseudomorphic two-dimensional phase.

In several cases, dislocation networks of screw, mixed, including 60°, dislocation or vernier networks were found to contribute to the misfit accommodation. (Refer to Table 5.5, and the discussion of the results of Chapter 5.). This means that periodic strain fields are introduced into the overgrowth, and the wave vectors corresponding to these dislocations are observable with diffraction techniques. As this wave vector is given by the difference between nearby overgrowth and substrate reciprocal lattice vectors (Chapter 5, figures 5.7) which are relatively close together, a fine structure around the reciprocal lattice positions contributing to the epitaxy may be observed. Gradmann and Waller (1982) have observed this directly in LEED diffraction patterns, as has Gradmann (1964) in RHEED observations. This interpretation is limited by multiple scattering effects, although the secondary diffraction spots may be distinguishable from intensity considerations.

The energy based models all involve an adatom-substrate interaction potential which was expressed as a truncated Fourier series, with wave vectors selected from the infinite set of the substrate reciprocal lattice. The choice of Fourier coefficients and their

relative magnitudes, the number of terms retained from the infinite series expression, the corrections for asymmetry of the actual atomic arrangement and stacking fault effects by using structure factors or secondary series, are all dictated by the features which one wishes to retain in the model. The final form of the series and magnitudes are discussed at length in Chapter 2.

The ideal epitaxial configurations were predicted from the purely rigid overgrowth model, in Chapter 3, and are tabulated in Table 3.5 and 3.6 for the bcc{110}/fcc{111} system, and in Table 3.2 and 3.3 for the fcc{111}/fcc{111} system. Also in Chapter 3, the reciprocal lattice formulation of the epitaxial criteria and the geometrical realization in the Ewald construction were derived.

In Chapter 4 the misfit strain, and rotation, necessary to achieve coherency for non-ideal systems, both one-dimensional and two-dimensional are obtained for the bcc{110}/fcc{111} system, the former as the overgrowth. It is here that anisotropy plays an important role. The elastic constants with the three anisotropy ratios used, ½, 1 and 5, designed in such a way that any effects are in fact due to the anisotropy are given in Table 4.1. Both analytical expressions derived from the reciprocal lattice criterion, and direct numerical minimization of interfacial energy were employed in this chapter, and the results were given in Tables 4.3-5.

With the overgrowth being allowed to strain to energetically optimal amounts, (possibly this means no strain), the effect of relaxation about "Minimum Strain" or O-lattice regions (Frank 1950, Bollmann 1970) was treated in Chapter 5, with a numerical implementation of the Finite Element technique. This produced the positions of the interfacial atoms, and the energies involved. The interfacial misfit structures, dislocation arrays or misfit verniers were obtained from the reciprocal lattice, and compared with the interfacial maps produced by the Finite Element techniques to interpret the latter. This comparison was possible after generalized expressions for misfit accommodation were obtained in

terms of the reciprocal lattice. Both interface structures (figures 5.11) and diagrams illustrating the energy behaviour of the misfit accommodation, pure vernier (rigid), misfit strain, and misfit dislocations were obtained and are shown in figures 5.8-10.

As the misfit strain could be predicted from the reciprocal lattice, (Chapter 4), as well as the dislocation arrays which accommodate the remaining misfit, (Chapter 5) the power of the reciprocal lattice formulation of the epitaxy problem has been adequately demonstrated. The convenience of numerical solution of the energy balance problems, from the rigid model, through the homogeneous strain to Finite Element -local strain- model has provided a useful adjunct to the idealised reciprocal lattice description. Conversely, the reciprocal lattice formulation has proved an almost indispensible tool during interpretation of the numerical results. The two approaches, used in parallel, have been shown to form a powerful, versatile and convenient combination.

The reciprocal lattice formulation of the epitaxial problem has been applied to two-dimensional substrates and overgrowths, or at least to systems with flat interfaces, and islands without strain gradients in the third, vertical direction. A three-dimensional generalization is straightforward, and would be able to describe the misfits and their accommodation in systems with essentially three-dimensional nature. Examples are the cases of Burgers vectors pointing out of the interface, as observed by Matthews (1966), Matthews and Jesser (1967), (refer to the reviews by Matthews 1975, 1979), in thicker overgrowths. Stepped interfaces, (Shiflet and van der Merwe 1986) should also be amenable to the further development of this approach.

REFERENCES

Abramowitz, M., Stegun, I.A., 1965, *Handbook of Mathematical Functions*, Dover Publications, New York

Amelinckx, S., 1979, *Dislocations in Solids*, Vol. 2, ed. F.R.N. Nabarro, North-Holland, Amsterdam, 67

Ashcroft, N.W., Mermin, N.D., 1975, *Solid State Physics*, Holt, Rhinehart and Winston

Auret, F.D., van der Merwe, J.H., 1974, *Thin Solid Films*, **23**, 257

Auret, F.D., van der Merwe, J.H., 1975, *Thin Solid Films*, **27**, 329

Ayrault, G., 1973, *Coordinated Science Lab. Rep. R-631*, University of Illinois, Urbana-Champaign

Ayrault, G., Ehrlich, G., 1974, *J. Chem. Phys.*, **60**, 281

Bacigalupi, R.J., Neustadter, H.E., 1970, *Surf. Sci.*, **19**, 396

Ball, C.A.B., 1970, *Phys. Stat. Sol.*, **42**, 357

Ball, C.A.B., van der Merwe, J.H., 1970, *Phys. Stat. Sol.*, **38**, 335

Bassett, D.W., 1973, *Surface and Defect Properties of Solids*, eds. M.W. Roberts and M.J. Thomas, Vol. 2, The Chemical Society, London

Bassett, D.W., Parsley, M.J. 1970, *J. Phys.* D, **3**, 707

Bassett, D.W., Webber, P.R., 1978, *Surf. Sci.*, **70**, 520

Batra, I.P., 1984, *Phys. Rev.* B **29**, 7108

Bauer, E., 1982, *Appl. Surf. Sci.*, **11/12**, 479

Bauer, E., Poppa, H., 1972, *Thin Solid Films*, **12**, 167

Bauer, E., Poppa, H., Todd, G., Davis, P.R., 1977, *J. Appl. Phys.*, **48**, 3773

Bauer, E., van der Merwe, J.H., 1986, *Phys. Rev.* B, **33**, 3657

Bilby, B.A., Bullough, R., Smith, E., 1955, *Proc. Roy. Soc.* A, **231**, 263

Bilby, B.A., Bullough, R., de Grinberg, D.K., 1964, *Disc. Faraday Soc.*, **38**, 61

Bollmann, W., 1967 a, *Phil. Mag.*, **16**, 363

Bollmann, W., 1967 b, *Phil. Mag.*, **16**, 383

Bollmann, W., 1970, *Crystal Defects and Crystalline Interfaces*, Springer Verlag, Berlin

Born, M., Huang, K., 1954, *Dynamical Theory of Crystal Lattices*, Oxford

Brooks, H., 1952, *Metal Interfaces*, Amer. Soc. Metals, 20

Bruce, L.A., Jaeger, H., 1977, *Phil. Mag.*, **36**, 1331

Bruce, L.A., Jaeger, H., 1978 a, *Phil. Mag.*, **37**, 337

Bruce, L.A., Jaeger, H., 1978 b, *Phil. Mag.*, **38**, 223

Busch, G., Schade, H., 1976, *Lectures on Solid State Physics*, Pergamon Press, Oxford

Carey, G.F., Oden, J.T., 1983, *Finite Elements, A Second Course*, Vol. II, Prentice-Hall, New Jersey

de Bono, E., 1967, 1977, *The Use of Lateral Thinking*, Pelican Books, Penguin, Middlesex

Davies, A.J., 1980, *The Finite Element Method, A First Approach*, Clarendon Press, Oxford

Ehrlich, G., Stolt, K., 1980, *Ann. Rev. Phys. Chem.*, **31**, 603

Fletcher, N.H., 1964, *J. Appl. Phys.*, **35**, 234

Fletcher, N.H., Adamson, P.L., 1966, *Phil. Mag.*, **14**, 99

Fletcher, N.H., Lodge, K.W., 1975, *Epitaxial Growth*, Part B, ed. J.W. Matthews, Academic Press, New York, 529

Forty, A.J., 1983, *Contemp. Phys.*, **24**, 271

Frank, F.C., 1950, *Conf. Plastic Deformation of Crystalline Solids*, Pittsburgh, 150
Frank, F.C., van der Merwe, J.H., 1949 a, *Proc. Roy. Soc. A*, **198**, 205
Frank, F.C., van der Merwe, J.H., 1949 b, *Proc. Roy. Soc. A*, **198**, 216
Frank, F.C., van der Merwe, J.H., 1950 a, *Proc. Roy. Soc. A*, **200**, 125
Frank, F.C., van der Merwe, J.H.,.1950 b, *Proc. Roy. Soc. A*, **201**, 261
Frenkel, J., Kontorowa, T., 1938, *Phys. Z. Sowjet.*, **13**, 1
Friedel, F.C., 1926, *Leçons de Cristallografie*, Berger Levrault, Paris
Gaigher, H.L., van der Berg, N.J., 1987, *Thin Solid Films*, **146**, 299
Goldstein, H., 1950, *Classical Mechanics*, Addison-Wesley, Reading, Massachusetts
Gotoh, Y., Arai, I., 1986, *Japan. J. Appl. Phys.*, **25**, L583
Gotoh, Y., Uwaha, M., 1987, *Japan. J. Appl. Phys.*, **26**, L17
Gradmann, U., 1964, *Physik Kondenzierten Mater.*, **3**, 91
Gradmann, U., Waller, G., 1982, *Surf. Sci.*, **116**, 539
Graham, W.R., Ehrlich, G., 1974, *Surf. Sci.*, **45**, 530
Halicioglu, I., Pound, G.M., 1979, *Thin Solid Films*, **57**, 241
Heinish, H.L., Jr., Sines, G., 1976, *Phil. Mag.*, **34**, 945
Hirth, J.P., Lothe, J., 1968, *Theory of Dislocations*, McGraw-Hill, New York
IMSL, 1980, *International Mathematical and Statistical Library*, Houston
Iverson, P.A., 1969, *Finite Element Methods in Stress Analysis*, eds. I Holand, K. Bell, Tapir, Trondheim, 97
Jesser, W.A., 1973, *Phys. Stat. Sol. a*, **20**, 63
Jesser, W.A., Kuhlmann-Wilsdorf, D., 1967 a, *Phys. Stat. Sol.*, **19**, 95
Jesser, W.A., Kuhlmann-Wilsdorf, D., 1967 b, *Phys. Stat. Sol.*, **21**, 533
Jesser, W.A., Matthews, J.W., 1967, *Phil. Mag.*, **15**, 1096
Jesser, W.A., Matthews, J.W., 1968 a, *Phil. Mag.*, **17**, 461
Jesser, W.A., Matthews, J.W., 1968 b, *Phil. Mag.*, **17**, 475
Jesser, W.A., Matthews, J.W., 1968 c, *Phil. Mag.*, **17**, 595
Kelly, A., Groves, G.W., 1973, *Crystallography and Crystal Defects*, Longman's, London
Kenty, J.L., 1975, *Thin Solid Films*, **26**, 181
Kishino, S., Ogirima, M., 1975, *Phil. Mag.*, **31**, 1239
Kittel, C., 1966, *Introduction to Solid State Physics*, 3rd Edition, John Wiley and Sons, New York
Kotzé, I.A., Lombaard, J.C., Henning, C.A.O., 1974, *Thin Solid Films*, **23**, 221
Kuk, Y., Feldman, L.C., Silverman, P.J., 1983, *Phys. Rev. Lett.*, **50**, 511
Kurdjumov, G., Sachs, G., 1930, *Z. Phys.*, **64**, 325
Lodge, K.W., 1970, *Structure and Energy of Crystal Interfaces*, M.Sc. Thesis, University of New England
Mackenzie, J.K., 1950, *Proc. Phys. Soc.* A, **LXIII**, 1370
Matthews, J.W., 1966, *Phil. Mag.*, **13**, 1207
Matthews, J.W., 1967, *Physics of Thin Films*, **4**, 137

Matthews, J.W., 1972, *Surf. Sci.*, **31**, 241
Matthews, J.W., 1974, *Phil. Mag.*, **29**, 797
Matthews, J.W., 1975, *Epitaxial Growth* Part B, ed. J.W. Matthews, Academic Press, New York, 559
Matthews, J.W., Jesser, W.A., 1969, *Phil. Mag.*, **20**, 999
Nabarro, F.R.N., 1947, *Proc. Phys. Soc.*, **59**, 256
Nabarro, F.R.N., 1967, *Theory of Crystal Dislocations*, Oxford
Nabarro, F.R.N., 1970, *Phil. Mag.* **178**, 803
Nishiyama, Z., 1934, *Sci. Rep. Res. Insts. Tôhoko Univ*, **23**, 637
Norrie, D.H., de Vries, G., 1973, *The Finite Element Method*, Academic Press, New York
Novaco, A.D., McTague, J.P., 1977, *Phys. Rev. Lett.*, **38**, 1286
Olsen, G.H., Jesser, W.A., 1971, *Acta Metall.*, **19**, 1009
Ramirez, R., Rahman, A., Schuller, I.K., 1984, *Phys. Rev.*, **30**, 6208
Reiss, H., 1968, *J. Appl. Phys.*, **39**, 5045
Ranganathan, S., 1966, *Acta Crystall.*, **21**, 197
Schlenk, W., Bauer, E., 1980, *Surf. Sci.*, **93**, 9
Shiflet, G.J., van der Merwe, J.H., 1986, *S. A. J. P.*, **9**, 31
Snyman, J.A., van der Merwe, J.H., 1974 a, *Surf. Sci.*, **42**, 190
Snyman, J.A., van der Merwe, J.H., 1974 b, *Surf. Sci.*, **45**, 619
Snyman, J.A., Snyman, H.C., 1981, *Surf. Sci.*, **105**, 357
Spiegel, M.R., 1963, *Advanced Calculus*, Schaum Outline Series, McGraw-Hill, New York
Spiegel, M.R., 1974, *Vector Analysis*, Schaum Outline Series, McGraw-Hill, New York
Steele, W.A., 1973, *Surf. Sci.*, **36**, 317
Stoop, L.C.A., van der Merwe, J.H., 1982 a, *Thin Solid Films*, **91**, 257
Stoop, L.C.A., van der Merwe, J.H., 1982 b, *Thin Solid Films*, **98**, 65
Stoop, L.C.A., van der Merwe, J.H., 1982 c, *Thin Solid Films*, **94**, 341
Stoop, P.M., 1986, *Computed Fourier Series Representations of the interaction potential of an Argon atom on an Argon Crystal Surface*, M.Sc. Thesis, University of Pretoria
Stoop, P.M., Snyman, J.A., 1987, *Thin Solid Films, Accepted for Publication*
Strozier, J.A., 1975, *Surface Physics of Materials*, Vol. I, ed. J.M. Blakely, Academic Press, New York, 1
Takayanagi, K., Yagi, K., Honjo, G., 1978, *Thin Solid Films*, **48**, 137
Timoshenko, S., Goodier, J.N., 1970, *Theory of Elasticity*, 3rd Edition, McGraw-Hill, New York
van der Merwe, J.H., 1950, *Proc. Phys. Soc. (London)*, A **63**, 616
van der Merwe, J.H., 1950, *Proc. Phys. Soc. (London)*, A **63**, 1370
van der Merwe, J.H., 1963 a, *J. Appl. Phys.*, **34**, 117
van der Merwe, J.H., 1963 b, *J. Appl. Phys.*, **34**, 123
van der Merwe, J.H., 1964, *Proc. Single Crystal Films, Pennsylvania, May 1963*, eds. H.H. Francombe, H. Sato, Pergamon Press, Oxford, 139.
van der Merwe, J.H., 1966, *Proc. Basic Problems in Thin Films*, eds. R. Niedermayer, H. Mayer, Vandenhoeck and Ruprecht, Göttingen, 122
van der Merwe, J.H., 1973, *Treatise on Materials Science and Technology*, Vol. 2, ed. H. Herman, Academic Press, New York, 1

van der Merwe, J.H., 1978, *CRC Crital Reviews in Solid State and Material Science*, *209*
van der Merwe, J.H., 1979, *Proc. Chemistry and Physics of Solid Surfaces*, ed. R. Vanselow, CRC Press, Baco Raton, Florida, 129
van der Merwe, J.H., 1980, *Thin Solid Films*, **74**, 129
van der Merwe, J.H., 1982 a, *Phil. Mag.*, **45**, 127
van der Merwe, J.H., 1982 b, *Phil. Mag.*, **45**, 145
van der Merwe, J.H., 1982 c, *Phil. Mag.*, **45**, 159
van der Merwe, J.H., Ball, C.A.B., 1975, *Epitaxial Growth*, Part B, ed. J.W. Matthews, Academic Press, New York, 493
van der Merwe, J.H., Braun, M.W.H., 1985, *Appl. Surf. Sci.*, **22/23**, 545
van der Merwe, J.H., Braun, M.W.H., 1987, (*Proc. Interfaces, Lattices, and Thin Films*, Dec. 1986, Boston Mass), *Mat. Res. Soc. Symp. Proc.*, vol **77**, ed. J.D. Dow and I.K. Schuller, Materials Research Society, p 133
Venables, J.A., Schabes-Retchkiman, P.S., 1978, *Surf. Sci.*, **71**, 27
Venables, J.A., Spiller, G.D.T., Hanbücken, M.,1984, *Rep. Prog. Phys.*, **47**, 399
Vook, R.W., 1982, *Intl. Metals Revs.*, **27**, 209
Wassermann, G., 1933, *Arch. Eissenhüttenw.*, **16**, 647
Waterman, P.C., 1959, *Phys. Rev.*, **113**, 1240
Wetzel, J.T., Machlin, E.S., 1984, *Surf. Sci.*, **144**, 124
Yagi, K., Takayanagi, K., Kobayashi, K., Honjo, G., 1976, *Thin Solid Films*, **32**, 185
Zienkiewicz, O.C., 1971, *The Finite Element Method in Engineering Science*, McGraw-Hill, New York

APPENDIX A

TRANSFORMATIONS

Listed here are the transformations, transformation parameters and identities relevant to the rigid and strained island models of Chapters 3, 4 and 5. Several transformations are given, in particular those relating the overgrowth and substrate crystallographic (skew) axes, as well as the relationship between these coordinates and cartesian coordinates referred to either substrate or overgrowth systems. Quantities in the substrate coordinates are indicated by a - symbols, and the overgrowth by b - symbols.

The crystallographic coordinates are defined in terms of lengths, angles, relative orientation and displacements. The lengths, in turn, are referred to single scaling parameters, a_{nn} and b_{nn}, usually chosen as the distance between nearest neighbour lattice sites or atoms. The ratio between these is used as a central parameter in the discussion of epitaxy, $r = b_{nn}/a_{nn}$.

The lengths are $a_1 = |\mathbf{a}_1| = c_1 a_{nn}$, $a_2 = |\mathbf{a}_2| = c_2 a_{nn}$ in the substrate and $b_1 = |\mathbf{b}_1| = d_1 b_{nn}$, $b_2 = |\mathbf{b}_2| = d_2 b_{nn}$ in the overgrowth. The angle α is the anti-clockwise angle between $\mathbf{a}_1$ and $\mathbf{a}_2$, while β is the equivalent angle in the overgrowth.

The angle θ gives the relative orientation of the two coordinate systems, and is the angle between $\mathbf{a}_1$ and $\mathbf{b}_1$, while the vector $\mathbf{r}_0 = x_0\mathbf{a}_1 + y_0\mathbf{a}_2$ gives the relative displacement of the origin of the overgrowth coordinate system.

Transformations between overgrowth and substrate quantities:

Overgrowth quantities in terms of the substrate:

$$\mathbf{b}_1 = r_{11}c_\theta \mathbf{a}_1 + r_{12}s_\theta \mathbf{a}_2 \quad , \quad x_b = (x_a - x_0)\frac{D_\theta}{r_{11}} + (y_a - y_0)\frac{T_{\theta\alpha}}{r_{12}}$$

$$\mathbf{b}_2 = r_{21}s_{\theta\beta}\mathbf{a}_1 + r_{22}c_{\theta\beta}\mathbf{a}_2 \quad , \quad y_b = (x_a - x_0)\frac{T_\theta}{r_{21}} + (y_a - y_0)\frac{D_{\theta\alpha}}{r_{22}} \quad . \quad \text{A1}$$

Conversely, substrate quantities in terms of the overgrowth are:

$$\mathbf{a}_1 = \frac{D_\theta}{r_{11}}\mathbf{b}_1 + \frac{T_\theta}{r_{21}}\mathbf{b}_2 \quad , \quad x_a = x_b r_{11}c_\theta + y_b r_{21}s_{\theta\beta} + x_0$$

$$\mathbf{a}_1 = \frac{T_{\theta\alpha}}{r_{12}}\mathbf{b}_1 + \frac{D_{\theta\alpha}}{r_{22}}\mathbf{b}_2 \quad , \quad y_a = x_b r_{12}s_\theta + y_b r_{22}c_{\theta\beta} + y_0 \quad . \quad \text{A2}$$

In these and subsequent transformations the transformation parameters are:

ratios:

$$r_{ij} = \frac{b_i}{a_j} = \frac{d_i}{c_j} r \quad , \text{ where } i,j = 1, 2 \ , \qquad \text{A3}$$

angular parameters:

$$c_\theta = \sin(\alpha-\theta)/\sin\alpha \quad , \quad s_\theta = \sin\theta/\sin\alpha$$
$$s_{\theta\beta} = \sin(\alpha-\beta-\theta)/\sin\alpha \quad , \quad c_{\theta\beta} = \sin(\beta+\theta)/\sin\alpha \ . \qquad \text{A4}$$

Substrate reciprocal lattice vectors are defined in terms of the 2-dimensional substrate lattice as:

$$\mathbf{a}_1^* = \frac{2\pi\ \mathbf{a}_2 \times \mathbf{n}}{\mathbf{n}\cdot(\mathbf{a}_1 \times \mathbf{a}_2)} \qquad \text{and} \qquad \mathbf{a}_2^* = \frac{2\pi\ \mathbf{n} \times \mathbf{a}_1}{\mathbf{n}\cdot(\mathbf{a}_1 \times \mathbf{a}_2)}$$

$$\text{with } \mathbf{n} = \frac{\mathbf{a}_1 \times \mathbf{a}_2}{|\mathbf{a}_1 \times \mathbf{a}_2|} \quad \text{the unit vector normal to } \mathbf{a}_1 \text{ and } \mathbf{a}_2 \ . \qquad \text{A5}$$

Overgrowth reciprocal vectors are similarly defined.

Transformations relating the reciprocal sets are given by:

$$\mathbf{a}_1^* = r_{11}c_\theta\ \mathbf{b}_1^* + r_{21}s_{\theta\beta}\ \mathbf{b}_2^* \quad , \ h = p\frac{D_\theta}{r_{11}} + q\frac{T_\theta}{r_{21}}$$
$$\mathbf{a}_2^* = r_{12}s_\theta\ \mathbf{b}_1^* + r_{22}c_{\theta\beta}\ \mathbf{b}_2^* \quad , \ k = p\frac{T_{\theta\alpha}}{r_{12}} + q\frac{D_{\theta\alpha}}{r_{22}} \qquad \text{A6}$$

and

$$\mathbf{b}_1^* = \frac{D_\theta}{r_{11}}\ \mathbf{a}_1^* + \frac{T_{\theta\alpha}}{r_{12}}\ \mathbf{a}_2^* \quad , \ p = hr_{11}c_\theta + kr_{12}s_\theta$$
$$\mathbf{b}_2^* = \frac{T_\theta}{r_{21}}\ \mathbf{a}_1^* + \frac{D_{\theta\alpha}}{r_{22}}\ \mathbf{a}_1^* \quad , \ q = hr_{21}s_{\theta\beta} + kr_{22}c_{\theta\beta} \ . \qquad \text{A7}$$

Components of the reciprocal vectors are obtained from the general formula valid for any vector $\mathbf{R}$ in terms of a set of vectors and is reciprocal set defined as in A5, and A8 (below):

$$\mathbf{R} = [(\mathbf{a}_1^*\cdot\mathbf{R})\mathbf{a}_1 + (\mathbf{a}_2^*\cdot\mathbf{R})\mathbf{a}_2]/2\pi = [(\mathbf{a}_1\cdot\mathbf{R})\mathbf{a}_1^* + (\mathbf{a}_2\cdot\mathbf{R})\mathbf{a}_2^*]/2\pi$$

Identities:

From these definitions and transformations it may be confirmed that several identities are satisfied by the various vectors and transformation parameters, i.e.

$$\mathbf{a}_i \cdot \mathbf{a}_j^* = 2\pi\delta_{ij} \quad \text{and} \quad \mathbf{b}_i \cdot \mathbf{b}_j^* = 2\pi\delta_{ij} \;, \; i, j = 1, 2. \qquad \text{A8}$$

The scalar product between a wave vector and a direct-space vector is the same in either coordinate system, and therefore invariant under the transformations, which leads to the identity:

$$[\mathbf{q}\cdot(\mathbf{r}-\mathbf{r}_0)]_a = [\mathbf{q}\cdot\mathbf{r}]_b \qquad \text{A9}$$

where: $\mathbf{q}_a = h\mathbf{a}_1^* + k\mathbf{a}_2^*$, $\mathbf{r}_a = x_a\mathbf{a}_1 + y_a\mathbf{a}_2$, $(\mathbf{r}_0)_a = x_0\mathbf{a}_1 + y_0\mathbf{a}_2$

and: $\mathbf{q}_b = p\mathbf{b}_1^* + q\mathbf{b}_2^*$, $\mathbf{r}_b = x_b\mathbf{b}_1 + y_b\mathbf{b}_2 = \mathbf{r}_a - \mathbf{r}_0$.

The angular transformation parameters satisfy the identities:

$$c_\theta D_\theta + s_\theta T_{\theta\alpha} = 1 = s_{\theta\beta} T_\theta + c_{\theta\beta} D_{\theta\alpha}$$

with $$\frac{r_{11}}{r_{21}} c_\theta T_\theta + \frac{r_{12}}{r_{22}} s_\theta D_{\theta\alpha} = 0 = \frac{r_{21}}{r_{11}} s_{\theta\beta} D_\theta + \frac{r_{22}}{r_{12}} c_{\theta\beta} T_{\theta\alpha} \;. \qquad \text{A10}$$

Cartesian components of the various sets of vectors.

When the reciprocal vectors are actually calculated, it is usual to express some of the vectors in suitable cartesian coordinates.

Two different choices of cartesian systems have proved useful, particularly in the reciprocal lattice formulations of the rigid and strained island models. The first choice of cartesian axes has the $\mathbf{e}_x$ unit vector parallel to the $\mathbf{a}_1$ substrate lattice direction, while in the second choice, the cartesian unit vector is parallel to the overgrowth vector $\mathbf{b}_1$.

Substrate Cartesian coordinates:

$$\mathbf{a}_1 = a_1\mathbf{e}_x = c_1 a_{nn}\,\mathbf{e}_x \quad , \quad \mathbf{a}_2 = a_{2x}\,\mathbf{e}_x + a_{2y}\,\mathbf{e}_y \qquad \text{A11}$$
$$, \quad = a_2\cos\alpha\,\mathbf{e}_x + a_2\sin\alpha\,\mathbf{e}_y$$
$$, \quad = c_2 a_{nn}(\cos\alpha\,\mathbf{e}_x + \sin\alpha\,\mathbf{e}_y)$$

$$\mathbf{a}_1^* = \frac{2\pi}{c_1 a_{nn}}\left[\mathbf{e}_x - \frac{\cos\alpha}{\sin\alpha}\,\mathbf{e}_y\right] \quad , \quad \mathbf{a}_2^* = \frac{2\pi\,\mathbf{e}_y}{c_2\,a_{nn}\sin\alpha} \qquad \text{A12}$$
$$= a_{2y}^*\,\mathbf{e}_y$$

$$\mathbf{b}_1^* = b_{1x}^* \mathbf{e}_x + b_{1y}^* \mathbf{e}_y \quad , \quad \mathbf{b}_2^* = b_{2x}^* \mathbf{e}_x + b_{2y}^* \mathbf{e}_y \qquad \text{A13}$$

$$b_{1x}^* = \frac{D_\theta}{r_{11}} a_{1x}^* + \frac{T_{\theta\alpha}}{r_{12}} a_{2x}^* \quad , \quad b_{2x}^* = \frac{T_\theta}{r_{21}} a_{1x}^* + \frac{D_{\theta\alpha}}{r_{22}} a_{2x}^*$$

$$b_{1y}^* = \frac{D_\theta}{r_{11}} a_{1y}^* + \frac{T_{\theta\alpha}}{r_{12}} a_{2y}^* \quad , \quad b_{2y}^* = \frac{T_\theta}{r_{21}} a_{1y}^* + \frac{D_{\theta\alpha}}{r_{22}} a_{2y}^*$$

$$\mathbf{b}_1 = \frac{2\pi}{b_{1x}^* b_{2y}^* - b_{1y}^* b_{2x}^*} \left[b_{2y}^* \mathbf{e}_x - b_{2x}^* \mathbf{e}_y \right] \qquad \text{A14}$$

$$\mathbf{b}_2 = \frac{2\pi}{b_{1x}^* b_{2y}^* - b_{1y}^* b_{2x}^*} \left[b_{1x}^* \mathbf{e}_y - b_{1y}^* \mathbf{e}_x \right]$$

Overgrowth Cartesian Coordinates:

$$\mathbf{b}_1 = b_1 \mathbf{e}_x = d_1 b_{nn} \mathbf{e}_x \quad , \quad \mathbf{b}_2 = b_{2x} \mathbf{e}_x + b_{2y} \mathbf{e}_y \qquad \text{A15}$$
$$= b_2 \cos\beta \, \mathbf{e}_x + b_2 \sin\beta \, \mathbf{e}_y$$
$$= d_2 b_{nn} (\cos\beta \, \mathbf{e}_x + \sin\beta \, \mathbf{e}_y)$$

$$\mathbf{b}_1^* = \frac{2\pi}{d_1 b_{nn}} \left[\mathbf{e}_x - \frac{\cos\beta}{\sin\beta} \mathbf{e}_y \right] \quad , \quad \mathbf{b}_2^* = \frac{2\pi \, \mathbf{e}_y}{d_2 \, b_{nn} \sin\beta} \qquad \text{A16}$$
$$= b_{2y}^* \mathbf{e}_y$$

$$\mathbf{a}_1^* = a_{1x}^* \mathbf{e}_x + a_{1y}^* \mathbf{e}_y \quad , \quad \mathbf{a}_2^* = a_{2x}^* \mathbf{e}_x + a_{2y}^* \mathbf{e}_y \qquad \text{A17}$$

$$a_{1x}^* = r_{11} c_\theta b_{1x}^* + r_{21} s_{\theta\beta} b_{2x}^* \quad , \quad a_{2x}^* = r_{12} s_\theta b_{1x}^* + r_{22} c_{\theta\beta} b_{2x}^*$$

$$a_{1y}^* = r_{11} c_\theta b_{1y}^* + r_{21} s_{\theta\beta} b_{2y}^* \quad , \quad a_{2y}^* = r_{12} s_\theta b_{1y}^* + r_{22} c_{\theta\beta} b_{2y}^*$$

$$\mathbf{a}_1 = \frac{2\pi}{a_{1x}^* a_{2y}^* - a_{1y}^* a_{2x}^*} \left[a_{2y}^* \mathbf{e}_x - a_{2x}^* \mathbf{e}_y \right] \qquad \text{A18}$$

$$\mathbf{a}_2 = \frac{2\pi}{a_{1x}^* a_{2y}^* - a_{1y}^* a_{2x}^*} \left[a_{1x}^* \mathbf{e}_y - a_{1y}^* \mathbf{e}_x \right]$$

Strains and their effects in direct and reciprocal spaces

Transformation matrices of both direct and reciprocal space are calculable from strains and have been derived in Chapter 4.

The coordinates are the overgrowth linked cartesian coordinates, with $\mathbf{r} = x\mathbf{e}_x + y\mathbf{e}_y$ a general position, and $\mathbf{u} = u_x\mathbf{e}_x + u_y\mathbf{e}_y$ the displacement field. Similar expressions are valid in any cartesian coordinates.

Strains:

$$\varepsilon_x = \frac{\partial u_x}{\partial x} \quad , \quad \varepsilon_y = \frac{\partial u_y}{\partial y} \quad , \quad \gamma_{xy} = \frac{\partial u_x}{\partial y} + \frac{\partial u_y}{\partial x} \qquad \text{A19}$$

Linear transformation in cartesian direct space

$$\mathbf{A} = \begin{bmatrix} \alpha_x & \tfrac{1}{2}\gamma_{xy} \\ \tfrac{1}{2}\gamma_{xy} & \alpha_y \end{bmatrix} = \begin{bmatrix} 1+\varepsilon_x & \tfrac{1}{2}\gamma_{xy} \\ \tfrac{1}{2}\gamma_{xy} & 1+\varepsilon_y \end{bmatrix} \qquad \text{A20}$$

Linear transformation in cartesian reciprocal space

$$\mathbf{A}^* = \begin{bmatrix} \alpha^*_x & \tfrac{1}{2}\gamma^*_{xy} \\ \tfrac{1}{2}\gamma^*_{xy} & \alpha^*_y \end{bmatrix} = \begin{bmatrix} 1+\varepsilon^*_x & \tfrac{1}{2}\gamma^*_{xy} \\ \tfrac{1}{2}\gamma^*_{xy} & 1+\varepsilon^*_y \end{bmatrix} = \frac{1}{(\alpha_x\alpha_y - \frac{1}{4}\gamma^2_{xy})} \begin{bmatrix} \alpha_y & -\tfrac{1}{2}\gamma_{xy} \\ -\tfrac{1}{2}\gamma_{xy} & \alpha_x \end{bmatrix} = \mathbf{A}^{-1} \qquad \text{A21}$$

Distorted lattice parameters:

$$\mathbf{b}'_1 = b_1 \begin{bmatrix} 1+\varepsilon_x \\ \tfrac{1}{2}\gamma_{xy} \end{bmatrix} \quad , \quad \mathbf{b}'_2 = b_2 \begin{bmatrix} (1+\varepsilon_x)\cos\beta + \tfrac{1}{2}\gamma_{xy}\sin\beta \\ \tfrac{1}{2}\gamma_{xy}\cos\beta + (1+\varepsilon_y)\sin\beta \end{bmatrix} \qquad \text{A22}$$

$$b'_1 = |\mathbf{b}'_1| = b_1[(1+\varepsilon^2_x) + \tfrac{1}{4}\gamma^2_{xy}]^{\frac{1}{2}}$$

$$b'_2 = |\mathbf{b}'_2|$$

$$= b_2\{[(1+\varepsilon_x)\cos\beta + \tfrac{1}{2}\gamma_{xy}\sin\beta]^2 + [\tfrac{1}{2}\gamma_{xy}\cos\beta + (1+\varepsilon_y)\sin\beta]^2\}^{\frac{1}{2}}$$

$$\cos\beta' = \mathbf{b}'_1\cdot\mathbf{b}'_2/(b'_1b'_2)$$

Orientation angle: $\theta' = \theta + \delta\theta$ A23

where $\cos\delta\theta = \mathbf{b}'_1\cdot\mathbf{b}_1/(b'_1b_1)$ and $\operatorname{sgn}(\delta\theta) = \begin{cases} +1 & \text{if } \gamma_{xy} \geq 0 \\ -1 & \text{if } \gamma_{xy} < 0 \end{cases}$

Strains from distorted lattice parameters

$$\mathbf{A} = \begin{bmatrix} a_{11} & a_{12} \\ a_{21} & a_{22} \end{bmatrix} = \begin{bmatrix} \frac{b'_1}{b_1}\cos\delta\theta & -\frac{b'_1}{b_1}\cdot\cos\delta\theta\ \cot\beta + \frac{b'_2}{b_2}\cdot\frac{\cos(\beta'+\delta\theta)}{\sin\beta} \\ \frac{b'_1}{b_1}\sin\delta\theta & -\frac{b'_1}{b_1}\cdot\sin\delta\theta\ \cot\beta + \frac{b'_2}{b_2}\cdot\frac{\sin(\beta'+\delta\theta)}{\sin\beta} \end{bmatrix} \qquad \text{A24}$$

with $\delta\theta = \theta'-\theta$.

The strains are then:

$$\begin{aligned} \varepsilon_x &= a_{11}\cos\phi + a_{21}\sin\phi - 1 \\ \varepsilon_y &= a_{22}\cos\phi - a_{12}\sin\phi - 1 \end{aligned} \qquad \text{A25}$$

and $\quad \tfrac{1}{2}\gamma_{xy} = a_{12}\cos\phi + a_{22}\sin\phi = a_{21}\cos\phi - a_{11}\sin\phi$

together with the essential rotation:

$$\tan\phi = \frac{a_{21} - a_{12}}{a_{11} - a_{22}} \qquad \text{A26}$$

Strains in any rotated coordinate system:

Rotate the coordinate system through θ_R the strains become:

$$\begin{aligned} \varepsilon'_x &= \varepsilon_x\cos^2\theta_R + \varepsilon_y\sin^2\theta_R + \tfrac{1}{2}\gamma_{xy}\sin2\theta_R \\ \varepsilon'_y &= \varepsilon_x\sin^2\theta_R + \varepsilon_y\cos^2\theta_R - \tfrac{1}{2}\gamma_{xy}\sin2\theta_R \\ \gamma'_{xy} &= (\varepsilon_y-\varepsilon_x)\sin2\theta_R + \gamma_{xy}\cos2\theta_R \end{aligned} \qquad \text{A27}$$

APPENDIX B

COMPUTER PROGRAMS

Several computer programs were written during the course of this project. The techniques for numerical minimization and solution of the non-linear simultaneous equations used the standard package of programs published by the International Mathematical and Statistical Library Inc. of Houston, Texas, U.S.A., referred to here and in the main text as IMSL. The descriptions of the essential techniques are briefly given in the IMSL manual, which also gives references to the source of the technique. These descriptions, including the references - if any, are repeated here *Verbatim.*

The answers derived from their procedures were tested in several ways, external to the actual routines, and in general were found to be stable and sufficiently precise. Minor changes were made to the program ZXMWD, the constrained minimization routine used in the program HOM3GEN. The changes allowed the subroutine to use an initial guess of the solution which was provided to the subroutine.

As these programs used the licensed subroutines from IMSL they are not listed in this appendix. In the interest of Scientific integrity however, they are available on magnetic tape or listing on request. Necessary licensing arrangements can be made with IMSL, who are usually amenable.

B.1 THE RECIPROCAL LATTICE PROGRAM - ORPHEUS

The reciprocal lattice problem was computerized for convenience, and to enable rapid testing of each development of the reciprocal lattice formulation. The program ORPHEUS was written in BASIC, and the language level used are the instructions common to GWBASIC 2.11

as supplied with MSDOS 2.11 for the Olivetti M24 computer, and BASICA as supplied with PCDOS 3.1 running on the IBM PC/AT - ENHANCED (model 5170). All the reciprocal lattice diagrams are direct printer copies of the computer screen, and these diagrams are modified continually during the execution of the program.

A working version of the program (compiled with Borland's Turbo Basic compiler) is supplied on 5 $\frac{1}{4}$" floppy disk with this book. The user is free to distribute it as he sees fit, but this author requests citation. A more powerful version is under development.

Capabilities:

The progam ORPHEUS manipulates the (surface) reciprocal lattices of the overgrowth and substrate from data supplied by the user in response to questions asked by the program.

Capabilities include interactive selection of reciprocal lattice vectors displayed on the computer screen, and manipulation, comparison of lengths, orientational calculations, strains, rotations, misfit dislocation spacings, Burgers vectors, orientations, line sense components, the strains and rotations needed for pseudomorphism.

The program may be stopped in two ways:

1) Normal ending is achieved by answering YES to the question : Are you finished?

2) Abnormal ending may be achieved by holding down the CTRL key and simultaneously pressing the BREAK key, thus the CTRL-BREAK combination, which immediately stops the program.

The version of ORPHEUS provided uses the IBM colour graphics adapter, or the Olivetti computer screen in 640 X 200 pixels resolution mode, referred to in BASIC as SCREEN 2, as well as the IBM enhanced adapter (ega) in 640 x 350 resolution.

For further information, please contact the author directly. as

Max W.H Braun
Physics Department
University of Pretoria
Pretoria
Republic of South Africa
2000

B.2 THE HOMOGENEOUS STRAIN PROGRAMS - HOM3GEN, HOM3PHAS and HOMSTRAN.

All three programs use the same method and share their major parts.

HOM3GEN:

Purpose This program calculates the homogeneous strains and distorted unit cell parameters which minimize the total interfacial energy defined as the sum of the misfit and strain energies.

Relevant parameters are the size of the overgrowth island as two integers, M and N. (Refer to Chapter 3 and 4 for their meanings.)

As energy minimization is done with the strains ε_x, ε_y and γ_{xy}, only, subject to plane stress boundary conditions no rigid rotation of the overgrowth is allowed. In addition the anisotropy ratio is requested by the program, which modifies the elastic constants to the required anisotropy ratio, as described in Chapter 4.

The minimization uses the constrained minimization routine ZXMWD, from the IMSL package, briefly described below.

Output from the program includes the strains, factors and angles by which the unit cell parameters change due to the strain, as well as the initial and final misfit enrgies, the strain energy and the total energy, all for an island with cubic lattice parameter 2.62Å, the lattice constant of Fe, for the selected orientation and nearest lattice parameter. Required as input are the Anisotropy ratio and the energy calibration factor W, as well as the second order relative amplitude A_{11}/A_{10} of the substrate potential called BLAM, and the stacking fault parameter DELTA.

This program calculates the required values over a range of r and theta which is set internally in the program.

The output is used in the program HOM3DRAW which uses the DISSPLA graphics package to produce the perspective energy diagrams and contours of Chapter 4.

HOMSTRAN, HOMPHAS

These programs are shortened special versions of the program HOM3GEN. The first needs additionally the input of r and theta as it solves the minimization problem only for a single pair. In addition, this program calculates W if the Van der Merwe configurational parameter, ℓ, is given, or calculates ℓ if W is given. The output is used by the finite element program RECLOADX as misfit strain component of the overgrowth misfit accommodation.

HOMPHAS calculates the strains, energies and cell parameters subject to homogeneous strain again as HOM3GEN, but for a range of configurational parameters and nearest neighbour ratios, for the two orientations, 30°, the Nishiyama-WAssermann orientation and 24.74°, the Kurdjumov-Sachs orientation. The output is used by PHASORT, which selects the epitaxial configuration and draws the phase diagrams.

B.3 THE FINITE ELEMENT SUITE

RECSYS:

Purpose Generation and assembly of the stiffness matrices for rectangular elements, using the standard elastic constants.

The program interactively requests the user to input the required anisotropy ratio, and modifies the elastic constants accordingly.

Output from the program are a raw stiffness matrix and a stiffness matrix which conforms to the boundary conditions described in chapter 5, the fixed average strain conditions, as well as the elastic constants and numbers of the degrees of freedom which are fixed.

KLUCOMP:

Purpose LU - decomposition of the bounded stiffness matrix $\mathbf{K}^B$.

This program employs the standard IMSL routine LUDAPB.

Output: The decomposed, bounded stiffness matrix.

RECLOADX:

Purpose Solves the finite element problem with strains input through a disk file.

This program uses the IMSL routine LUELPB to repeatedly solve the linear problem $\mathbf{K}^B\mathbf{U} = \mathbf{F}^B$, yielding $\mathbf{U}$. After each iteration the force matrix $\mathbf{F}^B$ is recalculated, until the linear solution exactly matches the solution to the non-linear problem $\mathbf{K}^B\mathbf{U} = \mathbf{F}^B(\mathbf{U})$. The exact convergence is finally proved by using the IMSL routine LUREPB.

To prevent random oscillation, the problem is treated as a relaxation problem, in which the system is allowed to respond slowly to the force field. Beginning with $\mathbf{U}$, $\mathbf{F}^B$ is calculated and using LUELPB, the new $\mathbf{U}^{(1)}$ is calculated. The displacement direction is determined from $\mathbf{U}^{(1)}-\mathbf{U}$. The distance along this direction that the system is allowed to move is limited by the following techniques:

1) No single degree of freedom may move more than 1/8 of a lattice parameter

2) The total energy for five short steps along the required direction is calculated and the distance which produces the smallest energy is used

3) Every second iteration, only half the step calculated in 2) is taken. This dramatically speeds convergence when the solution is close to finishing, as then the system tends to oscillate from one side of the minimum to the other, in nearly equal amounts. This halving of the step assures monotone convergence, or if the solution is oscillating, very rapid convergence.

The final solution is allowed to step as far as it likes. If no change is perceived within a predetermined number of significant digits when LUREPB has achieved solution, the linearized process has solved the nonlinear problem to the required precision. Most systems considered converged in this way to better than 10 significant digits in all the displacement components.

Output from the program are the nodal displacements, initial misfit energy, initial strain energy of a misfit strained overgrowth, and the final misfit, strain and total energies.

DSPLREC:

Purpose Plotting of the atom positions from the nodal displacements produced by RECLOADX

This program uses the finite element formulation to recreate the interface atom positions of the overgrowth from the nodal displacements. The DISSPLA package is used.

B.4 IMSL ROUTINES USED:

ZXMWD:

Purpose Global minimum (with constraints) of a function of N variables

The constrained minimization problem is equivalent to

$$\underset{(t_1 \ \cdots \ t_n)}{\text{Minimize}} \quad f(a_1+(b_1-a_1)\sin^2 t_1, \ \cdots \ a_n+(b_n-a_n)\sin^2 t_n)$$

where the t_i are now unconstrained. With this transformation, in fact, each possible global minimum, including any on the boundary, is transformed into a local minimum.

ZXMWD calls a modified version of ZXMIN to do about 30 iterations with each of NSRCH starting points generated by ZSRCH. The five which result in the lowest values of the funtion are allowed to continue to convergence. The local minimum found which, of these five, gives the lowest function value is taken to be the global minimum. As NSRCH is increased, the probability that this point is really the global minimum is increased.

See reference:

Box, M.J., *A Comparison of Several Current Optimization Methods and the Use of Transformations in Constrained Problems*, Computer Journal **9**, 1966, 67 - 77.

ZXMIN

Purpose Minimum of a function of N variables using a quasi-Newton method.

ZXMIN is based on Harwell Library Routine VA10A. It uses a quasi-Newton method to find the minimum of a function f(x) of N variables $x = (x_1, x_2, \ldots, x_N)$.

See reference:

Fletcher, R., *Fortran Subroutines For Minimization by Quasi-Newton Methods*, Report R7125 AERE, Harwell, England, June 1972.

ZSRCH

Purpose Generate points in an N dimensional space

ZSRCH generates starting points for algorithms which optimize functions of several variables - or, almost equivalently - algorithms which solve simultaneous non-linear equations.

ZSRCH is based on systematic placement of points to optimize the dispersion of the set.

ZSRCH may be used with any non linear optimization routine that requires starting points. The rectangle to be searched must be determined and the number of starting points must be chosen.

See reference:

Aird, T.J., and Rice, J.R., *Systematic Search in High Dimensional Sets*, SIAM Journal on Numerical Analysis, **14** (2) 1977, 296 - 312.

LUDAPB

Purpose Decomposition of a Positive Definite Band Symmetric Matrix - Band Symmetric Storage Mode

LUDAPB Decomposes the N by N matrix A into the product LL^T where L is a lower triangular band matrix. A is assumed to be a positive definite band symmetric matrix stored in band symmetric storage mode.

A is decomposed into LL^T by the Cholesky algorithm. This algorithm is stable without pivoting. The result, L, is stored in band storage mode in the matrix UL. The main diagonal values of UL are stored in reciprocal form.

LUELPB

Purpose. Elimination part of solution of AX = B - positive definitive band symmetric matrix - band symmetric storage mode.

LUELPB performs the elimination portion of the solution of a set of simultaneous equations AX = B where A is assumed to be a positive definite band symmetric matrix stored in band symmetric storage mode.

This routine was designed to be used in conjunction with LUDAPB. The input matrix UL for LUELPB should be the output matrix from LUDAPB.

UL is the LL^T decomposition of the original coefficient matrix A. The main diagonal elements of the LU decomposition are stored in reciprocal form.

See Reference:

Forsythe George and Moler Cleve B., *Computer Solution of Linear Algebraic Systems*, Prentice-Hall, Inc., Englewood Cliffs, New Jersey 1967, Chapter 23.

LUREPB

Purpose. Refinement of solution to linear equations - positive definite matrix - band symmetric storage mode

LUREPB refines the solution of a set of linear equations AX = B, where A is a positive definite band symmetric matrix stored in band symmetric storage mode. It is assumed that the LL^T decomposition of A is available as supplied by the IMSL Routine LUDAPB. This routine iterates upon the solution until machine accuracy is achieved.

The user supplies as input the N x N positive definite band symmetric matrix A, the lower triangle L of its LL^T decomposition (stored in UL) which is also N x N, and vectors X and B of length N. For further details see the algorithm and accuracy sections of IMSL Routine LUREFP.